

3D Printing of Highly Loaded Amorphous Solid Dispersions for Oral Drug Delivery

Inaugural-Dissertation

zur Erlangung des Doktorgrades
der Mathematisch-Naturwissenschaftlichen Fakultät
der Heinrich-Heine-Universität Düsseldorf

vorgelegt von

Nadine Gottschalk
aus Neuwied

Düsseldorf, September 2023

aus dem Institut für Pharmazeutische Technologie und Biopharmazie
der Heinrich-Heine-Universität Düsseldorf

Gedruckt mit der Genehmigung der
Mathematisch-Naturwissenschaftlichen Fakultät der
Heinrich-Heine-Universität Düsseldorf

Berichtersteller:

1. Prof. Dr. Jörg Breitzkreutz
2. Prof. Dr. Anne Seidlitz

Tag der mündlichen Prüfung: 08.03.2024

Table of contents

Abbreviations	III
1. Introduction	1
1.1. Additive manufacturing in pharmaceutical development.....	1
1.2. 3D printing techniques	2
1.2.1. Fused Deposition Modeling	2
1.2.1.1. Printing principle	2
1.2.1.2. Manufacturing of pharmaceutical filaments	3
1.2.1.3. Printing of pharmaceutical formulations.....	4
1.2.2. Drop-on-powder printing	7
1.2.2.1. Printing principle	7
1.2.2.2. Inkjet printing techniques.....	9
1.2.2.3. Material considerations for pharmaceutical printing.....	10
1.3. Poor drug solubility and enabling formulations	12
1.3.1. Relevance of poorly soluble drug substances.....	12
1.3.2. Amorphous solid dispersions	13
1.3.3. Manufacturing techniques: Hot-melt extrusion	15
1.3.4. Solid state characterization of amorphous solid dispersions	16
1.4. Model compounds.....	17
1.4.1. Ketoconazole.....	17
1.4.2. Peposertib	18
2. Aim of thesis.....	19
3. Results and discussion.....	20
3.1. Process considerations in Fused Deposition Modeling.....	20
3.1.1. Effects of high drug loads on mechanical properties of filaments.....	20
3.1.2. Effects of high drug loads on melt rheology and required process adjustments	34
3.1.3. Extrusion and printing of the pipeline substance peposertib	49
3.1.3.1. Introduction	49
3.1.3.2. Results and discussion	49

3.1.3.3. Conclusion	59
3.2. Drop-on-powder printing of highly drug loaded amorphous solid dispersions	61
3.2.1. Drop-on-powder process development for production of highly dosed formulations..	61
3.3. Comparing Fused Deposition Modeling and drop-on-powder printing	75
3.3.1. Comparative stability study of 3D printed amorphous solid dispersions	75
4. Summary and conclusion	87
5. Materials and methods	93
5.1. Materials	93
5.2. Methods	93
5.2.1. Manufacturing methods	93
5.2.1.1. Hot-melt extrusion	93
5.2.1.2. Printing	95
5.2.2. Analytical methods	96
5.2.2.1. Differential scanning calorimetry	96
5.2.2.2. Polarized light microscopy	96
5.2.2.3. X-ray powder diffraction	97
5.2.2.4. Three-point bending test	97
5.2.2.5. Feed force testing	97
5.2.2.6. Content and purity analysis	97
5.2.2.7. Dissolution	98
5.2.2.8. Tablet characterization	98
6. List of publications and conference contributions	99
6.1. Research papers	99
6.2. Patent application	99
6.3. Poster presentations	99
7. References	101
8. Danksagung	114
9. Eidesstattliche Erklärung	116

Abbreviations

3D	Three-dimensional
3DP	Three-dimensional printing
ACN	Acetonitrile
API	Active Pharmaceutical Ingredient
ASD	Amorphous Solid Dispersion
BCS	Biopharmaceutics Classification System
CAD	Computer-aided design
CCR	Critical cooling rate
CNC	Computer numerical control
DCS	Developability classification system
DoD	Drop-on-demand
DoP	Drop-on-powder
DSC	Differential scanning calorimetry
FaSSIF	Fasted State Simulated Intestinal Fluid
FDM	Fused Deposition Modeling
FDA	U.S. Food and Drug Administration
FFF	Fused filament fabrication
GFA	Glass forming ability
HME	Hot-melt extrusion
HPLC	High-performance liquid chromatography
MED	Melt Extrusion Deposition
pK_a	Negative base 10 log of the acid dissociation constant K_a
PLA	Polylactic acid
PLM	Polarized light microscopy
XRPD	Powder X-ray diffraction
SGF _{sp}	Simulated gastric fluid without pepsin
SLA	Stereolithography
SLS	Selective laser sintering
SME	Specific mechanical energy
SODF	Solid oral dosage form
T_g	Glass transition temperature
YM	Young's modulus

1. Introduction

1.1. Additive manufacturing in pharmaceutical development

Three-dimensional printing (3DP) is an emerging technology in the area of additive manufacturing (AM) and is gaining a huge interest in a broad range of industries in the past years. It started when the 3DP technology stereolithography was developed in the early 1980s by Charles Hull (Jamróz et al., 2018). From thereon, several 3DP techniques evolved. There are powder-based systems like selective laser sintering (SLS) and drop-on-powder (DoP) printing, extrusion-based systems like Fused Deposition Modeling (FDM) and semi-solid extrusion as well as liquid-based techniques, e.g., stereolithography (SLA). Even though the printing techniques differ, they have one principle in common: the three-dimensional (3D) object is created in a layer-by-layer fashion. The digital object design is created using computer-aided design (CAD) software and then typically transferred into a stereolithography file (.stl) format, which describes the surface of the object using triangles (Guo et al., 2019). A so called “slicing” software divides the object into a stack of layers and translates the printing directives into a machine-readable format using computer numerical control (CNC) programming language. Different formats are possible of which the “G-code” is most widely used. Through the fast adaptability of the object’s design, 3DP is used for rapid prototyping, e.g., in aerospace or in the automobile industry (Gross et al., 2014).

One of the potentials of 3DP in the pharmaceutical and biomedical industry is the production of personalized pharmaceutical products. 3DP can be used to produce personalized medical devices (Jammalamadaka and Tappa, 2018; Manero et al., 2019) and moreover, personalized solid oral dosage forms (SODFs). Compared to traditional manufacturing techniques, 3DP presents a flexible manufacturing approach, where tablet shapes and dosages can be easily adjusted to the patient’s needs by altering the 3D design. Personalized medicine could be produced on demand at point-of-care (e.g., in hospital pharmacies) and an efficient use of drug substances can reduce adverse drug reactions and may improve patient compliance.

The benefits of 3DP are not limited to point-of-care settings but also show potential for the pharmaceutical industry. Fast adaptability of dose-strength can facilitate dose-finding studies in early clinical trials and speed-up development timelines. In addition, conventional drug product manufacturing usually consists of multiple unit operations. 3DP is comparably simple, wherefore the number of processing steps as well as the total number of required excipients that facilitate manufacturing can possibly be reduced. An efficient use of pharmaceutical excipients within the formulation may reduce costs and enable higher drug loads. Furthermore, the pharmaceutical industry is challenged by a large number of poorly soluble compounds (Takagi et al., 2006; Ting

et al., 2018), requiring formulation strategies that provide solubility enhancement e.g., by manufacturing of amorphous solid dispersions (ASDs). Drug loads in ASDs are usually low (< 30%) and additionally required excipients, e.g., to enable tableting, further reduce the drug load, resulting in either tablets with high volume and mass, which can be difficult to swallow, or in a high pill burden for the patient (Kokott et al., 2023). Especially, the combination of new technologies, such as 3DP, combined with traditional solubility enhancement techniques has a high potential to offer new pathways in drug product development.

1.2. 3D printing techniques

1.2.1. Fused Deposition Modeling

1.2.1.1. Printing principle

FDM, also known as fused filament fabrication (FFF), belongs to the extrusion-based 3DP techniques. FDM has been invented by Scott Crump and patented in 1992 (Crump, 1992). Together with his wife Lisa Crump, he founded the company Stratasys Ltd. for the commercialization of 3D printers and related products. FDM uses a wire-like feed-stock material, called filament, which is produced from thermoplastic materials, usually by hot-melt extrusion (HME). The filament is conveyed into a heated printhead, and the molten or softened material is extruded layer-by-layer through a nozzle onto a build plate (Figure 1). The 3D structure is achieved by movement of the printhead relative to the building platform. Complex designs, such as donut-shaped tablets (Goyanes et al., 2015b), shell-core designs (Okwuosa et al., 2017) and hollow structures (Arafat et al., 2018; Fanous et al., 2020; Sadia et al., 2018) have been realized, which are impossible or difficult to achieve using traditional pharmaceutical manufacturing methods. Moreover, these novel designs are capable to modify release profiles (Goyanes et al., 2015b; Windolf et al., 2021). The use of different printheads with different formulations further enables the production of “polypills” consisting of different active pharmaceutical ingredients (APIs) usually separated in different compartments (Khaled et al., 2015). As a melt-based process, FDM is particularly suitable for the formulation of poorly soluble APIs, which can be transferred into a highly soluble amorphous state. Furthermore, high drug loads are possible, as the filament can be directly printed into a tablet-like geometry, without adding further excipients. However, the entire process contains two heating steps (HME and printing), wherefore FDM is considered for thermostable compounds only (Cui et al., 2021).

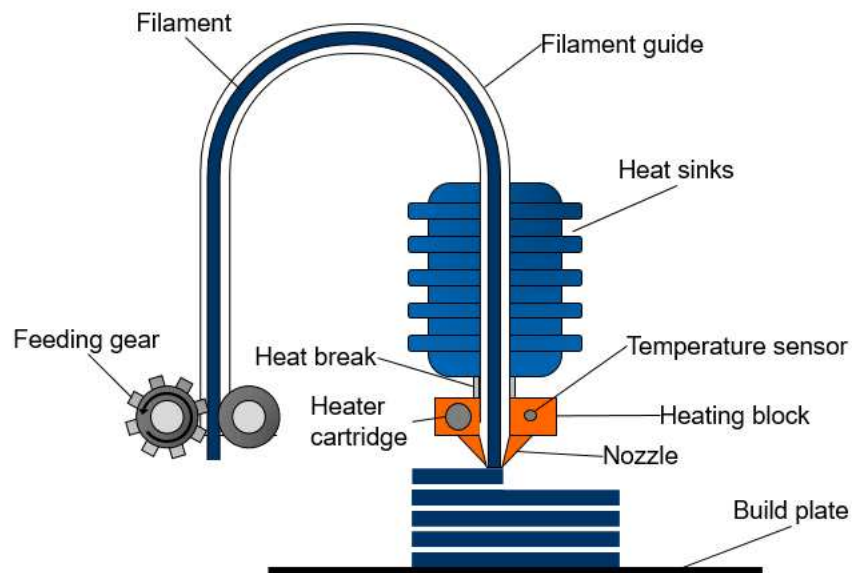


Figure 1: FDM principle of a bowden printer

1.2.1.2. Manufacturing of pharmaceutical filaments

Pharmaceutical filaments can be manufactured in several ways of which HME is most common. The API, a thermoplastic polymer and other excipients are heated up in an extruder barrel and the molten mass is homogenized by the screws and pushed forward through a cylindrical die. The resulting extrudate strand exiting the die can be pulled by a conveyor belt or an automated winder, which winds the filament on a spool. Another technique to produce drug-loaded filaments, which has been applied mainly in the early days of pharmaceutical 3DP, is immersion of commercially available technical filament in alcoholic solutions of API (Goyanes et al., 2014; Skowrya et al., 2015). However, immersion did not prevail since the achievable drug-loads were low ($< 2\%$ w/w), which is insufficient for most drug substances. In contrast to this, HME enables highly loaded filaments with up to 60% API (Verstraete et al., 2018).

Main quality attributes of pharmaceutical filaments are the absolute outer diameter, the diameter and content uniformity and the mechanical properties. Due to the primary use of commercially available 3D printers, common diameters are 1.75 mm and 2.85 mm. Filaments with larger diameters than the nominal diameter of the filament guide will get stuck in the printer and stop the printing process, whereas filaments with smaller diameter might bend, leading to discontinuous forward propulsion. There are two types of hot-melt extruders, which are mainly used for filament production: single- and twin-screw extruders. A homogenous distribution of the API in the polymer matrix is crucial for pharmaceutical filaments as the degree of homogeneity determines the content uniformity of the finished SODF. Therefore, mainly twin-screw extruders are used, since they provide higher shearing and mixing of the melt than single-screw extruders (Leister et al., 2012).

Adjusting the filament diameter and achieving a good dimensional uniformity can be challenging and requires thorough adaption of extrusion parameters. Korte and Quodbach (2018) showed that the powder feed rate and the conveyor belt speed were the main influencing factors when no filament winder is used. This confirms the theoretical consideration that the filament diameter increases with increasing powder feed rate, whereas the increase of conveyor belt speed results in thinner filaments. The major influence of the conveyor belt speed was later confirmed by Feuerbach et al. (2019). Prasad et al. (2019) further evaluated the influence of the die diameter, conveyor belt speed and screw speed on the absolute filament diameter of hypromellose filaments. As a result of die swelling, the filament diameter was generally higher than the die diameter and increased further when high screw speeds were applied.

Next to the absolute outer filament diameter, the extent of diameter fluctuations is of great importance. The minimum and maximum diameter of commercial available filaments are usually equal or smaller than ± 0.05 mm and this has been also recommended for pharmaceutical filaments (Melocchi et al., 2016). Ponsar et al. (2020) demonstrated that filament diameter quality determines the quality of printed tablets. Tablets, which had been printed from less uniform filaments, showed a lower mass uniformity. High diameter fluctuations were attributed to low barrel fillings, as a result of high screw speeds. It was further shown that fluctuations could be diminished by reducing the number of kneading zones in the screw configuration from three to two, allowing a uniform material transport in the extruder (Chamberlain et al., 2022). Nevertheless, filament production remains challenging. This is highlighted by the fact that several techniques have been employed to completely bypass filament production such as direct powder extrusion (Boniatto et al., 2021; Goyanes et al., 2019; Pflieger et al., 2022) or melt extrusion deposition (MED™, (Zheng et al., 2021)), where powdered or granulated materials are directly extruded into tablets.

1.2.1.3. Printing of pharmaceutical formulations

A printer hotend usually consists of several components. An integral part is the heating block. It contains a heating element (e.g., heater cartridge) and a metallic resistance sensor to control the temperature (Figure 1). The heating block is usually made from metals with high thermal conductivity such as aluminum or copper. A nozzle is directly attached to the heating block and is available in different geometries and nozzle sizes. The heat break is located above the heating block to reduce thermal energy from “creeping” up the filament path, which can lead to softening of the upper filament or extension and blockage. The heat sinks provide a large surface area and in combination with a ventilating fan providing active cooling of the upper filament.

Filaments can either be pulled into the hotend by rotating feeding gears inside the printhead (direct extruder) or be pushed by feeding gears outside of the printhead (bowden extruder). The filament acts as a piston that pushes the liquified material through the nozzle orifice. Feedability is a prerequisite for the FDM process and can be defined as the resistance of the filament to mechanical stress during the FDM feeding process. The feeding mechanism of commercially available 3D printers requires specific mechanical properties. A suitable 3DP material has to exhibit stiffness and toughness (Zhang et al., 2019). Stiffness describes the ability of material to withstand high loads, e.g., forces, without deformation (Zhang et al., 2019). Insufficient stiffness and high viscosities can lead to buckling of the filament (Nikzad et al., 2011), i.e., bending of the filament in the guide during printing. Venkataraman et al. (2000) found that filament buckling in the guide can be prevented if the ratio of elastic modulus of the material and its apparent viscosity in the hotend is larger than $3\text{-}5 \times 10^{-5} \text{ s}^{-1}$. Toughness is the ability of a material not to break upon being subjected to a sudden force (Perkins, 1999), defined as the area under the stress-strain curve until material fracture (Brostow et al., 2015), and is required to withstand the forces of the feeding gears during printing. If the material is too brittle, filament will break between the feeding gears (Ilyés et al., 2019; Zhang et al., 2017). Brittleness describes a material behavior, where the material fractures without or little plastic deformation when subjected to stress (Field, 1971). Commercially available materials for printing in the consumer sector, e.g., polylactic acid (PLA), are designed for the FDM printing process. However, the number of pharmaceutical polymers is limited and many polymers have been described of being too brittle for their use in FDM (Nasereddin et al., 2018; Tabriz et al., 2021). Therefore, the focus of pharmaceutical formulation development in FDM lies to a large extent on the optimization of the mechanical properties. In order to overcome poor feedability, the use of plasticizers is very common. Plasticizers are molecules of low molecular weight that, when incorporated into a polymer matrix, increase the free volume and reduce intermolecular friction of the polymer molecules (Nollenberger et al., 2012). They increase the mechanical flexibility of filaments and enable processing at lower temperatures (Lima et al., 2022). Commonly in use are non-toxic plasticizers such as glycerol or triethyl citrate (Goyanes et al., 2015a; Lima et al., 2022; Melocchi et al., 2016; Sadia et al., 2018; Santos et al., 2021). In addition, polymer blends containing polymers such as polyethylene oxide, can be used to improve the feedability (Alhijaj et al., 2016; Fuenmayor et al., 2018). However, adding excipients to a formulation increases the complexity and several factors such as miscibility, compatibility and stability during processing and storage have to be considered. Especially in formulations with high drug loads, the API can have a dominating effect on the filament properties leading, e.g., an embrittlement of a formulation (Aho et al., 2019; Prasad et al., 2019). Due to the

high proportion the possibilities for adjustments of the formulation are limited, demonstrating the need for novel printing approaches.

Several analytical methods have been employed to estimate feedability of pharmaceutical formulations and reduce trial-and-error printing. The three-point bending test is most commonly applied (Prasad et al., 2019; Xu et al., 2020; Zhang et al., 2017). Here, a moving blade moves downwards at a defined speed onto the filament placed on two support pins with fixed distance. The flexural modulus can be calculated from this setup as well as strain at break. Zhang et al. (2019) proposed the “stiffness test” in addition to the three-point bending test, where the test specimen is subjected to a force but in contrast to three-point bending test, the test specimen is placed on a solid plate without the possibility to bend. More complex techniques, similar to the actual printing process, have been developed such as the setup from Nasereddin et al. (2018), where longitudinal forces were applied onto the filament and flexibility profiles were correlated via principal component analysis to commercially available filaments. Xu et al. (2020) compared these three screening methods and found that the stiffness test is the most predictive method for direct extruders. Another method is the tensile test, where the test specimen is fixed between clamps and elongated at defined speed (Korte and Quodbach, 2018; Samaro et al., 2020) from which the young’s modulus (YM) can be calculated. It was proposed that a YM above 300 N/mm² is required to ensure proper stiffness, toughness and good printability. Tabriz et al. (2021) found that the maximum tensile strength until breakage in tensile testing is a good predictor for feedability in bowden extruders. The large number of test methods reflects the actual problem in pharmaceutical 3DP: there is a variety of FDM printers on the market, which can be used for pharmaceutical printing but with a lack of harmonized equipment (Feuerbach et al., 2018). Next to that, these printers are usually derived from the consumer 3DP sector and are repurposed for pharmaceutical printing, thus they often do not comply with the regulations for pharmaceutical products (Melocchi et al., 2021). The requirements for pharmaceutical products, medicinal products and medical devices differ significantly from those for rapid prototyping in the consumer sector. Hence, commercially available printers and their slicing software are designed to achieve good printability, high dimensional accuracy as well as suitable mechanical stability of printed objects. Printed pharmaceuticals, though, also must comply with the requirements specified in the pharmacopeias or regulations from competent authorities, which are, among others, mass variation and content uniformity. FDM printing offers huge flexibility in terms of parameter settings, but as printing will be performed with a broad range of excipient and API combinations, ideal print parameters must be elaborated for each individual formulation. Most commonly, a trial-and-error approach is used to find suitable printing settings, which is time- and material-consuming. Several methods have

been developed to estimate suitable and appropriate printing conditions. One of the key parameters, which has to be adapted to each respective formulation, is the nozzle temperature, which defines the viscosity of the melt in the hotend. Low nozzle temperatures may lead to incomplete melting and buckling of the filament, whereas high nozzle temperatures might result in premature material deposition and stringing (Fuenmayor et al., 2018) and, in case of thermosensitive APIs or excipients, in molecular degradation (Hoffmann et al., 2022; Kempin et al., 2018). In order to estimate suitable nozzle temperatures, rheological measurements have been applied. Coogan and Kazmer (2019) demonstrated that inline rheology measurements inside the printer nozzle are feasible. However, this measurement setup is difficult to establish. Elbadawi et al. (2020a) showed that prediction of print parameters is possible based on plate-plate rheological measurements and used those in a machine-learning tool (Elbadawi et al., 2020b). However, this approach did only confirm whether a material was printable or not at a certain temperature, neglecting other pharmaceutical considerations, such as batch uniformity. Furthermore, this approach solely focused on printing temperatures. As the printing process is a dynamic process, the melt viscosity in the nozzle depends not only on the nozzle temperature but also on various other factors, notably the printing speed, which determines the transition time of the filament through the hotend. A significant influence of the printing speed on the mass uniformity of printed tablets was demonstrated by Alhijaj et al. (2019), highlighting the importance of this parameter. The authors further showed that especially high printing speeds negatively correlated with the absolute printed mass. However, the FDM printing process is a comparably slow technique, wherefore high printing speeds are desirable to accelerate the manufacturing process. As FDM printers usually work with volumetric extrusion there are no control systems that measure the quantity of material being deposited. Deviations in mass as well as non-uniform tablet batches are possible, which are only detected when the material has been already printed. Therefore, predictive tools should be employed for the determination of print parameters, which ensure batch uniformity as well as content conformity with only low material input.

1.2.2. Drop-on-powder printing

1.2.2.1. *Printing principle*

DoP printing, also known as binder jetting, belongs to the powder-based 3DP techniques and has been invented for the fabrication of 3D objects from metallic or ceramic powders (Trenfield et al., 2018) by Emmanuel Sachs at the Massachusetts Institute of Technology in 1993 (Sachs et al., 1993). In DoP printing layers are created by spreading of thin powder layers (Figure 2). Powder particles are fused in-situ upon contact with small droplets of an ink or binder solution, which are jetted from a printhead onto each powder layer. Unbound powder acts as support enabling

complex geometries (Trenfield et al., 2018; Ziaee and Crane, 2019). After drying of the powder bed, unbound powder and solidified objects are separated. The technology was licensed to Therics, who developed the Theriform™ process for the production of pharmaceutical products. This technology uses drug-loaded ink, which is jetted onto a powder bed (Lee et al., 2003). However, the technique was limited in terms of dose due to the low applicable volumes of API ink. In contrast, the ZipDose® technology, patented by Yoo et al. in 2014 and assigned to Aprecia Pharmaceuticals, uses a binder to fuse a API-containing powder blends for the production of highly dosed and fast disintegrating dosage forms. The ZipDose® technology was used to produce the first 3D printed dosage form, which was approved by the U.S. Food and Drug Administration (FDA) in 2015 (Vaz and Kumar, 2021). The 3D printed product, Spritam®, is an orodispersible product containing the anticonvulsant levetiracetam for the treatment of partial-onset seizures of children.

One of the key benefits is that DoP printing enables manufacturing of highly drug loaded SODFs compared to traditional manufacturing techniques. Drug load in conventional tablets is often limited by poor compressibility and flowability of the API (Chen et al., 2022; Gentis and Betz, 2012; Khaled et al., 2018). Both factors are either not or only partially relevant in DoP printing. DoP printed dosage forms are further characterized by their high porosity, which can be used to produce, e.g., rapidly disintegrating dosage forms. Nevertheless, also dosage forms with controlled, sustained or pulsatile release (Trenfield et al., 2018) are possible, which is defined by the selection of excipients and print parameters (Okafor-Muo et al., 2020; Rowe et al., 2000; Wu et al., 1996). One of the drawbacks of this technology is the high porosity of SODFs, which can lead to high friability and poor breaking strength (Cui et al., 2021; Yu et al., 2009), impairing automatized processing and packaging of the final dosage forms (Trenfield et al., 2018). Further, it can be challenging to process moisture-sensitive APIs through binder jetting, as the inks, which are often aqueous, may lead to drug degradation through hydrolysis. However, unlike most other 3DP techniques, DoP printing is fast (Ziaee and Crane, 2019) and most suitable for scale-up (Hsiao et al., 2018; Sen et al., 2021), making this process particularly beneficial for the pharmaceutical industry. DoP printing has the potential to be used for early clinical trials supply (van den Heuvel et al., 2022), when different dosages are still under evaluation, as well as later stages of drug product development, where large quantities are required. Hence, DoP printing has the potential to accelerate development timelines and reduce resources in pharmaceutical development (Daly et al., 2015; Trenfield et al., 2018).

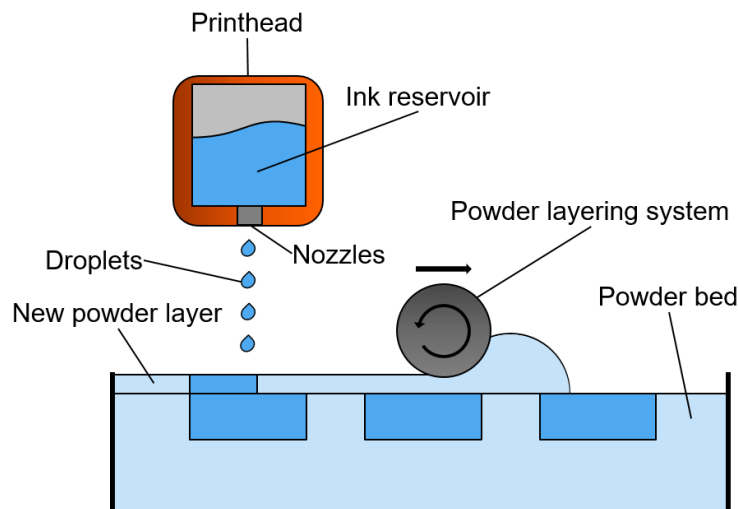


Figure 2: DoP printing principle

1.2.2.2. Inkjet printing techniques

DoP printing utilizes inkjet printing systems, which originally were invented for 2D printing on substrates, e.g., paper. Different printing processes, e.g., drop-on-demand (DoD) or continuous inkjetting are possible. In DoP printing, the inkjet process DoD is most widely used (Hue P. Le, 1998) as droplets can be generated as needed by individually activating nozzles. This process uses thermal or piezoelectric actuators for droplet generation that are closely located at the nozzle orifice (Hutchings et al., 2016). Thermal printheads generate droplets through a heating element, which is activated by an electric impulse leading to formation of a vapor sphere. The resulting positive pressure pushes the ink through the nozzle (J. Li et al., 2015; Sen et al., 2021; Ziaee and Crane, 2019). A second type of DoD printheads utilizes piezo-electric transducers in which the electric impulse results in deformation of a piezo element creating a pressure wave, which leads to the ejection of droplets (Vaz and Kumar, 2021). These printheads usually consist of several nozzles (up to 1000 per printhead (Daly et al., 2015; Vaz and Kumar, 2021)) enabling high printing speeds. Piezoelectric printheads can work with a broad range of liquids (Daly et al., 2015; Parhi, 2021), whereas thermal printheads are limited to inks that easily vaporize through temperature increase. Piezoelectric printheads are robust as they are not affected by heat damage like thermal printheads. However, these printheads come at high costs. In contrast, thermal printheads are more simple to fabricate and therefore cheaper (Cui et al., 2021). Concerns have been raised regarding the use of API-containing inks with thermal printheads as the heat impulse might trigger molecular degradation (Okafor-Muo et al., 2020). Nevertheless, it was shown that in various cases no degradation occurred, which was attributed to the short transition times in the nozzle (Buanz et al., 2011; Meléndez et al., 2008).

Next to DoD, droplets can also be generated continuously. Thabet et al. (2018b) demonstrated that continuous in-line printing is a feasible and fast approach to produce orodispersible films. Nevertheless, the system under evaluation was limited in terms of dose flexibility. Commercially available continuous inkjet printers provide this flexibility to deposit ink droplets at precise locations. This is achieved through deflection of non-print droplets by an electrostatic field from a continuous stream of droplets generated at high pressures (Daly et al., 2015; Ziaee and Crane, 2019). These inkjet systems are optimized for high throughputs, however, machines come at high costs and maintenance (Vaz and Kumar, 2021), wherefore this principle was not used in the following work.

1.2.2.3. Material considerations for pharmaceutical printing

The jettability of an ink is dependent on its properties and commonly described by the z-number, which is the reciprocal of the dimensionless Ohnesorge number (J. Li et al., 2015; Prasad and Smyth, 2016). The equation takes several factors into account: the nozzle diameter, fluid density, dynamic viscosity and surface tension. Values of 1 – 10 are generally described as printable, whereas values larger than 10 can result in formation of satellite drops, which reduce the resolution of the print. Ink jettability can further be characterized through droplet shape analysis (Schulz, 2020; Thabet et al., 2018a). Accurate determination of droplet size and shape helps to control droplet deposition and improve the printing process. Commercially available inks are usually optimized for the container system in order to provide good and stable drop ejection (Schulz, 2020).

The inks used for pharmaceutical applications are mainly water-based (Cader et al., 2019; Chang et al., 2021, 2020; Kiefer et al., 2021; Sen et al., 2020; Wang et al., 2006; Wickström et al., 2015; Yu et al., 2009). Also the use of volatile solvents such as ethanol, isopropyl alcohol, methanol or dichloromethane and aqueous mixtures thereof have been reported (Buanz et al., 2015; Infanger et al., 2019; Kozakiewicz-Latała et al., 2022; Rajjada et al., 2013; Scoutaris et al., 2011; Tian et al., 2019; Yu et al., 2007). Volatile solvents have the potential to reduce drying times and hence, accelerate the printing process. Several other additives can be used in inks, but it has to be considered that the higher the solid content in the ink, the higher the risk for nozzle clogging and printhead failure when the solvent evaporates, especially with DoD printheads (Ligon et al., 2017; Rajjada et al., 2013; Ziaee and Crane, 2019). Often surfactants, such as polysorbates, are used to reduce surface tension and enable stable droplet formation (Cader et al., 2019). Next to that, the addition of polymeric binders in the ink can enhance the mechanical properties of the printed dosage forms. Similar polymers as in wet granulation are used, e.g., different grades of povidone, cellulose ethers or polyvinyl alcohol (Chang et al., 2021, 2020; Kozakiewicz-Latała et al., 2022;

Schulz, 2020; Wang et al., 2021; Yu et al., 2009). API-loaded inks show very accurate drug dosing (Kiefer et al., 2021; Sen et al., 2020). However, the chemical and physical stability of the drug substance especially the thermodynamic solubility in the respective ink has to be considered. APIs with poor aqueous solubility will require the addition of solubility enhancers or toxic solvents such as methanol (Trenfield et al., 2018). Furthermore, final API loadings are usually very low (in the lower mg to μg range) due to the limited amounts of ink that can be applied per layer (Lee et al., 2003; Sen et al., 2020). In contrast, dosage forms with high drug loads up to 70% are achievable, when the API is included in the powder bed (Infanger et al., 2019; Yu et al., 2007). Nevertheless, the question whether unbound powder containing API can be reused remains. To address this issue, Aprelia Pharmaceuticals recently introduced their new technology “Z-Form”, that enables the direct printing of tablets into blisters.

The powder bed in pharmaceutical DoP printing can consist of almost any pharmaceutical powder material. Excipients used as fillers are sugar alcohols (e.g., lactose, mannitol, sucrose, dextrin, sorbitol), celluloses (e.g., microcrystalline cellulose) or inorganic materials (calcium sulfates, calcium phosphates (Antic et al., 2021; Chang et al., 2021, 2020; Kozakiewicz-Latała et al., 2022; Sen et al., 2020; Tian et al., 2019; van den Heuvel et al., 2021; Yu et al., 2009; Zhou et al., 2014)). Polymers can be added to the powder mixtures to enforce cohesion of particles, acting as a “solid binder” (Infanger et al., 2019) through polymer chain entanglement (Antic et al., 2021). Polymers typically used are cellulose ethers (hydroxypropyl cellulose, hypromellose, methyl cellulose (Antic et al., 2021; Infanger et al., 2019; Kozakiewicz-Latała et al., 2022; Wang et al., 2006), povidone (Kozakiewicz-Latała et al., 2022; Sen et al., 2020), copovidone (Antic et al., 2021; Chang et al., 2020) and polyvinyl alcohol (Zhang et al., 2021). It is important that the particle size is smaller than the set layer height, otherwise, larger particles can create furrows on the powder surface. The minimum layer height for DoP printing is stated to be 200 μm (Alhnan et al., 2016). The smaller the particle size, the smoother the surface properties and the higher the tensile strength of printed objects (Miyajima et al., 2020; Ziaee and Crane, 2019). However, with decreasing particle size the flowability of the powder decreases. Very fine powders with poor spreadability have been reported to result in an uneven powder surface (Gueche et al., 2021). A smooth powder surface is crucial for the printing process as defects in the powder bed can result in defects of the final dosage form. It was reported that the use of powders with bimodal particle size distribution shows advantages in terms of packing density (Sofia et al., 2018).

Binding of powder particles can be achieved through binder bridges and by recrystallization of dissolved material (Norman et al., 2017). The amount of printed ink or binder in relation to the respective powder material has to be carefully selected, as high amounts can result in “bleeding”

of the ink into powder areas, which were intended to remain unbound and low quantities might result in impaired mechanical properties of the finished dosage form (Souto et al., 2019; Ziaee and Crane, 2019). The required binder quantity depends on several factors, such as droplet size, spreadability as well as the number and size of voids in the powder. Good wettability is an additional factor to provide fast powder penetration and provide adequate binding properties (Kozakiewicz-Latała et al., 2022; Zhou et al., 2014). The wettability of the powder bed can be estimated by the droplet-penetration testing (Antic et al., 2021). In case the wettability is poor, the wettability can be improved using particle engineering, e.g., through crystal coating (Kozakiewicz-Latała et al., 2022). Nevertheless, the use of DoP printing has been mainly described for well soluble APIs. Amorphization of poorly soluble APIs, in order to enhance solubility, can be achieved when the API is dissolved in the ink and printed on substrates enabling fast solvent evaporation (Hirshfield et al., 2014; Prasad and Smyth, 2016; Raijada et al., 2013; Scoutaris et al., 2011; Wickström et al., 2015) or using rapidly solidifying resins (Clark et al., 2020). However, as mentioned in a previous section, resulting dose strengths are low. The processability of high dose and poorly soluble compounds in DoP printing was reported only to a limited extent and is part of the present work.

1.3. Poor drug solubility and enabling formulations

1.3.1. Relevance of poorly soluble drug substances

Despite representing a notable portion of drug substances in pharmaceutical development (Takagi et al., 2006), poorly soluble APIs still present a major challenge in the pharmaceutical industry. The oral administration route is preferred in patients (Alqahtani et al., 2021) but drug molecules have to be dissolved in the gastrointestinal tract before absorption in order to achieve a therapeutic effect. Amidon et al. proposed the biopharmaceutics classification system (BCS) in 1995 to provide a systematic approach for in vitro-in vivo correlations. Drug substances are classified by their thermodynamic solubility in aqueous media of different pH values as well as their intestinal membrane permeability based on human pharmacokinetic studies or Caco-2 cell assays. A compound is classified as poorly soluble when the highest dose strength is not soluble in 250 mL of aqueous medium in a pH range between 1.2 – 7.5. Poorly soluble compounds are categorized into BCS class II or IV, depending on good or limited permeability, respectively. The BCS was revised by Butler and Dressman in 2010, who established the developability classification system (DCS). The use of Fasted State Simulated Fluid (FaSSIF) as well as a volume increase to 500 mL were proposed in order to approximate biological conditions. The BCS class II was divided into two subcategories: class IIa, the dissolution rate limited compounds and class IIb, the solubility limited compounds. Solubility enhancement of class IIa compounds can be achieved by e.g.,

particle size reduction (Iwasaki et al., 2007) whereas Class IIb compounds require “enabling formulations” that increase their apparent solubility within the gastrointestinal fluids (Buckley et al., 2013). Poor solubility in combination with good permeability in case of BCS class II compounds can be addressed by several formulation strategies such as self-emulsifying systems, molecular complex forms like cyclodextrins or amorphous solid dispersion (Fridgeirsdottir et al., 2016) of which especially the latter is emerging. The FDA approval number of amorphous solid dispersion products has risen steadily in the past years (Jermain et al., 2018) showing that solid dispersions are a viable drug formulation strategy. However, the current market share of poorly soluble APIs makes up only 30%, whereas the number of BCS class II compounds in pharmaceutical development pipelines is estimated to be 60 – 70% (Ting et al., 2018), highlighting the necessity of investigating this class of compounds and related enabling formulations.

1.3.2. Amorphous solid dispersions

An amorphous material is characterized by its disordered intermolecular arrangement without long-range order or symmetry of the molecules in contrast to crystalline materials. The transformation from the crystalline to the amorphous state requires energy to overcome the crystal lattice energy, bringing the system to a higher free energy level (Hancock and Zografi, 1997). This can be achieved by several formulation strategies. The most prominent techniques are melt-fusion and solvent evaporation (Vasconcelos et al., 2016). In melt-fusion, the material is heated above its melting point followed by rapid cooling (quench-cooling) in order to “freeze” the melt in a glassy state. Solvent evaporation techniques use volatile solvents that are capable in dissolving the substance and the glassy state is achieved by rapid solvent removal. Amorphous materials lack a defined melting point but show a glass transition where the solid glass gradually turns from solid to a glassy semi-solid viscous state. The increased higher energy state results in a higher apparent solubility and dissolution rate by decreasing the energy barriers that have to be overcome when the molecules dissolve. However, the crystal lattice is thermodynamically preferred leading to recrystallization and phase separation over time. Regardless, maintaining physical stability of the amorphous state is crucial for bioavailability and shelf-life, which is dependent on several factors such as storage conditions, polymer choice or the API itself. Baird et al., (2010) investigated the recrystallization tendency of pure APIs and proposed a classification system where APIs are differentiated on the basis of their glass forming ability (GFA). APIs were divided into three classes according to their recrystallization behavior in a heating-cooling-heating cycle: class I drugs showed the lowest GFA and drug recrystallized upon cooling; class II drugs stayed amorphous during cooling but recrystallized upon reheating; class III drugs showed the lowest recrystallization tendency and stayed amorphous during cooling and reheating cycles. Blaabjerg et al. (2016)

redefined the GFA classes based on the cooling rate that is required to achieve the amorphous state. Low critical cooling rates (CCR) $< 2^{\circ}\text{C}/\text{min}$ indicate drugs with a low recrystallization tendency (class III), whereas a CCR of $> 750^{\circ}\text{C}/\text{min}$ indicates compounds with a high recrystallization tendency.

The use of an additional excipient can enhance the stability of the amorphous state. For this purpose, polymeric or non-polymeric excipients (e.g., mesoporous silica or amino acids (Dengale et al., 2016; Löbmann et al., 2013; Prestidge et al., 2007)) can be used as carriers. In case of polymeric carriers, the API is dispersed in the polymer matrix enhancing the physical stability by reducing molecular mobility. Several types of solid dispersions have been described by Chiou and Riegelman (1971), notably glass solutions and stabilized glass suspensions. The term ASD is used interchangeably for both conditions. A crystalline API can be soluble up to a certain level in a polymer matrix (Figure 3). The API is molecularly dispersed in the matrix representing a thermodynamically stable one-phase system, which is referred to as glass solution. In order to achieve high drugs loads and reduce pill burden in pharmaceutical development, the drug load often exceeds the solubility limit of the crystalline API resulting in a two-phase system, called glass suspension, which is kinetically stabilized. A glass suspension is meta-stable and sensitive to recrystallization of the API and/or phase separation (Luebbert et al., 2018). Isolated API-rich phases behave like neat amorphous API and will eventually recrystallize, as the glass transition temperature (T_g) of the API is usually low. The presence of crystalline traces, as a result of incomplete ASD transformation or insufficient solubility in the matrix, will also destabilize the ASD by triggering nucleation and crystal growth (Trasi and Taylor, 2012). The supersaturated state is kinetically stabilized by immobilization of the molecules. A high T_g and storage temperature below the T_g are beneficial for the physical stability. Above the T_g , the molecular mobility increases and the probability of recrystallization and phase separation rises. Additional excipients such as plasticizers lower the T_g , which also increases the mobility of the system and facilitates recrystallization. Solvents, including water, are well-known plasticizers that impair the physical stability of ASDs (Prudic et al., 2015). Nevertheless, many polymeric carriers are hygroscopic, so that humidity preventing containers are necessary. It is crucial to prevent API recrystallization during the shelf-life of a product as this decreases the apparent solubility and will probably reduce oral bioavailability. It was further shown that residual crystallinity in ASDs can negatively impact supersaturated dissolution profiles by accelerating nucleation and crystallization in related gastrointestinal fluids (Moseson et al., 2020). Systems can be described in two different parts according to the underlying effects: the spring and the parachute effect (Shah et al., 2014). The supersaturated API usually exhibits a “spring”, where supersaturation is only achieved for the initial

time period due to high thermodynamic pressure. The “parachute” describes the part of the dissolution profile where the supersaturation is maintained over a certain period of time. This profile is preferred as it increases the probability of drug absorption within the gastrointestinal tract. This can be achieved by the use of polymers, e.g., hydroxypropyl methyl cellulose acetate succinate, which act as precipitation inhibitors (Curatolo et al., 2009).

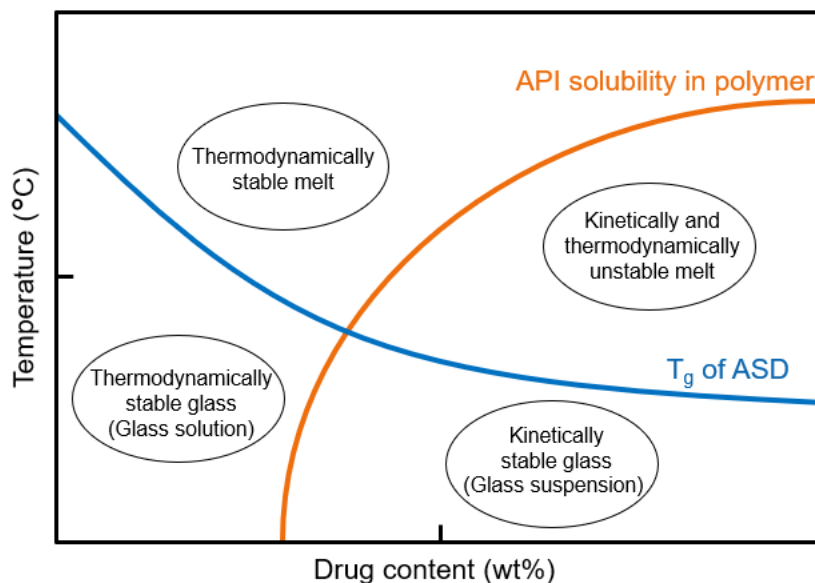


Figure 3: Phase diagram of an API-polymer system in dependence of drug content and temperature adapted from Lehmkemper et al. (2017)

1.3.3. Manufacturing techniques: Hot-melt extrusion

Several manufacturing techniques for ASDs have been described. HME belongs to the melt-fusion methods and offers the benefits of continuous and solvent-free manufacturing (Repka et al., 2018). It was shown that compared to other manufacturing techniques such as spray-drying, drug layering or milling, the highest amorphous drug loads could be achieved by HME (Dedroog et al., 2019), which was attributed to the high thermal energy input. In HME, the API is transferred into the amorphous state by melting and/or dissolution in the polymer matrix through thorough mixing. Quench-cooling freezes the melt in a glassy state. A considerate selection of extrusion parameters is crucial for a successful production of ASDs. An extruder usually consists of different heating elements, which can be controlled separately. High barrel temperatures above the melting point of the API will enable amorphization (Li et al., 2016). However, the thermal stability of the API has to be considered and parameters that enable amorphization but also prevent degradation have to be chosen (Matić et al., 2020). Other important factors are the residence time and the residence time distribution of the melt inside the barrel. Residence time is predominately affected by the feed rate and the screw speed parameters (Gao et al., 2000). The influence of the throughput on the

residence time is expected to be higher than the screw speed (Rudolf, 2008). Next to the applied thermal energy, the mechanical energy input is an important factor to ensure sufficient distribution of the API in the matrix. High screw speeds provide shearing of the melt and hence, contribute to amorphization of crystalline APIs (Lang et al., 2014; Li et al., 2016). The use of kneading elements in the screw configuration is considered to further enhance shearing and mixing and thereby dissolution of the API in the matrix material (M. Li et al., 2015). Twin-screw extruders are preferably used for the production of ASDs as they provide higher levels of mixing compared to single-screw extruders (Lawal and Kalyon, 1995).

1.3.4. Solid state characterization of amorphous solid dispersions

Several analytical methods exist to characterize the solid state of a solid dispersion.

Differential scanning calorimetry (DSC) is a thermal method where samples are heated at a constant rate in small pans. This technique is capable to detect endothermic or exothermic phase transitions by determining the difference in heat flow compared to an inert reference, e.g., an empty metallic pan, in the chosen temperature range. DSC can be used to determine first-order phase transitions, such as melting or crystallization, as well as second-order phase transition, such as the T_g . DSC is a sensitive technique and can provide information on the quantity of crystalline material (Chasse et al., 2022). However, thermal events, such as recrystallization or dissolution of crystals into the matrix, as a results of the heating during the measurement and matrix effects have to be considered (Dedroog et al., 2020).

Polarized light microscopy (PLM) can be utilized to visualize the solid state of a solid dispersion. While most crystalline substances show birefringence in polarized light, amorphous materials appear black due to their lack of long-range order (Nichols, 2006). PLM, as a visual analytical method, provides information on location and size of crystals and is capable to detect even small traces of crystallinity. Even though the sensitivity of this technique is very high, it lacks selectivity and quantitative determination is difficult (Chasse et al., 2022). Since only a small section is viewed, conclusions may not be representative for the entire material.

One of the techniques that provides the highest selectivity is X-ray powder diffraction (XRPD). The diffraction of X-rays as a function of the diffraction angle is unique for each crystal form and allows the detection of present polymorphs (Thakral et al., 2018). Conditions where constructive interference occurs are described by Bragg's law:

$$n \cdot \lambda = 2d \cdot \sin(\theta) \tag{1}$$

where n is the diffraction order, λ the incident X-ray wavelength, d the distance between the lattice planes of the crystalline system and θ the Bragg angle.

XRPD can also be used to quantify crystalline amounts, however, the detection of small crystalline traces is limited (Dedroog et al., 2020). The limits of detection and quantitation varies between formulations and is dependent on sample preparation (Chasse et al., 2022).

Next to DSC, PLM and XRPD, the solid state of a formulation can also be assessed via near-infrared or raman spectroscopy, terahertz spectroscopy or solid state nuclear magnetic resonance spectroscopy (Liu et al., 2018; Tambe et al., 2022). Due to blind spots and different detection and quantitation limits of each technique, the combination of several analytical methods is crucial.

1.4. Model compounds

1.4.1. Ketoconazole

Ketoconazole (Figure 4) is an antifungal agent for the treatment of a broad range of fungi such as candida albicans and dermatophytes (van Tyle, 2013). Ketoconazole belongs to the group of azol antifungals, which inhibit the ergosterol synthesis and thereby damage cell membrane integrity (Borgers et al., 1983). Being patented in 1977 by Janssen, ketoconazole was the first oral antifungal and is available on the market since 1981 (Gupta and Lyons, 2015). Nowadays, the main administration route is topical as market authorization in the European Union was suspended for oral use by the European Medicines Agency in 2013 due to its strong hepatotoxicity (EMA, 2013). Oral dosage forms are still available in the United States of America but the use was restricted by the FDA to endemic mycoses with no alternative treatment possibilities (FDA, 2013). Ketoconazole is available under the trademark Nizoral[®] with 200 mg per single dose (Gupta and Lyons, 2015). Even though its use is limited for oral administration, ketoconazole is frequently used as model compound in ASDs due to its representative API properties and good commercial availability. Ketoconazole is a weakly basic drug (pK_a 2.9 and 6.5, (van Tyle, 2013)) with a molecular weight of 531.4 g/mol. The API is hydrophobic (logP 3.54, (Baird et al., 2010)) and exhibits poor solubility in biorelevant media (22.2 $\mu\text{g/mL}$ in FaSSIF at pH 6.5, (Auch et al., 2018)) and has been categorized as BCS class IIb compound (Yasuhiro et al., 2014). Ketoconazole melts at 150 °C (Baird et al., 2010) and degradation occurs at high temperatures (221 °C, (Kanaujia et al., 2011)), wherefore its use as model compound in HME has been frequently described (Flügel et al., 2021; Kanaujia et al., 2011b; Monschke et al., 2021). It forms stable glasses upon melting without recrystallization upon cooling or reheating (GFA class III, (Baird et al., 2010)).

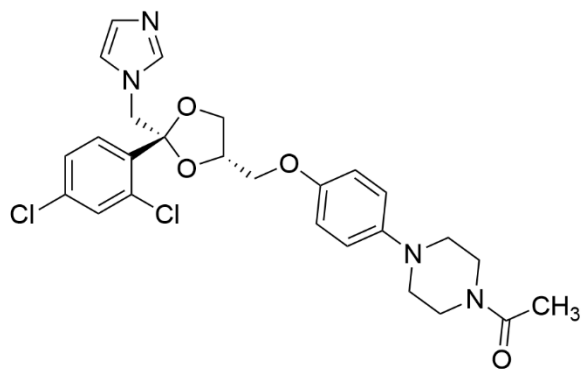


Figure 4: Structural formula of ketoconazole

1.4.2. Peposertib

The compound peposertib (Figure 5) is a pipeline compound of Merck Healthcare KGaA, Darmstadt. It is a DNA phosphokinase inhibitor and in evaluation for the treatment of solid tumors. Peposertib is weakly basic (pK_a 1.8 and 3.1; data received from Merck library) and lipophilic ($\log P$ 2.5, (Flügel et al., 2021)). Peposertib is further poorly soluble (1 $\mu\text{g/mL}$ in FaSSIF at pH 6.5). The molecular weight is 481.9 g/mol. Melting occurs at 207 °C followed by degradation at approximately 210 °C (data received from Merck library).

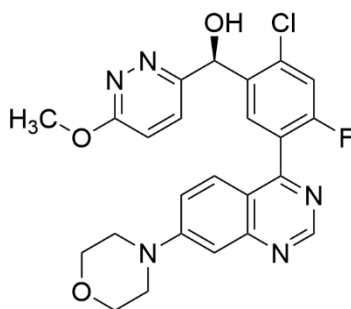


Figure 5: Structural formula of peposertib

2. Aim of thesis

The high number of poorly soluble APIs in development pipelines presents a challenge for the pharmaceutical industry. Poor solubility is often addressed by the development on ASDs, highlighting the need to investigate this formulation type. Especially highly dosed ASDs can be difficult to develop since the properties of the API may dominate the properties of the overall formulation and the high loading further limits the number and quantity of functional excipients. However, it is crucial to achieve the required dose by maintaining an adequate pill burden for patients. One benefit of 3DP is that tablet-like geometries can be directly printed from raw materials or intermediates, potentially reducing the number of unit operations and, hence, the number and quantity of excipients. Therefore, objective of this work was the development of amorphous dosage forms with high drug loads by means of 3DP. Two different 3DP techniques shall be compared for manufacturing of amorphous highly dosed tablets: FDM and DoP printing. The model compound ketoconazole is as a well-known BCS class II drug.

Regarding FDM 3DP, the focus of this work lies on the processability of highly dosed filaments. The influence of a high drug loadings of an amorphous API on the mechanical and rheological properties of filaments shall be investigated. In pharmaceutical FDM printing one of the key challenges are the mechanical properties of the filaments, as they are often very brittle and break between the feeding gears. Plasticizers may be added to the formulations, but this might affect the physical stability of highly loaded ASDs. Therefore, a FDM printer shall be modified to enable printing of brittle filaments. Another challenge in pharmaceutical FDM printing is the determination of suitable print parameters for each individual formulation. A predictive empirical method shall be developed in scope of this work to determine print parameters such as nozzle temperature and printing speed with regards to mass uniformity of the finished SODFs. Both approaches shall be validated using the pipeline compound, pepsertib, in a separate chapter from the cumulative part.

The 3DP technique DoP printing is known as a technique to produce either highly drug loaded formulations of well soluble APIs or low-dose formulations in which the API is amorphous. Therefore, aim of this work shall be to extend the scope of this printing technique to the production of highly dosed and amorphous SODFs by using ASDs as powder material. As this technique requires partial dissolution of powder particles to achieve powder binding, which may result in recrystallization when using ASDs, the solid state and physical stability of the resulting dosage forms shall be investigated. Finally, the two investigated 3DP techniques shall be compared in terms of processability, tablets properties and suitability to produce highly dosed and amorphous dosage forms.

3. Results and discussion

3.1. Process considerations in Fused Deposition Modeling

3.1.1. Effects of high drug loads on mechanical properties of filaments

Poor mechanical properties are a major issue in formulation development of pharmaceutical filaments. Especially in highly drug-loaded formulations, the mechanical properties are dominated by those of the API, leaving only little formulation design space to enhance these properties. Contrary to previous approaches that adapt the mechanical properties of the formulation, the following paper demonstrates that modification of the printer feeding system enables the printing of very brittle filaments. The paper focuses on the production and printing of filament with 40 % drug load of the model compound ketoconazole and selected brittle polymers. The modified feeding system enabled the production of tablets, which were then characterized in terms of mass uniformity, dimension, drug content and dissolution. Moreover, the solid-state properties of the filaments and their effects on the mechanical properties as well as solid-state transitions upon reheating in the printer hotend were assessed.

The idea for this paper as well as the study design were developed by Nadine Gottschalk, Malte Bogdahn and Julian Quodbach. Nadine Gottschalk performed the experimental work, i.e., establishing the printer modifications, extrusion and printing of filaments and related analytics and the main evaluation of the results. The initial draft was written by Nadine Gottschalk. Malte Bogdahn, Julian Quodbach and Meike Harms supported in data evaluation and revised the manuscript draft.

Evaluation of authorship:

Author	Idea	Study Design	Experimental	Evaluation	Manuscript
Nadine Gottschalk	40	40	100	60	65
Malte Bogdahn	30	30	0	15	15
Meike Harms	0	0	0	10	5
Julian Quodbach	30	30	0	15	15

Evaluation of copyright permission: The author of the article retains the right to include it in a thesis or dissertation, provided it is not published commercially (accessed 10.05.2024).

Article available online at: <https://doi.org/10.1016/j.ijpharm.2021.120216>

© 2022 Elsevier B.V. All rights reserved.

Brittle polymers in Fused Deposition Modeling: An improved feeding approach to enable the printing of highly drug loaded filament

Nadine Gottschalk^{a b}, Malte Bogdahn^b, Meike Harms^b, Julian Quodbach^a

^aInstitute of Pharmaceutics and Biopharmaceutics, Heinrich Heine University, Düsseldorf, Germany

^bDepartment of Pharmaceutical Technologies, Merck KGaA, Darmstadt, Germany

International Journal of Pharmaceutics, Volume 597, 120216, 2021

DOI: 10.1016/j.ijpharm.2021.120216

Abstract

Brittleness is often described as a restricting material property for the processability of filaments via Fused Deposition Modeling. Especially filaments produced from approved pharmaceutical polymers often tend to fracture between feeding gears, the commonly employed feeding mechanism. In order to enhance their mechanical properties, usually extensive formulation development is performed. This study presents a different strategy to enable the printing of brittle filaments without the use of additional excipients by adapting the feeding mechanism to piston feeding. The polymers Soluplus®, Kollidon® VA64 and Eudragit® E PO were used, which have been reported to be brittle. Ketoconazole was used as model compound at 40% drug load and the influence on the mechanical properties was investigated using the three-point flexural test. In order to gain a better understanding of the mechanism affecting brittleness, filaments were analyzed in terms of crystallinity and miscibility of the components using polarized microscopy, differential scanning calorimetry and X-ray diffraction. Printing was performed with the aim to obtain immediate release tablets. The addition of Ketoconazole resulted in filaments even more brittle than placebo filaments. Nevertheless, the adaption of the feeding mechanism enabled the successful manufacturing of uniform tablets from all formulations.



Contents lists available at ScienceDirect

International Journal of Pharmaceutics

journal homepage: www.elsevier.com/locate/ijpharm

Brittle polymers in Fused Deposition Modeling: An improved feeding approach to enable the printing of highly drug loaded filament

Nadine Gottschalk^{a,b}, Malte Bogdahn^{b,*}, Meike Harms^b, Julian Quodbach^a

^a Institute of Pharmaceutics and Biopharmaceutics, Heinrich Heine University, Düsseldorf, Germany

^b Department of Pharmaceutical Technologies, Merck KGaA, Darmstadt, Germany

ARTICLE INFO

Keywords:

Fused deposition modeling
Immediate release
High drug load
Mechanical properties
Additive manufacturing
Feedability

ABSTRACT

Brittleness is often described as a restricting material property for the processability of filaments via Fused Deposition Modeling. Especially filaments produced from approved pharmaceutical polymers often tend to fracture between feeding gears, the commonly employed feeding mechanism. In order to enhance their mechanical properties, usually extensive formulation development is performed. This study presents a different strategy to enable the printing of brittle filaments without the use of additional excipients by adapting the feeding mechanism to piston feeding. The polymers Soluplus®, Kollidon® VA64 and Eudragit® E PO were used, which have been reported to be brittle. Ketoconazole was used as model compound at 40% drug load and the influence on the mechanical properties was investigated using the three-point flexural test. In order to gain a better understanding of the mechanism affecting brittleness, filaments were analyzed in terms of crystallinity and miscibility of the components using polarized microscopy, differential scanning calorimetry and X-ray diffraction. Printing was performed with the aim to obtain immediate release tablets. The addition of Ketoconazole resulted in filaments even more brittle than placebo filaments. Nevertheless, the adaption of the feeding mechanism enabled the successful manufacturing of uniform tablets from all formulations.

1. Introduction

Additive manufacturing (AM), or three-dimensional printing (3DP), is gaining interest in the pharmaceutical field as a technology to produce solid oral dosage forms. AM techniques allow fast and easy fabrication of an object based on a digital design, usually created using computer-aided-design (CAD) software. Especially Fused Deposition Modeling (FDM) is a known AM technique that offers particular advantages for the production of prototypes. Originating in the field of plastic industry, the idea of rapid prototyping has also been reported for the production of solid oral dosage forms in the recent years. FDM facilitates the fabrication of tablets of different size, design and porosity and thereby adjusting drug dosage and release kinetics (Araújo et al., 2019; Tool et al., 2020). Therefore, FDM shows high potential in addressing the need of flexible dosage on-demand, for example in early phase development, where dosages can be variable, as well as the increasing need of

individualized patient treatment nowadays (Alhnan et al., 2016).

The incorporation of an active pharmaceutical ingredient (API) is commonly performed by hot melt extrusion (HME), which further allows the formation of amorphous solid dispersions (ASD). Solubility and dissolution rate of poorly soluble drugs, which still make up a large proportion of novel pipeline compounds (Ting et al., 2018), can thus be improved (Mooter, 2012). Thermoplastic polymers and API(s) are extruded as filament, which is the wire-like feedstock material for the printer and usually wound onto spools. The filament is then pushed through a heat-controlled nozzle, where it softens, and the mass is deposited onto the build plate or the object that is being constructed. Commercially available printers use feeding gears to feed the filament. Consequently, certain mechanical properties are required of the feedstock material. To withstand the punctual force of the feeding gears, materials for FDM must exhibit toughness. If the material is too soft, compression causes extension of filament diameter and the filament gets

Abbreviations: FDM, Fused Deposition Modeling; AM, Additive manufacturing; API, Active pharmaceutical ingredient; 3DP, Three-dimensional printing; SLP, Soluplus®; VA64, Kollidon® VA64; EPO, Eudragit® E PO; KTZ, Ketoconazole; ABS, Acrylonitrile butadiene styrene; PLA, Polylactic acid; ACN, Acetonitrile; Tg, Glass transition temperature; CV, Coefficient of variation; UPLC, Ultra performance liquid chromatography; HME, Hot melt extrusion; DSC, Differential scanning calorimetry; PXRD, X-Ray powder diffraction; YM, Young's modulus; ASD, Amorphous solid dispersion.

* Corresponding author at: Frankfurter Str. 250, 64293 Darmstadt, Germany.

E-mail address: malte.bogdahn@merckgroup.com (M. Bogdahn).

<https://doi.org/10.1016/j.ijpharm.2021.120216>

Received 22 October 2020; Received in revised form 18 December 2020; Accepted 21 December 2020

Available online 22 January 2021

0378-5173/© 2021 Elsevier B.V. All rights reserved.

stuck in the extruder. The filament can also be deformed by the feeding gears, leading to discontinuous forward propulsion of the softened material through the nozzle. In case of brittle materials, the filament can exhibit brittle fracture through the transversal forces applied by the feeding gears. A tight fixation of the filament between the gears is necessary to allow continuous feeding. Due to the pointy gear teeth, which enhance grip, the force is concentrated on a small area, facilitating breakage. Brittle fracture occurs for materials with low absorption of energy when subjected to stress with no or little plastic deformation prior to failure. Breakage of the filament during feeding leads to disruption of the printing process. Furthermore, small splinters of API-containing material might be distributed in the printhead. Residue-free cleaning of the contaminated printhead and the feeding gears is essential for further manufacturing, since remaining splinters can again lead to blockages or even to cross-contamination in following productions. However, cleaning can be difficult and time consuming because it often involves a complete disassembly of the extruder (Nasereddin et al., 2018).

Materials commonly used for FDM, such as polylactic acid (PLA) or acrylonitrile butadiene styrene (ABS) show proper toughness. Yet, for the manufacturing of solid oral dosage forms only approved materials of pharmaceutical quality are allowed. For this reason, the production of filaments made from pharmaceutical polymers is often described in literature (Melocchi et al., 2016), but many lack the required mechanical properties. Several techniques have been employed to assess the suitability of filament formulations for the FDM process, but currently there is no standard test method to screen filaments regarding their suitability for the FDM process.

Most frequently, the three-point flexural bending test is employed to assess brittleness. Here, a quasi-static test setup is used to examine the impact of a transversal force onto a test specimen. Resulting stress-strain curves provide information about the mechanical properties of the material. For example, strain at break or breaking distance can be used to compare the brittleness of different formulations (Verstraete et al., 2018; Zhang et al., 2017). However, results are highly dependent on the chosen test settings and dimensions of the test specimen.

In addition to this, several methods are used to determine the Young's modulus (YM). The YM indicates the stiffness of a material, which is also an important property for filaments, which have to be conducted through the printer without deformation. It has been stated that filaments with YM below 300 N/mm² are too flexible for printing via FDM (Korte and Quodbach, 2018). The YM can be measured in different modes that differ in the direction in which the force acts on the specimen (tensile, flexural or torsion). Next to quasi-static test setups, dynamic mechanical analysis (DMA) is also possible (Fuenmayor et al., 2018).

Recently, a promising screening tool has been published by Nasereddin et al. (2018), where a longitudinal force was applied to pieces of filament and flexibility profiles were compared to materials commonly used for FDM. Xu et al. (2020) compared several test methods, identifying the property "toughness" to be predictable for the feedability of filaments. Even software tools have been developed for the prediction of e.g. the mechanical properties of a formulation (Elbadawi et al., 2020b). Nevertheless, these predictions may not apply to every FDM printer because the forces applied on the filament can vary by the design of the feeding mechanism of different printers.

Pharmaceutical polymers that are suitable for HME are often very brittle and a common approach to overcome brittleness and reach mechanical resilience is the addition of plasticizers (Zhang et al., 2017) or the use of polymer blends (Alhijaj et al., 2016; Ilyés et al., 2019). Additional excipients increase the complexity of the formulation and the miscibility of polymer and polymer or polymer and plasticizer has to be considered. Plasticizers can further reduce the glass transition temperature (T_g) and enable the reduction of process temperatures, but they can also negatively affect drug absorption (Khizer et al., 2019). In case of ASDs, where the amorphous API is embedded and kinetically stabilized

in a polymer matrix, they are described to decrease the physical stability by increasing molecular mobility (Fung and Suryanarayanan, 2017). Moreover, when high doses of API or even drug combinations in form of a poly pill must be administered, the possibilities to improve mechanical properties by adding excipients are restricted, especially for ASDs, since addition may lead to a reduction of drug load as the highest achievable drug load is limited by the drug solubility in the polymer (Shah et al., 2014). The drug load of the formulation defines the amount of material that must be printed to obtain a specified dose. The resulting size and volume of the tablet must be easy to swallow to ensure patient compliance. When additional improvement of release kinetics is needed, which is usually done by altering shape (Goyanes et al., 2015) to increase surface or reduction of infill to create a porous structure inside the tablet (Goyanes et al., 2014), the volume of the tablet increases to maintain the dose. In consequence, it is crucial for the application of high dose drugs that the drug load of the filament is high, too. However, only few publications on FDM report high drug loads > 30% (Pietrzak et al., 2015; Samaro et al., 2020; Verstraete et al., 2018).

The aim of this study was to show that the extrusion and printing of brittle filaments and polymers with high drug loads without the use of plasticizers or additional polymers into amorphous immediate release dosage forms is feasible by modifying the feeding mechanism. Experiments were performed using a commercial printer from the consumer sector, similar to the majority of other studies on this topic. This is due to the fact that no pharmaceutical FDM-printers were available for a long time. Only recently, the M3dimaker™ was published by FabRX in the beginning of 2020.

The polymers Soluplus® (SLP) (Alhijaj et al., 2016; Nasereddin et al., 2018; Samaro et al., 2020), Kollidon® VA64 (VA64) (Fuenmayor et al., 2018; Nasereddin et al., 2018; Solanki et al., 2018) and Eudragit® E PO (EPO) (Alhijaj et al., 2016; Nasereddin et al., 2018) have been chosen in this study, since they are described in literature to be not feedable and thus not printable. As model compound Ketoconazole (KTZ) was used. KTZ is a poorly soluble (22.2 µg/mL in Fasted State Simulated Intestinal Fluid (Auch et al., 2018)), BCS class II and high dose (100–200 mg oral dose) antifungal agent.

2. Materials and methods

2.1. Materials

KTZ was purchased from LGM Pharma (Erlanger, USA). VA64 (Vinylpyrrolidone-vinyl acetate copolymer) and SLP (Polyvinyl caprolactam-polyvinyl acetate-polyethylene glycol graft copolymer) were purchased from BASF (Ludwigshafen, Germany). EPO (Poly[(dimethylaminoethyl methacrylate)-co-(methyl methacrylate)-co-(butyl methacrylate)]) and colloidal silicon dioxide were purchased from Evonik (Darmstadt, Germany). PLA (diameter: 1.75 mm) was purchased from Prusa Research s.r.o. (Prague, Czech Republic).

2.2. Methods

2.2.1. HME of filament sticks

Extrusion of the filament was performed using a twin-screw extruder (Pharma 11, ThermoFisher Scientific, Waltham, USA). Blend

Table 1
Formulations for HME (wt%).

Formulation	KTZ	VA64	SLP	EPO	Silicon dioxide
VA64-P	–	100	–	–	0
VA64-K	40	60	–	–	0
SLP-P	–	–	100	–	0
SLP-K	40	–	59	–	1
EPO-P	–	–	–	99	1
EPO-K	40	–	–	59	1

compositions and extrusion parameters are displayed in [Table 1](#) and [Table 2](#). Placebo (P) and KTZ (K) containing formulations were named based on the polymer used.

All components were blended using a turbula mixer for 15 min (T2A, Willy A. Bachofen Maschinenfabrik, Muttenz, Switzerland). Formulations SLP-K, EPO-P, EPO-K showed poor flow in the feeder and hence colloidal silicon dioxide was added to enable a uniform flow into the extruder. Blends containing colloidal silicon dioxide were sieved using a mesh size of 1 mm and blended for additional 15 min. The impact of silicon dioxide on brittleness of the filaments and other experiments is estimated to be low due to the low amount.

A conveyor belt (Brabender GmbH, Duisburg, Germany) was used to obtain straight filaments and modify the diameter by adjusting the conveyor belt speed ([Fig. 1](#)). Inline measurements of filament diameter were conducted after the conveyor belt using a laser measurement system (Odac 33 Trio, Zumbach, Orpund, Switzerland). Since the chosen material has been reported to be brittle and showed breakage, the filament was not wound on a spool but cut into filament sticks of approximately 30 cm length using diagonal pliers. Filament sticks with diameter exceeding $1.75 \text{ mm} \pm 0.1 \text{ mm}$ were discarded and not used for further experiments.

In case of VA64-K inline measurements were not possible due to breakage. Therefore, all filament sticks were collected during extrusion and measurement of filament diameter and sorting was performed subsequently by inserting sticks manually into the laser measurement system.

2.2.2. Printing of tablets

An Ultimaker 3 (firmware version: 4.0.1.20171023, Ultimaker, Geldermalsen, Netherlands), was used for printing. This printer uses a bowden extruder ([Fig. 2](#)), where the feeding gears are attached to the back of the printer and the filament is fed through a flexible bowden tube into the hotend. The printer is designed for filaments with a diameter of 2.85 mm, but was modified to work with a filament diameter of 1.75 mm. A smaller filament diameter was chosen to reduce thermal impact on the API due to shorter residence times in the hotend. Therefore, the originally used bowden tube was replaced with a tube with an inner diameter of 2 mm, which was fixed at the connection points with bushings.

To enable printing of brittle filament sticks, piston feeding was implemented by several modifications of the printer ([Fig. 2](#), [Supplementary Material Fig. S1](#)). Flexible PLA filament (feeding filament), which is moved by the feeding gears at the back of the printer through

the bowden tube, was used as piston to push the brittle filament stick through the hotend. In order to prevent bending of the brittle filament sticks during movement of the printhead, which may also cause breakage, a rigid guide, printed from PLA, was mounted on the print head ([Supplementary material Fig. S2](#)). Filament sticks were loaded into the guide through a reclosable opening in the bowden tube above the guide. The feeding filament was moved by the feeding gears through the bowden tube until it touched the filament stick in the guide. Further movement of the feeding filament pushed the filament stick through the heated nozzle. Cutting edges of both, feeding filament and filament stick, were planar to ensure good force transfer.

Tablets were designed in Fusion 360 (Autodesk, Farnborough, United Kingdom) and saved in a binary stereolithography file format (.stl) with high resolution. They were of cylindrical shape with a diameter of 10 mm and a height of 2.4 mm. Simplify3D (version 4.0.1., Simplify3D, Cincinnati, USA) was used for slicing and export of G-code. An infill density of 100% was chosen to obtain tablets with a dose of approximately 100 mg. The nozzle temperature was adapted individually for each material and was selected on the basis of visual assessment of the melt leaving the nozzle while pushing filament through until a continuous flow of glassy material was achieved. The behavior of the printing formulation at different settings was compared to PLA at 210 °C and the parameter set resulting in the most similar behavior was selected. The nozzle diameter was 0.4 mm. All prints were carried out at a speed of 30 mm/s, except for EPO-K, where a speed reduction showed improved amorphization of the API. First layer speed was reduced by 30%. Leveling of the build plate was performed prior to printing. EPO formulations and VA64-K showed strong adhesion to the glass build plate, which is why electrical insulation tape was used as printing surface to facilitate detachment. Printing parameters are displayed in [Table 3](#). For each formulation 20 tablets were printed.

For microscopical analysis, printing was performed on microscope slides. A single layer object consisting of 16 connected lines was designed ([Supplementary Fig. S3](#)). The length of each line was 70 mm, spacing between the lines was 1 mm. Object height and line width were chosen according to the set printing parameters. The speed of the initial layer was not reduced in this case. Prints were assessed after printing via microscopy.

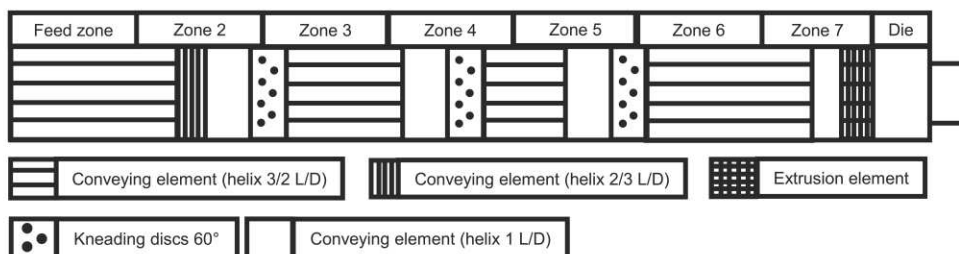
2.2.3. Tablet characterization

Mass of tablets was determined using an analytical balance (ME235S-OCE, Sartorius, Goettingen, Germany) and dimensions were measured using a digital caliper (TWIN-Cal IP67, TESA Technology,

Table 2
Extrusion parameters and screw configuration.

Formulation	Screw speed (rpm)	Feed rate (kg/h)	Zone 1 (°C)	Zone 2 (°C)	Zone 3 (°C)	Zone 4 (°C)	Zone 5 (°C)	Zone 6 (°C)	Zone 7 (°C)	Die (°C)	(mm)
VA64-P	200	0.2	80	180	180	180	180	180	180	180	2.0
VA64-K	150	0.2	80	160	160	160	160	160	160	160	2.0
SLP-P	250	0.3	80	180	180	180	180	180	180	180	2.0
SLP-K	250	0.3	80	160	160	160	160	160	160	145	2.0
EPO-P	250	0.3	75	100	140	140	140	140	140	130	2.0
EPO-K	300	0.3	90	140	160	160	160	160	140	130	2.0

Screw configuration:



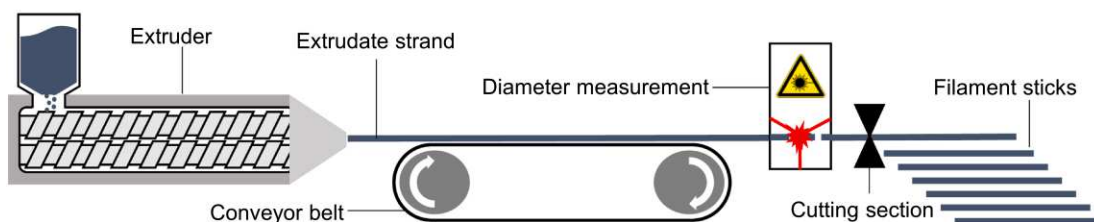


Fig. 1. Schematic illustration of filament stick production consisting of the extruder, conveyor belt, laser measurement device and cutting section.

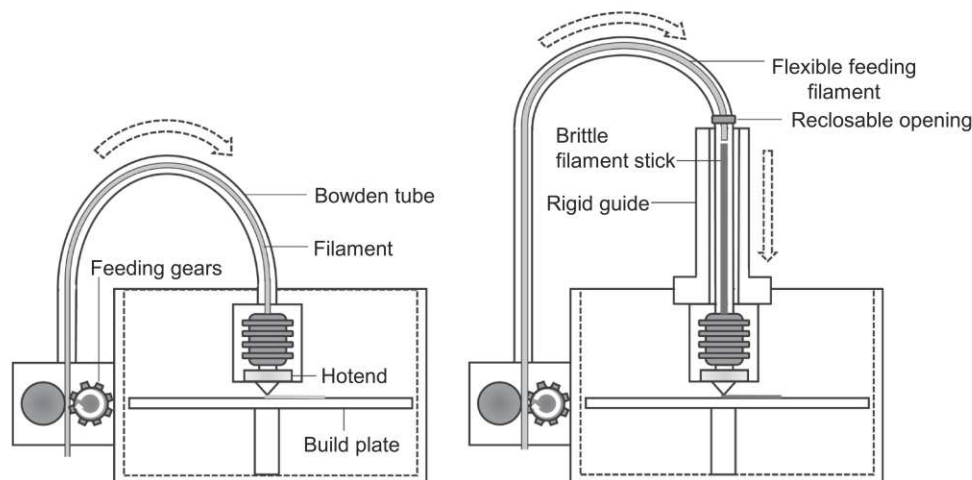


Fig. 2. Schematic illustration of FDM printer with original feeding system (left) and modification of feeding system to piston feeding (right).

Table 3

Parameters for the printing of tablets for each formulation.

	Line width (mm)	Layer height (mm)	Infill density (%)	Nozzle temperature (°C)	Build plate temperature (°C)	Printing speed (mm/s)	Printing time from G-code (min)
VA64-P	0.4	0.2	100	190	70	30	1:51
VA64-K	0.4	0.2	100	140	40*	30	1:51
SLP-P	0.4	0.2	100	190	40	30	1:51
SLP-K	0.4	0.2	100	140	50	30	1:51
EPO-P	0.4	0.2	100	170	20*	30	1:51
EPO-K	0.4	0.2	100	160	20*	10	6:38

* Electrical insulation tape was used to decrease adhesion of tablets to build plate.

Renens, Switzerland). Mean and standard deviation were calculated in all cases ($n = 20$).

2.2.4. Differential scanning calorimetry (DSC)

Pure substances, filaments and tablets were analyzed using a DSC 1 (Mettler Toledo, Gießen, Germany). Mortar and pestle were used to grind extrudates and printed tablets. Approximately 7–8 mg of sample were hermetically sealed in 100 μ L aluminum pans. Lids were pierced by the DSC piercing unit prior to analysis. An empty DSC pan was pierced and used as reference. Samples were heated to 110 °C at a rate of 20 °C/min and were kept at 110 °C for 1 min to evaporate water. Afterwards, samples were cooled down to 0 °C at 10 °C/min and heated up twice to 180 °C at a rate of 10 °C/min. In case of the EPO formulations the tempering step at 110 °C was omitted because hot-stage microscopy indicated recrystallization at this temperature. Tests were performed in triplicate.

2.2.5. X-Ray powder diffraction (PXRD)

PXRD measurements were performed to determine the crystalline state of blends, filaments and tablets using a D2 Phaser equipped with a SSD160 detector in 1D mode with a full opening of 4.875° (Bruker, Billerica, USA). A copper anode was used for X-ray generation at 30 kV and 10 mA. Nickel foil was used to reduce K β radiation. The scanning range was from 6 to 41° 2theta with a step size of 0.02° and a measurement time of 1 s per step. Approximately 70–100 mg of sample were prepared on a zero background holder and rotated with 5 rpm. The limit of detection for KTZ was determined by preparing blends using mortar and pestle with the corresponding polymer at different drug loads (1%, 2.5%, 5% and 10%). Tests were performed in triplicate.

2.2.6. Polarized light and hot-stage microscopy

Filaments and prints on microscope slides were examined using light microscopy (IX73P1F, Olympus, Tokyo, Japan) at 5x magnification. Samples were assessed visually in standard light to check for irregularities such as bubbles, which may affect breaking tendencies. In addition,

polarized light was applied to analyze the filaments qualitatively in terms of remaining traces of crystallinity. Therefore, filaments containing KTZ were compared to placebo filaments. Images were recorded using Olympus cellSens Standard software (version: 1.18). Hot-stage microscopy was performed for the EPO-K formulation to assess the influence of reheating to the sample using a LTS350 stage (Linkam, Waterfield, United Kingdom) at a heating rate of 10 °C/min to a maximum of 180 °C. The sample was analyzed under polarized light using a BX60 microscope (Olympus, Tokyo, Japan). Images were taken every 6 s and then processed using the Olympus Stream Essentials software (version 2.3.3.).

2.2.7. Mechanical testing

Mechanical properties were tested on a Texture Analyzer TA-XT (Stable Micro Systems, Godalming, United Kingdom) using a 3-point bending rig. Filament sticks were cut into 70 mm pieces and placed on supports with a gap of 30 mm. For calculation of stress–strain curves, diameters of each test sample were measured prior to analysis using the laser measurement system. The pretest speed was set to 5 mm/s and reduced upon a trigger force of 0.049 N to the test speed. Tests were performed at 1.0 mm/s and at 0.1 mm/s for better differentiation of strain at break values between the formulations. Nine replicate tests were performed for each formulation and each test speed. Data were acquired using Exponent software (version 6.1.16.0). Stress and strain were calculated according to Prasad et al. (2019).

2.2.8. Drug content of tablets and dissolution profile

Determination of drug content was performed for filaments (n = 3) and tablets (n = 6). Samples were chosen randomly, weighed (200–250 mg) and dissolved in a 1:1 mixture of acetonitrile (ACN) and water and further diluted to a concentration of 0.2 mg/mL (assuming 40% drug load).

Determination of in vitro drug release from printed tablets was carried out on a Sotax Smart AT7 Dissolution Tester (Sotax, Aesch, Switzerland) using the paddle method (USP II). Tablets (n = 6) were placed in 900 mL of 0.1 N hydrochloric acid (HCl) at a temperature of 37 °C and paddle rotation speed of 100 rpm. Samples (sampling volume = 3 mL) were drawn at various time points (5, 10, 15 and 30 min and 1, 1.5, 2, 4, 8, 12 and 24 h) and diluted with equal volumes of ACN. Chromatographic analysis of filaments, tablets and dissolution samples was done by an ultra performance liquid chromatography system (UPLC, Acquity H Class Plus, Waters, Massachusetts, USA) at a wavelength of 255 nm using an ACQUITY UPLC® CSH™ Phenyl-Hexyl column (1.7 µm 2.1x50 mm) constantly heated up to 60 °C. The eluents used were ammonium formate buffer (pH 4) and ACN, which were pumped at a flow rate of 1 mL/min through the system at ratios of 95:5 to 5:95 to 95:5 within 6 min.

3. Results and discussion

3.1. Extrusion

Neat polymer and blends were extruded in order to obtain filament sticks with an adequate filament diameter for FDM as well as amorphous filaments. It was necessary to adapt processing conditions for each formulation. Therefore, extrusion temperatures of at least 160 °C were chosen for the extrusion of formulations containing KTZ, which is above the melting temperature of KTZ (T_m (KTZ) = 151 °C (Kanaujia et al., 2011)), to obtain amorphous material. The temperature was maintained for the extrusion of the EPO-K formulation, even though the melt viscosity at the die was already low and production of filament sticks was difficult. A macroscopic decrease in melt viscosity for formulations containing KTZ was also observed for SLP and VA64 and the extrusion temperature was lowered compared to the placebo formulation. The extrusion temperatures were in all cases below the degradation temperatures of excipients and API.

The screw speeds were increased after the extrusion of VA64-K, since small crystalline agglomerations were observed occasionally. A higher screw speed increases the specific mechanical energy input (SME), leading to a better amorphization due to enhanced dispersion and dissolution of the API in the polymer matrix (Lang et al., 2014). In case of EPO-K, the screw speed was increased even further because it was observed that the opacity decreased. The throughput was adapted correspondingly to increase the specific feed load of the barrel, which facilitates the production of filaments with a uniform filament diameter (Ponsar et al., 2020).

The screw configuration was maintained for all formulations. Three kneading elements were distributed in even intervals along the screws to ensure proper distribution of KTZ in the polymer matrix.

Extrusion resulted in transparent and colorless filaments for all formulations except for EPO-K, which was slightly opaque, indicating phase separation.

3.2. Crystallinity assessment

Crystallinity analysis was performed using DSC, PXRD and polarized microscopy to evaluate whether KTZ was fully amorphous in the polymer matrix, since a crystalline state may affect the mechanical properties. Besides, amorphization of crystalline API may be even more difficult to reach in the hotend of the printer, where the residence time is short, and no mixing elements are present. Prior to extrusion, blends were analyzed using DSC to investigate polymer-API miscibility. In a binary system, a single T_g serves as indicator of a miscible system (Alhijaj et al., 2016). A single T_g was observed for the blends VA64-K and SLP-K during the second heating cycle and for filaments and tablets during the first heating cycle (Supplementary material Fig. S4), indicating full miscibility of 40% KTZ in the polymeric matrix, whereas the EPO-K blend showed two glass transition temperatures in the second heating cycle (Supplementary material Fig. S5), indicating a two-phase system, which was also observed for EPO-K filaments and tablets in the first heating cycle. However, amorphization of KTZ was possible for all formulations using DSC. In addition, a reduction of glass transition was observed for all formulations containing KTZ compared to placebo, which can be attributed to a plasticizing effect of KTZ (Table 4).

Microscopy was further used to identify irregularities in the filament matrix and polarized light was applied to assess whether crystals were present. A small number of birefringent spots was observed in placebo filament formulations (Fig. 3), which could be attributed to polymer particles or fibers based on their size and shape.

VA64-K filaments showed no endothermic events in DSC (Fig. 4) and no crystalline peaks in PXRD. Under polarized light, filaments proved to be mainly amorphous, but occasionally crystal agglomerations were observed that were not present in the placebo filament. The limit of detection for crystalline KTZ in a blend with VA64 was determined by spiking experiments and turned out to be 2.0% for DSC and 5% for PXRD. Possible explanations for small traces of crystallinity may be insufficient blending prior to extrusion or poor mixing inside the barrel due to low screw speeds. However, 40% of drug are a high amount when aiming for fully amorphous samples, making it a difficult and highly sensitive formulation. Printed tablets seemed to be amorphous

Table 4

Glass transition temperatures of placebo formulations and formulations with 40% drug load from filaments. Arithmetic means \pm SD (n = 3).

	T_g (°C)			
	VA64	SLP	EPO	KTZ
Neat	110.95 \pm	78.92 \pm	51.62 \pm 1.39	47.70 \pm
component	0.08	1.21		0.42 °C
KTZ (40% w/w)	74.54 \pm	51.56 (*)	33.04 \pm 1.07,	n/a
	0.72		46.59 \pm 0.16	

* n = 1 due to strong drift in baseline.

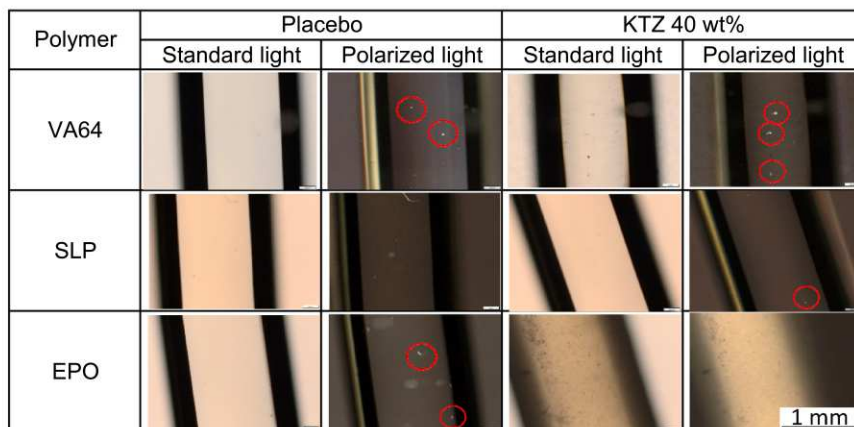


Fig. 3. Images of filament sticks from polymers VA64, SLP and EPO as placebo filaments and containing KTZ (40% w/w) in standard light and polarized light at 5x magnification. Birefringent spots are marked with circles with the exception of EPO-K, which was highly opaque.

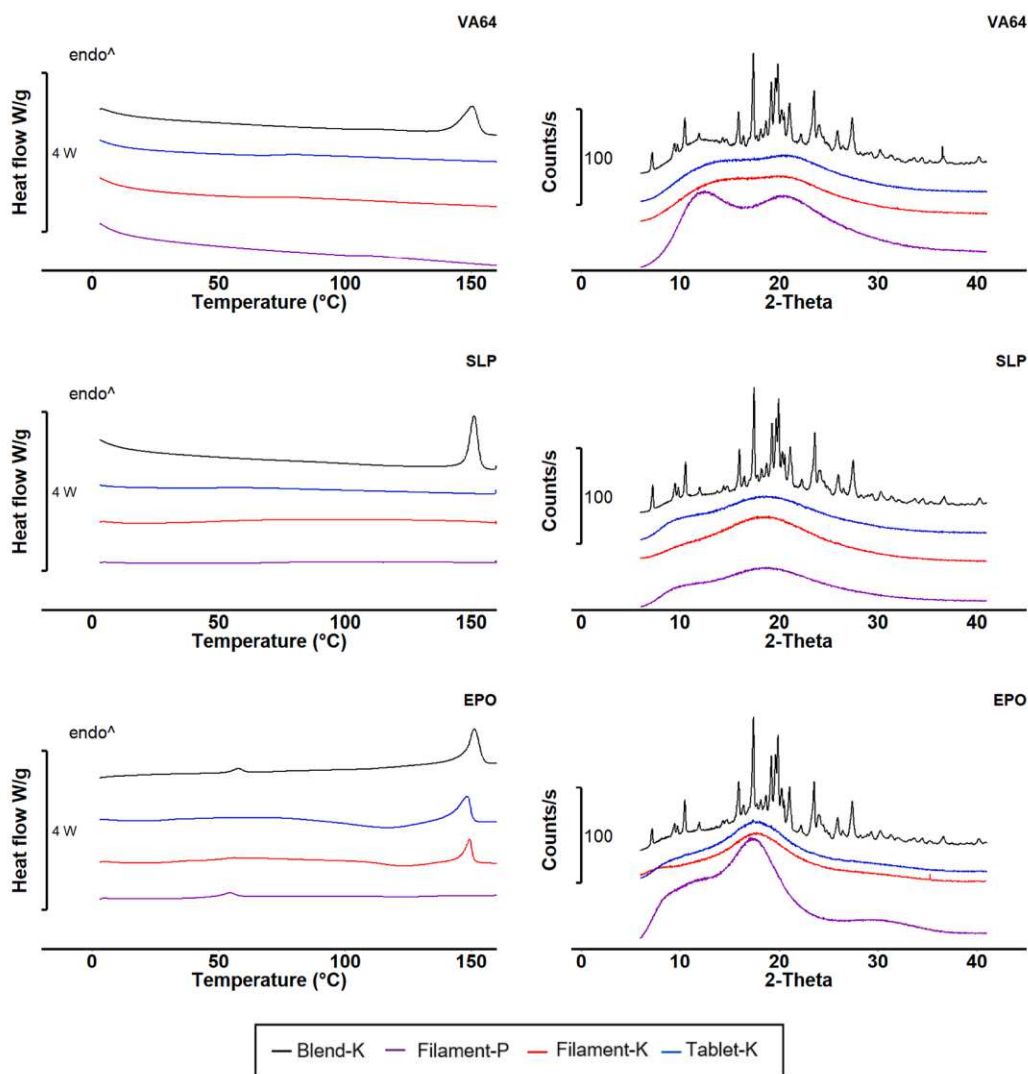


Fig. 4. DSC thermograms (left) of first heating cycle and PXRD graphs (right) of formulations with polymers VA64, SLP and EPO.

according to DSC and PXRD, too. Since polarized light microscopy has shown that the limit of detection of the aforementioned technique was too low to detect small traces of crystallinity, filaments were printed directly on microscope slides using equal printing parameters. A volume of 400 mm³ was printed over the whole slide, resembling two tablets. No traces of crystallinity were observed over the whole print (Supplementary material Fig. S6), from which can be concluded that the tablets were probably amorphous.

SLP-K filaments and tablets showed no melting peaks in DSC and no crystalline peaks in PXRD. Polarized microscopy confirmed that the filaments were fully amorphous.

The EPO-K filaments were opaque in contrast to the other formulations including EPO-P filaments. This is a hint at a multiphase system. From this macroscopic observation it cannot be concluded on the crystallinity of the phases. Polarized light microscopy showed an irregular surface and a very bright strand. However typical birefringence effects hinting at crystalline particles were not observed. This is in contradiction to the DSC measurements showing a distinct endothermic signal at 148 °C, which can be attributed to the melting point of KTZ. However, this melting peak was preceded by a very broad exothermic event from 90 °C to 140 °C, which might be caused by recrystallization during the heating process. Therefore, further experiments were performed. Hot-stage microscopy proved the suspected recrystallization at approximately 90 °C. The phenomenon of recrystallization upon reheating was described by Baird et al. (2010), who established a classification system

for compounds depending on their glass forming ability. KTZ is actually strong glass former (class III) which remains amorphous upon cooling and reheating. In contrast to the first observation, the apparent fully amorphous sample on the microscope slide was reheated, showing no such recrystallization. This hints at small nuclei being present in the filaments, which have been reported to cause crystal growth upon reheating (Trasi and Taylor, 2012), triggering the recrystallization of KTZ. The recrystallization potential triggered by reheating makes EPO-K a challenging but interesting formulation for the FDM process. PXRD showed no peaks, indicating a crystalline fraction in case of the formulation of EPO-K below the limit of detection of 2.5%.

Printing pretests were performed on microscope slides to investigate the influence of nozzle temperature and printing speed on the recrystallization behavior with the aim to print amorphous tablets (Fig. 5). A high density of crystals was observed for all prints at the beginning of the print, even at temperatures above the melting point of KTZ, lessening gradually. The Ultimaker 3 starts to print directly after the heating element has reached the set temperature, but it is likely that the set temperature was yet not reached inside the hotend and the filament, causing this phenomenon. The amount of crystalline material appeared to be higher than in the filaments, especially when considering the smaller height of the printed strand (0.2 mm) compared to the filament diameter (1.75 mm), where multiple layers overlap, indicating that recrystallization occurred also during printing. Naturally, printing at nozzle temperatures above the melting point as well as reducing printing

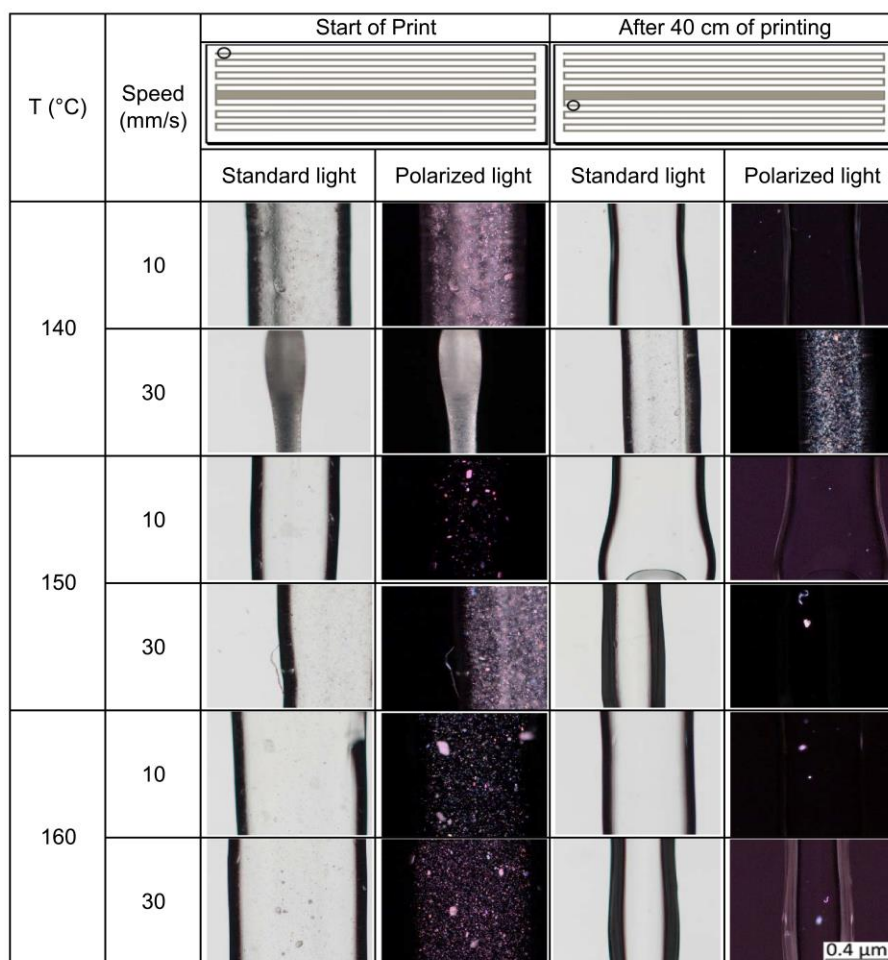


Fig. 5. Pretest printing of EPO-K on microscope slides at 5x magnification.

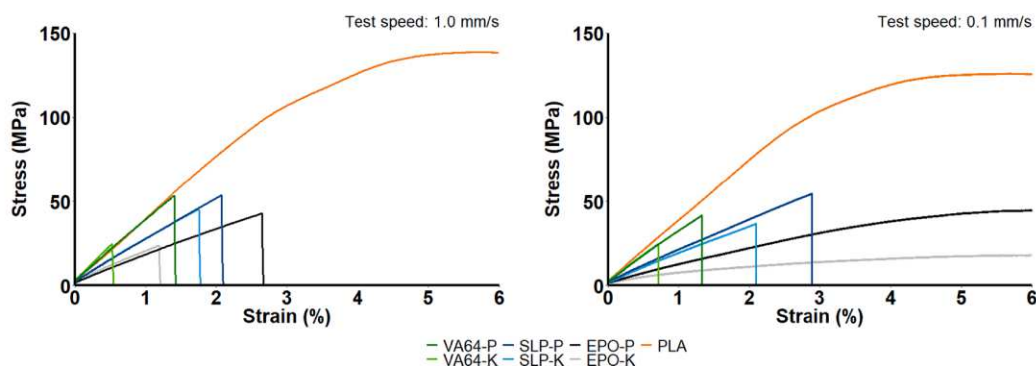


Fig. 6. Stress–strain graphs from 3-point bending test of filament formulations at 1.0 mm/s (left) and 0.1 mm/s (right) test speed.

speed, which increases residence time of the filament inside the hotend, resulted in a visible lower fraction of crystalline API. Best results in terms of amorphism were obtained using 160 °C and a printing speed of 10 mm/s. However, tablets printed at these parameters also showed recrystallization in DSC, indicating that traces of crystallinity were still present.

3.3. Mechanical properties of filaments

The mechanical toughness of the filaments was tested by placing filament sticks carefully between the original feeding gears of the Ultimaker 3. The pressure of the gears is adapted by a spring and was set to the lowest tension possible. All filament formulations broke upon manual movement of the feeding gears (Supplementary material Fig. S7), demonstrating lacking feedability using the conventional feeding mechanism. Mechanical properties were further analyzed using a three-point flexural bending test, since differences in brittleness were noticed during handling of the different filament formulations. Two different test speeds were compared.

At a test speed of 1.0 mm/s, all formulations showed brittle fracture (Fig. 6) with a defined linear increase of stress without plastic deformation prior to breakage, whereas PLA filament, which is commonly used for FDM, showed elastic behavior up to approximately 2.5% strain followed by plastic deformation. PLA did not break under these test conditions. The strain at break for the different placebo polymers was $EPO > SLP > VA64$ (Fig. 7). In addition, KTZ seemed to further decrease strain at break. In case of EPO-K, a strong reduction was observed compared to EPO-P, which is likely due to phase separation and the presence of crystals in the polymer matrix, leading to microcracks in the material facilitating breakage. Remarkably, filaments containing amorphous KTZ also showed a decrease in strain at break. DSC experiments of the filaments had shown a single T_g , indicating that no phase separation had occurred, which may affect the mechanical properties. VA64-K showed a significant ($p < 0.05$) reduction of strain at break compared to VA64-P. SLP-K also exhibited breakage at lower strain values, but mean values for SLP-P and SLP-K differed only slightly. In order to increase sensitivity of the test, the test speed was reduced from 1.0 mm/s to 0.1 mm/s. Both, VA64-K and SLP-K showed a significant ($p < 0.05$) reduction of strain at break compared to placebo, with VA64-K being the most brittle among the tested formulations, indicating that amorphous KTZ or crystalline concentrations below the lowest detection limit (2.0%) also led to an embrittlement of the filament. A possible explanation of this phenomenon may be that the high drug load of 40% leaves only few interaction points of the polymer and thereby reduces the toughness of the material.

Interestingly, EPO formulations exhibited plastic deformation under these test conditions similar to PLA, but the plateau was reached at lower stresses. This shows nicely how mechanical behavior can vary

depending on the test parameters. A variety of test conditions have been reported for the assessment of mechanical properties of filaments to predict their suitability for FDM. Hence, comparison of results should only be conducted with caution. In addition, feedability depends on the specific printer and a predictive method must be developed individually.

3.4. Printing

Printing of the brittle filament sticks using the modified setup was feasible, since only longitudinal forces were applied to the filaments and bending was prevented by the guide. All printing parameters were kept equal except for nozzle temperature. Melocchi (2016) has already described that, compared to HME, higher temperatures are needed for printing, which was true for placebo formulations in this experiment. Remarkably, formulations containing 40% KTZ were printable at temperatures approximately 20 °C lower than the extrusion temperature. This may be caused by a reduction of melt viscosity, which was already observed macroscopically during HME. A reduction of nozzle temperatures due to the addition of API was also described by Elbadawi et al. (2020a, 2020b). However, printing of EPO-K was performed at higher temperatures and at lower printing speed to increase residence time in the hotend to aim for fully amorphous tablets.

Printing resulted in tablets of uniform dimensions (Fig. 8). Small deviations of height (up to 0.26 mm) from the original design of the tablet and a higher coefficient of variation (CV) (Table 5) were observed for EPO-K and VA64 formulations. The upper tablet surface for these formulations was slightly uneven, most likely caused by the hot nozzle during printing. High temperatures might have led also to an increased mass flow through the nozzle, probably caused by decreased melt viscosity, resulting in the height being larger than stated in the G-code. In the following layer the same volume is extruded, but the distance between nozzle and object is smaller than the set layer height, resulting in a displacement of the low viscous material to the sides, which can be observed in the last layer. In this study nozzle temperatures were set by visual assessment of the melt. Further investigations have to be done to find optimal printing parameters for individual formulations. Tablets printed from formulations SLP-K, EPO-P and EPO-K were mainly transparent, even though EPO-K filaments were opaque, whereas tablets printed from the other formulations were opaque, which can be attributed to the presence of bubbles in the matrix, which were observed macroscopically.

The tablets showed a low variability in mass ($CV \leq 4$, Table 5), indicating that transfer of force from feeding filament to printing filament resulted in a continuous mass flow. Tablet masses between the different formulations differed from 212.1 mg to 251.6 mg. Densities of milled extrudates were determined using a gas pycnometer, which showed differences between the formulations (data not shown), but these could not explain mass variations. A possible explanation may be

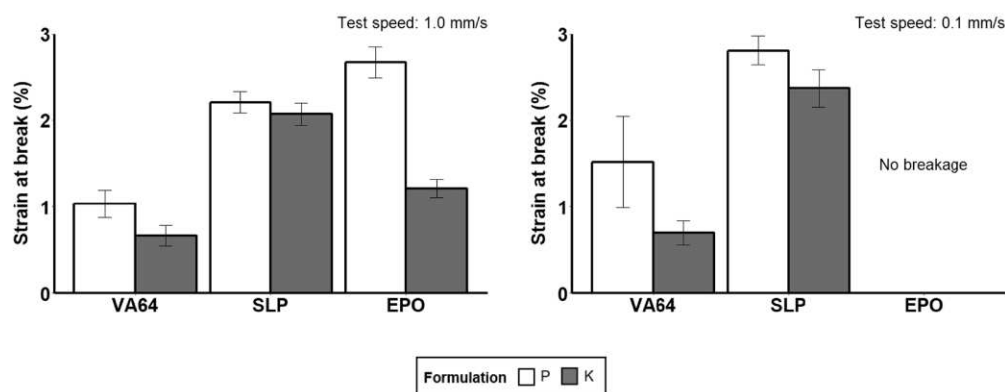


Fig. 7. Strain at break (\pm SD, $n = 10$) from 3-point bending test at 1.0 mm/s (left) and 0.1 mm/s (right) test speed for polymers VA64, SLP and EPO. Comparison of placebo filaments and filaments containing KTZ.

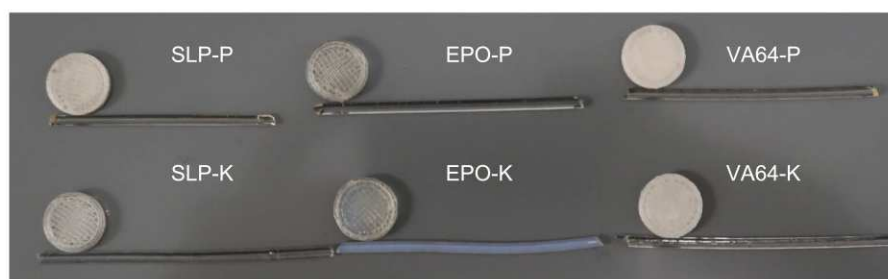


Fig. 8. Printed tablets and corresponding filaments.

Table 5

Mass and dimension of tablets. Arithmetic means \pm CV ($n = 20$).

	Mass (mg)	Height (mm)	Diameter (mm)
VA64-P	229.8 \pm 3.4	2.57 \pm 1.98	10.58 \pm 0.83
VA64-K	251.6 \pm 2.9	2.66 \pm 2.81	10.50 \pm 0.71
SLP-P	212.1 \pm 4.0	2.40 \pm 1.50	10.43 \pm 0.35
SLP-K	228.3 \pm 3.2	2.41 \pm 1.01	10.12 \pm 0.64
EPO-P	213.6 \pm 2.0	2.38 \pm 1.01	10.36 \pm 0.54
EPO-K	225.2 \pm 3.9	2.53 \pm 1.96	10.32 \pm 0.81

differences in melt viscosity due to different nozzle temperatures, causing resistance and slippage of the feeding filament between the feeding gears.

3.5. Content and in vitro release

Content uniformity of filaments is an important criterion to ensure correct dosing. Fluctuations of content can result in over- or underdosing and the aim should be to keep these as low as possible. Filament and tablet content for VA64-K and SLP-K was approximately 4% lower than the theoretical drug load of 40% (Table 6). This is possibly due to inhomogeneities in the powder blend or demixing during extrusion, since particle sizes of API and both polymers differed (average size of KTZ 1.2 μ m vs. VA64 79.8 μ m and SLP 253.7 μ m), which was determined using

Table 6

Mean content \pm SD of filaments ($n = 3$) and tablets ($n = 6$).

	Filament content (%)	Tablet content (%)
VA64-K	37.4 \pm 0.3	36.6 \pm 0.2
SLP-K	36.3 \pm 1.4	36.2 \pm 0.6
EPO-K	41.3 \pm 2.0	42.2 \pm 2.3

light microscopy of the raw materials. Further investigations need to be performed on blend composition and processing. No or little reduction of content between filaments and tablets was observed. The tablet content of VA64-K was slightly lowered compared to the filament, but no degradation products were observed in the chromatograms, indicating no degradation of KTZ had occurred during printing.

Considering that tablets had been printed with 100% infill, all formulations showed a fast release (Fig. 9). It is likely that the high content of KTZ strongly influenced the dissolution rate. The dissolution rate differed slightly between the polymers. For EPO-K and VA64-K 80% release was reached after approximately 25 min, whereas release from SLP-K printed tablets was slightly slower (80% release after

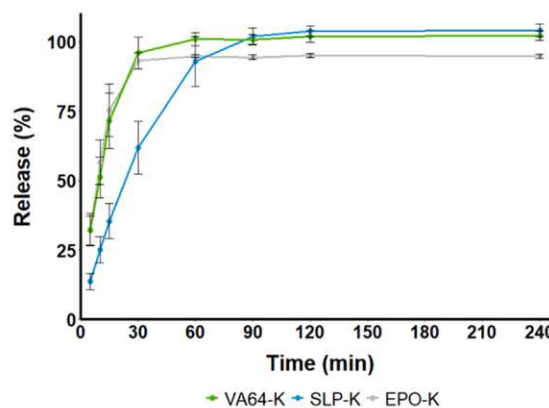


Fig. 9. Mean release (\pm SD, $n = 6$) of tablets in 0.1 N HCl based on the mean KTZ content of tablets. Release > 240 min is not displayed.

approximately 45 min). Dissolution enhancement could likely be improved in this case by reducing infill without excessive enlargement of the tablet volume while maintaining an equivalent dose, since a high drug load was chosen.

4. Conclusion

The feedability of filaments is a prerequisite for printing via the AM technique FDM and is strongly dependent on the mechanical properties of the respective material. Due to a limited number of approved materials, a common strategy to enhance mechanical properties is extensive formulation development either by addition of plasticizers or the use of polymer blends. This study presents a novel approach for brittle filaments that were not feedable with existing feeding systems and, thus, not printable. We demonstrated that printing of these filaments was feasible by adapting the feeding mechanism of the printer from feeding gears to piston feeding. Printing resulted in reproducible tablets of uniform mass and dimensions. It was further shown that a high drug load (40%) of the model compound KTZ led to an embrittlement of all filament formulations, even if the material was an amorphous one-phase system. This underlines the importance of the printer being able to process materials with a wide range of mechanical properties, since a high drug load can be essential for high dose compounds to acquire the specified dosage at an adequate tablet size. Tablets showed fast release at 100% infill, still holding the potential of reducing the release time further by reducing infill density. Besides, the study showed that a high drug load can also be challenging when complete miscibility of polymer and API is not achieved. Consequently, the number of suitable polymers for a specific API might be even more limited and addition of excipients to alter mechanical properties may be more challenging. The modification of the feeding mechanism can simplify formulation development in many cases and enables the production of tablets from filaments within a broader range of mechanical properties. In addition to this, feeding gears are difficult to clean and further create abrasion, which is a risk factor for cross-contamination of the product and safety of the operator. All parts of the printer that come in contact with the product should be easily cleanable. Admittedly, the modification of the printer, as it is described in this study, lacks continuous production, since each filament has to be loaded separately, which needs to be addressed by technical engineering. However, commercially available FDM-printers are far from what is appropriate for the production of medicinal products in this regard. It has already been pointed out that several printer adaptations are needed to comply with pharmaceutical production standards (Araújo et al., 2019). Nevertheless, current research is mainly performed on consumer FDM-printers, which is due to their good availability and low cost. With the aim of manufacturing medicinal products, development of a novel pharmaceutical FDM-printer is essential and should also concern machine adaptations. An alternative feeding mechanism may be one of them.

CRediT authorship contribution statement

Nadine Gottschalk: Conceptualization, Investigation, Formal analysis, Writing - original draft. **Malte Bogdahn:** Conceptualization, Supervision, Writing - review & editing. **Meike Harms:** Writing - review & editing. **Julian Quodbach:** Conceptualization, Supervision, Writing - review & editing.

Declaration of Competing Interest

The authors declare that they have no known competing financial interests or personal relationships that could have appeared to influence the work reported in this paper.

Acknowledgements

The authors would like to thank the initiative ProMatLeben by the Bundesministerium für Bildung und Forschung (reference no. 13XP5064), who funded the work of this paper. The authors would also like to thank Alessandro-Giuseppe Elia for his support during the conduction of the hot melt extrusion.

Funding

This work was supported by the Bundesministerium für Bildung und Forschung (reference no. 13XP5064).

Appendix A. Supplementary data

Supplementary data to this article can be found online at <https://doi.org/10.1016/j.ijpharm.2021.120216>.

References

- Alhijaj, M., Belton, P., Qi, S., 2016. An investigation into the use of polymer blends to improve the printability of and regulate drug release from pharmaceutical solid dispersions prepared via fused deposition modeling (FDM) 3D printing. *Eur. J. Pharm. Biopharm.* 108, 111–125. <https://doi.org/10.1016/j.ejpb.2016.08.016>.
- Alhnan, M.A., Okwuosa, T.C., Sadia, M., Wan, K., Ahmed, W., 2016. Emergence of 3D Printed Dosage Forms : Opportunities and Challenges. *Pharm. Res.* 33, 1817–1832. <https://doi.org/10.1007/s11095-016-1933-1>.
- Araújo, M.R.P., Sa-barreto, L.L., Gratieri, T., Gelfuso, G.M., Cunha-filho, M., 2019. The Digital Pharmacies Era : How 3D Printing Technology Using Fused Deposition Modeling Can Become a Reality. *Pharmaceutics* 11, 128. <https://doi.org/10.3390/pharmaceutics11030128>.
- Auch, C., Harms, M., Mäder, K., 2018. Melt-based screening method with improved predictability regarding polymer selection for amorphous solid dispersions. *Eur. J. Pharm. Sci.* 124, 339–348. <https://doi.org/10.1016/j.ejps.2018.08.035>.
- Baird, J.A., Eerdenbrugh, B.V.A.N., Taylor, L.S., 2010. A Classification System to Assess the Crystallization Tendency of Organic Molecules from Undercooled Melts. *J. Pharm. Sci.* 99, 3787–3806. <https://doi.org/10.1002/jps.22197>.
- Elbadawi, M., Gustafsson, T., Gaisford, S., Basit, A.W., 2020a. 3D printing tablets : Predicting printability and drug dissolution from rheological data. *Int. J. Pharm.* 590, 119868. <https://doi.org/10.1016/j.ijpharm.2020.119868>.
- Elbadawi, M., Muñoz Castro, B., Gavins, F.K.H., Ong, J.J., Gaisford, S., Pérez, G., Basit, A. W., Cabalar, P., Goyanes, A., 2020b. M3DISEEN: A novel machine learning approach for predicting the 3D printability of medicines. *Int. J. Pharm.* 590, 119837. <https://doi.org/10.1016/j.ijpharm.2020.119837>.
- Fuenmayor, E., Forde, M., Healy, A.V., Devine, D.M., Mcconville, C., Major, I., 2018. Material Considerations for Fused-Filament Fabrication of Solid Dosage Forms. *Pharmaceutics* 10 (2), 44. <https://doi.org/10.3390/pharmaceutics10020044>.
- Fung, M.H., Suryanarayanan, R., 2017. Use of a Plasticizer for Physical Stability Prediction of Amorphous Solid Dispersions. *Cryst. Growth Des.* 17 (8), 4315–4325. <https://doi.org/10.1021/acs.cgd.7b00625>.
- Goyanes, A., Buanz, A.B.M., Basit, A.W., Gaisford, S., 2014. Fused-filament 3D printing (3DP) for fabrication of tablets. *Int. J. Pharm.* 476, 88–92. <https://doi.org/10.1016/j.ijpharm.2014.09.044>.
- Goyanes, A., Robles, P., Buanz, A., Basit, A.W., Gaisford, S., 2015. Effect of geometry on drug release from 3D printed tablets. *Int. J. Pharm.* 494, 657–663. <https://doi.org/10.1016/j.ijpharm.2015.04.069>.
- Ilyés, K., Krisztián, N., Balogh, A., Farkas, B., 2019. The applicability of pharmaceutical polymeric blends for the fused deposition modelling (FDM) 3D technique : Material considerations – printability – process modulation, with consecutive effects on in vitro release, stability and degradation. *Eur. J. Pharm. Sci.* 129, 110–123. <https://doi.org/10.1016/j.ejps.2018.12.019>.
- Kanaujia, P., Lau, G., Ng, W.A.I.K., Widjaja, E., Hanefeld, A., Fischbach, M., Maio, M., Tan, R.B.H., 2011. Nanoparticle Formation and Growth During In Vitro Dissolution of Ketoconazole Solid Dispersion. *J. Pharm. Sci.* 100, 2876–2885. <https://doi.org/10.1002/jps>.
- Khizer, Z., Akram, M.R., Sarfraz, R.M., Nirwan, J.S., Farhaj, S., Yousaf, M., Hussain, T., Lou, S., Timmins, P., Conway, B.R., Ghori, M.U., 2019. Plasticiser-Free 3D Printed Hydrophilic Matrices : Pharmacokinetic Studies. *Polymers (Basel)*. 11, 1095.
- Korte, C., Quodbach, J., 2018. Formulation development and process analysis of drug-loaded filaments manufactured via hot-melt extrusion for 3D-printing of medicines. *Pharm. Dev. Technol.* 23, 1117–1127. <https://doi.org/10.1080/10837450.2018.1433208>.
- Lang, B., Mcginty, J.W., Iii, R.O.W., Lang, B., Mcginty, J.W., Iii, R.O.W., 2014. Hot-melt extrusion – basic principles and pharmaceutical applications Hot-melt extrusion – basic principles and pharmaceutical applications. *Drug Dev. Ind. Pharm.* 9045 <https://doi.org/10.3109/03639045.2013.838577>.
- Melocchi, A., Parietti, F., Maroni, A., Foppoli, A., Gazzaniga, A., Zema, L., 2016. Hot-melt extruded filaments based on pharmaceutical grade polymers for 3D printing by fused deposition modeling. *Int. J. Pharm.* 509, 255–263. <https://doi.org/10.1016/j.ijpharm.2016.05.036>.

- Mooter, G. Van Den, 2012. The use of amorphous solid dispersions : A formulation strategy to overcome poor solubility and dissolution rate. *Drug Discov. Today Technol.* 9, 79–85. <https://doi.org/10.1016/j.ddtec.2011.10.002>.
- Nasereddin, J.M., Wellner, N., Albhijaj, M., Belton, P., Qi, S., 2018. Development of a Simple Mechanical Screening Method for Predicting the Feedability of a Pharmaceutical FDM 3D Printing Filament. *Pharm. Res.* 35, 151. <https://doi.org/10.1007/s11095-018-2432-3>.
- Pietrzak, K., Isreb, A., Alhnan, M.A., 2015. A flexible-dose dispenser for immediate and extended release 3D printed tablets. *Eur. J. Pharm. Biopharm.* 96, 380–387. <https://doi.org/10.1016/j.ejpb.2015.07.027>.
- Ponsar, H., Wiedey, R., Quodbach, J., 2020. Hot-Melt Extrusion Process Fluctuations and Their Impact on Critical Quality Attributes of Filaments and 3D-Printed Dosage Forms. *Pharmaceutics* 12, 511. <https://doi.org/10.3390/pharmaceutics12060511>.
- Prasad, E., Islam, M.T., Goodwin, D.J., Megarry, A.J., Halbert, G.W., Florence, A.J., Robertson, J., 2019. Development of a hot-melt extrusion (HME) process to produce drug loaded Affinisol™ 15LV filaments for fused filament fabrication (FFF) 3D printing. *Addit. Manuf.* 29, 100776. <https://doi.org/10.1016/j.addma.2019.06.027>.
- Samaro, A., Janssens, P., Vanhoorne, V., Renterghem, J. Van, Eeckhout, M., Cardon, L., 2020. Screening of pharmaceutical polymers for extrusion-Based Additive Manufacturing of patient-tailored tablets. *Int. J. Pharm.* 586, 119591. <https://doi.org/10.1016/j.ijpharm.2020.119591>.
- Shah, N., Shandhu, H., Choi, D.S., Chokshi, H., Malick, A.W., 2014. *Amorphous Solid Dispersions - Theory and Practice*. Springer.
- Solanki, N.G., Shah, A.V., Serajuddin, A.T.M., 2018. Formulation of 3D Printed Tablet for Rapid Drug Release by Fused Deposition Modeling : Screening Polymers for Drug Release, Drug-Polymer Miscibility and Printability. *J. Pharm. Sci.* 107, 390–401. <https://doi.org/10.1016/j.xphs.2017.10.021>.
- Ting, M., Porter, W.W., Mecca, J.M., Bates, F.S., Reineke, T.M., 2018. Advances in Polymer Design for Enhancing Oral Drug Solubility and Delivery. *Bioconjugate Chem.* 29, 939–952. <https://doi.org/10.1021/acs.bioconjchem.7b00646>.
- Tool, R., Thakkar, R., Pillai, A.R., Zhang, J., Zhang, Y., Kulkarni, V., Maniruzzaman, M., 2020. Tablets Using Fill Density as an Effective. *Polymers (Basel)*. 12, 1–21.
- Trasi, N.S., Taylor, L.S., 2012. Effect of polymers on nucleation and crystal growth of amorphous acetaminophen. *CrystEndComm* 14, 5188–5197. <https://doi.org/10.1039/c2ce25374g>.
- Verstraete, G., Samaro, A., Grymonpré, W., Vanhoorne, V., Snick, B. Van, Boone, M.N., 2018. 3D printing of high drug loaded dosage forms using thermoplastic polyurethanes. *Int. J. Pharm.* 536, 318–325. <https://doi.org/10.1016/j.ijpharm.2017.12.002>.
- Xu, P., Li, J., Meda, A., Osei-yeboah, F., Matthew, L., 2020. Development of a quantitative method to evaluate the printability of filaments for fused deposition modeling 3D printing. *Int. J. Pharm.* 119760 <https://doi.org/10.1016/j.ijpharm.2020.119760>.
- Zhang, J., Feng, X., Patil, H., Tiwari, R.V., Repka, M.A., 2017. Coupling 3D printing with hot-melt extrusion to produce controlled-release tablets. *Int. J. Pharm.* 519, 186–197. <https://doi.org/10.1016/j.ijpharm.2016.12.049>.

3.1.2. Effects of high drug loads on melt rheology and required process adjustments

In contrary to commercially available printing materials in the consumer sector, pharmaceutical filaments consist not only of a single material but of a variety of materials, e.g., API, plasticizers or polymers. The type and quantity of excipient or API can affect the melt rheology of the formulation, requiring an adjustment of print parameters. Furthermore, pharmaceutical printing has different requirements for the printed dosage forms than what commercially available printer were designed for. Mass conformity of a tablet batch is just one important quality criterion among others. The following paper introduces an empirical method, the feed force tester, measuring the required forces to push a filament through the hotend at a certain nozzle temperature and printing speed. Feed force data were transferred to actual printing processes with focus on the absolute mass and mass uniformity. Tests were performed with different commercially available materials as well as pharmaceutical formulations with different drug loads. This method presents a systematic approach to identify print parameters in terms of printing speed and nozzle temperature and optimize them for the respective formulation.

The idea and the study design were developed by Nadine Gottschalk, Malte Bogdahn and Julian Quodbach. The feed force tester was implemented and assessed by Nadine Gottschalk. She also performed the remaining experimental work, such as extrusion, printing and analytics. Alessandro-Giuseppe Elia and Florian Hess contributed to the development of the rheology method. Main data evaluation and writing of the initial manuscript draft was performed by Nadine Gottschalk. Julian Quodbach and Malte Bogdahn supported data evaluation and revised the manuscript draft.

Evaluation of authorship:

Author	Idea	Study Design	Experimental	Evaluation	Manuscript
Nadine Gottschalk	30	50	98	60	70
Julian Quodbach	25	25	0	20	15
Alessandro-Giuseppe Elia	0	0	1	0	0
Florian Hess	0	0	1	0	0
Malte Bogdahn	45	25	0	20	15

Evaluation of copyright permission: The author of the article retains the right to include it in a thesis or dissertation, provided it is not published commercially (accessed 10.05.2024).

Article available online at: <https://doi.org/10.1016/j.ijpharm.2021.121416>

© 2022 Elsevier B.V. All rights reserved.

Determination of feed forces to improve process understanding of Fused Deposition Modeling 3D printing and to ensure mass conformity of printed solid oral dosage forms

Nadine Gottschalk ^{a b}, Julian Quodbach ^a, Alessandro-Giuseppe Elia ^b, Florian Hess ^b, Malte Bogdahn ^b

^aInstitute of Pharmaceutics and Biopharmaceutics, Heinrich Heine University, Düsseldorf, Germany

^bMerck KGaA, Darmstadt, Germany

International Journal of Pharmaceutics, Volume 614, 121416, 2022

DOI: 10.1016/j.ijpharm.2021.121416

Abstract

Fused Deposition Modeling is a suitable technique for the production of personalized solid oral dosage forms. For widespread application, it is necessary to be able to print a wide range of different formulations to address individual therapeutic needs. Due to the complexity of formulation composition (e.g., due to different compounds, excipients for enhancement of release and mechanical properties) and limited mechanical understanding, determination of suitable printing parameters is challenging. To address this challenge, we have developed a feed force tester using a Texture Analyser setup that mimics the actual printing process. Feed force data were compared to the mass of tablets printed from technical materials as well as pharmaceutical filaments containing ketoconazole at high drug loads of 20% and 40% and polyvinyl alcohol. By determining a feed force limit for the 3D printer from feed force data of several formulations printed, it was possible to specify the operable printing range, where printing is reproducible and printed mass corresponds the target mass. Based on these results, rational optimization of the printing process in terms of speed, time and temperature for different materials and formulations is possible.



Contents lists available at ScienceDirect

International Journal of Pharmaceutics

journal homepage: www.elsevier.com/locate/ijpharm

Determination of feed forces to improve process understanding of Fused Deposition Modeling 3D printing and to ensure mass conformity of printed solid oral dosage forms

Nadine Gottschalk^{a,b}, Julian Quodbach^a, Alessandro-Giuseppe Elia^b, Florian Hess^b, Malte Bogdahn^{b,*}

^a Institute of Pharmaceutics and Biopharmaceutics, Heinrich Heine University, Düsseldorf, Germany

^b Merck KGaA, Darmstadt, Germany

ARTICLE INFO

Keywords:

Additive manufacturing
Fused Deposition Modeling
Feed forces
Process optimization
Printing parameters
Texture analyzer
Melt rheology

ABSTRACT

Fused Deposition Modeling is a suitable technique for the production of personalized solid oral dosage forms. For widespread application, it is necessary to be able to print a wide range of different formulations to address individual therapeutic needs. Due to the complexity of formulation composition (e.g., due to different compounds, excipients for enhancement of release and mechanical properties) and limited mechanical understanding, determination of suitable printing parameters is challenging. To address this challenge, we have developed a feed force tester using a Texture Analyser setup that mimics the actual printing process. Feed force data were compared to the mass of tablets printed from technical materials as well as pharmaceutical filaments containing ketoconazole at high drug loads of 20% and 40% and polyvinyl alcohol. By determining a feed force limit for the 3D printer from feed force data of several formulations printed, it was possible to specify the operable printing range, where printing is reproducible and printed mass corresponds the target mass. Based on these results, rational optimization of the printing process in terms of speed, time and temperature for different materials and formulations is possible.

1. Introduction

The three-dimensional printing (3DP) technique Fused Deposition Modeling (FDM) has been vastly explored recently in the pharmaceutical field, due to its high potential to produce personalized pharmaceutical products (Dumpa et al., 2021). In FDM, the desired object is created layer-by-layer by a deposition of molten or softened thermoplastic polymer onto a build plate. The FDM process requires wire-like filament, which is commonly moved by feeding gears into the hotend, where the material is softened and pushed through the heated nozzle. Pharmaceutical filament is produced by hot-melt extrusion (HME) of a polymer and active pharmaceutical ingredient (API) blend at elevated temperatures (Prasad et al., 2019). The extrudate strand exiting the die can be pulled by a conveyor belt (Dumpa et al., 2020; Korte and

Quodbach, 2018a; Zhang et al., 2017) or a winder (Ponsar et al., 2020) in order to adjust to a certain filament diameter, which is usually in the range of 1.75 mm or 2.85 mm. The filament diameter uniformity is crucial to ensure mass conformity of the printed tablet (Ponsar et al., 2020). Typical filament diameter fluctuations should not exceed absolute values of ± 0.05 mm in case of a 1.75 mm filament (Melocchi et al., 2015).

FDM is particularly suitable for the on-demand production of personalized solid oral dosage forms, since the tablet design can be easily changed in terms of size, shape and porosity using computer-aided design (CAD) software (Cailleaux et al., 2021). As a result, dose and release properties can be adjusted according to individual needs (Goyanes et al., 2015; Korte and Quodbach, 2018b; Tool et al., 2020; Windolf et al., 2021). In a point-of-care manufacturing setting, an

Abbreviations: 3DP, three-dimensional printing; FDM, fused deposition modeling; HME, hot melt extrusion; CAD, computer-aided design; API, active pharmaceutical ingredient; PETG, polyethylene terephthalate glycol-modified; PLA, polylactic acid; PVA, polyvinyl alcohol; KITZ, ketoconazole; DSC, differential scanning calorimetry; PXRD, X-ray powder diffraction; CE, conveying element; EE, extrusion element; ME, mixing element; ACN, acetonitrile; SD, standard deviation; CV, coefficient of variation; T_g , glass transition temperature.

* Corresponding author.

E-mail address: malte.bogdahn@merckgroup.com (M. Bogdahn).

<https://doi.org/10.1016/j.ijpharm.2021.121416>

Received 28 September 2021; Received in revised form 17 December 2021; Accepted 18 December 2021

Available online 25 December 2021

0378-5173/© 2022 Elsevier B.V. All rights reserved.

additional benefit is that no powder materials are required (Quodbach et al., 2021). Regarding the production of tablets, the composition of each formulation may vary greatly and excipients, e.g., plasticizers, dissolution enhancers or API(s), are likely to affect melt properties (Prasad et al., 2016). Consequently, adjustment of printing parameters is necessary for each formulation.

In the early days of 3DP, adjustment of printing parameters was mainly done by trial-and-error and visual assessment of the melt at the nozzle. It was stated that the printing temperature is generally higher than the extrusion temperature (Pereira et al., 2020). A couple of attempts have been reported to predict printing temperatures for general printability. Rheology measurements have been performed to determine adequate nozzle temperatures in dependence of the applied shear rate (Elbadawi, 2018). However, the actual shear stress inside the hotend is a function of the applied extrusion rate, temperature and the design of the hotend. Moreover, heat absorption of the filament is dependent on the filament diameter, the distance of the filament to the heating element and the respective composition of the formulation. Inline rheology measurements are possible (Coogan and Kazmer, 2019), but difficult to establish. The prediction of printing temperatures via a machine learning approach has been shown by Elbadawi et al. (2020b) in their software tool M3DIseen on the basis of in-house conducted experiments. Muñiz Castro et al. (2021) further showed that by the means of machine learning it was possible to determine e.g., printing temperatures for a variety of formulation from literature data very precisely. Nevertheless, these methods require a lot of data regarding the material properties and interaction of polymers, additives and especially API(s), which may not be available at an early stage of drug development. The printing process is complex and the choice of process parameters can affect the quality of the printed object. Regarding the production of solid oral dosage forms, the printed tablet mass should match the intended to ensure the correct API dose. However, printing temperature and printing speed can have a distinct influence on tablet properties such as the total weight and weight uniformity (Alhijaj et al., 2019). This highlights the importance of determining printing parameters that ensure the desired quality attributes of solid oral dosage forms.

The aim of this work was the development of an analytical tool to determine printing parameters based on the forces needed to convey filament through a heated 3DP hotend at different speeds. The feed forces determined should then be transferred to a printer and correlated to the printed mass at equal printing conditions. For this purpose, the technical 3DP materials polylactic acid (PLA), polyethylene terephthalate glycol-modified (PETG) and polyvinyl alcohol (PVA) have been used to develop the method due to their good availability and low diameter fluctuations. The method was also applied to an internally produced pharmaceutical filament based on PVA extruded with varying drug loads of ketoconazole (KTZ), a poorly soluble antifungal agent (Taupitz et al., 2013). The influence of KTZ on printing conditions, mechanical properties and dissolution at the different drug loads was evaluated.

2. Materials and methods

2.1. Materials

KTZ was purchased from LGM Pharma (Erlanger, USA). PVA (Par-teck® MXP) was supplied by Merck KGaA (Darmstadt, Germany). Technical PLA and PVA filament (diameter: 1.75 mm) were purchased from Prusa Research s.r.o. (Prague, Czech Republic). PETG filament was purchased from Polymaker (Shanghai, China).

A fully assembled RepRap Arduino Mega Pololu Shield basic kit (RAMPS 1.4) was purchased from Reprapworld, which was originally developed by UltiMachine (South Pittsburg, USA). An E3D amplifier board was purchased from E3D (Oxford, United Kingdom) and an axial 24 V fan (4500 rpm) was purchased from RND Components (Nänikon, Switzerland).

2.2. Methods

2.2.1. Setup for assessment of feed forces

The forces needed to convey filament at a certain speed through a heated nozzle are further called feed forces; the system developed to determine such forces is referred to as a feed force tester. Feed forces were measured using a Texture Analyser TA-XT (Stable Micro Systems, Godalming, UK) equipped with tensile grips and a custom-built rig. A mount (Fig. 1) was designed for an Ultimaker print core (Ultimaker, Geldermalsen, Netherlands) using Fusion 360 software (Autodesk, Farnborough, UK). A rigid guide was attached on top of the mount to prevent buckling of the filament. The Ultimaker 3 print core is designed for filament with a diameter of 2.85 mm. Since filament with a diameter of 1.75 mm was used for this test, a PTFE tube (length approximately 20 cm, inner diameter 2 mm) was placed inside the print core and guide. A lid on top of the setup was used to prevent the guiding tube from moving upwards during the test. A metal rod (\varnothing 1.5 mm) was used as piston to move the filament stick through the heated nozzle. The metal rod was attached to a small, 3D printed cuboid that was placed between the clamps of the tensile grips. A fan was placed in front of the setup for cooling of the heat sinks to prevent heat creep, which can lead to decreasing stiffness or thermal expansion of the filament, which can result in obstruction of the hotend.

The hotend was controlled by standalone electronics derived from open-source components intended to control entire FDM systems. The electronics were chosen to resemble an actual 3D printer. The electronics were built around a RepRap RAMPS board and an Arduino Mega 2560 microcontroller board. Marlin firmware (Version 1.1.9) was configured for the hotend and compiled and flashed onto the Arduino controller using Arduino software (1.8.5). To mimic the 3D printer used in transferring experiments as closely as possible, an original Ultimaker 3 print core 0.4 mm type B was used. To adapt the PT100 temperature sensor to the RAMPS circuit, which is designed for NTC type temperature sensors, an E3D amplifier board was used. Prior to each experiment, a PID autotune cycle was initiated via Marlin firmware and temperature for the conducted experiments was set manually via Arduino software. Temperature data were recorded during the tests using Marlin debug modus on the serial port. Tests were only started when the set temperature was constant.

Tests were performed in quintuplicate. Therefore, filament was cut into pieces of approximately 15 cm length and loaded through the lid into the feed force tester. The piston was attached to the clamp and moved downwards until the tip was located a few millimeters above the end of the filament. The distance between the clamp and setup was 80 mm. A pretest speed of 1 mm/s was selected that altered upon a trigger force of 1.0 N to the actual test speeds of 0.33 mm/s, 1.00 mm/s and 1.66 mm/s, mimicking 10 mm/s, 30 mm/s and 50 mm/s printing speed, respectively. Printing speeds, such as 10 mm/s, refer to the movement of the printhead in xy-direction and not to the forward propulsion of the filament. The feeding speed of the filament is dependent on the filament diameter as well as the volume of a single printed line. Calculations were performed on the basis of a filament diameter of 1.75 mm, considering a layer height of 0.2 mm and 0.4 mm line width. The target distance was 70 mm. The remaining filament in the setup was fully removed by pushing it through the heated nozzle when loading a new filament piece. Data were acquired using Exponent software (version 6.1.16.0, Stable Micro Systems, Godalming, UK). The material, which was pushed through the nozzle, was collected and weighed using an analytical balance (ME235S-OCE, Sartorius, Goettingen, Germany). Tested nozzle temperatures for the respective material are displayed in Table 1. Initial printing temperatures of the technical materials were chosen according to the suggested printing temperatures of the manufacturer: 200–220 °C (PLA), 180–210 °C (PVA) and 230–240 °C (PETG).

2.2.2. Blend composition and HME of filament

Blending was performed using a turbula mixer (T2A, Willy A.

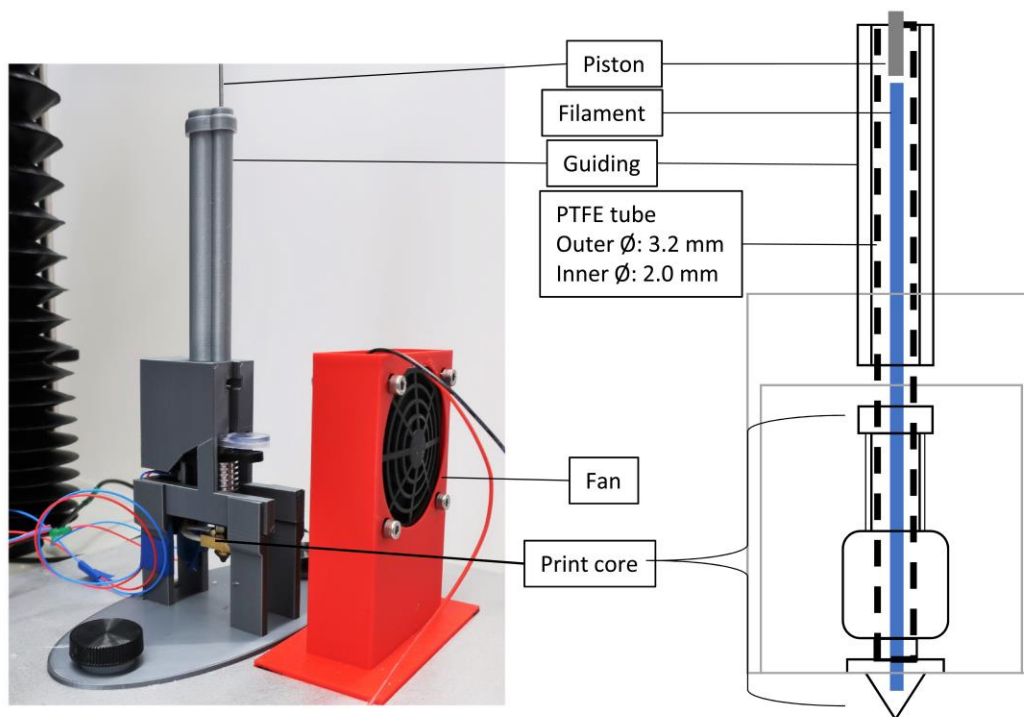


Fig. 1. Setup for assessment of feed forces.

Table 1

Assessment of feed forces: tested nozzle temperatures.

Materials		Tested nozzle temperature (°C)								
		180	190	200	210	220	230	240	250	260
Technical materials	PLA			x	x	x	x	x	x	
	PVA		x	x	x	x	x	x		
	PETG						x	x	x	x
Pharmaceutical formulations	PVA-K0			x	x	x	x			
	PVA-K20		x	x	x	x				
	PVA-K40	x	x	x	x					

Bachofen Maschinenfabrik, Muttenz, Switzerland). Polymer and KTZ were premixed for 15 min and colloidal silicon dioxide was added stepwise to the premix. The blend was sieved using a mesh size of 1 mm and blended for additional 15 min. Colloidal silicon dioxide was added to enhance flow of the blend into the hot-melt extruder. Blend compositions are displayed in Table 2. Formulations were named according to the proportion of KTZ in the composition.

Extrusion of the filament was performed on a co-rotating twin-screw extruder (Pharma 11, Thermofisher Scientific, Waltham, USA) with a 2 mm die. A screw configuration consisting of conveying elements (CE), mixing elements (ME) and extrusion elements (EE) was used. The screw configuration is displayed in detail in the supplementary material (Table S1). Extrusion parameters are displayed in Table 3. The extrusion and die temperature were decreased with increasing drug load to obtain a suitable melt viscosity at the die, resulting in a self-supporting strand.

Table 2

Formulations for HME (wt%).

Formulation	KTZ (%)	PVA (%)	Silicon dioxide (%)
PVA-K0	–	99	1
PVA-K20	20	79	1
PVA-K40	40	59	1

Temperature selection was performed via visual assessment of the melt at the die. The measured temperature of the melt at the die was approximately 5–6 °C lower than the set temperature. Extrusion processes were performed below the degradation temperature of the API (221 °C (Kanaujia et al., 2011)). A high screw speed was selected to enable good distribution of KTZ in the polymer matrix. Extrusion parameters were recorded during extrusion.

In order to modify the filament diameter, the speed of the conveyor belt (Brabender GmbH, Duisburg, Germany) was adjusted. Inline measurements of filament diameter were conducted behind the conveyor belt using a 3-axis laser measurement system (Odad 33 Trio, Zumbach, Orpund, Switzerland). The obtained filament was cut into filament sticks of approximately 25 cm length using diagonal pliers. Filaments were collected during extrusion at different time points, representing the beginning, middle and end of the extrusion process (approximately 1 h for each time point). Extrusion was initially performed to obtain uniform filaments with a diameter of 1.75 mm ± 0.1 mm. Since mass deviations of the collected material, which had been pushed through the printer nozzle during assessment of feed forces were observed, material was classified to meet the range of 1.75 mm ± 0.05 mm for printing experiments to reduce deviations.

Table 3

Set extrusion parameters and temperatures.

Formulation	Screw speed (rpm)	Feed rate (kg/h)	Zone 1 (°C)	Zone 2 (°C)	Zone 3 (°C)	Zone 4 (°C)	Zone 5 (°C)	Zone 6 (°C)	Zone 7 (°C)	Die (°C)
PVA-K0	300	0.2	80	160	200	200	200	200	200	200
PVA-K20	300	0.2	80	160	190	190	190	190	190	180
PVA-K40	300	0.2	80	160	180	180	180	180	180	170

2.2.3. 3D printing

An Ultimaker 3 (firmware version: 4.0.1.20171023, Ultimaker, Geldermalsen, Netherlands), was used for printing, which had been modified to work with a filament diameter of 1.75 mm instead of 2.85 mm. A detailed description of the printing setup and procedure can be found in Gottschalk et al. (2021). Printing tests were performed at various parameter combinations and printed objects were characterized according to their mass deviation from the target mass. The printed volume is stated in the G-code and the theoretical mass was calculated with the respective material density. A deviation of 5% from the target mass was defined as lower limit. Two different objects were designed for printing in Fusion 360 (Autodesk, Farnborough, United Kingdom): a cuboid (10 mm × 20 mm × 2.4 mm) for transferring experiments from the feed force tester to the printer due to its higher volume and easier determinable dimensions ($n = 3$) and cylindrical tablets ($\varnothing = 10$ mm, $h = 2.4$ mm) for the assessment of drug release and solid-state characterization ($n = 20$). 3D objects were saved with high resolution in a binary stereolithography file format (.stl) and sliced using Simplify 3D (version 4.0.1. Simplify3D, Cincinnati, USA). For transferring experiments, printing speed and nozzle temperatures corresponding to feed force tester experiments were used. Cylindrical tablets were printed from three different pharmaceutical formulations. Filaments from the middle of the extrusion were used for printing. PVA-K0, PVA-K20 and PVA-K40 were printed at 30 mm/s and 200, 220 and 240 °C according to feed force test results and cuboid printing. All other printing parameters were kept equal and are displayed in Table 4. The only exception was the build plate temperature in case of technical PVA, which had to be reduced to 40 °C due to strong adhesion of the printed objects to the build plate. A nozzle with a diameter of 0.4 mm was used for printing. Manual leveling of the build plate was performed prior to printing.

2.2.4. Characterization of printed objects

The dimensions of both, cuboids and tablets, were determined using a digital caliper (TWIN-Cal IP67, TESA Technology, Renens, Switzerland). Measuring was performed in triplicate. Samples (cuboids $n = 3$, tablets $n = 20$) were weighed using an analytical balance (ME235S-OCE, Sartorius, Goettingen, Germany).

2.2.5. Differential scanning calorimetry (DSC)

Pure substances, blends, filaments and tablets were analyzed using a DSC 1 (Mettler Toledo, Gießen, Germany). A Tube Mill Control (IKA, Staufen, Germany) was used to crush the extrudates and printed tablets at 25,000 rpm. Milling time varied between 30 and 60 s depending on the formulation. Approximately 7–8 mg of sample were hermetically sealed in 100 μ L aluminum pans that were pierced by the DSC piercing unit prior to analysis to enable evaporation of water vapor. An empty and pierced DSC pan was used as reference. Samples were heated up and

Table 4

Printing parameters.

Line width	0.4 mm
Layer height	0.2 mm
Initial layer height	0.2 mm
Build plate temperature	60 °C (40 °C for technical PVA)
Infill density	100%
Infill pattern	Rectilinear
Initial layer flow	100%
Printing speed	10, 30, 50 mm/s
Shell	2

cooled down twice in a range of 0 °C to 220 °C at a rate of 10 K/min. Tests were performed in triplicate.

2.2.6. X-Ray powder diffraction (PXRD)

PXRD measurements were performed to determine the solid state of blends, filaments and tablets. A D2 Phaser (Bruker, Billerica, USA) equipped with an SSD160 detector in 1D mode with a full opening of 4.875° was used. X-rays were generated by a copper anode at 30 kV and 10 mA and reduction of $K\beta$ radiation was done by the utilization of nickel foil. Sample preparation was performed on a zero-background holder with well and scanned from 6° to 41° with a step size of 0.02° and measurement time of 1 s per step. Sample rotation speed was set to 5 rpm.

2.2.7. 3-Point bending test

A 3-point bending test was employed to assess the influence of the drug load on the mechanical properties. Therefore, filament was cut into pieces of 70 mm and tested with a Texture Analyser TA-XT (Stable Micro Systems, Godalming, UK) equipped with a 3-point bending rig with a 30 mm gap. Upon contact of the blade with the sample (trigger force: 0.049 N) the pre-test speed of 5 mm/s reduced to 0.1 mm/s. Nine replicate tests were performed for each formulation. Stress and strain curves were calculated using the diameter of each sample, which was determined prior to the analysis using the laser measurement system. Data were acquired using Exponent software (version 6.1.16.0).

2.2.8. Drug content and dissolution

Blend, filament and tablet drug content was determined. Blend samples were taken prior to extrusion from the top, middle and bottom of the blend: four samples each at different positions. Filaments were tested in triplicate for each timepoint of extrusion. Six randomly selected tablets were tested. Test solutions were prepared by weighing 200–250 mg of sample into a volumetric flask and dissolving the sample using 50 mL of 0.1 N HCl. The solution was further diluted to a concentration of 0.2 mg/mL using a mixture of 1:1 acetonitrile (ACN) and water.

Dissolution profiles were acquired by placing a printed tablet in the vessels of a Sotax Smart AT7 Dissolution Tester (Sotax, Aesch, Switzerland) filled with 900 mL of 0.1 N HCl at 37 °C ($n = 6$). The paddle method (USP II) was used. Paddle rotation speed was set to 100 rpm. Samples (sampling volume = 3 mL) were drawn at various time points (5, 10, 15, 30 and 45 min and 1, 1.5, 2, 4, 8, 12 and 24 h) and diluted with equal volumes of ACN. Ultra performance liquid chromatography is described in detail in Gottschalk et al. (2021).

2.2.9. Density measurements

Density measurements of milled extrudate were performed on an Ultracyc 1200e gas expansion pycnometer (Quantachrome, Boynton Beach, USA). Nitrogen was used as purging gas and the target pressure was 1.4 bar. Approximately 4–5 g of milled extrudates were analyzed. Tests were performed in triplicate.

2.2.10. X-ray microtomography

Measurements of printed cuboids were performed with a Skyscan 1176 by Bruker (Billerica, USA) at a source voltage of 80 kV and a source current of 312 μ A. A copper–aluminum filter was used to reduce beam hardening effects by the sample. Samples were scanned in steps of 0.2° over 360° and a resolution of 8.8 μ m per pixel. Reconstruction was performed using NRecon (Version 1.7.4.6., Bruker, Billerica, USA). Post

alignment and ring artefact reduction were applied for each sample individually. Porosity analysis was performed using CTAn (Version 1.20.8.0, Bruker, Billerica, USA) by selecting a representative volume centered inside the cuboid with a size of 10 mm × 7 mm 1.8 mm (n = 1).

2.2.11. Melt rheology

The melt viscosity of the different formulations was determined using a Haake™ Mars™ plate-plate rheometer (ThermoFisher Scientific, Waltham, USA). Approximately 550 mg of powder blend was applied to the plate ($\varnothing = 20$ mm), heated to 200 °C and excess material trimmed after a gap height of 1 mm was reached. The temperature of 200 °C was maintained for 5 min and thereafter reduced to 170 °C. Viscosity was determined in a range from 170 °C to 250 °C with a heating rate of 2 K/min. Oscillatory tests were performed in triplicate at a constant frequency (6.28 rad/s) and strain rate (0.1%).

3. Results and discussion

3.1. Feed force tester

3.1.1. Assessment of feed forces (technical materials)

Feed force profiles at the varying test speeds and nozzle temperatures

are exemplary shown for technical PVA in Fig. 2. Profiles for PLA and PETG were similar to PVA and can be found in the supplementary material (Figs. S1 and S2).

Forces were low during the first 5 mm of the test distance of 70 mm. After approximately 5 mm, an increase of force was observed, which resulted in a force plateau for the remaining 40 mm of the test distance. This initial profile shape, with a certain lag followed by a force increase, is likely a result of compression of the softened material during pressure build-up in the nozzle. Once sufficient pressure is reached, material is pushed out of the nozzle until an equilibrium is reached, which then results in constant material flow (force plateau). Oscillations were observed in the force plateau that were more pronounced at high test speeds, demonstrating the interplay between material movement and pressure build-up in the nozzle at equilibrium. The general shape of the feed force profile was similar for nearly all tested settings and materials, differing mainly by the absolute value of the force plateau, which was dependent on the combination of nozzle temperature and test speed. One exception was observed for PVA at 240 °C and 0.33 mm/s test speed, where sharp drops of force were observed in the course of the profile. Each drop was accompanied by the sound of bursting bubbles, a phenomenon, which has been reported in previous studies (Chung et al., 2018; Wu et al., 2018). Bubbles are not desired as they can impair the

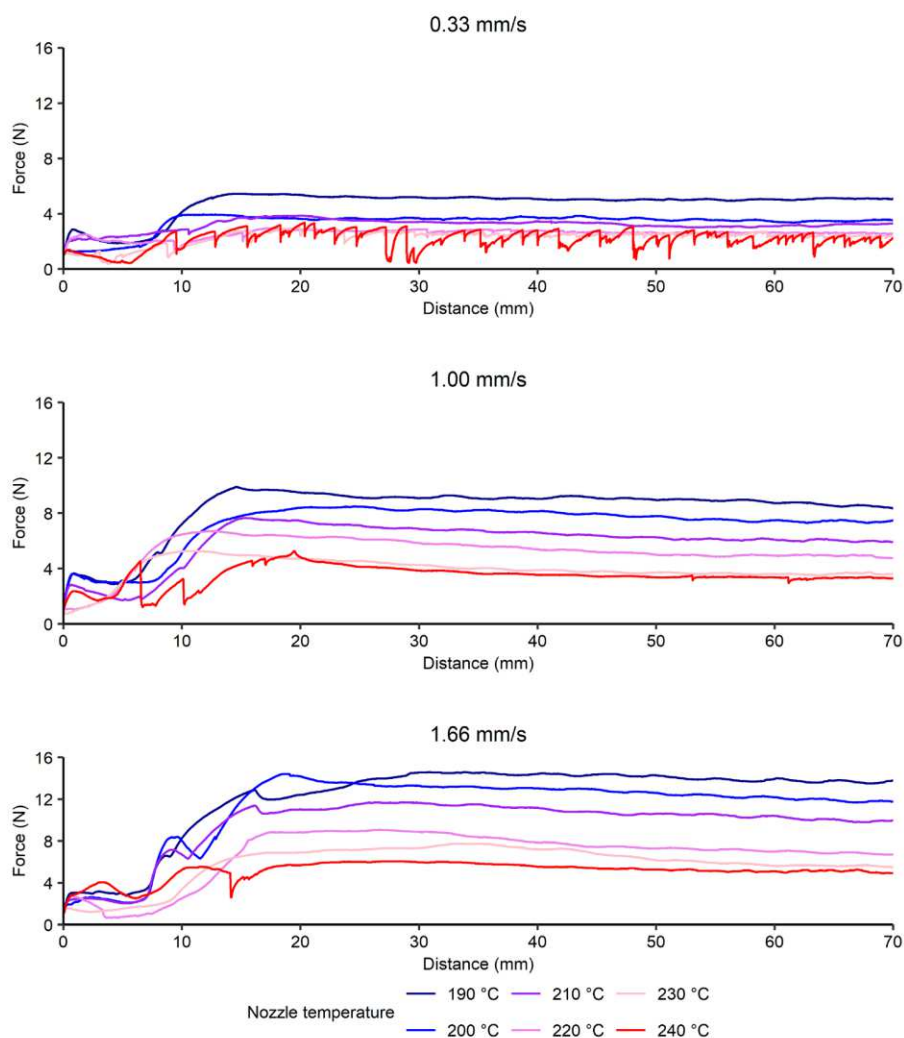


Fig. 2. Feed force profile for technical PVA at varying test speeds and temperatures.

dimensional quality and dosage of the tablet (Crişan et al., 2021). This can be a result of evaporating moisture from the hygroscopic PVA filament, despite the material having been dried in a vacuum drier prior to the experiment. This effect might be caused by the prolonged residence time in the hotend and low polymer viscosity. At low test speeds the material remains longer in the hotend and material has more time to absorb thermal energy leading to a vaporization of residual moisture, resulting in the formation and, due to the low melt viscosity, bursting of vapor bubbles. Another potential explanation is the degradation of PVA. PVA undergoes elimination of hydroxyl side groups upon heating up to temperatures > 200 °C, generating water (Dong et al., 2014; Holland and Hay, 2001). This behavior was not observed for PLA and PETG. Within one test speed, the force plateau decreased with increasing nozzle temperature, possibly caused by a reduction of melt viscosity. In contrast, at a given nozzle temperature the force plateau increased when increasing the test speed. This force increase is probably caused by a shortened residence time due to the high test speed (Simon et al., 2018) and lower heat absorption in the hotend leading to increased melt viscosity and increased pressure due to the higher quantity of material being fed. Recorded nozzle temperatures revealed a decrease of only 1–2 °C during printing at the highest test speed (Fig. S3). This is assumed to have only a minor effect on the overall melt viscosity. The true temperature of the melt in the nozzle would provide valuable information but determination is difficult.

The initial compression phase of the profile showed high variability in terms of force onset and slope as a result of manual loading. However, the absolute values of the force plateau were reproducible, wherefore mean force values of the last 40 mm of the plateau were used to calculate the feed forces for each setting (Table 5).

In addition to the force measurements, the material exiting the die was analyzed in terms of mass conformity (Fig. S4). Coefficients of variation (CV) of all extruded masses at the tested parameter combinations were low ($CV < 4\%$), especially for PETG ($CV < 2.0\%$). These results show that even if feed forces were high, it was still possible to extrude homogeneous amounts of material. The rigid design of the piston feeding mechanism may contribute to the uniformity of the results. Regarding PLA and PETG, the extruded mass was 6–8 mg lower than the theoretical mass of 70 mm of filament corresponding to approximately 2–3 mm of filament. This is in accordance with the distance of the initial compression phase of these materials (Figs. 2, S1 and S2). PVA showed a longer compression phase (approximately 6–8 mm) resulting in a higher corresponding mass difference of approximately 18 mg. Since this phenomenon may affect the printed mass in further printing experiments, printing of skirt lines prior to printing of the objects was added to the G-code next to a purging step at the start of printing.

Table 5
Feed forces for technical materials at different test speeds.

Material	Nozzle temperature (°C)	Mean feed force (N) \pm SD (n = 5)		
		0.33 mm/s	1.00 mm/s	1.66 mm/s
PLA	200	4.63 \pm 0.08	11.43 \pm 0.13	17.11 \pm 0.09
	210	3.06 \pm 0.16	8.11 \pm 0.44	10.96 \pm 0.73
	220	2.44 \pm 0.22	6.15 \pm 0.42	9.53 \pm 0.48
	230	1.64 \pm 0.11	4.94 \pm 0.47	7.96 \pm 0.28
	240	1.43 \pm 0.18	4.31 \pm 0.37	7.08 \pm 0.36
	250	1.21 \pm 0.23	3.17 \pm 0.32	4.87 \pm 0.39
PVA	190	4.9 \pm 0.06	8.7 \pm 0.08	17.1 \pm 0.10
	200	4.0 \pm 0.33	8.1 \pm 0.60	12.5 \pm 0.55
	210	3.2 \pm 0.03	6.4 \pm 0.23	10.0 \pm 0.72
	220	2.6 \pm 0.08	5.3 \pm 0.07	7.8 \pm 0.19
	230	2.4 \pm 0.10	4.1 \pm 0.21	6.1 \pm 0.75
	240	2.1 \pm 0.07	3.4 \pm 0.05	5.3 \pm 0.12
PETG	230	4.95 \pm 0.02	12.51 \pm 0.12	18.48 \pm 0.08
	240	3.66 \pm 0.06	9.36 \pm 0.11	12.68 \pm 0.25
	250	2.66 \pm 0.08	7.12 \pm 0.07	10.52 \pm 0.18
	260	1.69 \pm 0.13	5.26 \pm 0.24	8.05 \pm 0.24

3.1.2. Transferring of feed forces to 3D-printer of technical materials

The feed force tester was constructed to resemble the printer and the printing process. Printing experiments were performed at equivalent printing conditions with the aim of transferring the data acquired from the feed force tester to the printer, to determine suitable printing parameters with regards to the target mass. Feed forces and cuboid masses at corresponding settings are displayed in Fig. 3. Parameter combinations leading to high feed forces resulted in negative deviations from the target cuboid mass. This effect is likely caused by under extrusion of the material. Under extrusion occurs during printing if the back pressure of the material in the nozzle is too high due to high melt viscosity (Alsoufi et al., 2019) and when the feeding gears are not capable of moving the filament forward, which leads to slippage of the filament between the gears. Compensation was achieved by lowering the printing speed, however, at speeds of 10 mm/s, printing a single cuboid lasted 15 min, which is not acceptable in terms of efficiency for real-life application. To improve efficiency of FDM printing, a feed force limit for the printer was determined by identifying the highest feed force that still resulted in masses within the specification of 5% for each material. For PLA and PETG feed force limits of 4.87 ± 0.4 N and 4.95 ± 0.02 N were identified whereas the feed force limit for PVA was lower (4.1 ± 0.2 N). For verification of the results, feed force and printing tests at selected parameter combinations were repeated on different days and after disassembly, cleaning and reassembly of the printer setup and feed force tester. Results indicated a good reproducibility in terms of feed forces (Fig. S5). Cuboid mass was reproducible when parameter combinations resulted in feed forces < 4 N. However, cuboid mass showed poor reproducibility (tested for PVA and PLA) when parameter combinations were used that resulted in feed force values ≥ 4 N. An explanation may be the susceptibility of the printing setup to mechanical obstruction, e. g., bending in the bowden tube, which may differ slightly after new assembly. Especially at parameter combinations resulting in feed forces > 4 N filament can slip between the feeding gears leading to an increase of surface roughness of the filament. Due to that, higher friction can occur in the bowden tube, which has been reported to result in printing inaccuracies (Hernandez, 2015). The extend of surface roughness probably depends on the set feeder tension. The feeder tension is adjusted manually by a screw and may vary slightly after reassembly. In addition to that, the bowden tube was not fixed during printing and the way it bends during printing possibly affects the friction between the tube and the filament. Therefore, cuboid masses printed at parameter combinations close to the limit should be considered with caution. In consequence, only parameter combinations resulting in feed forces < 4 N were considered for following experiments.

Dimensions of the cuboids differed slightly from the dimensions of the CAD (10 mm \times 20 mm \times 2.4 mm). Width and length of the cuboids differed in a range of ± 0.4 –0.8 mm. Width and length of the cuboid increased with increasing nozzle temperatures at all printing speeds. A possible explanation for this phenomenon could be material oozing out from the nozzle due to low viscosity at elevated temperatures also known as over extrusion (Butt et al., 2021). In some cases, the cuboid mass was slightly higher than the target mass. However, an increase in width and length was also observed for cuboids where this was not the case. Here, the increase of width and length was possibly due to higher temperature of the material exiting the nozzle and prolonged solidification. In addition to that, width and length increased with decreasing printing speed, likely caused by the nozzle maintaining contact with the object for a longer period, resulting in higher mobility until solidification. Cuboid height corresponded to the theoretical height of 2.4 mm and was elevated ($+ 0.1$ mm) at a low printing speed of 10 mm/s and high nozzle temperatures.

3.2. Processing and characterization of internally produced formulations

3.2.1. Transfer to internally produced formulations

Internally produced formulations showed similar behavior compared

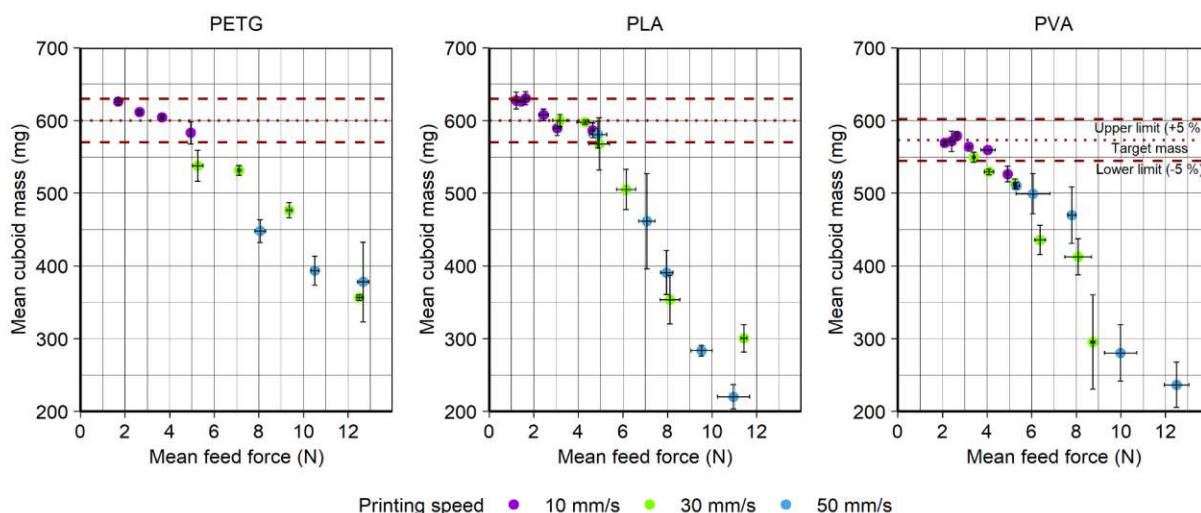


Fig. 3. Mean cuboid mass \pm SD ($n = 3$) vs. mean feed forces \pm SD ($n = 5$) at the respective print settings for PLA, PVA and PETG. The dotted line displays the calculated target mass. The dashed lines display the upper and lower 5 % limit of the target mass for each material.

to the technical materials in terms of feed force profile and of printed cuboid mass at different parameter combinations. The feed force plateau values and mass of printed cuboids for each formulation at different parameter combinations are displayed in Fig. 4. Furthermore, the formulation PVA-K0 showed similar values to technical PVA, differing by <1 N. The identified limit of 4 N was applied to the formulations with different drug loads. It was confirmed that parameter combinations leading to feed forces > 4 N resulted in cuboids with a mass decreased by $> 5\%$, whereas feed forces < 4 N resulted in cuboids within the specification. These results demonstrate that the transfer from feed force results to printed cuboids was also successful for the internally produced filaments. Only few exceptions were observed for parameter combinations that resulted in feed forces close to the limit of 4 N, e.g., PVA-K0 at 30 mm/s and 230 °C, which was likely due to low reproducibility of printing at parameter combinations resulting in values > 4 N, as already mentioned in the previous section. Printing at 50 mm/s and at nozzle temperatures of 190 °C and 200 °C failed to produce solid cuboids from PVA-K20, since only small amounts of material were extruded. Printing was accompanied by an audible sound of the filament slipping between the feeding gears, a strong indicator of an irregular process. This parameter combination, although resulting in high mean feed forces and a higher standard deviation, was still feasible in the feed force tester. This demonstrates that the tool is capable of identifying parameter combinations in advance to prevent increased wear of the feeding motor of the printer.

Mass reduction could be observed visually with X-ray microtomography measurements and is displayed for PVA-K20 at different parameter combinations in Fig. 5. It was apparent that cuboids were not completely solid but had small voids. The voids were located between printed lines and evenly distributed over the whole cuboid except for the bottom layer. The build plate of the printer was leveled manually, therefore it is likely that the distance between nozzle and build plate was slightly smaller than the stated layer height of 0.2 mm. This can lead to the material being pushed to the sides in the first layer and fusion of printed lines (Alhijjaj et al., 2019). In contrast, printed lines were not fully fused in xy-direction e.g., at 30 mm/s and 190 °C and 200 °C, resulting in large voids up to 220 μm . However, even at parameter combinations that resulted in a good fusion of printed lines (e.g., cuboids printed at 10 mm/s), small voids were still detectable. When round strands are placed next and on top of each other, cavities are created. These cavities appear to decrease with increasing nozzle temperature, which is probably a result of lower melt viscosity, which leads to more

pronounced spreading of the softened material after deposition. The proportion of voids also increased by either increasing the printing speed or decreasing the nozzle temperature. For cuboids printed at 10 mm/s the void space was approximately 1–3% of the total cuboid volume, 1–33% for cuboids printed at 30 mm/s and 3–5% for those parameter combinations where printing at 50 mm/s was possible. These data roughly correspond to the mean mass reduction of the cuboids. These results demonstrate that the mass reduction at certain parameter combinations was a result of continuous under extrusion over the whole printing process.

Regarding the proportion of KTZ in the formulations, lower nozzle temperatures were feasible with increasing KTZ proportion, resulting in feed forces < 4 N. This effect could also be attributed to a lower melt viscosity due to the addition of KTZ. The reduction of melt viscosity due to the addition of an API has been reported in earlier studies (Aho et al., 2019; Chivate et al., 2021; Elbadawi et al., 2020a; Solanki et al., 2018). This effect was already evident during extrusion, where a reduction of melt viscosity with increasing drug load was observed at the die and was further confirmed by determining the melt viscosities of the blends using a rheometer (Fig. 6). KTZ had a plasticizing effect, lowering the melt viscosity with increasing concentration, also explaining why extrusion and printing were feasible at lower temperatures. A sharp decrease in melt viscosity was observed at 203 °C, a few degrees above the melting point of the polymer (195 °C, see Section 3.2.2.2.). The lowest viscosity was observed at 223 °C, after which the viscosity only slightly increased. Since brown discolorations in the material were observed after the rheology measurements, it is likely that this increase is due to degradation of the polymer. Printing and feed force tests were also performed for PVA-K0 at temperatures > 230 °C, but no discoloration was observed. It is likely that the temperature of the material in the hotend is generally lower than the set nozzle temperatures due to the short transition times during testing and printing (Boetker et al., 2016; Ilyés et al., 2019).

3.2.2. Filament and tablet characterization

3.2.2.1. Mass conformity and dimension of tablets. Cylindrical tablets were printed at 30 mm/s at the lowest possible nozzle temperature that resulted in cuboids masses within the specification (Table 6). Tablet mass and dimension were uniform and did not result in tablets out of specification. Mean diameter of PVA-K0 tablets was in accordance with the CAD file, whereas the tablet height was slightly elevated, which was

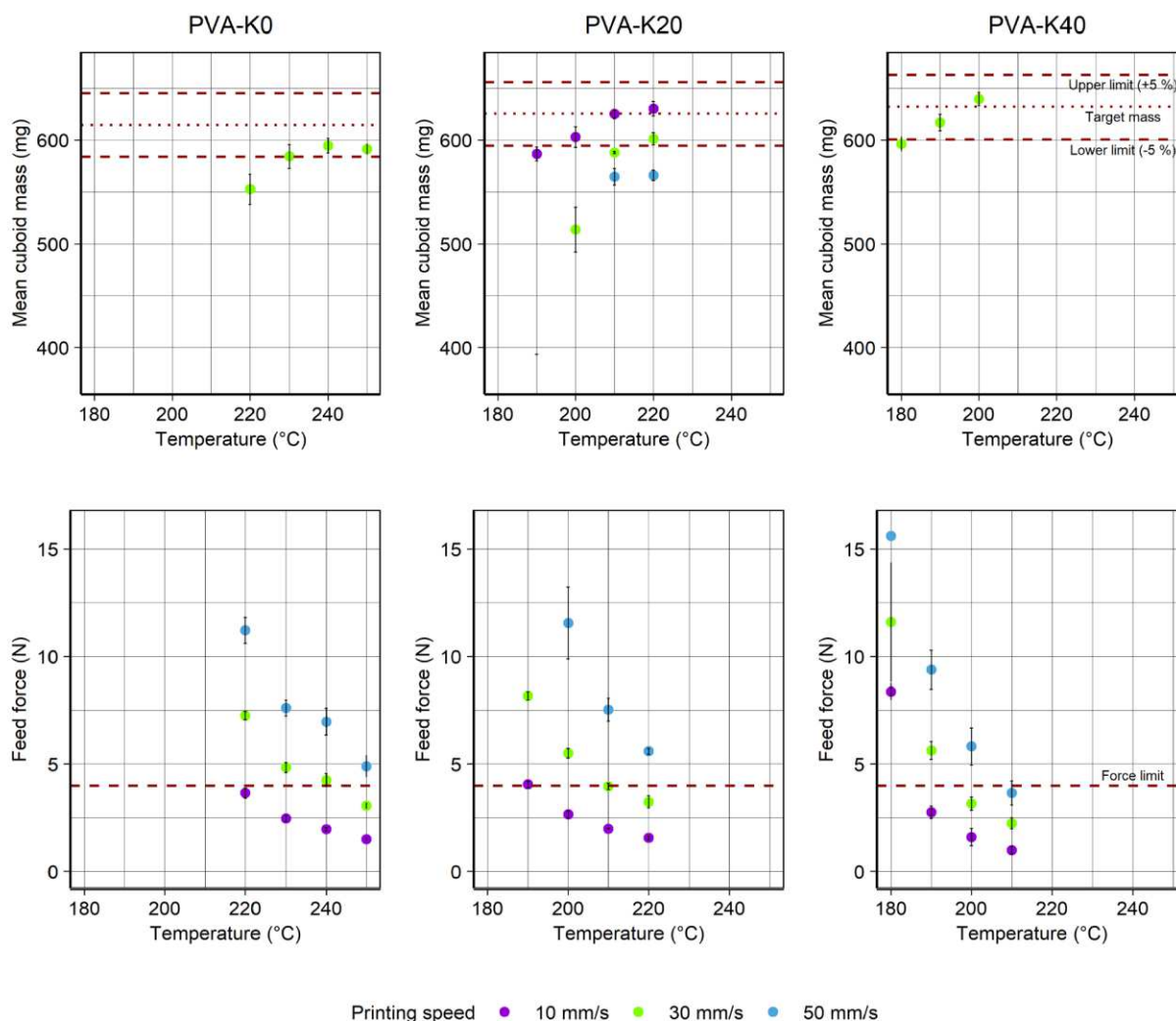


Fig. 4. Mean cuboid mass \pm SD ($n = 3$) and mean feed forces \pm SD ($n = 5$) of internally produced filament.

due to an uneven tablet surface caused by the hot nozzle during printing of the last layer. In contrast, tablet height of PVA-K20 and PVA-K40 corresponded to the initial design but the tablet diameter was slightly larger. Solidification of the softened material in these two cases was probably slightly slower compared to PVA-K0, potentially as a result of a lower melt viscosity.

3.2.2.2. Crystallinity assessment. PXRD (Fig. 7) indicated that filament and tablets were partially crystalline, which can be attributed to the semi-crystalline structure of PVA. The peak profile of the KTZ containing formulations was equal to the peak profile of extruded PVA. No peaks indicating crystalline KTZ were detected.

A broad melting peak was observed in DSC thermograms at approximately 195 °C, corresponding the melting point of PVA, which confirms PXRD results (Fig. 8). At the melting point of KTZ (150 °C), no endothermic event was observed for PVA-K20, demonstrating that KTZ was embedded in the amorphous state. In the case of PVA-K40 a peak at 150 °C was detected, indicating that traces of crystalline KTZ were still present, which were not detectable via PXRD, possibly due to a lower limit of detection. The glass transition temperature (T_g) of the composition decreased with increasing drug load from 69 °C to 60 °C (Table 7).

3.2.2.3. 3-Point bending test. The influence of KTZ addition on the mechanical properties of the filaments was assessed via a 3-point bending test. Here, a distinct influence of the proportion of KTZ in the formulation on the mechanical behavior of the filaments was observed (Fig. 9). Placebo filaments produced from PVA-K0 showed elastic deformation at low strains, turning into plastic deformation at higher strains. These filaments did not fracture during the test, whereas PVA-K20 filament fractured at strains of approximately 5%. PVA-K40 filaments showed brittle fracture already at strains around 2%, indicated by the linear increase and sudden drop of stress without plastic deformation prior to breakage. These results highlight that even though a decrease of T_g was observed, embrittlement of the material occurred. The embrittlement increased with increasing drug load. This is likely due to microstructural flaws in the polymer created by the addition of KTZ, which facilitate breakage (Argon and Cohen, 2003) in the polymer. Since a modified printer setup was used for printing where only longitudinal forces were applied to the filaments, printing of all formulations was feasible.

3.2.2.4. Dissolution and drug content. To ensure accurate dosing, it is necessary that the API is well distributed in the powder blend and segregation of the components does not occur during extrusion. The KTZ content of the blend, filament and tablets was compared and found to be

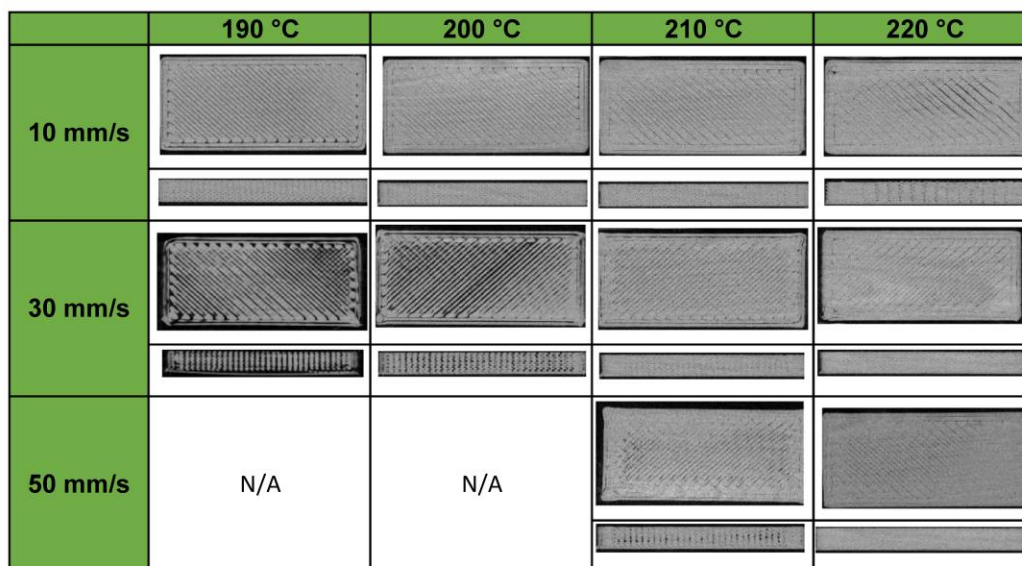


Fig. 5. X-ray microtomography slices of cuboids (top and side) from PVA-K20 at varying printing speeds and nozzle temperatures.

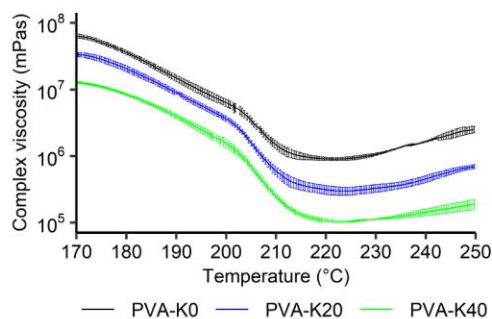


Fig. 6. Melt rheology of different blends containing PVA and KTZ over a temperature sweep of 170 °C to 250 °C (Mean complex viscosity \pm SD, $n = 3$).

Table 6

Mass of printed tablets. Arithmetic means \pm SD ($n = 20$).

	PVA-K0	PVA-K20	PVA-K40
Target mass (mg)	241.3	245.7	248.3
Mean mass (mg)	238.3 \pm 4.3	245.4 \pm 4.7	246.2 \pm 4.7
Mean height (mm)	2.52 \pm 0.07	2.40 \pm 0.03	2.41 \pm 0.05
Mean diameter (mm)	10.08 \pm 0.08	10.31 \pm 0.09	10.24 \pm 0.09
Mass deviation from target mass > 5%	0	0	0

similar (Table 8), except for the tablet content of the PVA-K20 formulation, which was slightly lower. This was mainly due to the content of one tablet and is reflected by the higher SD. No degradation of the API was observed after extrusion or printing. The SD after the different process steps was lowest for the blends and increased for filament and tablets, probably indicating segregation of KTZ and PVA during extrusion. The effect was more pronounced for the PVA-K40 formulation and could be due to the high proportion of KTZ. In this case, an increased feeding speed in the powder feeder was observed during extrusion.

Furthermore, the dissolution of tablets (Fig. 10) showed 80% release of the dose within 45 min in case of PVA-K40 and 120 min in case of PVA-K20. An increased release rate for PVA with increasing drug load was also described by Hasimi et al. (2014) and was reasoned to be caused by higher inter-chain mobility due to the plasticization of the API leading to accelerated water absorption. A drop of T_g was also observed with increasing amounts of KTZ and may explain the increase in drug release.

4. Conclusion and outlook

Herein, an empirical tool for the assessment of feed forces in the FDM process to gain deeper insights into the printing process was successfully developed, the results of which were then successfully transferred to an actual printing process. Furthermore, it was demonstrated that this tool was suitable for determining appropriate printing parameters by determining a feed force limit for the printer to specify the operable range. Printing below the feed force limit allowed reproducible printing of tablets within < 5% of the target mass. The proportion of KTZ in the pharmaceutical filaments had a high impact on melt viscosity. The feed force tester was able to detect these differences and the printing parameters could be adapted accordingly. Trial-and-error formulation development of filaments to enhance material and release properties is common and likely affects the melt viscosity of a formulation. By applying the developed feed force tester, printing parameters can be easily adapted to the respective formulation, reducing overall time and resource requirements in formulation development of 3D printed tablets.

In addition, it was demonstrated that optimization of the printing process in terms of printing time or nozzle temperatures is possible. FDM is a relatively slow manufacturing process and the time needed to print a single object is mainly defined by printing speed, which also determines the residence time of the filament in the hotend. By using the feed force tester, it is possible to reduce print time by accurately increasing the nozzle temperature. In addition, optimization of nozzle temperature when printing thermosensitive compounds can be achieved by decreasing the printing speed. Deviations in printed tablet mass from target masses is generally a result of specific printer limitations and the

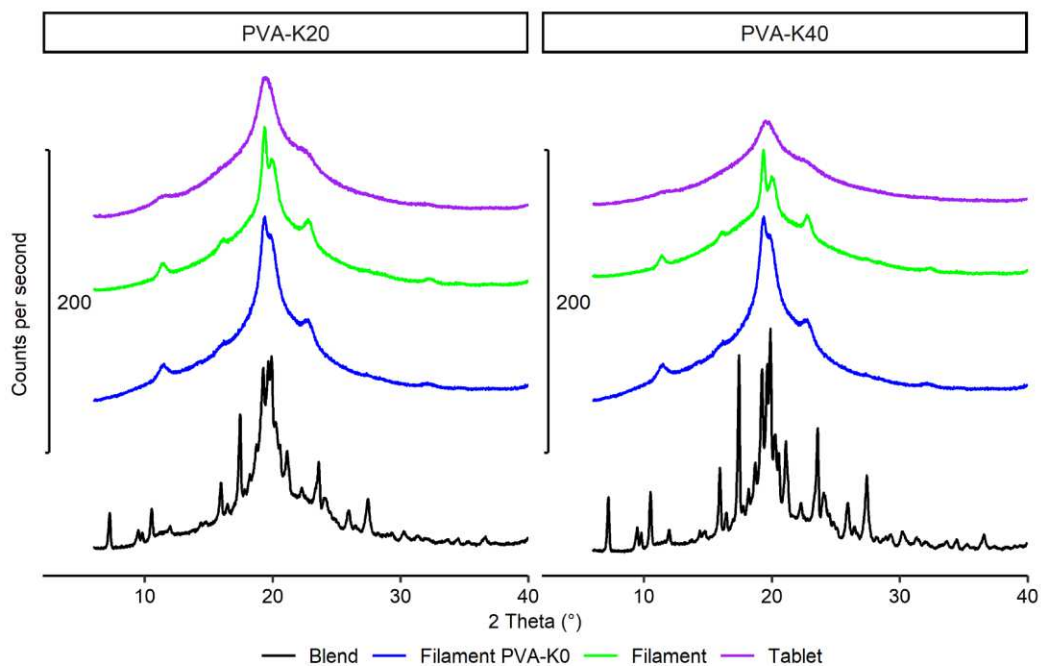


Fig. 7. PXRD results for blend, filament and tablets for PVA-K20 and PVA-K40.

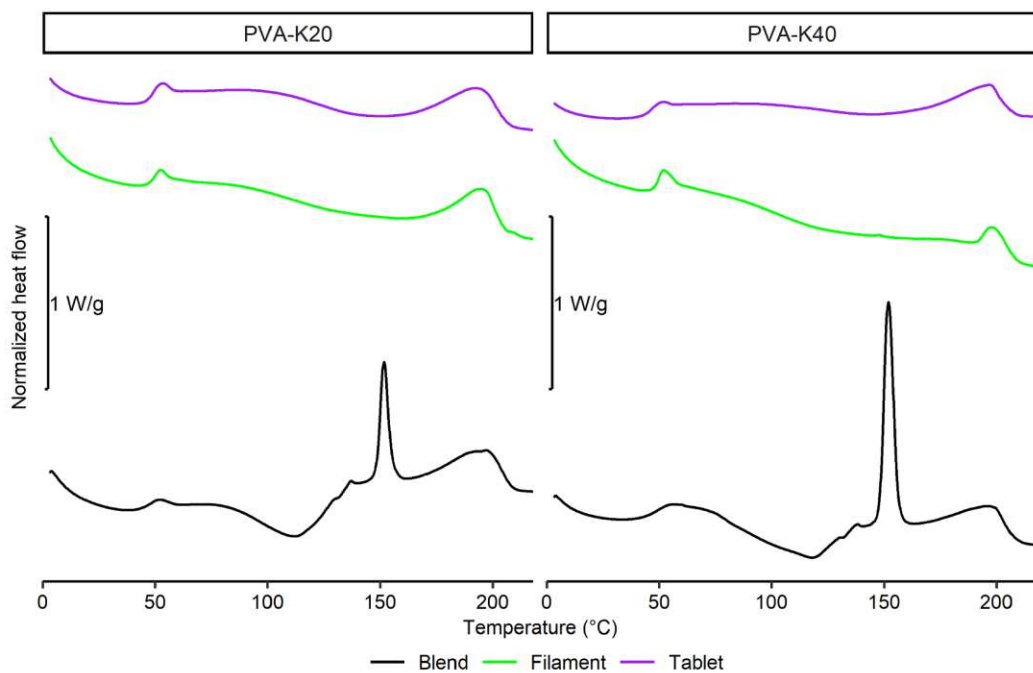


Fig. 8. DSC graphs of blend, filament and tablet for PVA-K20 and PVA-K40.

feed force limit determined in this study applies specifically to an Ultimaker 3 FDM printer. That said, such a limit is likely to be definable to any printer and nozzle type with just a few printing and feed force tests of readily available technical material.

Until now, the FDM printers being applied in the production of oral solid dosage forms are commercially available units, primarily targeted for the consumer sector. It has been highlighted that development of

pharmaceutical printers is necessary. It may be possible to implement sensors that measure the applied forces and distance for the forward propulsion of the filament. In addition, it would be possible to improve the feeding system to achieve higher forces in order to increase the printing speed even further. Nevertheless, printing speed will still be limited by the transition time that is necessary to ensure good heat transfer and softening of the material.

Table 7
T_g of different compositions from DSC ± SD, n = 3 (2nd heating cycle).

	T _g (°C)			
	PVA-K0	PVA-K20	PVA-K40	Pure KTZ
Blend	69.2 ± 0.1	64.0 ± 0.2	60.3 ± 0.1	47.7 ± 0.4
Filament	68.9 ± 0.2	64.2 ± 0.7	60.2 ± 0.1	–
Tablet	–	63.8 ± 0.2	59.8 ± 0.1	–

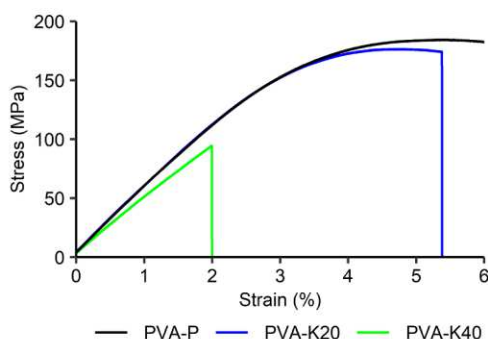


Fig. 9. Stress-strain profiles for different formulations of 3-point bending measurements.

Table 8
KTZ content for different formulations. Arithmetic means ± SD.

	KTZ Content (%)	
	PVA-K20	PVA-K40
Blend (n = 12)	19.4 ± 0.3	38.1 ± 0.8
Filament (n = 3) *	19.4 ± 0.5	37.9 ± 1.6
Tablets (n = 6)	18.8 ± 1.0	38.6 ± 1.6

* Filament content from middle of extrusion.

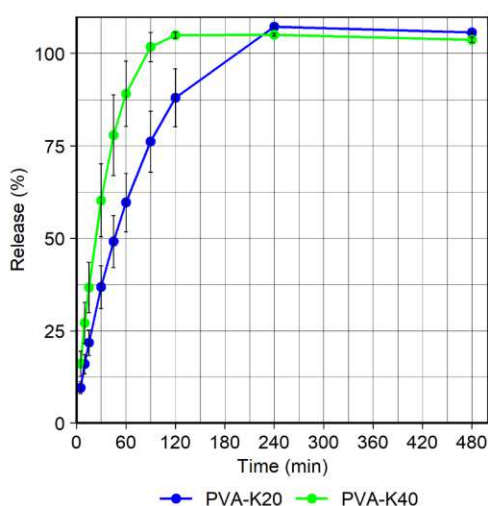


Fig. 10. Dissolution of tablets in 0.1 N HCl. Arithmetic means ± SD (n = 6).

CRediT authorship contribution statement

Nadine Gottschalk: Conceptualization, Investigation, Methodology, Formal analysis, Writing – original draft. **Julian Quodbach:** Conceptualization, Supervision, Writing – review & editing. **Alessandro-Giuseppe Elia:** Methodology. **Florian Hess:** Methodology. **Malte**

Bogdahn: Conceptualization, Supervision, Writing – review & editing.

Declaration of Competing Interest

The authors declare that they have no known competing financial interests or personal relationships that could have appeared to influence the work reported in this paper.

Acknowledgements

The authors would like to thank the initiative ProMatLeben by the German Federal Ministry of Education and Research (reference no. 13XP5064), who funded the work of this paper. The authors would also like to thank Christian Brenneis, Mara Balthasar, Torsten Friedmann and Sebastian Bollmann for their support with X-ray microtomography measurements.

Funding: This work was supported by the German Federal Ministry of Education and Research (reference no. 13XP5064).

Appendix A. Supplementary material

Supplementary data to this article can be found online at <https://doi.org/10.1016/j.ijpharm.2021.121416>.

References

- Aho, J., Bøtker, J.P., Genina, N., Edinger, M., Arnfast, L., 2019. Roadmap to 3D-Printed Oral Pharmaceutical Dosage Forms: Feedstock Filament Properties and Characterization for Fused Deposition Modeling. *J. Pharm. Sci.* 108, 26–35. <https://doi.org/10.1016/j.xphs.2018.11.012>.
- Alhijaj, M., Nasereddin, J., Belton, P., Qi, S., 2019. Impact of Processing Parameters on the Quality of Pharmaceutical Solid Dosage Forms Produced by Fused Deposition Modeling (FDM). *Pharmaceutics* 11, 633. <https://doi.org/10.3390/pharmaceutics11120633>.
- Alsoufi, M.S., Alhazmi, M.W., Suker, D.K., Alghamdi, T.A., 2019. Experimental Characterization of the Influence of Nozzle Temperature in FDM 3D Printed Pure PLA and Advanced PLA +. *Am. J. Mech. Eng.* 7 (2), 45–60.
- Argon, A.S., Cohen, R.E., 2003. Toughenability of polymers. *Polymer (Guildf)*. 44 (19), 6013–6032. [https://doi.org/10.1016/S0032-3861\(03\)00546-9](https://doi.org/10.1016/S0032-3861(03)00546-9).
- Boetker, J., Water, J.J., Aho, J., Arnfast, L., Bohr, A., Rantanen, J., 2016. Modifying release characteristics from 3D printed drug-eluting products. *Eur. J. Pharm. Sci.* 90, 47–52. <https://doi.org/10.1016/j.ejps.2016.03.013>.
- Butt, J., Bhaskar, R., Mohaghegh, V., 2021. Investigating the effects of extrusion temperatures and material extrusion rates on FFF-printed thermoplastics. *Int. J. Adv. Manuf. Technol.* 117, 2679–2699. <https://doi.org/10.1007/s00170-021-07850-5>.
- Cailleaux, S., Sanchez-ballester, N.M., Gueche, Y.A., Bataille, B., Soulaïrol, I., 2021. Fused Deposition Modeling (FDM), the new asset for the production of tailored medicines. *J. Control. Release* 330, 821–841. <https://doi.org/10.1016/j.jconrel.2020.10.056>.
- Chivate, A., Garkal, A., Hariharan, K., Mehta, T., 2021. Journal of Drug Delivery Science and Technology Exploring novel carrier for improving bioavailability of Itraconazole: Solid dispersion through hot-melt extrusion. *J. Drug Deliv. Sci. Technol.* 63, 102541. <https://doi.org/10.1016/j.jddst.2021.102541>.
- Chung, M., Radacs, N., Robert, C., McCarthy, E.D., Callanan, A., Conlisk, N., Hoskins, P. R., Koutsos, V., 2018. On the optimization of low-cost FDM 3D printers for accurate replication of patient-specific abdominal aortic aneurysm geometry. *3D Print. Med.* 4 <https://doi.org/10.1186/s41205-017-0023-2>.
- Coogan, T.J., Kazmer, D.O., 2019. In-line rheological monitoring of fused deposition modeling. *J. Rheol.* 63 (1), 141–155. <https://doi.org/10.1122/1.5054648>.
- Crîșan, A.G., Porfire, A., Ambrus, R., Katona, G., Rus, L.M., Porav, A.S., Ilyés, K., Tomuță, I., 2021. Polyvinyl alcohol-based 3d printed tablets: Novel insight into the influence of polymer particle size on filament preparation and drug release performance. *Pharmaceutics* 14, 418. <https://doi.org/10.3390/ph14050418>.
- Dong, W., Wang, Y., Huang, C., Xiang, S., Ma, P., Ni, Z., Chen, M., 2014. Enhanced thermal stability of poly (vinyl alcohol) in presence of melanin. *J. Therm. Anal. Calorim.* 115 (2), 1661–1668. <https://doi.org/10.1007/s10973-013-3419-2>.
- Dumpa, N., Butreddy, A., Wang, H., Komanduri, N., Bandari, S., Repka, M.A., 2021. 3D printing in personalized drug delivery: An overview of hot-melt extrusion-based fused deposition modeling. *Int. J. Pharm.* 600, 120501. <https://doi.org/10.1016/j.ijpharm.2021.120501>.
- Dumpa, N.R., Bandari, S., Repka, M.A., 2020. Novel Gastroretentive Floating Pulsatile Drug Delivery System Produced via Hot-Melt Extrusion and Fused Deposition Modeling 3D Printing. *Pharmaceutics* 12, 52 <https://doi.org/10.3390/ph12050418>.
- Elbadawi, M., 2018. Polymeric Additive Manufacturing: The Necessity and Utility of Rheology. *Polymer Rheology*. 45–46. <https://doi.org/10.5772/intechopen.77074>.

- Elbadawi, M., Gustaffson, T., Gaisford, S., Basit, A.W., 2020a. 3D printing tablets: Predicting printability and drug dissolution from rheological data. *Int. J. Pharm.* 590, 119868. <https://doi.org/10.1016/j.ijpharm.2020.119868>.
- Elbadawi, M., Muñiz Castro, B., Gavins, F.K.H., Ong, J.J., Gaisford, S., Pérez, G., Basit, A.W., Cabalar, P., Goyanes, A., 2020b. M3DISEEN: A novel machine learning approach for predicting the 3D printability of medicines. *Int. J. Pharm.* 590, 119837. <https://doi.org/10.1016/j.ijpharm.2020.119837>.
- Gotschalk, N., Bogdahn, M., Harms, M., Quodbach, J., 2021. Brittle polymers in Fused Deposition Modeling: An improved feeding approach to enable the printing of highly drug loaded filament. *Int. J. Pharm.* 597, 120216. <https://doi.org/10.1016/j.ijpharm.2021.120216>.
- Goyanes, A., Robles Martinez, P., Buanz, A., Basit, A.W., Gaisford, S., 2015. Effect of geometry on drug release from 3D printed tablets. *Int. J. Pharm.* 494 (2), 657–663. <https://doi.org/10.1016/j.ijpharm.2015.04.069>.
- Hasimi, A., Papadokostaki, K.G., Sanopoulou, M., 2014. Mechanisms of diphyllyne release from dual-solute loaded poly(vinyl alcohol) matrices. *Mater. Sci. Eng. C* 34, 369–376. <https://doi.org/10.1016/j.msec.2013.09.027>.
- Hernandez, D.D., 2015. Factors Affecting Dimensional Precision of Consumer 3D Printing. *Int. J. Aviat. Aeronaut. Aerosp.* 2 <https://doi.org/10.15394/ijaaa.2015.1085> 6.
- Holland, B.J., Hay, J.N., 2001. The thermal degradation of poly (vinyl alcohol). *Polymer (Guildf)*. 42, 6775–6783. [https://doi.org/10.1016/S0032-3861\(01\)00166-5](https://doi.org/10.1016/S0032-3861(01)00166-5).
- Ilyés, K., Krisztián, N., Balogh, A., Farkas, B., 2019. The applicability of pharmaceutical polymeric blends for the fused deposition modelling (FDM) 3D technique: Material considerations – printability – process modulation, with consecutive effects on in vitro release, stability and degradation. *Eur. J. Pharm. Sci.* 129, 110–123. <https://doi.org/10.1016/j.ejps.2018.12.019>.
- Kanaujia, P., Lau, G., Ng, W.A.L.K., Widjaja, E., Hanefeld, A., Fischbach, M., Maio, M., Tan, R.B.H., 2011. Nanoparticle Formation and Growth During In Vitro Dissolution of Ketoconazole Solid Dispersion. *J. Pharm. Sci.* 100, 2876–2885. <https://doi.org/10.1002/jps.10837450.2018.1433208>.
- Korte, C., Quodbach, J., 2018a. Formulation development and process analysis of drug-loaded filaments manufactured via hot-melt extrusion for 3D-printing of medicines. *Pharm. Dev. Technol.* 23 (10), 1117–1127. <https://doi.org/10.1080/10837450.2018.1433208>.
- Korte, C., Quodbach, J., 2018b. 3D-Printed Network Structures as Controlled-Release Drug Delivery Systems: Dose Adjustment, API Release Analysis and Prediction. *AAPS PharmSciTech* 19, 3333–3342. <https://doi.org/10.1208/s12249-018-1017-0>.
- Melocchi, A., Parietti, F., Loreti, G., Maroni, A., Gazzaniga, A., Zema, L., 2015. Journal of Drug Delivery Science and Technology 3D printing by fused deposition modeling (FDM) of a swellable / erodible capsular device for oral pulsatile release of drugs. *J. Drug Deliv. Sci. Technol.* 30, 360–367. <https://doi.org/10.1016/j.jddst.2015.07.016>.
- Muñiz Castro, B., Elbadawi, M., Jie, J., Pollard, T., Song, Z., Gaisford, S., Gilberto, P., Basit, A.W., Cabalar, P., Goyanes, A., 2021. Machine learning predicts 3D printing performance of over 900 drug delivery systems. *J. Control. Release* 337, 530–545. <https://doi.org/10.1016/j.jconrel.2021.07.046>.
- Pereira, G.G., Figueiredo, S., Fernandes, A.I., Pinto, J.F., 2020. Polymer Selection for Hot-Melt Extrusion Coupled to Fused Deposition Modelling in Pharmaceutics. *Pharmaceutics* 12 (9), 795. <https://doi.org/10.3390/pharmaceutics12090795>.
- Ponsar, H., Wiedey, R., Quodbach, J., 2020. Hot-Melt Extrusion Process Fluctuations and Their Impact on Critical Quality Attributes of Filaments and 3D-Printed Dosage Forms. *Pharmaceutics* 12, 511. <https://doi.org/10.3390/pharmaceutics12060511>.
- Prasad, E., Islam, M.T., Goodwin, D.J., Megarry, A.J., Halbert, G.W., Florence, A.J., Robertson, J., 2019. Development of a hot-melt extrusion (HME) process to produce drug loaded Affinisol™ 15LV filaments for fused filament fabrication (FFF) 3D printing. *Addit. Manuf.* 29, 100776. <https://doi.org/10.1016/j.addma.2019.06.027>.
- Prasad, L.K., Smyth, H., Prasad, L.K., Smyth, H., 2016. 3D Printing technologies for drug delivery: a review 3D Printing technologies for drug delivery: a review. *Drug Dev. Ind. Pharm.* 42, 1019–1031. <https://doi.org/10.3109/03639045.2015.1120743>.
- Quodbach, J., Bogdahn, M., Breikreutz, J., Chamberlain, R., Eggenreich, K., Kapote, D., Kipping, T., Klinken, S., Loose, F., Marquetant, T., Windolf, H., 2021. Quality of FDM 3D Printed Medicines for Pediatrics: Considerations for Formulation Development, Filament Extrusion, Printing Process and Printer Design. *Ther. Innov. Regul. Sci.* <https://doi.org/10.1007/s43441-021-00354-0>.
- Simon, T.R., Lee, W.J., Spurgeon, B.E., Boor, B.E., Zhao, F., 2018. An Experimental Study on the Energy Consumption and Emission Profile of Fused Deposition Modeling Process. *Procedia Manuf.* 26, 920–928. <https://doi.org/10.1016/j.promfg.2018.07.119>.
- Solanki, N.G., Shah, A.V., Serajuddin, A.T.M., 2018. Formulation of 3D Printed Tablet for Rapid Drug Release by Fused Deposition Modeling: Screening Polymers for Drug Release, Drug-Polymer Miscibility and Printability. *J. Pharm. Sci.* 107, 390–401. <https://doi.org/10.1016/j.xphs.2017.10.021>.
- Taupitz, T., Dressman, J.B., Klein, S., 2013. In Vitro Tools for Evaluating Novel Dosage Forms of Poorly Soluble, Weakly Basic Drugs: Case Example Ketoconazole. *Pharm. Drug Deliv. Pharm. Technol.* 102, 3645–3652. <https://doi.org/10.1002/jps.23666>.
- Tool, R., Thakkar, R., Pillai, A.R., Zhang, J., Zhang, Y., Kulkarni, V., Maniruzzaman, M., 2020. Tablets Using Fill Density as an Effective. *Polymers (Basel)*. 12, 1–21. <https://doi.org/10.3390/polym12091872>.
- Windolf, H., Chamberlain, R., Quodbach, J., 2021. Predicting drug release from 3D printed oral medicines based on the surface area to volume ratio of tablet geometry. *Pharmaceutics* 13, 1453. <https://doi.org/10.3390/pharmaceutics13091453>.
- Wu, J., Chen, N., Bai, F., Wang, Q.L., 2018. Preparation of poly(vinyl alcohol)/poly(lactic acid)/hydroxyapatite bioactive nanocomposites for fused deposition modeling. *Polym. Compos.* 39, E508–E518. <https://doi.org/10.1002/pc.24642>.
- Zhang, J., Feng, X., Patil, H., Tiwari, R.V., Repka, M.A., 2017. Coupling 3D printing with hot-melt extrusion to produce controlled-release tablets. *Int. J. Pharm.* 519 (1–2), 186–197. <https://doi.org/10.1016/j.ijpharm.2016.12.049>.

3.1.3. Extrusion and printing of the pipeline substance peposertib

3.1.3.1. Introduction

Peposertib is a poorly soluble drug substance, which is currently in clinical trials at Merck. In order to achieve immediate release tablets and a good bioavailability, solubility enhancement is necessary. In addition, high doses of API are potentially required, leading to a high number of tablets that have to be taken by the patients in clinical trials. To reduce the pill burden, tablets with high drug loads are preferred. The 3DP technique FDM was evaluated for the manufacturing of peposertib SODFs as it combines two important benefits, which may prove effective in this case. First, the amorphization of the poorly soluble API in a melt-based process. Second, directly printing the highly drug loaded extrudate into dosage forms with high dosages. However, peposertib has a high melting point of 207 °C and degrades shortly after melting, which complicates the manufacturing of a fully amorphous formulation with also a low number of impurities. Therefore, the effects of extrusion process parameters and print parameters on the purity will be discussed in the following sections. Tablets were characterized with regards to solid-state, purity and drug release. Moreover, this formulation was further used to test the applicability of the feed force tester and the modified printer setup, which have been described in the previous sections, and discuss their benefits and limitations for the development of a poorly soluble pipeline compound.

3.1.3.2. Results and discussion

Extrusion of peposertib

A compacted powder blend with improved flow properties, compared to the physical mixture of peposertib and copovidone, was used for extrusion, which is further referred to as “compactate”. The polymer copovidone was used in the formulation as Flügel et al. (2021) suggested good miscibility of API and polymer, which would facilitate embedding of peposertib in the polymer matrix below its melting point (Guo et al., 2014; Marsac et al., 2006). Peposertib degrades upon melting at approximately 210 °C, wherefore extrusion was performed below the melting temperature of peposertib to reduce molecular degradation. Further, the aim was to produce fully amorphous extrudate during extrusion, since trials by Gottschalk et al. (2021) had shown that amorphization in the hotend is challenging due to low transition times and the lack of mechanical energy input. In order to obtain an amorphous filament with low quantities of impurities, high screw speeds were utilized to ensure high shearing and mixing of the components and facilitate dissolution of peposertib in the polymer matrix. DSC measurements showed a melting point depression, indicating dissolution of peposertib in copovidone at an onset of approximately 150 °C – 160 °C, wherefore an initial barrel temperature of 160 °C was chosen.

Figure 6 displays the reduction of residual crystallinity of the API in the extrudate with increasing screw speeds from 300 to 600 rpm. Barrel and die temperatures were adapted in the range of 160 – 170 °C and 170 – 180 °C, respectively, to aid the amorphization process. At screw speeds of 600 rpm and 160 °C the extrudate showed still traces of crystallinity. An increase in extrusion temperature to 170 °C and die temperature up to 175 °C was necessary to achieve a fully amorphization. DSC and XRPD measurements confirmed this observation (data not shown). Several publications showed the influence of high shearing on reducing the degree of crystallinity as a result of high mechanical energy input (Evans et al., 2018; Huang et al., 2017; Hughey et al., 2010). The die temperature was further increased to 180 °C to improve filament diameter uniformity. However, a color change from bright yellow to a darker yellow was observed as well as a trend in terms of peposertib content, which decreased gradually with increasing screw speeds (Figure 7). The chromatogram showed several impurities of which the oxidized form, where the secondary hydroxylic group is oxidized to the ketone, was the most pronounced impurity. The “ketone impurity” increased corresponding to the decrease in peposertib with increasing screw speeds. Matić et al. (2020) also reported an increase in screw speed leading to API degradation. An increase in screw speed increases the specific mechanical energy input (SME), which is proportional to the screw speed (Thompson and Williams, 2021).

$$SME \left(\frac{kJ}{kg} \right) = \frac{KW (applied)}{Feed\ rate \left(\frac{kg}{h} \right)} \quad (2)$$

$$KW (applied) = Motor\ rating (kW) * Torque (\%) * 0.97 * \frac{Screw\ speed\ running (rpm)}{Screw\ speed\ max (rpm)} \quad (3)$$

Motor rating refers to the maximum power the engine can exert. High mechanical energy will also translate in thermal energy (Schenck et al., 2019) and can promote degradation reactions such as oxidation. However, high screw speeds also facilitate amorphization of the API, wherefore sweet spot identification is crucial.

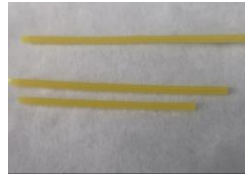
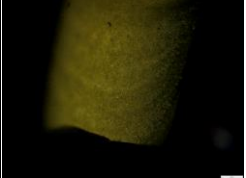

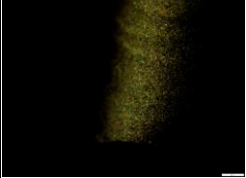
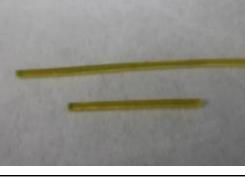
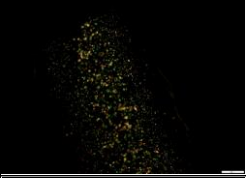


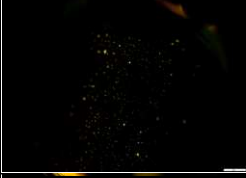



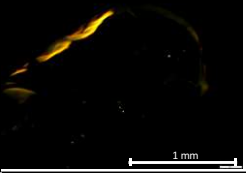
Test run	Barrel temperature (°C)	Die temperature (°C)	Screw speed (rpm)	Images of filaments	Polarized light image (5x magnification)	Comments
1.1	160	170	300			- Filament not transparent - Birefringence
1.2	160	170	400			- Filament not transparent - Birefringence
1.3	160	170	500			- Filament transparent - Birefringence
1.4	165	170	500			- Filament transparent - Birefringence
2.1	165	170	600	-		- Filament transparent - Few birefringent spots
2.5	170	170	600	-		- Filament transparent - Few birefringent spots
2.6	170	175	600	-		- Filament transparent - No birefringent spots
2.7	170	180	600			- Filament transparent - Few birefringent spots due to air bubbles

Figure 6: Images of melt extrudate containing copovidone and peposertib at different extrusion settings

Adding to this, the use of copovidone and already contained peroxides could have contributed to drug oxidation. Copovidone forms peroxides upon contact with atmospheric oxygen and the amount can increase upon storage (Bühler, 2005). Butreddy et al. (2021) and Sarabu et al. (2022) demonstrated in their studies the effect of peroxide levels in copovidone on drug oxidation. The authors demonstrated that even though peroxides levels were below the limit defined by the Ph. Eur. (400 ppm), pronounced drug oxidation was observed in comparison to a copovidone grade with lower peroxide levels.

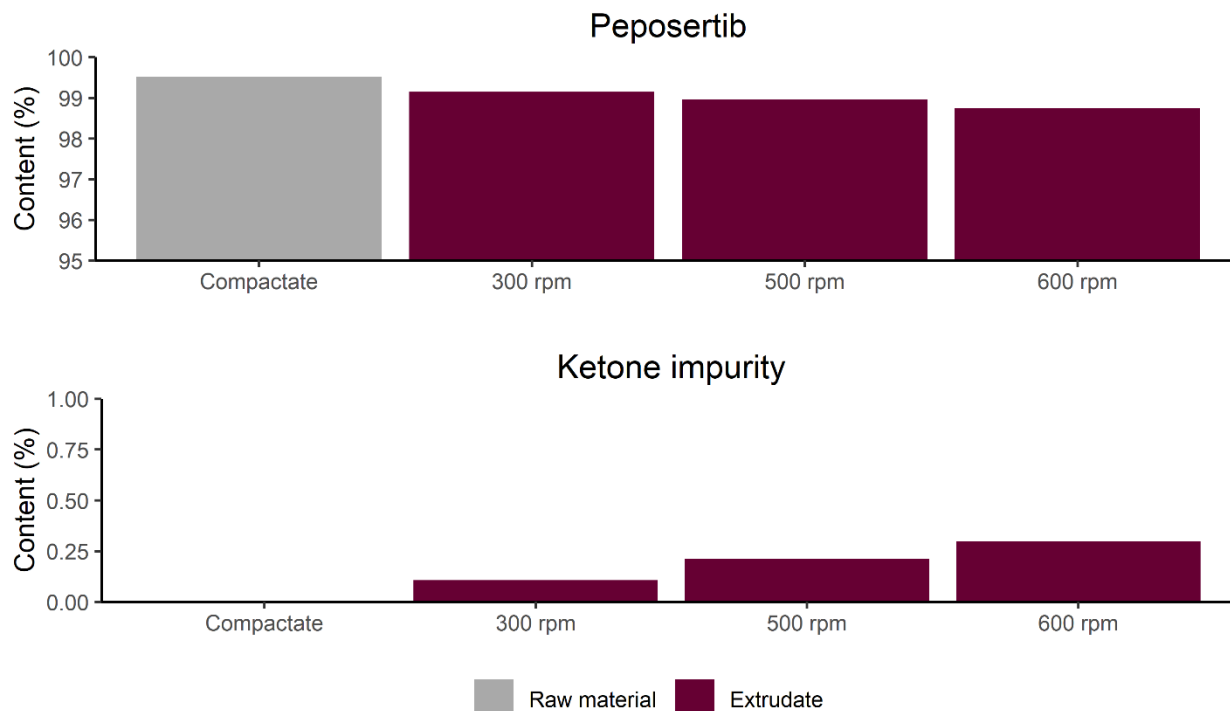


Figure 7: Peposertib content (top) and ketone impurity (bottom) of compactate and extruded material processed at different screw speeds related to extrusion run 1.1,1.3,2.7 (n = 1)

The fluctuations of filament diameter were approximately in the range of ± 0.15 mm instead of the targeted ± 0.05 mm. It was reported that high screw speeds negatively correlate with the filament diameter uniformity (Ponsar et al., 2020) by reducing the barrel filling. Regarding the experiment runs 2.1 – 2.7, which had been performed at 600 rpm, the powder feed rate was increased from 0.2 kg/h to 0.3 kg/h to compensate this effect. Still, filament diameter fluctuations were comparably high. Due to the narrow extrusion window in which amorphous filaments were obtained and limited amount of material, the extrusion process was not further optimized. For the following experiments only filament sticks in a range of ± 0.1 mm were selected.

Printing of peposertib

The extrudate was very brittle and showed a low strain at break of $1.57 \% \pm 0.44 \%$. The strain at break was in between a 20 % and 40 % drug loaded formulation of copovidone and ketoconazole (20 %: $2.5 \% \pm 0.6 \%$; 40 %: $0.7 \% \pm 0.1 \%$). Due to the high brittleness the formulation was not printable using the conventional feeding mechanism, requiring the modified printer setup from Gottschalk et al. (2021). Feed force analysis at 30 mm/s indicated that nozzle temperatures greater than 170 °C were necessary for printing as forces of approximately 4 N and smaller were reached (Table 1).

Table 1: Feed forces of peposertib extrudate at 30 mm/s (n = 3)

Nozzle temperature	170 °C	180 °C	190 °C
Feed force (N)	4.26	2.20	1.04
SD (N)	0.27	0.06	0.09

Even though this formulation was similar in terms of composition and mechanical properties to the formulations containing ketoconazole, printing of peposertib was more challenging. The formulation containing peposertib showed poor adhesion to the build plate and poor inter-layer bonding leading to full or partial detachment of tablets during printing. Flügel et al. (2021) investigated the mechanical properties of peposertib and ketoconazole in copovidone and found that peposertib formulations resulted in a higher hardness and resistance to deformation compared to equivalent formulations containing ketoconazole. The reason for this was attributed to the strong intermolecular interaction between peposertib and copovidone, due to the ability of the hydroxylic group in peposertib to form hydrogen bonds with copovidone. These strong intermolecular interactions and resulting mechanical properties could possibly also lead to poor build plate adhesion and inter-layer bonding in FDM printing. In order to enable reproducible printing, several attempts have been assessed:

- Increasing the build plate temperature from 60 °C up to 85 °C to reduce contractions of the molten material and increase area of contact between material and build plate.
- Application of adhesion tape.
- Increasing the nozzle temperature with the aim to decrease the melt viscosity and enhance layer spreading on the build plate.
- Reducing the printing speed to 10 mm/s, which presumably has two effects: first to prevent fast jerky movements of the printhead to reduce vibrations and second, prolonging transition times of filament in the nozzle and reduce the melt viscosity.

An increase of build plate temperature alone or in combination with increasing printing temperatures did not lead to sufficient build plate adhesion. Tablets did either detach immediately after the first layer or during the print. In case of 180 °C and 185 °C nozzle temperature and 80 °C and 70 °C build plate temperature, respectively, the printing of a single full tablet was possible, but printing could not be reproduced. It has to be added that leveling of the build plate was performed manually and it is likely that even small changes in the distance between nozzle and build plate can have a huge effect on the adhesion of the material. Alhijaj et al. (2019) and Melocchi et al. (2016) reported a significant influence on object dimension and mass, when the build plate was leveled by different operators or at different days.

Three cases are possible when the leveling is performed (Figure 8):

1. The distance of nozzle to build plate equals the set layer height (ideal case)
2. The distance between nozzle and build plate is larger than the set layer height
3. The distance between nozzle and build plate is smaller than the set layer height

If the distance between nozzle and build plate is too large the extruded strand is not pressed onto the surface and the contact area is small, which increases the probability of detaching during the print (case 2). However, if the actual distance between nozzle and build plate is smaller than the set first layer height material is squeezed to the side leading to an uneven surface with small parts sticking out (case 3). The objects detach in the next layer when the nozzle bumps into these parts. Next to that, the build plate of the Ultimaker is made of glass, which was described to lead to reduced spreading of the first layer (Alhijaj et al., 2019), further reducing adhesion. The application of adhesion tape with a rough surface increased the adhesion to the build plate. However, it became apparent that brittleness of the material led to breaking of tablets during printing (Figure 9a) and poor inter-layer cohesion of the formulation was further leading to layer separation (Figure 9b). Even small vibrations during printing can lead to cracks of the printed material. Therefore, the printing speed had been decreased to 10 mm/s to reduce vibrations. However, printing at nozzle temperatures ranging from 170 °C to 180 °C resulted into bubble formation, indicated by the opaque appearance of the tablet (Figure 9c). This phenomenon had also been observed in Gottschalk et al. (2022) for polyvinyl alcohol filaments. Copovidone is, like polyvinyl alcohol, a hygroscopic polymer and it is likely that residual moisture in the filaments vaporizes at high printing temperatures. This is facilitated by the low melt viscosity as a result of increased residence time in the hotend at low printing speeds and high nozzle temperatures. Bubble formation did further exacerbate the adhesion to the build plate and inter-layer bonding. Nevertheless, printing tablets at a lower nozzle temperature (165 °C), where no bubble formation was observed, also led to

tablet detachment. A possible explanation for this might be the low printing speed. In case of slow printing material overextrusion is more likely due to higher residence times in the nozzle and low melt viscosities, leading to non-uniform print lines and material parts sticking out. This may also lead to detachment as soon as the nozzle bumps into these outstanding parts (similar to case 3 in Figure 8).

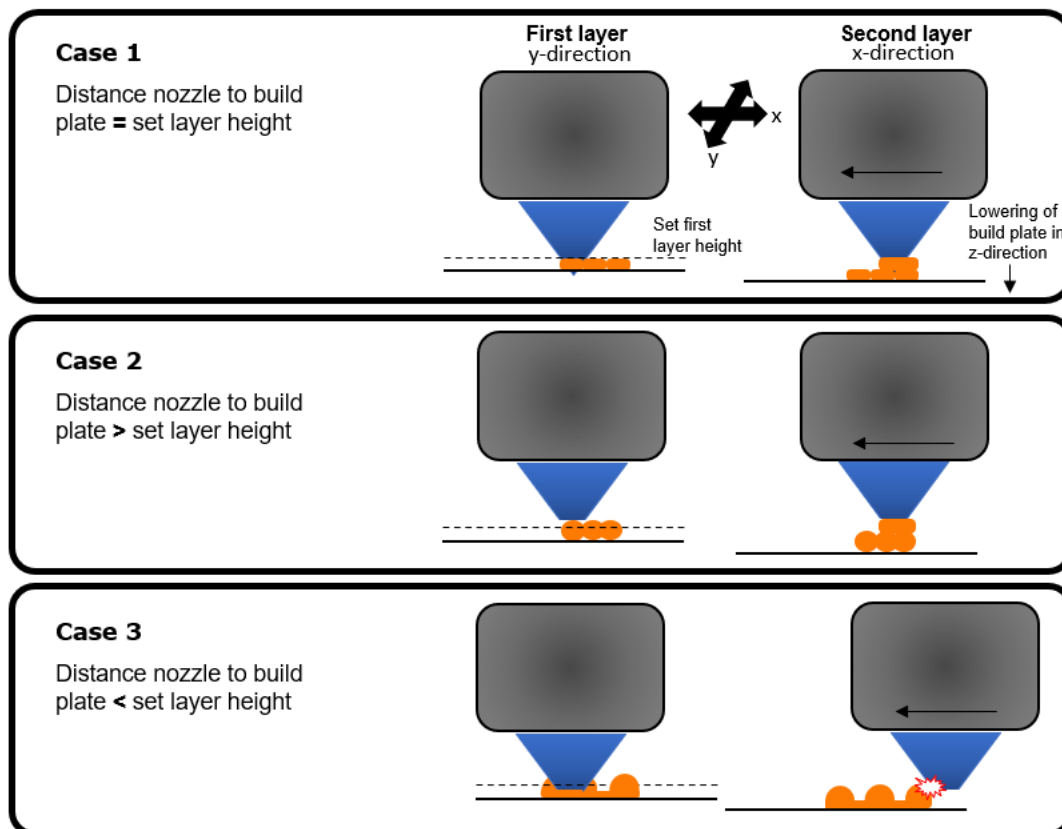


Figure 8: Possible cases for deposition of the first layer dependent on leveling of the build plate

From these observations, process parameters were selected that enabled reproducible printing. These were printing at a lower temperature (165 °C) and at 30 mm/s to reduce the probability of material overextrusion, printing on adhesion tape and the addition of ten circle lines that were connected to the tablet to further enhance adhesion (Figure 9d). Next to identification of suitable print parameters, the influence of the different settings on the purity profile of peposertib was investigated. Figure 10 displays the content of peposertib and the ketone impurity in tablets, material after the feed force test, extrudate and compactate. Enhanced oxidation at 185 °C and 190 °C was observed for printed tablets compared to the extrudate.

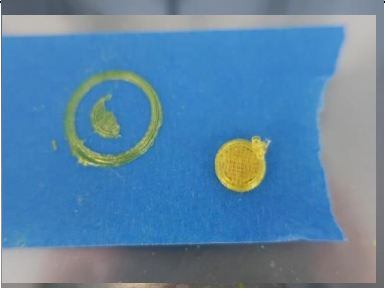
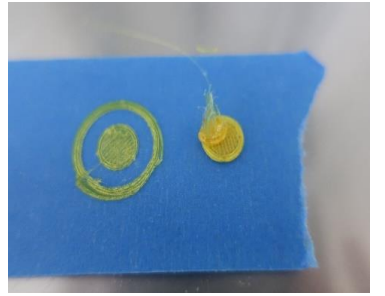

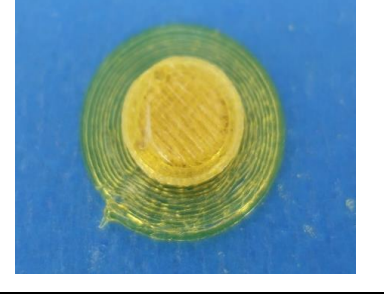
#	Observations	Temperature [°C]		Print speed (mm/s)	Appearance
		Printcore	Build plate		
a	Brittleness	165	70	10	
b	Layer-layer separation	165	80	10	
c	Air bubbles in tablet	175	70	30	
d	Tablet with brim	165	70	30	

Figure 9: Printing observations

Interestingly, extruded samples from the feed force tester showed no enhanced oxidation. In the feed force tester material is simply pushed through, whereas in case of printing the nozzle is in longer contact with the material. Printing of an additional layer onto a freshly printed layer and slower cooling rates are likely to increase thermal stress and promote formation of impurities. These results indicate that not only the residence time in the hotend is decisive for the thermal stress on the formulation and all print parameters should be considered in terms of impurities of heat-sensitive APIs.

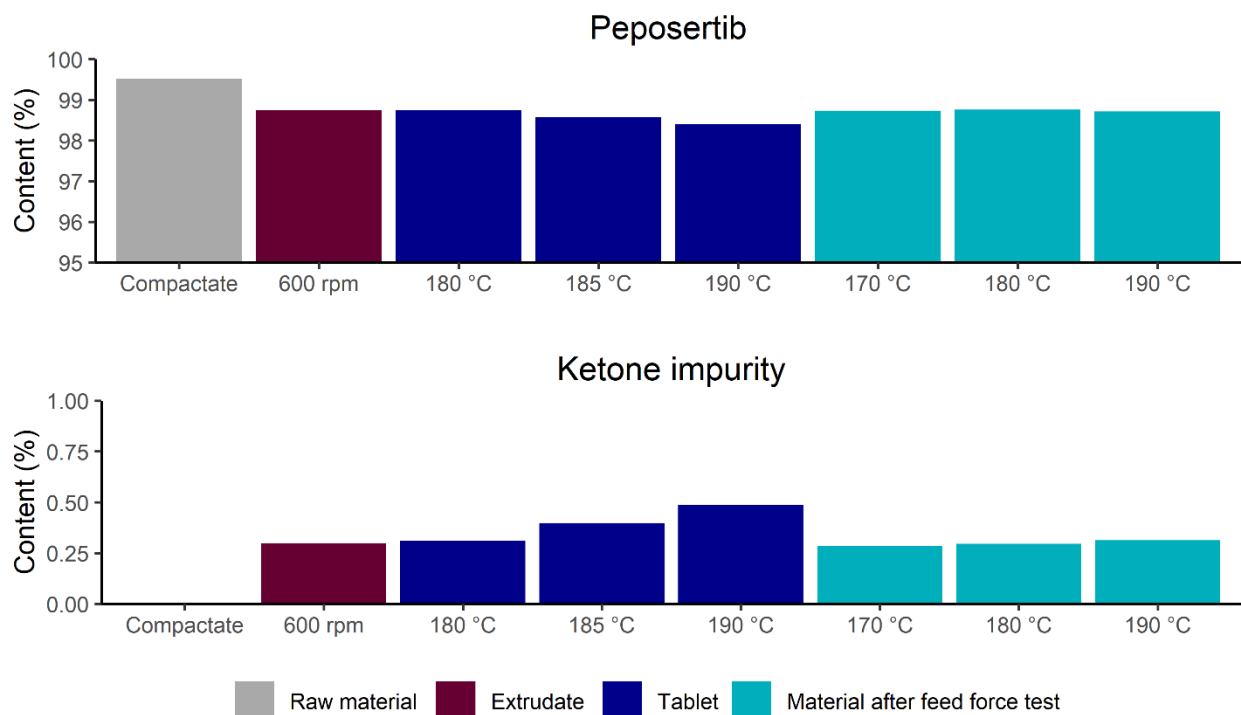


Figure 10: Peposertib content (top) and ketone impurity (bottom) of compactate, extrudate (extrusion run 2.7), printed samples (related to print run 5, 6 and 9) and samples after assessment in feed force tester (n = 1)

Tablet characterization

In total, 23 tablets were printed with an average mass of $223.5 \text{ mg} \pm 7.7 \text{ mg}$. One of the tablets differed more than 7.5% of the mean mass, however, the pharmacopeia test “Uniformity of mass” (Ph. Eur. 2.9.5.) was passed. A slightly lower nozzle temperature was selected than the nozzle temperature selected with the feed force tester. It was shown in Gottschalk et al., (2022) that printing at process parameters that result in feed forces $> 4 \text{ N}$ can lead to higher fluctuations in tablet mass, which is a possible explanation for the higher deviation.

Solid state characterization via PLM indicated that tablets were fully amorphous (Figure 11). The amorphous state was further confirmed by DSC and XRPD (data not shown).

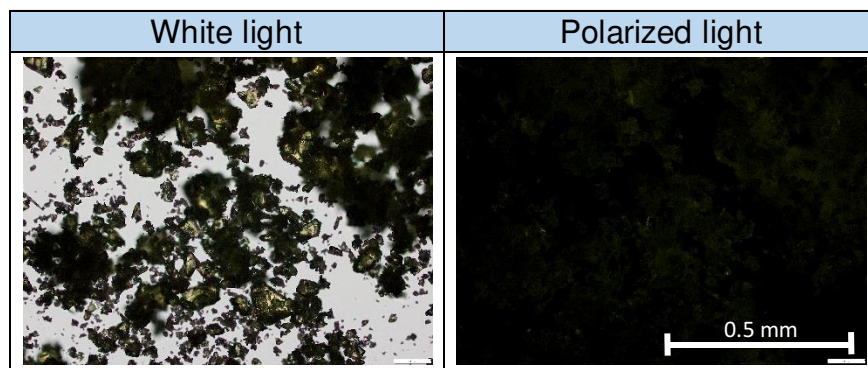


Figure 11: Microscope images of crushed peposertib tablets at 10x magnification using white light (left) and polarized light (right). Absence of birefringence using polarized light indicates an amorphous sample.

Although, dissolution tests at sink conditions showed no immediate but a slow and linear ($R^2 = 0.9919$) release of peposertib (Figure 12). The dissolution mechanism of most FDM printed tablet was reported to be through diffusion and erosion due to their inherently dense structure and large proportion of polymer in the formulation (Arafat et al., 2018; Goyanes et al., 2014; Sadia et al., 2018). A Korsmeyer-Peppas analysis resulted in a release exponent of $n = 0.85$, indicating an anomalous release mechanism, accounting for both, drug diffusion and tablet erosion. The fact that the release exponent was close to the limit of 0.89, indicates that the release was almost zero-order.

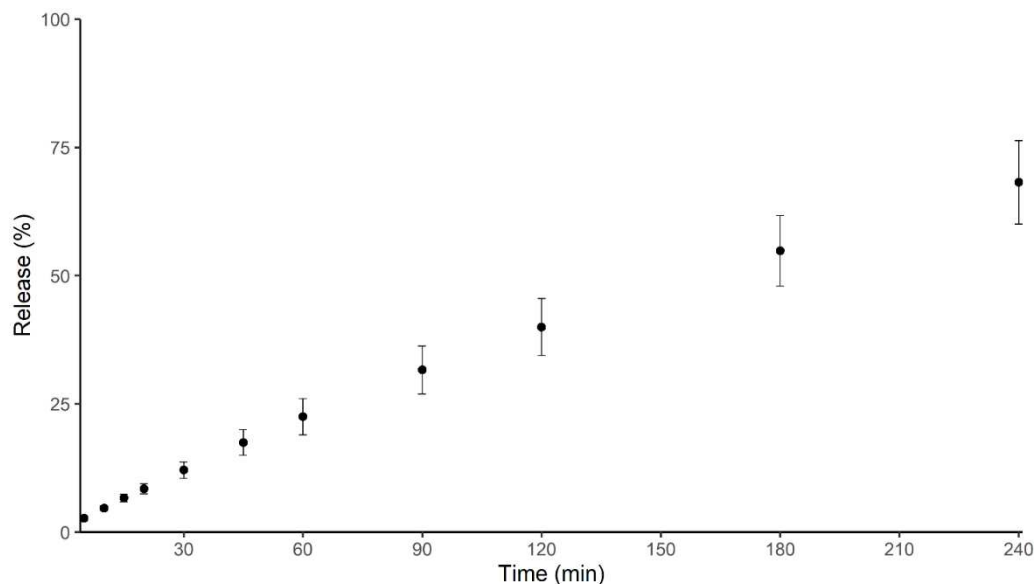


Figure 12: Dissolution under sink conditions of FDM printed tablets containing peposertib (30 % drug load) SGF_{sp} at 37 °C, mean release \pm SD (n = 6)

Next to that, it was observed that upon contact with the dissolution medium, peposertib tablets turned from transparent to opaque, indicating drug recrystallization at the tablet surface. After 240 min tablets were still present in the vessel in form of paste-like mass (Figure 13) and 68 % of

drug was released. The slow drug dissolution is likely a result of drug recrystallization combined with tablet erosion. As immediate release is desired for peposertib, further enhancement of the tablet design would be necessary. Therefore, the addition of disintegration enhancers into the formulation might be necessary, combined with advanced porous 3D structures that enforce disintegration into mini-structures as proposed by Arafat et al. (2018). It has to be considered though, that this will likely increase the tablet volume and the pill burden of the patient.



Figure 13: Peposertib tablet after dissolution. Left: After taking the tablet out of the vessel. Right: After crushing with a spatula

3.1.3.3. Conclusion

Through FDM 3DP, it was possible to achieve highly drug loaded and amorphous tablets at a small tablet size. Printing of the highly brittle formulation was enabled using the modified printer setup from Gottschalk et al. (2021) and the feed force tester had been employed to determine suitable printing temperature. However, final print parameters slightly deviated from the predicted. High brittleness of the formulation combined with strong intermolecular interactions of peposertib and copovidone, resulting in poor build-plate adhesion and inter-layer bonding required temperature reduction and additional measures to improve tablet adhesion and cohesion. The feed force tester is an empirical tool, measuring the forces that are necessary to push a filament through the nozzle at a certain temperature and speed. The data are linked to a 3D printer in order to determine the maximum force the printer can reach in order to achieve a uniform tablet mass not varying from the target mass. However, this method does not take into account the printability of a formulation in terms of adhesion to the build-plate or between layers, which are also affected by nozzle temperature and printing speed. In case the determined nozzle temperature does not match the temperature that is required to ensure reproducible printing, deviations in tablet mass and uniformity are possible. In this case, a printing system that is capable to use higher feed forces would be desirable. Next to that, experiments demonstrated that the extend of drug degradation of an API is not solely dependent on the nozzle temperature, but also affected by the contact of

the nozzle to the printed layers during printing and presents another limitation of the feed force tester.

In order to achieve amorphous filament, high mechanical energy was necessary in order to disperse peposertib in the polymer matrix during HME. As the FDM process does not provide mixing in the hotend, the filament needs to be fully amorphous after extrusion. Nevertheless, the increase in screw speeds during extrusion also resulted in peposertib degradation. High screw speeds also resulted in high filament diameter fluctuations, showing that extrusion parameters for amorphous filaments can be contradictory to those for dimensional uniform filaments.

Even though tablets were fully amorphous, they did not show immediate release, as a result of both, their inherently high density and recrystallization of peposertib during dissolution. Further improvements on tablet design and formulation will be necessary with the aim to enhance disintegration without increasing the tablet size.

The pipeline compound peposertib presented a challenging compound for the use in FDM but highlights the limitations of this technique. Some of them could potentially be overcome, e.g., through the development of a novel printer. Still, the inherent density of FDM printed tablets can present a challenge for highly drug loaded formulations containing a poorly soluble API, which could possibly be overcome using alternative 3DP techniques, e.g., DoP printing.

3.2. Drop-on-powder printing of highly drug loaded amorphous solid dispersions

3.2.1. Drop-on-powder process development for production of highly dosed formulations

The powder-based 3DP technique DoP printing is an appropriate method to produce highly dosed SODFs but is primarily employed for highly soluble APIs. The following paper introduces a feasibility approach for the use of amorphous powder material containing a poorly API in the DoP printing process. The challenge in using an amorphous powder material is the recrystallization potential upon contact with the ink. Therefore, the influence of different inks and ink-to-powder ratios on the solid-state, physical stability as well as the mechanical properties of the final dosage forms were evaluated. The solid state was assessed using DSC, XRPD and PLM. The latter was used to identify even small traces of crystallinity and their effect on ASD stability. High drug loads of 20 % and 40 % of the model compound ketoconazole were used to assess the limits of this approach.

The idea and study design were mainly developed by Nadine Gottschalk under support from Julian Quodbach and Malte Bogdahn. The experimental work, including extrusion, milling, printing and characterization of tablets was shared between Nadine Gottschalk and Alicia Burkard. Main data evaluation was performed by Nadine Gottschalk, and supported by Alicia Burkard, Julian Quodbach and Malte Bogdahn. The initial manuscript draft was written by Nadine Gottschalk and revised by Julian Quodbach and Malte Bogdahn.

Evaluation of authorship:

Author	Idea	Study Design	Experimental	Evaluation	Manuscript
Nadine Gottschalk	75	80	50	65	70
Alicia Burkard	0	0	50	25	0
Julian Quodbach	10	10	0	5	15
Malte Bogdahn	15	10	0	5	15

Evaluation of copyright permission: This article is available under the Creative Commons CC-BY-NC-ND license and permits non-commercial use of the work as published, without adaptation or alteration provided the work is fully attributed (accessed 10.05.2024).

Article available online at: <https://doi.org/10.1016/j.ijpx.2022.100151>

© 2022 Published by Elsevier B.V.

Drop-on-powder 3D printing of amorphous high dose oral dosage forms: Process development, opportunities and printing limitations

Nadine Gottschalk ^{a b}, Alicia Burkard ^b, Julian Quodbach ^{a c}, Malte Bogdahn ^b

^aInstitute of Pharmaceutics and Biopharmaceutics, Heinrich Heine University, Düsseldorf,
Germany

^bMerck KGaA, Darmstadt, Germany

^cDepartment of Pharmaceutics, Utrecht Institute for Pharmaceutical Sciences, Utrecht
University, Netherlands

International Journal of Pharmaceutics: X, Volume 5, 100151, 2022

DOI: 10.1016/j.ijpx.2022.100151

Abstract

Drop-on-powder 3D printing is able to produce highly drug loaded solid oral dosage forms. However, this technique is mainly limited to well soluble drugs. The majority of pipeline compounds is poorly soluble, though, and requires solubility enhancement, e.g., via formation of amorphous solid dispersions. This study presents a detailed and systematic development approach for the production of tablets containing high amounts of a poorly soluble, amorphized drug via drop-on-powder 3D printing (also known as binder jetting). Amorphization of the compound was achieved via hot-melt extrusion using the exemplary system of the model compound ketoconazole and copovidone as matrix polymer at drug loadings of 20% and 40%. The milled extrudate was used as powder for printing and the influence of inks and different ink-to-powder ratios on recrystallization of ketoconazole was investigated in a material-saving small-scale screening. Crystallinity assessment was performed using differential scanning calorimetry and polarized light microscopy to identify even small traces of crystallinity. Printing of tablets showed that the performed small-scale screening was capable to identify printing parameters for the development of amorphous and mechanically stable tablets via drop-on-powder printing. A stability study demonstrated physically stable tablets over twelve weeks at accelerated storage conditions.



Contents lists available at ScienceDirect

International Journal of Pharmaceutics: X

journal homepage: www.sciencedirect.com/journal/international-journal-of-pharmaceutics-x

Drop-on-powder 3D printing of amorphous high dose oral dosage forms: Process development, opportunities and printing limitations

Nadine Gottschalk^{a,b}, Alicia Burkard^b, Julian Quodbach^{a,c}, Malte Bogdahn^{b,*}

^a Institute of Pharmaceutics and Biopharmaceutics, Heinrich Heine University, Düsseldorf, Germany

^b Merck KGaA, Darmstadt, Germany

^c Department of Pharmaceutics, Utrecht Institute for Pharmaceutical Sciences, Utrecht University, Netherlands

ARTICLE INFO

Keywords:

Drop-on-powder printing
Binder jetting
Amorphous solid dispersion
Solubility enhancement
3D Printing
Process development
Additive manufacturing

ABSTRACT

Drop-on-powder 3D printing is able to produce highly drug loaded solid oral dosage forms. However, this technique is mainly limited to well soluble drugs. The majority of pipeline compounds is poorly soluble, though, and requires solubility enhancement, e.g., via formation of amorphous solid dispersions. This study presents a detailed and systematic development approach for the production of tablets containing high amounts of a poorly soluble, amorphized drug via drop-on-powder 3D printing (also known as binder jetting). Amorphization of the compound was achieved via hot-melt extrusion using the exemplary system of the model compound ketoconazole and copovidone as matrix polymer at drug loadings of 20% and 40%. The milled extrudate was used as powder for printing and the influence of inks and different ink-to-powder ratios on recrystallization of ketoconazole was investigated in a material-saving small-scale screening. Crystallinity assessment was performed using differential scanning calorimetry and polarized light microscopy to identify even small traces of crystallinity. Printing of tablets showed that the performed small-scale screening was capable to identify printing parameters for the development of amorphous and mechanically stable tablets via drop-on-powder printing. A stability study demonstrated physically stable tablets over twelve weeks at accelerated storage conditions.

1. Introduction

Three-dimensional printing (3DP) demonstrated to be a capable set of techniques for the production of individualized solid oral dosage forms (SODFs) in the last years. 3DP or additive manufacturing (AM) is a generic term for the layer-by-layer production of three-dimensional (3D) objects from computer-based design. The creation of pharmaceutical SODFs in a layer-by-layer fashion can be done in several ways. There are techniques based on powder and liquid solidification as well as extrusion-based methods (Seoane-Viaño et al., 2021). What they have in common is fast adjustability of the 3D tablet design and by that adapting the dose and release properties (Goyanes et al., 2015; Windolf et al., 2021). Although, 3DP techniques have gained great popularity in the pharmaceutical research sector, for a long time Spritam® by Aprelia Pharmaceuticals was the only approved drug product by the U.S. Food and Drug Administration (FDA), which is produced using the technique

drop-on-powder (DoP). Recently, Triastek received IND clearance for clinical studies by the FDA for their product T19, produced by Melt Extrusion Deposition (MED™) (Sen et al., 2021a). 3D printed products can be beneficial in clinical studies due to flexible dose adjustment and easy scalability (Sen et al., 2021a; Seoane-Viaño et al., 2021).

Besides the benefits for the manufacturing of clinical trial supply, 3DP techniques can also help solving the challenges of poor drug solubility. The majority of newly discovered compounds are poorly soluble and belong to the Biopharmaceutics Classification System (BCS) class II (Gala et al., 2020; Ting et al., 2018). A common strategy to enhance solubility and bioavailability of these compounds is the formulation of amorphous solid dispersions (ASD), where the amorphous active pharmaceutical ingredient (API) is kinetically stabilized in a polymer matrix. A kinetically stabilized system will eventually transform into a thermodynamically stable system, which means in case of an ASD that the amorphous API will recrystallize over time. Several factors such as the

Abbreviations: 3D, three-dimensional; 3DP, three-dimensional printing; AM, additive manufacturing; API, active pharmaceutical ingredient; ASD, amorphous solid dispersion; BCS, Biopharmaceutics Classification System; DoP, drop-on-powder; dpmm, dots per millimeter; DSC, differential scanning calorimetry; FDA, U.S. Food and Drug Administration; FDM, fused deposition modeling; HME, hot-melt extrusion; KTZ, ketoconazole; SODF, solid oral dosage form.

* Corresponding author.

E-mail address: malte.bogdahn@merckgroup.com (M. Bogdahn).

<https://doi.org/10.1016/j.ijpx.2022.100151>

Received 27 September 2022; Received in revised form 21 December 2022; Accepted 22 December 2022

Available online 23 December 2022

2590-1567/© 2022 Published by Elsevier B.V. This is an open access article under the CC BY-NC-ND license (<http://creativecommons.org/licenses/by-nc-nd/4.0/>).

storage temperature, moisture content and remaining traces of crystallinity affect the physical stability (Shah et al., 2014). An ASD can be obtained by a variety of techniques among which hot melt extrusion (HME) is widely used. By the means of HME an API-polymer mixture is blended in a heated barrel and the API can become amorphous by either heating above the melting temperature or/and dissolving in the polymer matrix (Shah et al., 2014).

HME has been coupled frequently with the 3DP technique Fused Deposition Modeling (FDM), also a melt-extrusion based process, to achieve amorphous drug products. However, the mechanical properties of the filaments are a great issue (Fuenmayor et al., 2018; Ilyés et al., 2019; Nasereddin et al., 2018) and especially high drug loads may result in very brittle filaments, which are not printable using commercially available printers (Gottschalk et al., 2021). Therefore, the addition of plasticizers in the formulation is necessary in many cases, which can impair the physical stability of the ASD (Wei et al., 2020). Another promising 3DP technique is DoP. The DoP process can be described as an in-situ wet granulation, where small ink or binder droplets are jetted on thin powder layers resulting in fusion of the powder particles. The iterative process of powder spreading and ink application proceeds until the 3D objects is printed. Since the single powder particles are applied loosely onto each other, drug release from DoP printed SODFs benefits from the porous structure (Jennotte et al., 2020). In addition to that, high drug loads up to 70% are feasible, which is usually not the case for classical manufacturing techniques such as tableting due to poor compressibility of most APIs. However, in DoP printing tablet hardness and tablet friability can be impaired (Infanger et al., 2019; Wang et al., 2022a), which requires the usage of polymeric binders. The binder can be included in the ink (Chang et al., 2021; Goole and Amighi, 2016; Kozakiewicz-Latala et al., 2022; Sen et al., 2021b; Wang et al., 2021; Wilts et al., 2019) as well as in the powder bed (Wang et al., 2022b; Antic et al., 2021; Infanger et al., 2019; Tian et al., 2019; Wang et al., 2006; Zhang et al., 2021). The production of ASDs is possible by the means of DoP printing, if the API is included in the ink in combination with a volatile solvent due to fast evaporation from small droplets similar to spray-drying (Scoutaris et al., 2011; Wickström et al., 2015). The proportion of API in the ink depends on its solubility in the solvent and high API concentrations increase the likelihood of recrystallization of the API at the nozzle leading to nozzle clogging (Parhi, 2021). Furthermore, the achieved drug loads and dosages are low, being in the lower microgram-range up to a maximum of 5 mg (Clark et al., 2020; Rajjada et al., 2013; Sharma et al., 2013). High drug loads, though, may be necessary to achieve high drug dosages by maintaining an adequate tablet size.

In the current literature, the use of DoP printing for high dose formulations is mainly described for highly soluble compounds. This study investigates the possibility of coupling HME with DoP printing by using hot-melt extruded ASDs as powder bed material. We present a systematic development approach for SODFs via DoP printing with the aim to produce fully amorphous dosage forms. Ketoconazole (KTZ), an antifungal agent with a poor solubility (22.2 µg/mL in Fasted State Simulated Intestinal Fluid (Auch et al., 2018) was used as model compound. As matrix polymer copovidone (Kollidon® VA64) was selected because of its suitability to produce ASDs with ketoconazole, especially in a melt-based approach (Auch et al., 2018), and because it has been reported to have strong binding properties when used as a solid binder in DoP printing (Antic et al., 2021; Chang et al., 2020). Water-based and water-free inks as well as various ink-to-powder ratios were assessed regarding their suitability to print high dose amorphous dosage forms. The selected key quality attributes for development were degree of recrystallization, physical stability and mechanical properties of the printed tablets.

2. Material and methods

2.1. Materials

KTZ was purchased from LGM Pharma (Boca Raton, USA). Copovidone (Kollidon® VA64, Vinylpyrrolidone-vinyl acetate copolymer) was purchased from BASF (Ludwigshafen, Germany). Methylene blue and the solvents ethanol, methanol and isopropyl alcohol (purity ≥99.9%) were provided by Merck (Darmstadt, Germany). Colloidal silicon dioxide was purchased from Evonik Industries (Essen, Germany).

2.2. Methods

2.2.1. Blending and extrusion

Two blends were prepared by weighing polymer and API and blending them using a Turbular® mixer (T2C, Willy A. Bachofen AG, Muttens, Switzerland) for 15 min. Colloidal silicon dioxide was manually added to the premix and the mixture was sieved (mesh size: 1 mm) and blended again for 15 min. This was necessary to enable a uniform powder feeding of the KTZ-containing blends during extrusion. The composition of the blends is displayed in Table 1.

Extrusion was performed on a Pharma 11 twin-screw extruder (Thermo Fisher Scientific, Waltham, USA) with a screw configuration consisting of three kneading zones to achieve good mixing of API and polymer. A gravimetric feeder (Congrav® OPI T) and conveyor belt from Brabender GmbH & Co. KG (Duisburg, Germany) were used. The conveyor belt was used to pull the extrudate strand to facilitate cooling. Extrudate was further cut into smaller pieces using diagonal pliers. A slow feed rate of 0.2 kg/h was chosen to prolong the residence time of the melt in the barrel and a high screw speed of 300 rpm to create a high input of mechanical energy to produce fully amorphous extrudates with homogeneously distributed API. Extrusion was performed above the melting point of KTZ (151 °C) and below the degradation temperature of 221 °C (Kanaujia et al., 2011). Barrel temperatures had to be adapted for each formulation to produce a self-supporting extrudate strand and are displayed in Table 2.

2.2.2. Milling and particle size determination

A typical layer height in DoP printing to achieve good resolution of printed objects is 100 µm (Chang et al., 2021; Wang et al., 2022b), hence, particles should be smaller than the intended layer height. Therefore, the aim was to produce particles <100 µm. For initial printing tests a small batch of approximately 15 g of extrudate (VA64-K0 and VA64-K40) was milled using a Tube Mill control (IKA, Staufen, Germany). The milling chamber was filled with a maximum of 5 g and milling was performed in steps of 1 min at 25,000 rpm with cooling steps of approximately 1 min in between to reduce thermal impact on the powder and prevent aggregation of particles. Each formulation was milled for 5–8 min in total. Milled extrudate was sieved with a mesh size of 200 µm. Using the Tube Mill, it was not possible to produce an appropriate amount of powder with a particle size <100 µm. As the initial screening was performed on trays with cavities deeper than 100 µm the powder was suitable. To reach a smaller particle size for the printing of tablets, an ultra-centrifugal mill (ZM 200, Retsch, Haan, Germany) was used. Formulations VA64-K20 and VA64-K40 were milled using a twelve-teeth rotor and a sieve with a mesh size of 200 µm with a distance ring at 10,000 rpm. Particle size was determined via dynamic image analysis using a Camsizer X2 (Retsch, Haan, Germany).

Table 1
Blend composition in wt%.

	VA64-K0	VA64-K20	VA64-K40
KTZ (%)	0	20	40
Copovidone (%)	100	79	59
Silicon dioxide (%)	0	1	1

Table 2
Extrusion parameters.

Formula-tion	Feed rate (kg/h)	Screw speed (rpm)	Zone 1 (°C)	Zone 2 (°C)	Zone 3 (°C)	Zone 4 (°C)	Zone 5 (°C)	Zone 6 (°C)	Zone 7 (°C)	Die (°C)
VA64-K0	0.2	200	80	180	180	180	180	180	180	180
VA64-K20	0.2	300	60	120	180	180	180	180	180	175
VA64-K40	0.2	300	60	120	160	160	160	150	150	150

The X-jet module was used. Dispersing pressure was set to 50 kPa and gap width to 4 mm. As D90 values of the milled extrudates were below 100 μm (supplementary material, Table S1), the whole powder fraction was used as powder bed material for printing.

2.2.3. Preparation of inks

Ink composition is displayed in Table 3. Ink was prepared by mixing the corresponding volumes. For pretests, methylene blue was added to the inks in a concentration of 0.16 mg/mL. No further characterization of the inks was performed.

2.2.4. Printing

2.2.4.1. Printer setup. Commercial binder jetting printers for pharmaceutical use are not available, yet. Therefore, a custom-made powder bed printer comprising an active powder reservoir, a roller, a powder bed with building platform and a printing station had to be modified. A schematic drawing of the printing process is displayed in Fig. 1.

The mechanical setup is controlled by an off-the-shelf motion control system compatible to the G-code standard. The build platform can move in xyz-direction, whereas the printing station is fixed. To create a powder layer the build plate is lowered by the intended layer height. For each printed layer the build platform moves under the orifice of a powder reservoir. A screw inside the reservoir distributes a powder pile onto the platform. In the next step, the platform moves at constant speed under the counter-rotating roller to spread the powder pile into a single layer. Hereafter, ink is deposited on the smoothed powder bed. The printing station was specifically designed. While industrial piezo inkjet printheads are suitable for large production setups with high throughput, they require advanced parameter tuning. For this study, modified HP C6602 cartridges (thermal printhead) were chosen because of their robustness. The cartridge was controlled via an Arduino Mega 2560 microcontroller board with an open-source extension board (Ink-shield) and in-house developed firmware. The twelve nozzles of the printhead are arranged in a line with a length of 3.175 mm. Each of the twelve nozzles could be controlled individually. The motion controller of the printer generated a pulse signal to sync the print head controller to the printing motion. The distance between the nozzles and the powder bed was approximately 5 mm. The functionality of the nozzles was tested by checking the electrical resistance of each nozzle using a multimeter after each print. Broken nozzles are indicated by a greatly increased nozzle resistance.

The HP cartridge C6602 is a commercially available, prefilled printhead for 2D inkjet printing and therefore, had to be opened and thoroughly cleaned to allow filling with the prepared inks. Customized lids were printed from polylactic acid on a Prusa i3 MK3S (Prusa Research s.r.o., Prague, Czech Republic) and glued on the cartridge. The lids had been modified with a male luer-lock adapter to enable the connection to a vacuum pump. A meniscus vacuum of -1.96 mbar (-20 mm H_2O) was applied to prevent the ink from oozing. Approximately 10 mL of ink were filled in the cartridge using a syringe to ensure a comparable filling level for all experiments.

2.2.4.2. Determination of droplet volume. The droplet volume of the inks containing methylene blue was determined by jetting 1800 droplets per nozzle into a UV transparent 96 well plate (Corning, New York, USA). Ink was diluted with 200 μL of demineralized water and absorption of methylene blue at 665 nm was measured using a microplate reader (Spark, Tecan, Männedorf, Switzerland). A calibration in the wells with 200 μL of five aqueous solutions of methylene blue in a range from 1.6 to 5.7 $\mu\text{g}/\text{mL}$ was performed ($n = 3$). The droplet volume was calculated from the jetted amount of methylene blue and the total number of droplets. Five replicate tests were performed for each ink.

2.2.4.3. Parameter screening. For the initial print parameter screening only the print station and the build platform were used. Extrudate milled using the Tube Mill was spread manually using cardboard on small trays with cavities of 500 μm depth. Various ink-to-powder ratios were evaluated, by printing single layer objects with a fixed layer height. The ink-to-powder ratio is referred to as dots per mm in printing direction (dpmm). All twelve nozzles were used to print a band, wherefore the distance between the droplet orthogonal to the printing direction was fixed. Material and parameter combination are listed in Table 4. The build plate moved at constant speed in x-direction below the print head during droplet generation. Additional tests were performed to evaluate the influence of enhanced drying on printed layers using a 1 kW halogen lamp (Philips, Amsterdam, Netherlands) on samples printed with E70 at 50 dpmm at full and half intensity for 0.5, 5 and 10 min. The lamp was placed approximately 15 cm above the freshly printed samples.

2.2.4.4. Printing of tablets. For printing of multilayer objects, the combination of printing station, build platform, powder reservoirs and roller was used. Cylindrical tablets (height: 2.4 mm, diameter: 10 mm) were designed in Fusion 360 (Autodesk, Farnborough, United Kingdom) and

Table 3
Ink composition (v/v%) and ink properties from literature.

Ink	Composition (v/v%)				Ink properties at 20 °C ¹		
	Methanol	Ethanol	Isopropyl alcohol	Purified water	Vapor pressure (kPa)	Surface tension (mN/m)	Viscosity (mPa*s)
M100	100	–	–	–	13.0 ^a	22.6 ^b	0.6 ^b
E70	–	70	–	30	5.9 ^c	27.5 ^d	1.2 ^e
IPA90	–	–	90	10	–	22.2 ^f	2.7 ^f

¹Literature data:

^a (Gibbard and Creek, 1934).

^b (Wanchoo and Narayan, 1992).

^c Safety data sheet "Ethyl alcohol 70% v/v"

^d (Khatab et al., 2012).

^e (Vazquez et al., 1995).

^f (Pang et al., 2007).

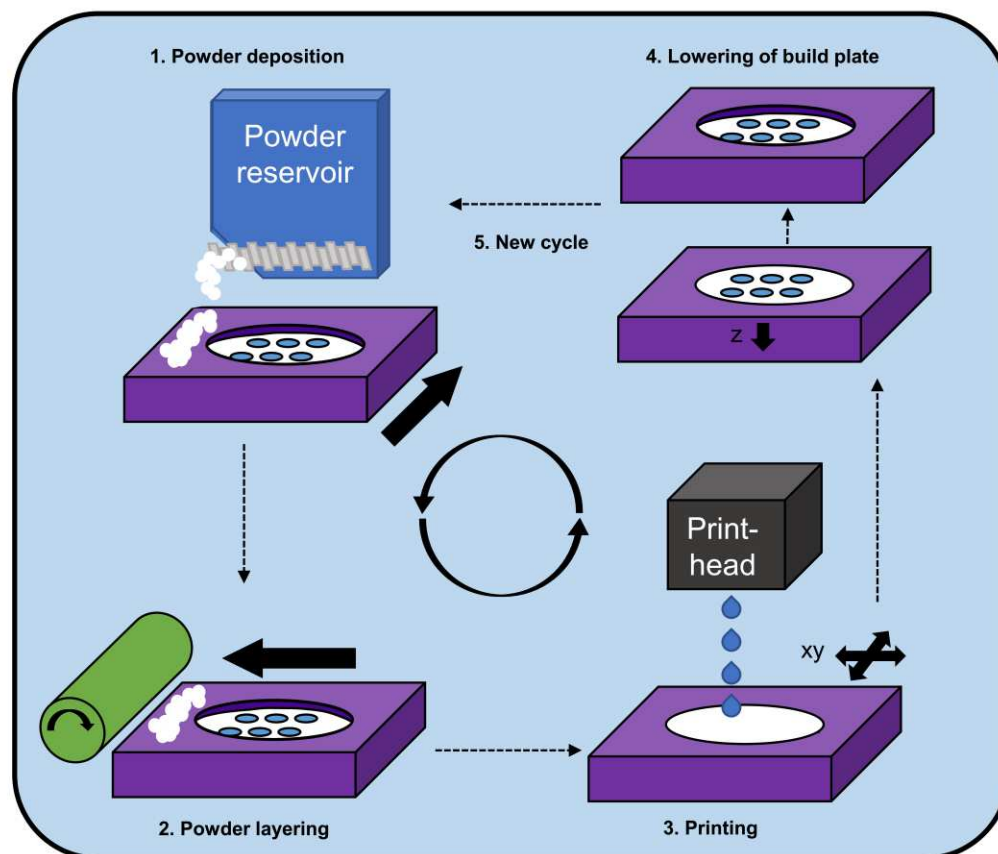


Fig. 1. Schematic drawing of printing process.

Table 4
Screening of printing parameters.

Screening experiment	Material	Ink-to-powder ratio (dpmm)	Printing length (mm)	Inks
... to estimate ink-to-powder ratio	VA64-K0	10, 50, 100, 150, 200, 250	5	E70
		30, 40, 50, 60, 70, 80	5	E70
	VA64-K40	30, 40, 50, 60, 70, 80	5	E70
		30, 40, 50, 60	60	M100
... to assess the influence of ink-to-powder ratio on recrystallization	VA64-K40	30, 40, 50, 60	60	E70
		40, 50, 60	60	IPA90
	VA64-K40	50	60	E70
... to assess the influence of drying with lamp on recrystallization	VA64-K40	50	60	E70

saved in a binary stereolithography file format (.stl) with high resolution. The file resembling the tablet geometry was converted into printing and motion data via a specifically developed script written in Python 3.7. The script accepted all print settings as input parameters. The motion commands were saved as G-code file and imported into the motion control software of the printer. The corresponding graphical information were sent to the print head controller via USB connection during the print job. The powder was automatically deposited from the powder

reservoir and spread via the counter-rotating roller set to 350 rpm. The platform moved at a speed of 600 mm/min. Layer height was set to 0.1 mm. After ink jetting, the powder bed was left to rest for 15 s before the next powder layering step. Twelve tablets were printed at the same time. The powder bed was dried in a vacuum drier (VacuTherm VT6060MBL, Thermo Fisher Scientific, Waltham, USA) at <100 mbar at room temperature overnight.

2.2.5. Storage

To assess the physical stability, printed tablets were stored in open glass vessels in a desiccator with silica gel at 40 °C in a climate chamber for 2, 4 and 12 weeks (KBF 240, Binder, Tuttlingen, Germany).

2.2.6. Polarized light microscopy

Single layer objects and printed tablets were crushed using mortar and pestle prior to analysis. Furthermore, the top layer of tablets was cut off using a cutter knife, to allow a 2D view on the samples. Samples were qualitatively analyzed using polarized light microscopy (IX73P1F, Olympus, Tokyo, Japan) at 5× and 10× magnification with regards to traces of crystallinity and their location in the tablet. Images were recorded using Olympus cellSens standard software (version: 1.18).

2.2.7. Differential scanning calorimetry (DSC)

Crystallinity assessment of samples was performed using a DSC 1 (Mettler Toledo, Gießen, Germany). Neat substances, blends, milled extrudates and ground printed samples were analyzed. Approximately 7–9 mg were weighed into a 100 µL aluminum pan and hermetically sealed. The lid was pierced prior to analysis using the automatic piercing unit. Samples containing methylene blue were heated twice from 0 °C to

200 °C, samples without methylene blue were heated from 0 °C to 170 °C at heating and cooling rates of 10 K/min. Tests were performed in triplicate.

2.2.8. Tablet hardness

Printed tablets were analyzed using an Erweka tablet hardness tester (THB 125, Erweka, Langen, Germany). Tablets were placed in the hardness tester in such a way that the force acted in the direction of printing. Tests were performed in triplicate. In case of VA64-K20 tablets printed with E70, ten tablets were tested. Tensile strength was calculated according to Pitt and Heasley, 2013.

3. Results and discussion

The approach of using already amorphous API as powder bed material has not been described in the literature so far. The single steps from ink selection and parameter optimization to the printing process and characterization of printed tablets will be described in the following sections. A flowchart of the work performed in this study is displayed in Fig. 2.

3.1. Small-scale prescreening: identification of printing parameters

3.1.1. Ink and ink-to-powder ratio screening

Aim of initial printing pretests was to test whether the milled hot-

melt extrudate from copovidone was suitable as solid binder and to which extend recrystallization of the amorphously embedded API in the polymer matrix would occur by varying ink-to-powder ratios. Tests were performed with highly drug loaded material (40% w/w). The high proportion of API molecules in the extrudate makes the formulation more susceptible to recrystallization. It was assumed that this would facilitate differentiation between the different settings and inks. Pretests were further designed to consume as little time and material as possible.

First, single layer objects were printed with ink E70 to estimate the approximate amount of ink necessary to fuse extrudate particles from VA64-K0 and VA64-K40 leading to mechanically stable flakes. It was assumed that parameters leading to stable flakes would lead to mechanically stable tablets or can be used as starting point for tablet optimization. The dye methylene blue was used to visualize ink distribution in the flakes. Initially, a broad range of ink-to-powder ratios was selected and used with VA64-K0. With regards to potential recrystallization of KTZ in the following experiments, ink-to-powder ratios were selected, which were as low as possible but still resulted in stable flakes. Visual assessment of the samples (Fig. 3) indicated excess amounts of ink at volumes >100 dpmm. Here, the amount of ink was too high to be absorbed by the powder material leading to fusion of ink droplets and the formation of an “ink pool”. In contrast, 10 dpmm did not lead to fusion of the powder particles and the printed sample was very fragile. Consequently, a range from 30 to 80 dpmm was selected. The samples were assessed on whether they could be picked up and removed from the

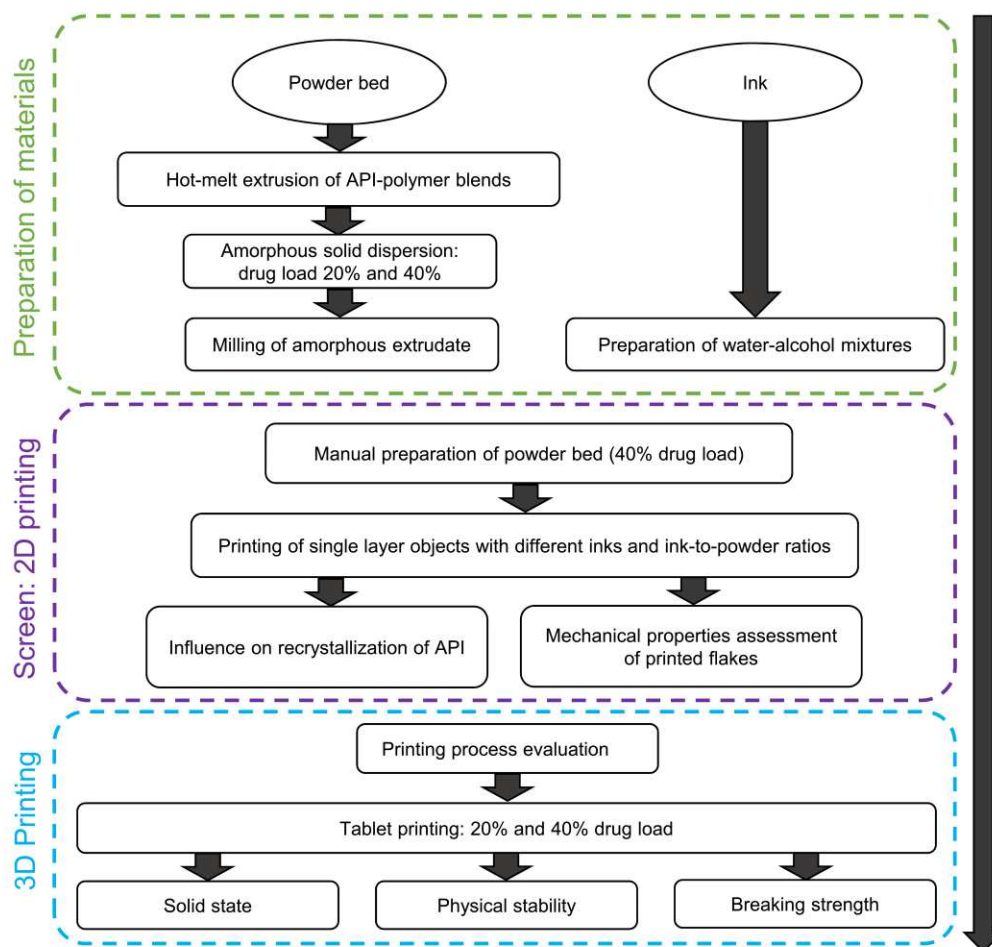


Fig. 2. Flowchart of the development approach in this study.

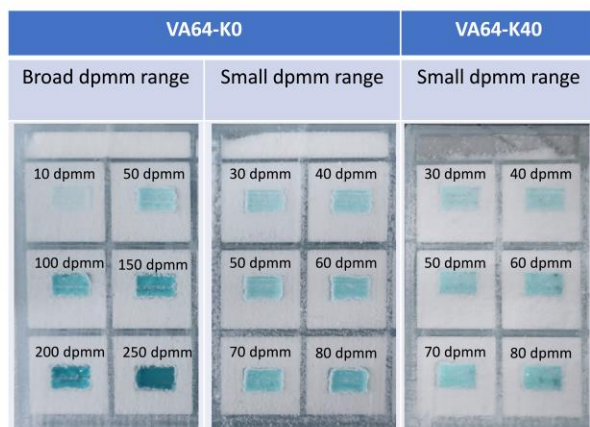


Fig. 3. Various ink-to-powder ratios in a range of 10–250 dpmm with E70 ink containing methylene blue on milled extrudate (VA64-K0 and VA64-K40). (For interpretation of the references to colour in this figure legend, the reader is referred to the web version of this article).

powder bed in one piece using tweezers. Tests were performed using VA64-K0 and VA64-K40, which resulted in stable flakes starting at 40 dpmm in case of VA64-K0 and 50 dpmm in case of VA64-K40, indicating that due to the reduction of the amount of solid binder, mechanical stability was impaired. In case of VA64-K0 the samples slightly bent upwards. The warping effect is not desired in powder bed printing since it may lead to removal of printed layers during recoating of a new powder layer, stopping the printing process (Tian et al., 2019). The reason for warping is that upon contact with water, polymers like copovidone undergo swelling due to sorption of water (Li et al., 2011). Hence, warping was stronger at higher ink-to-powder ratios. However, during swelling, inter-particle bonds are created, which contribute to the mechanical strength of the samples. Subsequent drying, which does not occur uniformly over the whole wetted area as the edges dry faster, results in contraction and warping. To ensure a continuous printing

process and mechanically stable samples, a sweet spot regarding the ink-to-powder ratio has to be identified. In case of VA64-K40, strong warping was only present at high ink-to-powder ratios >70 dpmm, possibly due to a lower proportion of the binder copovidone.

Next to the E70 ink another water-based ink, IPA90, and a water-free ink, M100, were tested in a range of 40–60 dpmm. Visual assessment of the prints (supplementary material Fig. S1) with inks containing ethanol and methanol indicated good distribution of the ink on the powder surface, whereas the IPA90 ink led to neither a good distribution nor mechanically stable samples. The droplet volume of IPA90 was smaller (IPA90: 72 pL ± 2 pL, E70: 124 pL ± 3 pL, M100: 131 pL ± 4 pL) A likely reason is the more as twice as high viscosity of the IPA90 ink (Table 3). Due to the small droplet volume and high viscosity, it is unlikely that proper particle fusion and good mechanical strength of tablets will be achieved. Therefore, IPA90 was excluded from following experiments.

3.1.2. Assessment of recrystallization behavior

In the next step, the effects on recrystallization of the inks E70 and M100 in various ink-to-powder ratios were assessed. Extruded and milled powder was analyzed in advance and was fully amorphous prior to the screening (supplementary material Fig. S2). In addition, the miscibility of API and polymer was demonstrated using DSC. A single glass transition was observed, which indicates a miscible system (supplementary material, Fig. S3). Assessment of single layer objects via polarized light microscopy (Fig. 4) showed birefringence starting from 50 dpmm, indicating recrystallization. To rule out that birefringence was possibly a result of light refraction where particles had fused, samples were compared to printed single layers of VA64-K0 (supplementary material Fig. S4). Here, no such birefringence was observed indicating that the birefringence in VA64-K40 was due to recrystallization upon contact with the inks. The proportion of recrystallization appeared to be slightly higher for the water-containing ink E70, which is possibly a result of a lower vapor pressure and slower evaporation of the solvent (Table 3). The droplet volume of E70 and M100 was almost identical. The observed recrystallization was too low to be detected via DSC (data not shown). The limit of detection had been determined in prior experiments (Gottschalk et al., 2021) and was found to be 2.0% leading us to assume that the proportion of crystallinity is below this

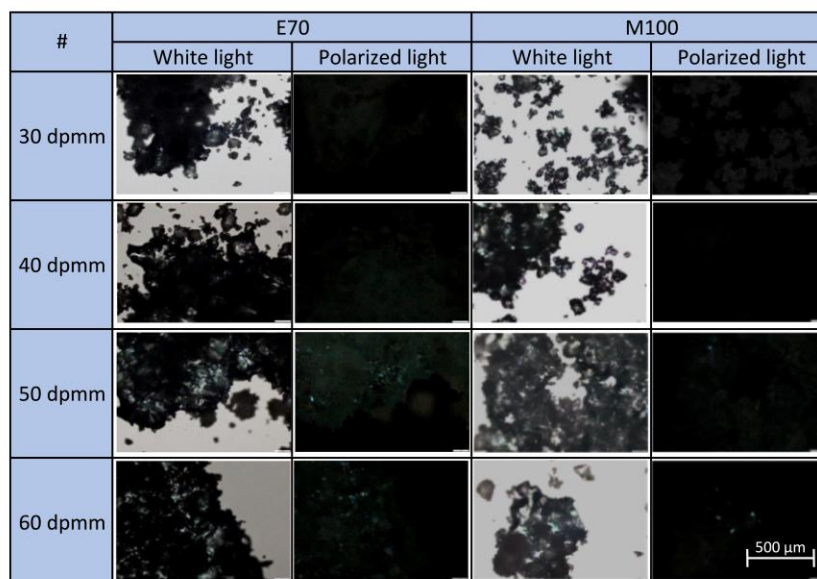


Fig. 4. Influence of ink-to-powder ratios on recrystallization of amorphous KTZ at 40% drug load comparing E70 and M100 containing methylene blue. Microscope images with white and polarized light at 10× magnification. (For interpretation of the references to colour in this figure legend, the reader is referred to the web version of this article).

limit. It has to be pointed out that variations between printheads may lead to variations of the droplet volume. Several printheads were used in this study since single nozzles stopped working occasionally, indicated by an increased electrical nozzle resistance.

Additional drying with a halogen lamp directly after printing was performed to evaluate whether this would reduce recrystallization due to faster evaporation. To our surprise, the opposite was observed and drying induced recrystallization (Fig. 5). After using the lamp for 30 s at maximum intensity, samples were not dry and it appeared that the energy input provided the activation energy for recrystallization. All samples demonstrated recrystallization to a greater extent compared to samples, which had not been dried. The intensity was reduced to prevent initial recrystallization but even though samples were dry after 5 and 10 min of drying, recrystallization could not be prevented and an additional drying step was considered not suitable regarding this process.

Pretests already indicated that the amorphous extrudate was susceptible to recrystallization upon wetting with the inks, possibly due to higher molecular mobility in the wetted areas. It became also apparent that mechanical strength decreased with decreasing ink-to-powder ratios, which requires the definition of optimal conditions. It has to be mentioned that only a single layer was printed and the drying rate will be impaired when printing a multilayer object. In contrast, samples will probably be mechanically more stable since fusion of the particles will not only occur in xy-direction but also in z-direction. In the pretests, milled extrudate with a particle size range of 100–200 μm was used. Particle sizes $<100 \mu\text{m}$ were used for printing of multilayer objects. This should further lead to an enhanced mechanical stability of the printed samples because of additional binding locations. Considering all these aspects, an ink-to-powder ratio of 30 dpmm was selected for printing of multilayer objects. Methylene blue was not used in follow-up experiments. Comparative experiments were performed with a E70 ink without methylene blue leading to comparable results regarding recrystallization and mechanical properties of printed layers (supplementary material, Fig. S5).

3.2. Transfer of identified printing parameters to multilayer objects

3.2.1. Printing process

The results from the pre-screening in 3.1 were transferred to the actual printing process of multilayer dosage forms. Observations in the following section are described for the formulation VA64-K20. Conclusions from these initial printing experiments were transferred to formulation VA64-K40. No differences in powder behavior between VA64-K20 and VA64-K40 were observed.

First, powder layer spreadability was assessed using the roller. Milled extrudate showed good powder-layering properties: the powder layers

were smooth and homogenous in a broad range of roller speed settings (50–400 rpm) without throwing the powder over the roll during powder distribution or shearing powder against each other. A uniform powder bed is important to ensure quality of tablets. Powder bed defects may impair the mechanical strength of the printed tablets and, when the API is included in the powder bed, will probably lead to poor mass and dosing conformity of the tablets. Occasionally, extrudate particles attached to the roll (Fig. 6), resulting in furrows on the powder surface. This phenomenon was observed more frequently when the milled extrudate was exposed to air humidity for longer periods of time. Drying of the powder could reduce this effect but since the polymer copovidone is highly hygroscopic (Liu et al., 2013) and due to the great surface area of the fine powder, absorption can occur fast. To prevent this effect, working in an environment with controlled air humidity would have been necessary. Since this was not possible, particles that had adhered to the roll had to be removed manually using a wiper to ensure a smooth powder bed.

Differences in terms of processability were observed during testing of the inks E70 and M100. M100 printed at 30 dpmm resulted in a smooth first layer, whereas in case of E70 the first layer showed warping at the edges of the printed area as already observed during the prescreening. Due to warping, the printed layers were removed by the roller in the next powder layering step and the print job had to be aborted. To overcome this phenomenon, the ink-to-powder ratio was decreased to 10 dpmm and the roller speed was varied. These attempts were not successful, indicating that barely visible warping effects can interrupt the printing process. In addition to that, the initial build plate layer height was adapted stepwise to create a very thin first powder layer (0.2 mm) so the first printed layer would be in contact to the build plate (Fig. 7). Adhesion of the first printed layer prevented warping and printing was feasible. However, printing was only feasible in a narrow first layer height range: first layer heights $\geq 0.3 \text{ mm}$ resulted in removal of the first printed layer whereas first layer height $\leq 0.1 \text{ mm}$ led to a strong adhesion to the build plate, making removal of printed tablet without breaking them impossible.

3.2.2. Tablet properties

Tablets were printed from formulations VA64-K20 and VA64-K40 with the inks E70 and M100 and a representative tablet is displayed in Fig. 8a. Tablets were white and slightly yellowish where the ink wetted the powder bed. Three darker stripes were visible on the tablet surface, which is a result of the printhead moving four times over the powder bed to cover the whole area. The twelve nozzles of the printhead are arranged in a line with a length of 3.175 mm and the tablet diameter was 10 mm. It was observed that if only a single nozzle would break during printing, the tablets would fall apart at this location (supplementary

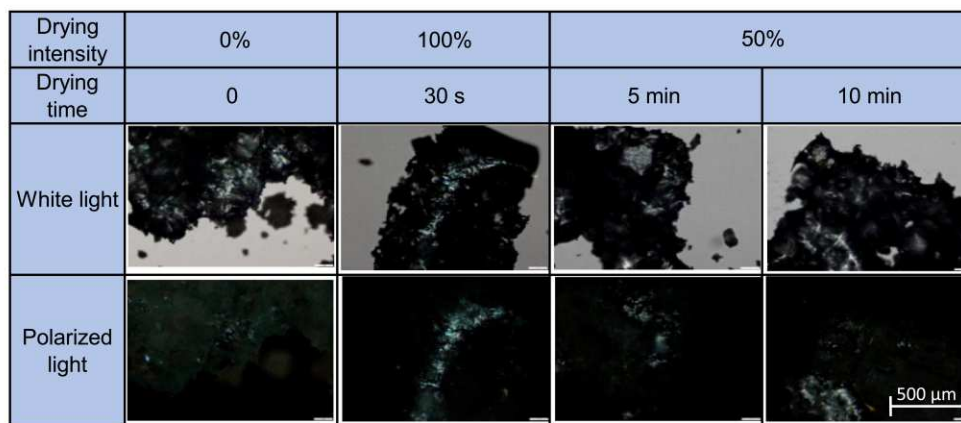


Fig. 5. Influence of drying intensity and time on recrystallization of KTZ at 40% drug load at 50 dpmm printed with E70.

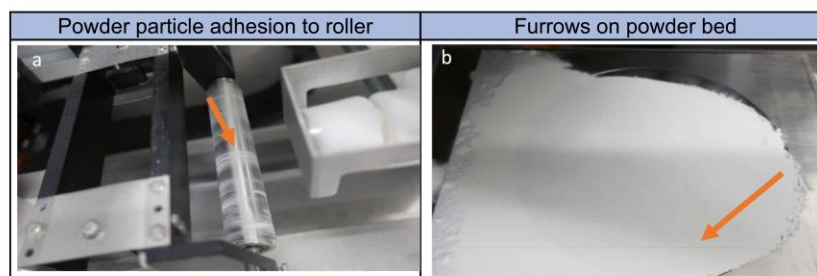


Fig. 6. Adhesion of powder particles on distributing roller (a) and the resulting furrows in the powder bed (b).

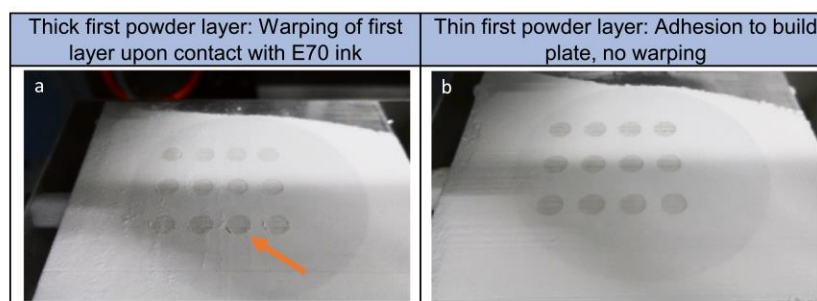


Fig. 7. Warping of first layer (orange arrow) when printing on a thick first powder layer (a) and a thin first powder layer (b).

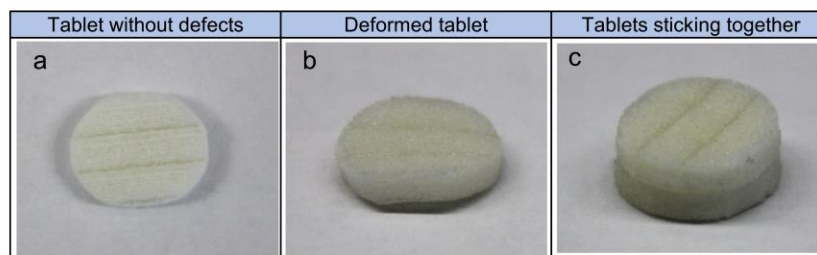


Fig. 8. Tablet without defects (VA64-K20 printed with E70) after printing and drying (a), deformed tablet (b) and tablets sticking together after 2 weeks of storage (c).

material, Fig. S6). Therefore, the slicer had been programmed to produce a slight overlap on print passes to prevent tablets falling apart. This resulted in areas with higher ink-to-powder ratio visible as stripes on the tablets.

Tablets printed with E70 had nearly twice the tensile strength of tablets printed with M100 (Table 5) and are close to 1 MPa, which is a reported target value in the literature (Leane et al., 2015). As already

Table 5
Tensile strength of tablet with 20% and 40% drug load printed with E70 and M100 ($n = 3$).

Formulation	Ink	Tablet tensile strength at stability time point (MPa) \pm SD			
		T0	2 weeks	4 weeks	12 weeks
VA64-K20	E70	0.93 \pm 0.30*	1.76 \pm 0.31*	2.33 \pm 0.28*	1.83 \pm 0.47*
	M100	0.64 \pm 0.19	0.76 \pm 0.12	0.70 \pm 0.41	0.79 \pm 0.13
VA64-K40	E70	1.05 \pm 0.21	N/A	N/A	N/A
	M100	0.51 \pm 0.14	0.56 \pm 0.15	0.64 \pm 0.13	0.59 \pm 0.13

* $n = 10$.

described in Section 3.2.1., strong warping, which had been observed with E70, probably correlates with strong particle fusion. The tensile strength was independent from the proportion of solid binder in the formulation highlighting the importance of ink selection for the mechanical properties of printed tablets.

The tensile strength of tablets printed with E70 increased during storage. It was also observed that printed tablets before storage showed a strong decrease in glass transition temperature compared to the neat milled extrudate ($54.2 \text{ }^\circ\text{C} \pm 0.9 \text{ }^\circ\text{C}$ vs. $34.0 \text{ }^\circ\text{C} \pm 12.1 \text{ }^\circ\text{C}$ for VA64-K20). A pronounced endothermic event was observed at $90\text{--}100 \text{ }^\circ\text{C}$ in DSC data indicating the evaporation of water. Water acts as powerful plasticizer and reduces the glass transition temperature (Pereira et al., 2019). Samples were kept at $40 \text{ }^\circ\text{C}$ during storage, which was above the glass transition temperature of the printed tablets, and it is likely that higher molecular mobility of the polymer resulted in an enhanced fusion of particles increasing the tablet strength. Contributing to that, some of the tablets were slightly deformed and occasionally stucked together (Fig. 8b and c). The glass transition temperature increased during storage to $69.4 \text{ }^\circ\text{C} \pm 0.6 \text{ }^\circ\text{C}$ indicating a loss of water.

Regarding the recrystallization in dependence of the ink, printing of VA64-K40 with E70 resulted in enhanced recrystallization of KTZ compared to M100 as already indicated in the pre-screening. The effect

on recrystallization was more pronounced than in the pre-screening (Fig. 9) and 2.8% crystalline KTZ was detected via DSC. The reason for this is most likely the lower surface area-to-volume ratio of stacked wet powder layers resulting in a slower drying process compared to single layer objects.

By means of the fast-evaporating solvent methanol the degree of recrystallization was minimized but could not be completely eliminated. Even small traces of solvent can impair the physical stability of a formulation, which was the case of VA64-K40 tablets printed with M100. Additional recrystallization occurred after 12 weeks of storage at accelerated conditions. Analysis of single tablet layers indicated that recrystallization was localized to where material had been directly wetted by the ink (Fig. 10). Areas in between showed no recrystallization. As a result of the fixed nozzle spacing, areas in between are wetted only indirectly by ink diffusion leading to a lower moisture content.

In a supersaturated formulation with a drug load of 40%, the distance between API molecules is small. The addition of liquid even at small amounts increases the mobility of the molecules in the wetted areas, facilitating recrystallization. Therefore, DoP printing is considered unsuitable for the production of physically stable tablets at such high drug loads. Here, an approach where the tablet contains loose powder and only the shell and top and bottom layers are printed as described by Yu et al. (2009) would be conceivable. Mechanical strength and physical stability of the inner phase would have to be assessed separately in this case.

At a lower drug load of 20%, the difference between the two inks was less pronounced. Tablets printed with M100 were fully amorphous and remained amorphous during storage. Regarding tablets printed with E70, in the ground samples a few particles >100 μm were detected that contained a high number of crystalline spots (Fig. 9). These large particles were a result of the printing process and fusion of particles, where, due to the slicer settings, overlapping of printed lines occurred. After storage for twelve weeks at accelerated conditions crystals were still only localized there (Fig. 10) and samples were fully amorphous in areas where no overlapping occurred. The crystalline amount was too low to be detected via DSC.

The low drug load as well as the high porosity of the tablets contribute to the enhanced physical stability. This example shows that even small amounts of excess ink and recrystallization can be compensated when using lower drug loads. An overview on all formulations and

their results can be found in the supplementary material (Table S2).

4. Conclusion

In this study, we demonstrated that DoP printing of hot-melt extruded ASD powder containing KTZ was successful. The screening method developed for this purpose has proven to be capable of identifying suitable printing parameters. Printing of single layer objects was time-efficient and material-saving and close observations of the material behavior were a good indicator of a successful printing process and quality of the printed tablets. Tablets printed in this study showed satisfactory results in terms of mechanical strength and solid-state properties. Even though only small amounts of ink were used, tablets exhibited high tensile strengths up to 2.33 MPa when printed with a water-based ink. Fully amorphous and physically stable tablets were produced with 20% drug load printed with a water-free ink. A higher drug load of 40% KTZ was also feasible, but the presence of small crystalline traces induced recrystallization after twelve weeks of storage at accelerated conditions, demonstrating the limits of this approach. However, at drug loads of 20% small crystalline traces did not induce recrystallization during storage as they remained localized, which was attributed to the porous structure of the tablets. Further evaluations on additional APIs and polymers need to be performed.

DoP printing has so far been rarely used for the formulation of ASDs. Our approach shows that DoP printing coupled with HME has the potential to produce amorphous high dose tablets. This technique represents an alternative to other 3DP techniques such as FDM, which is often limited by the mechanical properties of the feedstock materials. Furthermore, the combination of an amorphous and highly porous formulation is advantageous for the formulation of poorly soluble drugs as it will increase solubility and dissolution and thereby likely enhance oral bioavailability. In a follow-up study, we will compare this technique to the FDM process in terms of processability and dosage form performance.

Funding

Parts of this work were supported by the German Federal Ministry of Education and Research [grant number 13XP5064].

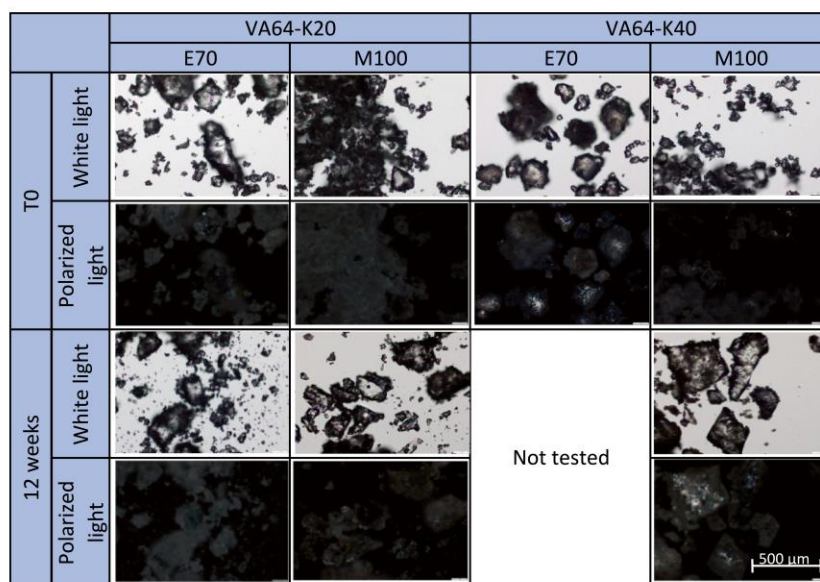


Fig. 9. Ground tablets with 20% and 40% drug load printed with E70 and M100. Images using white and polarized light at 10 \times magnification.

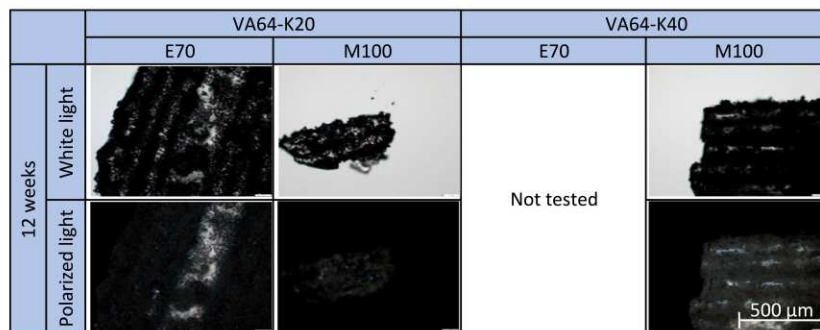


Fig. 10. Microscope images of tablet fragments at 5× magnification using white and polarized light.

CRedit authorship contribution statement

Nadine Gottschalk: Conceptualization, Investigation, Methodology, Formal analysis, Writing – original draft, Visualization. **Alicia Burkard:** Investigation, Formal analysis. **Julian Quodbach:** Conceptualization, Supervision, Writing – review & editing. **Malte Bogdahn:** Conceptualization, Supervision, Writing – review & editing.

Declaration of Competing Interest

The authors declare the following financial interests/personal relationships which may be considered as potential competing interests:

Malte Bogdahn has patent Process for the manufacture of a solid pharmaceutical administration form pending to Merck Patent GmbH. Nadine Gottschalk has patent Process for the manufacture of a solid pharmaceutical administration form pending to Merck Patent GmbH. Julian Quodbach has patent Process for the manufacture of a solid pharmaceutical administration form pending to Merck Patent GmbH.

Data availability

No data was used for the research described in the article.

Acknowledgements

The authors would like to thank Marcel Wedel for his technical support during the experiments. The authors would also like to thank the German Federal Ministry of Education and Research, as parts of this work were funded through the initiative ProMatLeben (grant number 13XP5064).

Appendix A. Supplementary data

Supplementary data to this article can be found online at <https://doi.org/10.1016/j.ijph.2022.100151>.

References

- Antic, A., Zhang, J., Amini, N., Morton, D.A.V., Hapgood, K.P., Ft, F., 2021. Screening pharmaceutical excipient powders for use in commercial 3D binder jetting printers. *Adv. Powder Technol.* 32, 2469–2483. <https://doi.org/10.1016/j.apt.2021.05.014>.
- Auch, C., Harms, M., Mäder, K., 2018. Melt-based screening method with improved predictability regarding polymer selection for amorphous solid dispersions. *Eur. J. Pharm. Sci.* 124, 339–348. <https://doi.org/10.1016/j.ejps.2018.08.035>.
- Chang, S., Wan, S., Kowsari, K., Shetty, A., Sorrells, L., Sen, K., Nagapudi, K., Chaudhuri, B., Ma, A.W.K., 2020. Binder-Jet 3D printing of indomethacin-laden pharmaceutical dosage forms. *J. Pharm. Sci.* 109, 3054–3063. <https://doi.org/10.1016/j.xphs.2020.06.027>.
- Chang, S., Jin, J., Yan, J., Dong, X., Chaudhuri, B., 2021. Development of a pilot-scale HuskyJet binder jet 3D printer for additive manufacturing of pharmaceutical tablets. *Int. J. Pharm.* 605, 120791. <https://doi.org/10.1016/j.ijpharm.2021.120791>.
- Clark, E.A., Alexander, M.R., Irvine, D.J., Roberts, C.J., Wallace, M.J., Yoo, J., Wildman, R.D., 2020. Making tablets for delivery of poorly soluble drugs using

- photoinitiated 3D inkjet printing. *Int. J. Pharm.* 578, 118805. <https://doi.org/10.1016/j.ijpharm.2019.118805>.
- Ethyl Alcohol, 70% v/v; MSDS No. VT270 [Online]; Val Tech Diagnostics: Zelenople, PA, USA, August 13, 2013; <http://www.labchem.com/tools/msds/msds/VT270.pdf>. (accessed January 4, 2023).
- Fuenmayor, E., Forde, M., Healy, A., Devine, D., Lyons, J., McConville, C., Major, I., 2018. Material considerations for fused-filament fabrication of solid dosage forms. *Pharmaceutics* 10, 44. <https://doi.org/10.3390/pharmaceutics10020044>.
- Gala, U.H., Miller, D.A., Williams, R.O., 2020. Harnessing the therapeutic potential of anticancer drugs through amorphous solid dispersions. *Biochim. Biophys. Acta - Rev. Cancer* 1873, 188319. <https://doi.org/10.1016/j.bbcan.2019.188319>.
- Gibbard, H.F., Creek, J.L., 1934. Vapor pressure of Methanol from 288.15 to 337.65 K. *J. Chem. Eng. Data* 19, 308–310. <https://doi.org/10.1021/jc60063a013>.
- Goole, J., Amighi, K., 2016. 3D printing in pharmaceutics: a new tool for designing customized drug delivery systems. *Int. J. Pharm.* 499, 376–394. <https://doi.org/10.1016/j.ijpharm.2015.12.071>.
- Gottschalk, N., Bogdahn, M., Harms, M., Quodbach, J., 2021. Brittle polymers in Fused Deposition Modeling: an improved feeding approach to enable the printing of highly drug loaded filament. *Int. J. Pharm.* 597, 120216. <https://doi.org/10.1016/j.ijpharm.2021.120216>.
- Goyanes, A., Robles Martinez, P., Buaz, A., Basit, A.W., Gaisford, S., 2015. Effect of geometry on drug release from 3D printed tablets. *Int. J. Pharm.* 494, 657–663. <https://doi.org/10.1016/j.ijpharm.2015.04.069>.
- Ilyés, K., Kovács, N.K., Balogh, A., Borbás, E., Farkas, B., Casian, T., Marosi, G., Tomuța, I., Nagy, Z.K., 2019. The applicability of pharmaceutical polymeric blends for the fused deposition modelling (FDM) 3D technique: Material considerations—printability—process modulation, with consecutive effects on in vitro release, stability and degradation. *Eur. J. Pharm. Sci.* 129, 110–123. <https://doi.org/10.1016/j.ejps.2018.12.019>.
- Infanger, S., Haemmerli, A., Iliev, S., Baier, A., Stoyanov, E., Quodbach, J., 2019. Powder bed 3D-printing of highly loaded drug delivery devices with hydroxypropyl cellulose as solid binder. *Int. J. Pharm.* 555, 198–206. <https://doi.org/10.1016/j.ijpharm.2018.11.048>.
- Jennotte, O., Koch, N., Lechanteur, A., Evrard, B., 2020. Three-dimensional printing technology as a promising tool in bioavailability enhancement of poorly water-soluble molecules: a review. *Int. J. Pharm.* 580, 119200. <https://doi.org/10.1016/j.ijpharm.2020.119200>.
- Kanauija, P., Lau, G., Ng, W.K., Widjaja, E., Hanefeld, A., Fischbach, M., Maio, M., Tan, R.B.H., 2011. Nanoparticle Formation and growth during in Vitro Dissolution of Ketoconazole Solid Dispersion. *J. Pharm. Sci.* 100, 2876–2885. <https://doi.org/10.1002/jps.22491>.
- Khattab, I.S., Bandarkar, F., Fakhree, M.A.A., Jouyban, A., 2012. Density, viscosity and surface tension of water+ethanol mixtures from 293 to 323 K. *Korean J. Chem. Eng.* 29, 812–817. <https://doi.org/10.1007/11814-011-0239-6>.
- Kozakiewicz-Latała, M., Nartowski, K.P., Dominik, A., Malec, K., Gólkowska, A.M., Ziocińska, A., Rusińska, M., Szymczyk-Ziółkowska, P., Ziółkowski, G., Górnica, A., Karolewicz, B., 2022. Binder jetting 3D printing of challenging medicines: from low dose tablets to hydrophobic molecules. *Eur. J. Pharm. Biopharm.* 170, 144–159. <https://doi.org/10.1016/j.ejpb.2021.11.001>.
- Leane, M., Pitt, K., Reynolds, G., 2015. A proposal for a drug product Manufacturing Classification System (MCS) for oral solid dosage forms. *Pharm. Dev. Technol.* 20, 12–21. <https://doi.org/10.3109/10837450.2014.954728>.
- Li, J., Tao, L., Dali, M., Buckley, D., Gao, J., Hubert, M., 2011. The effect of the physical states of binders on high-shear wet granulation and granule properties: a mechanistic approach toward understanding high-shear wet granulation process. Part II. Granulation and granule properties. *J. Pharm. Sci.* 100, 294–310. <https://doi.org/10.1002/jps.22261>.
- Liu, J., Cao, F., Zhang, C., Ping, Q., 2013. Use of polymer combinations in the preparation of solid dispersions of a thermally unstable drug by hot-melt extrusion. *Acta Pharm. Sin.* B 3, 263–272. <https://doi.org/10.1016/j.apsb.2013.06.007>.
- Nasereddin, J.M., Wellner, N., Alhijaj, M., Belton, P., Qi, S., 2018. Development of a simple mechanical screening method for predicting the feasibility of a pharmaceutical FDM 3D printing filament. *Pharm. Res.* 35, 151. <https://doi.org/10.1007/s11095-018-2432-3>.

- Pang, F.-M., Seng, C.-E., Teng, T.-T., Ibrahim, M.H., 2007. Densities and viscosities of aqueous solutions of 1-propanol and 2-propanol at temperatures from 293.15 K to 333.15 K. *J. Mol. Liq.* 136, 71–78. <https://doi.org/10.1016/j.molliq.2007.01.003>.
- Parhi, R., 2021. A review of three-dimensional printing for pharmaceutical applications: Quality control, risk assessment and future perspectives. *J. Drug Deliv. Sci. Technol.* 64, 102571 <https://doi.org/10.1016/j.jddst.2021.102571>.
- Pereira, B.C., Isreb, A., Forbes, R.T., Dores, F., Habashy, R., Petit, J.-B., Alhnan, M.A., Oga, E.F., 2019. "Temporary Plasticiser": a novel solution to fabricate 3D printed patient-centred cardiovascular "Polypill" architectures. *Eur. J. Pharm. Biopharm.* 135, 94–103. <https://doi.org/10.1016/j.ejpb.2018.12.009>.
- Pitt, K.G., Heasley, M.G., 2013. Determination of the tensile strength of elongated tablets. *Powder Technol.* 238, 169–175. <https://doi.org/10.1016/j.powtec.2011.12.060>.
- Raijada, D., Genina, N., Fors, D., Wisaeus, E., Peltonen, J., Rantanen, J., Sandler, N., 2013. A step toward development of printable dosage forms for poorly soluble drugs. *J. Pharm. Sci.* 102, 3694–3704. <https://doi.org/10.1002/jps.23678>.
- Scoutaris, N., Alexander, M.R., Gellert, P.R., Roberts, C.J., 2011. Inkjet printing as a novel medicine formulation technique. *J. Control. Release* 156, 179–185. <https://doi.org/10.1016/j.jconrel.2011.07.033>.
- Sen, K., Mehta, T., Sansare, S., Sharifi, L., Ma, A.W.K., Chaudhuri, B., 2021a. Pharmaceutical applications of powder-based binder jet 3D printing process – a review. *Adv. Drug Deliv. Rev.* 177, 113943 <https://doi.org/10.1016/j.addr.2021.113943>.
- Sen, K., Mukherjee, R., Sansare, S., Halder, A., Kashi, H., Ma, A.W.K., Chaudhuri, B., 2021b. Impact of powder-binder interactions on 3D printability of pharmaceutical tablets using drop test methodology. *Eur. J. Pharm. Sci.* 160, 105755 <https://doi.org/10.1016/j.ejps.2021.105755>.
- Seoane-Viño, I., Trenfield, S.J., Basit, A.W., Goyanes, A., 2021. Translating 3D printed pharmaceuticals: from hype to real-world clinical applications. *Adv. Drug Deliv. Rev.* 174, 553–575. <https://doi.org/10.1016/j.addr.2021.05.003>.
- Shah, N., Sandhu, Ha, Choi, D.S., Chokshi, H., Mallick, A.W. (Eds.), 2014. *Dissolution of Amorphous Solid Dispersions: Theory and Practice*. Springer. https://doi.org/10.1007/978-1-4939-1598-9_15.
- Sharma, G., Mueannoom, W., Buanz, A.B.M., Taylor, K.M.G., Gaisford, S., 2013. In vitro characterisation of terbutaline sulphate particles prepared by thermal ink-jet spray freeze drying. *Int. J. Pharm.* 447, 165–170. <https://doi.org/10.1016/j.ijpharm.2013.02.045>.
- Tian, P., Yang, F., Yu, L., Lin, M.-M., Lin, W., Lin, Q., Lv, Z., Huang, S., Chen, Y., 2019. Applications of excipients in the field of 3D printed pharmaceuticals. *Drug Dev. Ind. Pharm.* 45, 905–913. <https://doi.org/10.1080/03639045.2019.1576723>.
- Ting, J.M., Porter, W.W., Mecca, J.M., Bates, F.S., Reineke, T.M., 2018. Advances in polymer design for enhancing oral drug solubility and delivery. *Bioconjug. Chem.* 29, 939–952. <https://doi.org/10.1021/acs.bioconjchem.7b00646>.
- Vazquez, G., Alvarez, E., Navaza, J.M., 1995. Surface tension of alcohol water + water from 20 to 50 °C. *J. Chem. Eng. Data* 40, 611–614. <https://doi.org/10.1021/je00019a016>.
- Wanchoo, R.K., Narayan, J., 1992. Excess properties of (Methanol + Toluene or p-xylene) binary liquid mixture. *Phys. Chem. Liq.* 25, 15–26. <https://doi.org/10.1080/00319109208027283>.
- Wang, C.-C., Tejwani, M.R., Roach, W.J., Kay, J.L., Yoo, J., Surprenant, H.L., Monkhouse, D.C., Pryor, T.J., 2006. Development of near zero-order release dosage forms using three-dimensional printing (3-DPTM) technology. *Drug Dev. Ind. Pharm.* 32, 367–376. <https://doi.org/10.1080/03639040500519300>.
- Wang, Z., Han, X., Chen, R., Li, J., Gao, J., Zhang, H., Liu, N., Gao, X., Zheng, A., 2021. Innovative color jet 3D printing of levetiracetam personalized paediatric preparations. *Asian J. Pharm. Sci.* 16, 374–386. <https://doi.org/10.1016/j.ajps.2021.02.003>.
- Wang, Y., Müllertz, A., Rantanen, J., 2022a. Additive manufacturing of solid products for oral drug delivery using binder jetting three-dimensional printing. *AAPS PharmSciTech* 23, 196. <https://doi.org/10.1208/s12249-022-02321-w>.
- Wang, Y., Müllertz, A., Rantanen, J., 2022b. Structured approach for designing drug-loaded solid products by binder jetting 3D printing. *Eur. J. Pharm. Sci.* 178, 106280 <https://doi.org/10.1016/j.ejps.2022.106280>.
- Wei, C., Solanki, N.G., Vasoya, J.M., Shah, A.V., Serajuddin, A.T.M., 2020. Development of 3D Printed Tablets by Fused Deposition Modeling using polyvinyl Alcohol as Polymeric Matrix for Rapid Drug Release. *J. Pharm. Sci.* 109, 1558–1572. <https://doi.org/10.1016/j.xphs.2020.01.015>.
- Wickström, H., Palo, M., Rijckaert, K., Kolakovic, R., Nyman, J.O., Määttä, A., Ihalainen, P., Peltonen, J., Genina, N., de Beer, T., Löbmann, K., Rades, T., Sandler, N., 2015. Improvement of dissolution rate of indomethacin by inkjet printing. *Eur. J. Pharm. Sci.* 75, 91–100. <https://doi.org/10.1016/j.ejps.2015.03.009>.
- Wilts, E.M., Ma, D., Bai, Y., Williams, C.B., Long, T.E., 2019. Comparison of linear and 4-arm star poly(vinyl pyrrolidone) for aqueous binder jetting additive manufacturing of personalized dosage tablets. *ACS Appl. Mater. Interfaces* 11, 23938–23947. <https://doi.org/10.1021/acsami.9b08116>.
- Windolf, H., Chamberlain, R., Quodbach, J., 2021. Predicting drug release from 3D printed oral medicines based on the surface area to volume ratio of tablet geometry. *Pharmaceutics* 13, 1453. <https://doi.org/10.3390/pharmaceutics13091453>.
- Yu, D., Branford-White, C., Yang, Y.-C., Zhu, L., Welbeck, E.W., Yang, X., 2009. A novel fast disintegrating tablet fabricated by three-dimensional printing. *Drug Dev. Ind. Pharm.* 35, 1530–1536. <https://doi.org/10.3109/03639040903059359>.
- Zhang, J., Allardyce, B.J., Rajkhowa, R., Wang, X., Liu, X., 2021. 3D printing of silk powder by Binder Jetting technique. *Addit. Manuf.* 38, 101820 <https://doi.org/10.1016/j.addma.2020.101820>.

3.3. Comparing Fused Deposition Modeling and drop-on-powder printing

3.3.1. Comparative stability study of 3D printed amorphous solid dispersions

Even though DoP printing and FDM are categorized as 3DP techniques, they differ strongly in terms of material requirements and mode of action. This final paper focuses on the comparison of both printing techniques. Using the same material, a hot-melt extruded formulation containing copovidone and 20 % of the model compound ketoconazole, both techniques were compared regarding processability, resulting tablet properties and solid state of freshly prepared samples and after storage at accelerated conditions. Optimized processing conditions were applied according to the previously developed and described methods. The paper aims at highlighting the advantages and disadvantages of each technique and shall serve as decision guide for development of amorphous 3D printed dosage forms.

The idea and study design were mainly developed by Nadine Gottschalk. The experimental work was entirely performed by Nadine Gottschalk, who also performed the main data evaluation and wrote the initial manuscript draft. Malte Bogdahn and Julian Quodbach contributed to idea creation, study design and data evaluation and revised the initial manuscript draft.

Evaluation of authorship:

Author	Idea	Study Design	Experimental	Evaluation	Manuscript
Nadine Gottschalk	80	80	100	80	80
Malte Bogdahn	10	10	0	10	10
Julian Quodbach	10	10	0	10	10

Evaluation of copyright permission: This article is available under the Creative Commons CC-BY-NC-ND license and permits non-commercial use of the work as published, without adaptation or alteration provided the work is fully attributed (accessed 10.05.2024).

Article available online at: <https://doi.org/10.1016/j.ijpx.2023.100179>

© 2022 Published by Elsevier B.V.

3D Printing of Amorphous Solid Dispersions: A Comparison of Fused Deposition Modeling and Drop-on-Powder Printing

Nadine Gottschalk ^{a b}, Julian Quodbach ^{a c}, Malte Bogdahn ^b

^aInstitute of Pharmaceutics and Biopharmaceutics, Heinrich Heine University, Düsseldorf, Germany

^bMerck KGaA, Darmstadt, Germany

^cDepartment of Pharmaceutics, Utrecht Institute for Pharmaceutical Sciences, Utrecht University, Netherlands

International Journal of Pharmaceutics: X, Volume 5, 100179, 2023

DOI: 10.1016/j.ijpx.2023.100179

Abstract

Nowadays, a high number of pipeline drugs are poorly soluble and require solubility enhancement by e.g., manufacturing of amorphous solid dispersion. Pharmaceutical 3D printing has great potential in producing amorphous solid oral dosage forms. However, 3D printing techniques differ greatly in terms of processing as well as tablet properties. In this study, an amorphous formulation, which had been printed via Fused Deposition Modeling and drop-on-powder printing, also known as binder jetting, was characterized in terms of solid-state properties and physical stability. Solid state assessment was performed by differential scanning calorimetry, powder X-ray diffraction and polarized microscopy. The supersaturation performance of the amorphous solid dispersion was assessed via non-sink dissolution. We further evaluated both 3D printing techniques regarding their processability as well as tablet uniformity in terms of dimension, mass and content. Challenges and limitations of each 3D printing technique were discussed. Both techniques are feasible for the production of amorphous formulations. Results indicated that Fused Deposition Modeling is better suited for production, as the recrystallization tendency was lower. Still, filament production and printing presented a major challenge. Drop-on-powder printing can be a viable alternative for the production of amorphous tablets, when a formulation is not printable by Fused Deposition Modeling.



Contents lists available at ScienceDirect

International Journal of Pharmaceutics: X

journal homepage: www.sciencedirect.com/journal/international-journal-of-pharmaceutics-x

3D printing of amorphous solid dispersions: A comparison of fused deposition modeling and drop-on-powder printing

Nadine Gottschalk^{a,b}, Malte Bogdahn^{b,*}, Julian Quodbach^{a,c,1}

^a Institute of Pharmaceutics and Biopharmaceutics, Heinrich Heine University, Düsseldorf, Germany

^b Merck KGaA, Darmstadt, Germany

^c Department of Pharmaceutics, Utrecht Institute for Pharmaceutical Sciences, Utrecht University, Netherlands

ARTICLE INFO

Keywords:

Fused deposition modeling
Drop-on-powder
Binder jetting
Amorphous solid dispersion
Solubility enhancement
3D printing
Additive manufacturing

ABSTRACT

Nowadays, a high number of pipeline drugs are poorly soluble and require solubility enhancement by e.g., manufacturing of amorphous solid dispersion. Pharmaceutical 3D printing has great potential in producing amorphous solid oral dosage forms. However, 3D printing techniques differ greatly in terms of processing as well as tablet properties. In this study, an amorphous formulation, which had been printed via Fused Deposition Modeling and drop-on-powder printing, also known as binder jetting, was characterized in terms of solid-state properties and physical stability. Solid state assessment was performed by differential scanning calorimetry, powder X-ray diffraction and polarized microscopy. The supersaturation performance of the amorphous solid dispersion was assessed via non-sink dissolution. We further evaluated both 3D printing techniques regarding their processability as well as tablet uniformity in terms of dimension, mass and content. Challenges and limitations of each 3D printing technique were discussed. Both techniques are feasible for the production of amorphous formulations. Results indicated that Fused Deposition Modeling is better suited for production, as the recrystallization tendency was lower. Still, filament production and printing presented a major challenge. Drop-on-powder printing can be a viable alternative for the production of amorphous tablets, when a formulation is not printable by Fused Deposition Modeling.

1. Introduction

The majority of new drug entities nowadays is poorly soluble. It is estimated that poorly soluble compounds make up around 70% of pipeline compounds (Ting et al., 2018). One of the most used techniques to enhance their solubility is the production of amorphous solid dispersions (ASD). The amorphous state is unstable and can be stabilized by polymers. The incorporation of an active pharmaceutical ingredient (API) can be performed e.g., by hot-melt extrusion (HME) in which the API and polymer are transformed into the amorphous state by means of thermal and mechanical energy (Shah et al., 2014). Regarding the production of solid oral dosage forms (SODF) a classical process chain would be to mill the extrudate, add additional excipients and perform

tableting. In early clinical trials, this can lead to issues as different dosages are in evaluation, requiring different tablet formulations. Formulation development can be challenging especially in early stages of development because only small quantities of active pharmaceutical ingredient (API) are available.

Novel manufacturing techniques, such as three-dimensional printing (3DP), can be valuable for the pharmaceutical industry, due to fast adaptability of the 3D tablet design. Among the wide range of 3DP techniques, the most reported techniques to produce SODFs are Fused Deposition Modeling (FDM), due the good availability of affordable printers (Araújo et al., 2019), and drop-on-powder (DoP) printing, being the first 3DP technique to result in a FDA approved pharmaceutical product (Vaz and Kumar, 2021).

Abbreviations: 3DP, three-dimensional printing; ACN, acetonitrile; API, active pharmaceutical ingredient; ASD, amorphous solid dispersion; CAD, computer-aided design; CV, coefficient of variation; DoP, drop-on-powder; dpmm, dots per millimeter; DSC, differential scanning calorimetry; FaSSIF, fasted state simulated intestinal fluid; FDM, fused deposition modeling; T_g, glass transition temperature; HME, hot-melt extrusion; KTZ, ketoconazole; pXRD, powder X-ray diffraction; SODF, solid oral dosage form; UPLC, ultra-performance liquid chromatography.

* Corresponding author.

E-mail address: Malte.Bogdahn@Merckgroup.com (M. Bogdahn).

¹ Both authors contributed equally.

<https://doi.org/10.1016/j.ijpx.2023.100179>

Received 28 December 2022; Received in revised form 16 March 2023; Accepted 17 March 2023

Available online 20 March 2023

2590-1567/© 2023 The Authors. Published by Elsevier B.V. This is an open access article under the CC BY-NC-ND license (<http://creativecommons.org/licenses/by-nc-nd/4.0/>).

FDM belongs to the material extrusion processes. Filament, the wirelike feedstock material, is pushed through a heated nozzle and the 3D object is created through layer-by-layer deposition of molten material. In FDM, the mechanical properties of filaments are of great importance as they are decisive for printability (Fuenmayor et al., 2018; Ilyés et al., 2019; Nasereddin et al., 2018; Zhang et al., 2017). The mechanical properties depend on different factors, such as the type and proportions of API, polymer and additional excipients. FDM, as a melt-based manufacturing method, is well suited for the production of ASDs. Amorphization of the API can be achieved either during HME or during the printing process (Prasad et al., 2019). Several studies have demonstrated the possibility to produce amorphous FDM-printed SODFs (Buyukgoz et al., 2021; Gottschalk et al., 2021; Jamróz et al., 2018; Kissi et al., 2021; Prasad et al., 2019).

DoP printing can be referred to the additive manufacturing category binder jetting and is part of the powder-based 3DP techniques. Ink droplets are generated and jetted onto powder layers. The ink fuses powder particles in-situ, resulting in porous systems. Polymeric binders are necessary to provide the required mechanical stability of the tablet and can be included in the ink (Chang et al., 2021; Yu et al., 2009) as well as in the powder bed (Antic et al., 2021; Infanger et al., 2019). There is also the possibility to include the API in the ink (Clark et al., 2020; Wickström et al., 2015). Solvent evaporation from droplets can be fast and similar to other solvent evaporation methods like spray drying, ASDs can be produced. However, this kind of binder jetting is mainly restricted to printing on edible paper or of oral films instead of powder-based dosage forms. Due to this, the achievable dosages in the final SODFs are low (Clark et al., 2020; Rajjada et al., 2013; Wickström et al., 2015). In contrast, adding the API to the powder bed enables high drug loads up to 70% but is mainly limited to highly soluble drugs (Infanger et al., 2019; Wang et al., 2021). Recently, we published a printing approach, which uses milled extrudate as powder bed material to enable higher drug loadings up to 40% of a poorly soluble API in its amorphous form (Gottschalk et al., 2022a) and on which we will elaborate further in this study.

Both techniques, FDM and DoP printing, can be used to produce amorphous SODFs. In this study we directly compare these techniques by using exactly the same raw material, a hot-melt extruded ASD. We demonstrate opportunities and challenges that arise during material processing and the influence of the different printing techniques on tablet properties and physical stability of an ASD. The poorly soluble API ketoconazole (KTZ) was used as model compound. Copovidone was used due to its versatile use as a matrix former for ASDs as well as good binding capacities in DoP printing. Process development was described in an earlier study on DoP printing (Gottschalk et al., 2022a) and FDM (Gottschalk et al., 2022b; Gottschalk et al., 2021) and optimized printing conditions were applied. This study is meant to display the advantages and disadvantages of each technique and act as a decision guide for drug product development.

2. Material and methods

2.1. Materials

KTZ was used as model compound. KTZ is poorly soluble (0.08 mg/mL in phosphate buffer pH 6.8 (Ullrich and Schiffter, 2018)) and melts at 151 °C (Kanaujia et al., 2011). KTZ was purchased from LGM Pharma (Boca Raton, USA). Copovidone, which was used as matrix polymer (Kollidon® VA64, vinylpyrrolidone-vinyl acetate copolymer), was purchased from BASF (Ludwigshafen, Germany). Colloidal silicon dioxide was used as flowability enhancer and was purchased from Evonik Industries (Essen, Germany).

Fasted State Simulated Intestinal Fluid (FaSSIF) powder was purchased from Biorelevant.com Ltd. (London, UK). Hydrochloric acid (HCl, 0.1 M), acetonitrile (ACN, hypergrade, purity ≥99.9%), sodium hydroxide solution (1 M), formic acid, ammonia solution (25%), sodium

chloride and di-sodium hydrogen phosphate were purchased from Merck KGaA (Darmstadt, Germany). All reagents used in this study were of analytical grade.

2.2. Extrusion and filament production

The powder blend was prepared using a Turbular® mixer (T2C, Willy A. Bachofen AG, Muttenz, Switzerland). First, KTZ (20%) and copovidone (79%) were blended for 15 min. Hereafter, colloidal silicon dioxide (1%) was added to the premix and blended for another 15 min.

Extrusion was performed on a Pharma 11 hot-melt extruder (Thermo Fisher Scientific, Waltham, USA) with a 1.75 mm die with a length of 3 cm. The screw configuration consisted of three mixing elements to achieve good mixing of all components. The detailed screw configuration is displayed in the supplementary material (Table S1). Heating zone 1 was set to 60 °C, zone 2 to 120 °C, zones 3–7 to 180 °C and the die to 175 °C. Feeding was performed using a gravimetric feeder (Congrav® OP 1 T, Brabender Technologie GmbH & Co. KG, Duisburg, Germany) at 0.2 kg/h. The screw speed was set to 300 rpm. A conveyor belt (Brabender Technologie GmbH & Co. KG, Duisburg, Germany) was used to adjust the filament diameter to 1.75 mm by adapting the conveyor belt speed. The diameter was measured using a laser axis measurement system (Odac Trio33, Zumbach Electronic AG, Orpund, Switzerland). The intended filament diameter was 1.75 mm ± 0.05 mm and only filament within this specification was used for FDM printing.

2.3. Feed force testing

The feed force tester as described in Gottschalk et al. (2022b) was used to determine suitable printing conditions on a Texture Analyser (TA-XT, Stable Micro Systems, Godalming, UK). A test speed (piston movement speed) of 1.00 mm/s was chosen, which equals a printing speed of 30 mm/s. For further details see Gottschalk et al. (2022b). Tests were performed in quintuplicate at 130 °C, 140 °C and 150 °C. Feed forces were determined in the last 40 mm of testing distance.

2.4. Printing FDM

Printing was performed on an Ultimaker 3 (Ultimaker, Utrecht, Netherlands) equipped with an Ultimaker print core (0.4 mm, BB). The printer had been modified according to Gottschalk et al. (2021) to enable the printing of brittle filaments as well as printing with a filament diameter of 1.75 mm. The tablet design was cylindrical and was created in Fusion 360 (Autodesk, San Rafael, USA) with a height of 2.4 mm and a diameter of 10 mm. The design was saved as binary stereolithography file format (.stl). Slicing was performed using Simplify3D (version 4.0.1., Simplify3D, Cincinnati, USA). The nozzle was heated to 150 °C and the build plate up to 70 °C. Printing was performed at 30 mm/s, a line width of 0.4 mm and a layer height of 0.2 mm. The infill density was 100%. Printed tablets are referred to as FDM tablets in the following text.

2.5. Milling

Part of the filaments was milled to achieve fine powder for DoP printing. Samples were milled using an ultra-centrifugal mill (ZM 200, Retsch, Haan, Germany). A twelve-tooth rotor and a sieve with a mesh size of 200 µm with a distance ring were employed. Filaments were milled at 10,000 rpm. Particle size was determined using a Camsizer X2 (Retsch, Haan, Germany) equipped with the X-jet module and applying a dispersing pressure of 50 kPa. Gap width was set to 4 mm. Milled powder is referred to as DoP powder in the following text.

2.6. Printing DoP

A custom-made powder bed printer was used for DoP printing of

tablets. The printer consisted of a powder reservoir, a roller for powder deposition, a building platform, which can be controlled in xyz-direction, and a fixed printhead, a modified HP C6602 cartridge. The printer setup is described in detail in [Gottschalk et al. \(2022a\)](#). The same computer-aided design (CAD) file as in 2.4. was used for printing of DoP tablets. Slicing was performed with an in-house developed script. Tablets were printed at 30 dots per mm (dpmm) in printing direction with an ink containing ethanol and water (70:30 wt%) and an infill density of 100%. The parameters had been determined in a previous study and have been selected since the settings led to best results regarding mechanical properties and solid state. Printed tablets are referred to as DoP tablets in the following text.

2.7. Tablet dimension and mass

Tablet height and diameter were determined using a digital caliper (TWIN-Cal IP67, TESA Technology, Renens, Switzerland) for all printed tablets. Measurements were performed in triplicate. Tablet mass of all tablets was determined using an analytical balance (ME235S-0 CE, Sartorius, Goettingen, Germany).

2.8. Differential scanning calorimetry (DSC)

Blend, filament, tablets and DoP powder were analyzed regarding their solid state with a DSC 1 (Mettler Toledo, Gießen, Germany). Filament (approximately 500 mg) and tablets (3 each) were ground using mortar and pestle. Approximately 7–8 mg were weighed into 100 μ L aluminum pans and sealed. The lid was pierced prior to the analysis using the automatic piercing unit. A pierced pan was used as reference. Two heating cycles from 0 to 170 $^{\circ}$ C were applied at 10 K/min.

2.9. Powder X-Ray diffraction (pXRD)

pXRD measurements were performed on ground tablets, filament and DoP powder to determine the solid state using a D2 Phaser (Bruker, Billerica, USA) equipped with an SSD160 detector in 1D mode. A full opening of 4.875 $^{\circ}$ was used. A copper anode at 30 kV and 10 mA was used to generate X-rays. Reduction of K β radiation was done by nickel foil. Sample preparation was performed on a zero-background holder with well. Sample rotation speed was set to 5 rpm and sample was scanned from 6 $^{\circ}$ to 35 $^{\circ}$ with a step size of 0.02 $^{\circ}$ and measurement time of 6 s per step.

2.10. Polarized light microscopy

Ground tablets, filament and DoP powder were analyzed in white and polarized light under a microscope (IX73P1F, Olympus, Tokyo, Japan) at 5 \times and 10 \times magnification for the detection of crystalline traces. In addition to that, the powder raw materials were assessed regarding their particle size in white light at 10 \times magnification. Microscopical images were recorded and evaluated using Olympus cellSens Standard software (version: 1.18).

2.11. Content

KTZ concentration was determined using ultra-performance liquid chromatography (UPLC). The method is described in [Gottschalk et al., 2021](#). FDM and DoP tablets were assessed as well as the corresponding feedstock materials (filament and DoP powder). Regarding filament, coherent pieces were analyzed instead of milled samples to assess possible effects on API distribution. Samples were weighed into small glass vessels and diluted with a mixture of ACN and MilliQ water (50:50) to a concentration of 0.2 mg/mL (assuming a drug load of 20% KTZ). Tests were performed in triplicate.

2.12. Non-sink dissolution

Non-sink dissolution of tablets, filament and milled filament was performed in FaSSiF. FaSSiF was prepared by using FaSSiF powder at a concentration of 22 mg/mL in phosphate buffer pH 6.5. Ground samples were accurately weighed using a micro balance (MCA6.6S-2S00-M Cubis $\text{\textcircled{R}}$, Sartorius, Goettingen, Germany) into 2 mL Eppendorf caps (approximately 3 mg). By adding 1.2 mL of heated FaSSiF (37 $^{\circ}$ C) the experiment was started. First, samples were vortexed for 30 s (Vortex-Genie $\text{\textcircled{R}}$ 2, Scientific Instruments, Schwäbisch Gmünd, Germany) and placed in an incubator (Thermomixer comfort, Eppendorf, Hamburg, Germany) heated up to 37 $^{\circ}$ C. Prior to each sampling point, samples were centrifuged at 15,000 rpm (Mikro 200R, Hettich, Tuttlingen, Germany). At each sampling point 50 μ L of supernatant was removed and diluted with 50 μ L of ACN to prevent precipitation. The cycle of vortexing, incubation and centrifugation was repeated after each sampling. The removed volume was not replaced. Sampling points were 5, 10, 15, 20, 30, 45, 60, 90 and 120 min. The maximum possible API concentration was 500 μ g/mL. Tests were performed in triplicate.

2.13. Sink-dissolution

Dissolution was performed according to the Ph. Eur. 2.9.3. and 5.17.1. in a dissolution tester (Smart AT7, Sotax, Aesch, Switzerland) equipped with paddles (USP dissolution apparatus 2). Paddle rotation speed was set to 100 rpm. DoP and FDM tablets ($n = 3$, respectively) were dissolved in 900 mL of 0.1 N HCl at 37 $^{\circ}$ C. 3 mL of sample was drawn at 5, 10, 15, 30, 45, 60, 90 and 120 min. Sink-dissolution was performed with the aim to investigate differences in terms of drug release from the different dosage forms. As the surface area to volume ratio strongly influences the release ([Windolf et al., 2021](#)), the same tablet designs were compared. However, as printing resulted in different tablet weights, the absolute API mass differed, being approximately 48 mg for FDM printed tablets and approximately 30 mg for DoP printed tablets.

2.14. Three-point bending test

The three-point bending flexural test is commonly applied to assess and compare the mechanical properties of filaments for the FDM process. A Texture Analyser TA-XT equipped with a three-point bending rig (Stable Micro Systems, Godalming, UK) was used. The gap between the supports was 30 mm. The test punch was moved at 5 mm/s prior to the test and reduced to 0.1 mm/s upon contact with the test specimen. Filament diameter was assessed using the laser measurement system ([Section 2.2](#)) prior to the test and stress and strains were calculated for each run. Tests were carried out in tenfold. The strain at break was determined to evaluate the brittleness of the material. Data were acquired using Exponent software (version 6.1.16.0).

2.15. Material density

Extrudate density was analyzed using a nitrogen pycnometer (Ultracyc 1200e gas expansion pycnometer, Quantachrome, Boynton Beach, USA). The target pressure was 1.4 bar. Extrudate was milled using a Tube Mill Control (IKA, Staufen, Germany) at 25,000 rpm. Tests were performed in triplicate and approximately 4–5 g of sample were analyzed in each run.

2.16. Storage conditions

Samples of each feedstock material (filament and DoP powder) and tablets (FDM and DoP) were placed in glass vessels and stored for 2, 4 and 12 weeks in a desiccator in a climate chamber (KBF 240, Binder, Tuttlingen, Germany) at 40 $^{\circ}$ C.

3. Results and discussion

3.1. Processing

In FDM, filament diameter homogeneity is of great importance as fluctuations $>1.75 \text{ mm} \pm 0.05 \text{ mm}$ may lead to deviations in tablet mass (Ponsar et al., 2020). The filament diameter during extrusion is displayed in Fig. 1. It shows that the diameter was not always in the range of $1.75 \text{ mm} \pm 0.05 \text{ mm}$. The filament diameter was manually adapted by adjusting the speed of a conveyor belt. A small die swell was observed at the extruder die, wherefore stretching of the extrudate strand was necessary. To find the appropriate conveyor belt speed was difficult and a trial-and-error process. Oscillating fluctuations in diameter were observed approximately every 30–60 s. These signals did not correlate with other extrusion parameters such as torque, die pressure or actual throughput as these were constant (supplementary material Fig. S1). Earlier extrusion experiments on the Pharma 11 had also shown these oscillations and it is assumed that these are likely a result of the pulsatile material transport in twin-screw extruders, which is correlated to high screw speeds (Ponsar et al., 2020). High screw speeds of 300 rpm were used in this setup as they have been reported to be a critical parameter for the production of ASDs. They provide mechanical energy input and facilitate molecular dispersion of the API in the polymer matrix (Keen et al., 2014) as well does the use of kneading zones. It was shown that the use of three kneading zones in the screw configuration, which was the case in this study, leads to discontinuous material transport and fluctuations in filament diameter (Chamberlain et al., 2022). For the following experiments it was important to use fully amorphous material. In case of FDM printing it was assumed that the short residence in the hot end would not provide sufficient thermal energy to amorphize the API. Since the extruded material was also used as starting material for DoP printing, it was necessary that the API was fully amorphous and well distributed in the polymer matrix since crystalline traces and local supersaturation were likely to result in recrystallization upon contact with the ink. Due to that, higher diameter fluctuations were accepted during extrusion. However, FDM printing of tablets was performed only with selected filament within the specification of $1.75 \text{ mm} \pm 0.05 \text{ mm}$ to reduce tablet mass deviations.

The FDM printing temperature was determined using the feed force tester. Forces below the printer force limit of 4 N were achieved at 140 °C. Even though the melt flow was suitable at 140 °C, printing had to be performed at 150 °C as the material did not stick to the build plate. Tablets detached during printing, stopping the printing process.

Handling indicated that filament was very brittle. The strain at break

determined via the 3-point bending test was low ($2.5\% \pm 0.6\%$) and further decreased during storage at accelerated conditions to 1.5–1.7% (Table 1). The decrease in breaking strength was a result of fine hairline cracks (supplementary material Fig. S2), which had formed during storage in a desiccator at 40 °C, most likely a result of subsequent drying (see chapter 3.3.). In FDM, suitable mechanical properties of the filament are crucial for their printability.

The brittleness of the material was beneficial for the production of DoP powder bed material as it facilitated milling to a small particle size without the use of liquid nitrogen. However, milling was only possible batchwise as the fine particles did block the sieve after approximately 1 h. The milling chamber reached up to 50 °C during milling. Milled powder proved easy to in handling during printing. As described in Gottschalk et al. (2022a), milled extrudate was easily spreadable over a broad range of settings and resulted in a smooth powder bed. The only drawback here was the hygroscopicity of the material combined with a high surface area of the finely milled material. Water sorption led to attachment of particles to the roller-recoater system, which had to be removed manually before each layering process.

3.2. Tablet properties

Due to the different manufacturing processes, tablet appearance differed strongly between FDM and DoP printed tablets. FDM tablets had a glassy appearance and were transparent (Fig. 2). Grooves from the printer nozzle were clearly visible on the tablet surface and tablet edges were sharp. In contrast, DoP tablets were white and had a powdery surface. Edges were slightly rounded compared to FDM tablets. Darker lines on the tablet surface of DoP tablets were a result of the slicer setting. The intention was to produce a slight overlap of the jetted ink to prevent tablets from falling apart at potential printing gaps. This is discussed in detail in Gottschalk et al. (2022a). In addition, the shape of these tablets was slightly elliptical compared to FDM printed tablets. The reason for this is that FDM tablets were produced by printing two circular shell layers and a rectilinear infill pattern, while DoP tablets were produced by depositing the ink as stripes, since the twelve nozzles were

Table 1

Strain at break in 3-point bending test of filaments over storage (Mean strain at break and SD, $n = 10$).

	T0	2 weeks	4 weeks	12 weeks
Strain at break (%)	2.5	1.5	1.7	1.7
SD (%)	0.6	0.5	0.2	0.2

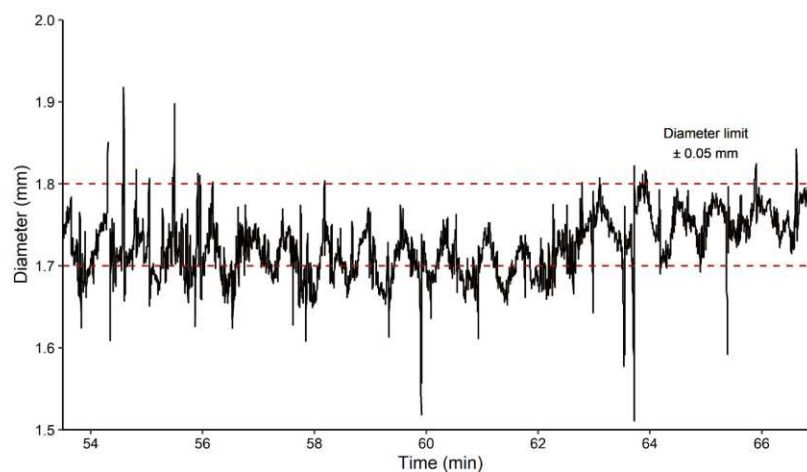


Fig. 1. Filament diameter during extrusion.



Fig. 2. FDM and DoP tablets.

arranged in line.

Printing using the same CAD file resulted in different tablet masses (Table 2). Mean FDM tablet mass was approximately 1.6× higher than DoP tablet mass. In FDM, the molten material solidifies, resulting in very dense objects with only few voids (Gottschalk et al., 2022b). The tablet mass-to-volume ratio (1.21 g/mL) corresponds approximately the material density (1.23 g/mL) of the intended 3D design. Fine powder material, which was used for DoP printing, had a smaller bulk density and, corresponding to that, tablets had a lower density (0.8 g/mL compared to 1.2 g/mL assuming mean values for tablet dimension and mass from Table 2).

The tablet height and diameter of FDM tablets were slightly elevated compared to the CAD design (approximately +0.1 mm in terms of tablet height and +0.4 mm in terms of diameter). Elevated height is possibly a result of the bumpy tablet surface, whereas the elevated tablet diameter is possibly a result of the nozzle pushing the softened material to the sides. DoP tablet height differed between the batches and was also slightly higher compared to the CAD file design in most cases. Elevated height of DoP tablets is possibly a result of the polymer swelling upon contact with the ink. Copovidone is known to swell upon contact with water (Antic et al., 2021). The tablet diameter was only slightly lower (approximately 0.15 mm) than the target design.

Regarding the deviations in tablet mass and dimensions, differences were observed between the various batches of DoP tablets (Table 2). A maximum of twelve tablets was printed in one run. The number of suitable tablets of each run differed because some of the tablets stuck to the build plate and broke during removal. Tablets had to be printed in a way that the ink in the first layer was in contact to the build plate to reduce warping (Gottschalk et al., 2022a). Further, printing had to be performed on different days to reach the number of tablets necessary for the stability testing, whereas FDM tablets were printed within one day. Here, a number of ten tablets was defined as one batch to facilitate comparison between FDM and DoP tablets and evaluate whether there were trends during printing.

Regarding DoP tablets, a mass increase was observed between the

different prints. The total difference between the first and the last batch was approximately 20 mg. However, the variations within one DoP tablet batch were significantly lower than the variations of the FDM tablets ($p < 0.05$). As described in Section 3.1., copovidone is very hygroscopic and the powder surface area was large. The powder cartridge had been stored over-night in a plastic bags, therefore it is likely that the increase in mass is a result of water sorption. The coefficient of variation (CV) of the FDM batches was higher in most cases, ranging from 1.0% - 4.4%, which can probably be attributed to filament diameter deviations. Filament was produced in a range of 1.7–1.8 mm, which can result in mass deviations up to 5.8% in theory. Mass conformity is crucial in the production of high dose SODFs as tablet mass deviations can result in dosage fluctuations. An optimized extrusion process and filament uniformity may improve the mass uniformity of printed tablets. Other factors contributing to impaired mass conformity related to the printing process may be inconsistent filament forward propulsion as a result of high viscosities in the nozzle, which can be excluded since optimized conditions according to the feed force tester were used. However, it might be possible that oozing occurred, since a higher printing temperature was necessary to ensure that tablets adhered to the build plate. Adding to that, the build plate height may be another factor. It has been shown that printed mass differed significantly when the build plate was leveled by different operators (Melocchi et al., 2016) and on different days of leveling (Alhijaj et al., 2019). In this study leveling was performed by one person at the start of printing and was not altered until all FDM tablets required were printed. However, it is possible that build plate height changes slightly during removal of printed tablets.

3.3. Solid state and physical stability

Every step in the process chain can influence the solid state and physical stability of an ASD. Therefore, all steps from filament, milled DoP powder and printed tablets were considered. Polarized microscopic images as well as DSC measurements indicated that the feedstock materials were fully amorphous, demonstrating that extrusion was successful in producing amorphous material and furthermore, that milling did not promote recrystallization. Reheating of amorphous filaments during FDM printing did not affect the solid state either. However, small birefringence was occasionally observed for DoP printed tablets (Fig. 3). This effect was already described in our previous study and is due to local overwetting of ink. The analytical methods DSC and pXRD were not capable of detecting these small amounts of crystals, concluding that the amount was below the limit of detection of 2% and 5%, respectively, which was determined in a previous study (Gottschalk et al., 2021). During storage over twelve weeks, samples remained amorphous or, in case of DoP tablets, no further increase of recrystallization was observed (Fig. 3), which can be attributed to the porous structure of the tablets. The porous structure prevents the spread of recrystallization by forming crystallization barriers in form of voids.

Table 2

Dimensions and weight of DoP and FDM tablets for the respective batches. Number of tablets denotes the usable tablets from a batch and the total number printed in a batch. Batch numbering: first number refers to the day of printing and second number to the printing order on that day.

Tablet type	Batch	Number of tablets	Mean height (mm)	CV (%)	Mean diameter (mm)	CV (%)	Mean mass (mg)	CV (%)	
DoP	1.1	3/3	2.43	2.65	9.82	1.60	138.7	0.1	
	2.1	7/12	2.44	2.12	9.86	0.75	143.8	0.9	
	2.2	8/12	2.41	1.75	9.80	0.45	145.3	1.2	
	3.1	11/12	2.40	1.49	9.84	0.36	148.1	1.5	
	3.2	12/12	2.46	2.17	9.86	0.68	149.7	1.0	
	3.3	12/12	2.46	1.60	9.83	0.53	149.6	1.0	
	4.1	10/12	2.50	1.22	9.85	0.49	156.3	1.1	
	4.2	12/12	2.49	1.30	9.86	0.44	160.8	1.2	
	FDM	1.1	10	2.48	1.82	10.36	0.63	239.9	1.8
		1.2	10	2.48	1.49	10.43	0.74	240.6	1.0
1.3		10	2.50	2.43	10.49	0.53	242.0	2.8	
1.4		10	2.53	3.32	10.44	0.71	238.4	4.4	
Target value	–	–	2.40	–	10.00	–	–	–	

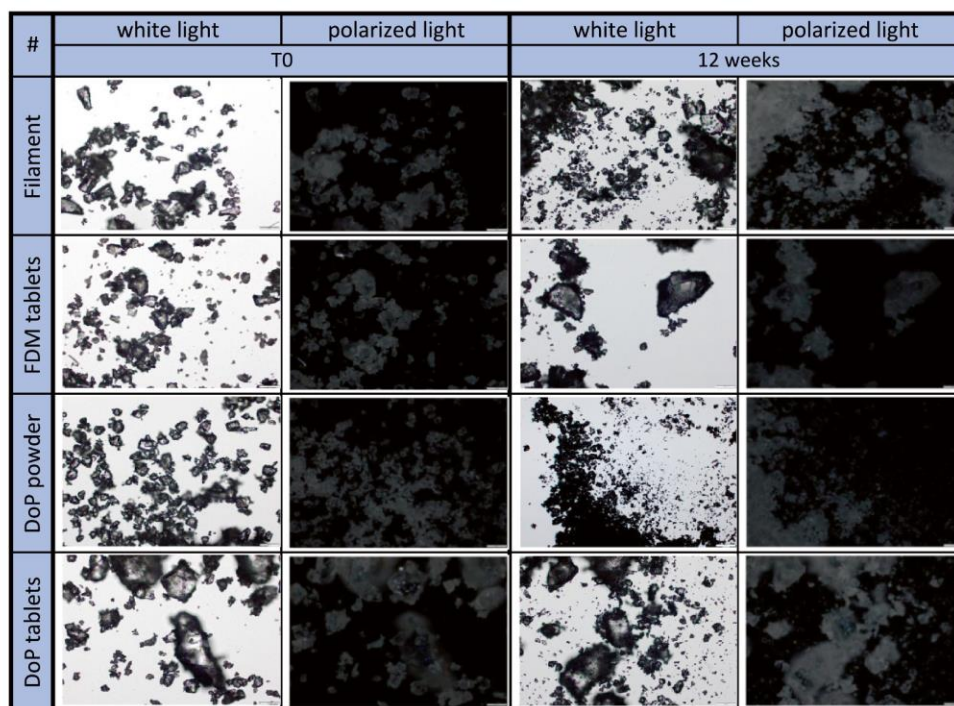


Fig. 3. Microscopic images of ground filament, tablets and DoP powder at 10 \times magnification at T0 and after twelve weeks of storage at 40 °C in desiccator (images of DoP tablets from Gotschalk et al., 2022b).

Non-sink dissolution (Fig. 4) confirmed the presence of small crystalline traces in DoP printed tablets as the supersaturation declined faster (101 $\mu\text{g}/\text{mL}$ after 120 min dissolution for stability samples before storage) compared to the other materials (161–181 $\mu\text{g}/\text{mL}$ after 120 min dissolution for stability samples before storage). Anwar et al. (2015) described that the presence of small crystal nuclei can induce precipitation in a supersaturated solution. Similar supersaturation profiles were obtained for stored samples, indicating no further recrystallization. There was only one exception in case of FDM tablets after two weeks of storage, where supersaturation reduced faster. It is likely that this was due to content fluctuations in the filament, which will be discussed in the following section. Since the material was ground and homogenized for non-sink dissolution, error bars were low.

The storage conditions might have contributed to the good physical stability of the material. Samples had been stored at 40 °C in a desiccator, since pretests had shown that storage at 75% r.h. led to strong recrystallization due to water sorption. Copovidone is known to be a hygroscopic polymer. Humidity in an ASD can lower the glass transition temperature (T_g) and increase the mobility of the API facilitating recrystallization (Patel and Serajuddin, 2022). However, storage at elevated temperature and dry conditions resulted in subsequent drying of the materials, indicated by an increase of T_g (Table 3) in all cases. The T_g was lowest for DoP tablets, which can be attributed to the use of a water-based ink and residual moisture.

3.4. Content and drug release

In order to ensure the correct dose of 3D printed SODFs, it is necessary that the API is well distributed in the polymer matrix. Local supersaturations of API in the polymer can further lead to enhanced recrystallization. The content and content uniformity were evaluated during the whole process chain. Table 4 displays the blend content prior extrusion, the filament content and the content of the remaining material in the feeder after extrusion. The mean content of the blend was

slightly higher than the targeted content but also showed high deviations. This was probably related to the high differences in particles size of the different material. The particle size of KTZ ranged between 1 and 5 μm whereas in case of copovidone particles up to 200 μm were observed using a microscope. We observed a significant increase ($p < 0.05$) of drug content of the remaining material in the feeder and a significant decrease of filament content during extrusion ($p < 0.05$), indicating segregation of the powder blend during extrusion. It is likely that due to the cohesiveness of the smaller KTZ particles and adhesion to the feeder walls, small portions of KTZ remained in the extruder, thereby reducing the filament content and increasing the content of the remaining powder material in the feeder. This is supported by an increase of powder screw speed from approx. 25 rpm to 29 rpm towards the end of extrusion. Since extrusion was performed approximately 40 °C below the degradation temperature of KTZ (221 °C, Kanaujia et al. (2011)) and no impurities were observed in UPLC chromatograms, it is unlikely that content decrease was due to degradation.

Content of feedstock materials and tablets are displayed in Fig. 5. In two cases, the deviations of FDM tablets and filaments were higher compared to the other samples (ranging from 3.5 to 6.6%), indicating inhomogeneities in the filament. Content deviations were very low for DoP powder material and DoP tablets being mainly in a range of <1% (with a maximum of 2.7%). DoP powder material was milled post extrusion and blended, which probably contributes to the content uniformity.

The mean content of DoP powder and tablets was in all cases lower than the targeted content, whereas FDM filament and tablet content was higher in many cases. Comparing the feedstock materials, DoP powder showed a significantly lower content than the filament at T0 ($p < 0.05$). It is likely that the increased powder surface of the DoP powder accelerated water sorption during handling and intermittent storage of the samples as no indications on drug degradation were observed. Water sorption increases the tablet mass and leads to a lower apparent drug content. Filaments on the other hand, have a lower surface area-to

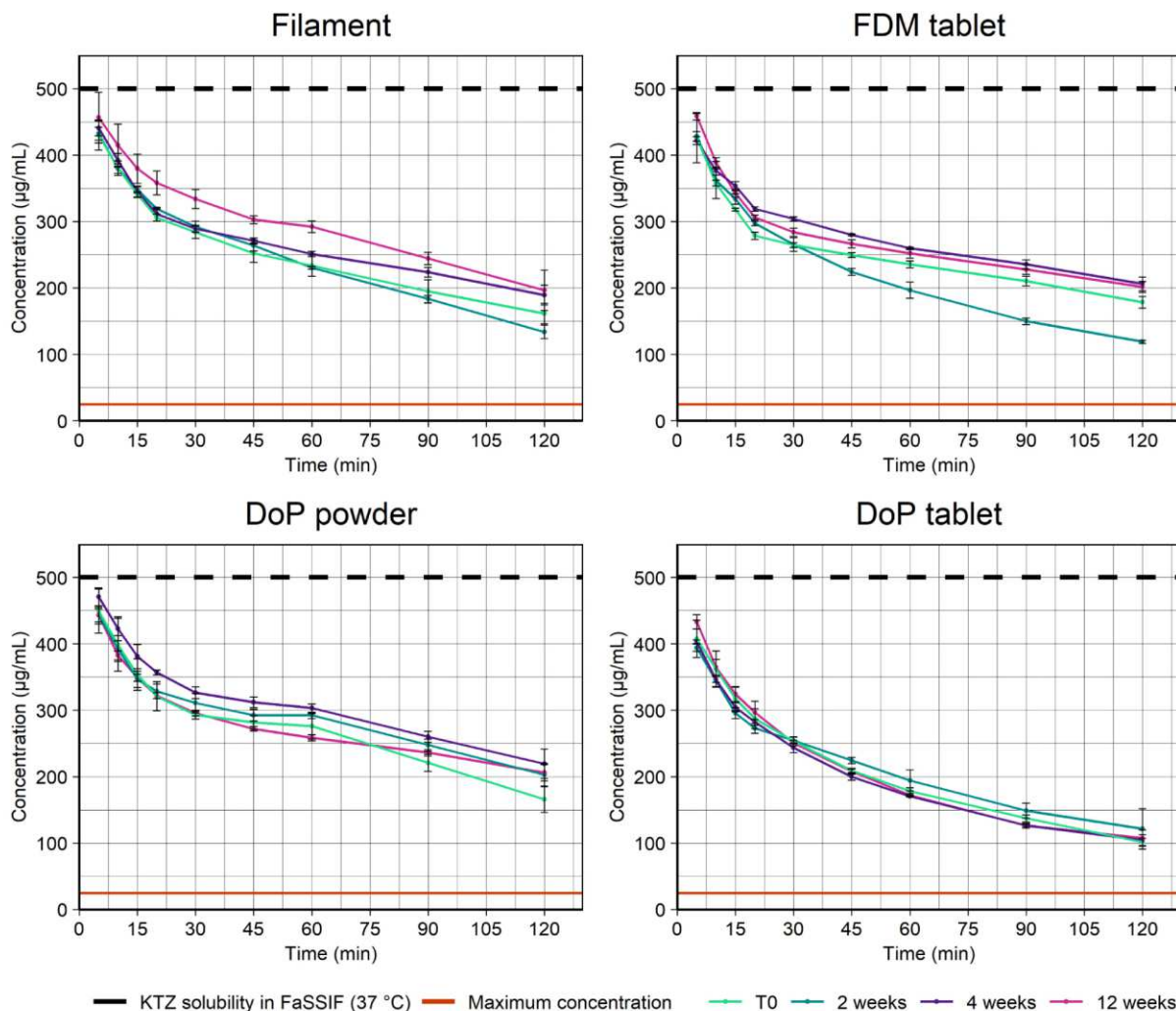


Fig. 4. Non-sink dissolution of filament, tablets and DoP powder (mean concentration \pm SD, $n = 3$).

Table 3

T_g s of materials during storage.

Samples	T_g (°C) \pm SD ($n = 3$)			
	Filament	FDM tablet	DoP powder	DoP tablet
T0	51.9 \pm 4.4	55.5 \pm 2.4	54.2 \pm 0.9*	34.0 \pm 12.1*
2 weeks	59.1 \pm 0.5	61.6 \pm 0.3	66.5 \pm 4.5	58.3 \pm 0.5
4 weeks	66.6 \pm 1.1	65.1 \pm 2.2	56.1 \pm 9.9	64.2 \pm 0.7
12 weeks	68.3 \pm 1.5	72.3 \pm 1.0	74.6 \pm 0.4	69.4 \pm 0.6*

* Data were shown in previous study (Gottschalk et al., 2022a).

Table 4

Content of powder blend, filament and of blend in feeder after extrusion (Mean \pm SD).

	Blend ($n = 12$)	Filament ($n = 9$)	Feeder after extrusion ($n = 3$)
Content (%)	103.6 \pm 1.8	98.6 \pm 1.3	106.0 \pm 0.8

volume ratio slowing down water sorption. Furthermore, the drug content of DoP printed tablets at T0 was significantly lower ($p < 0.05$) than drug content of the DoP tablets, whereas no significant differences were observed after storage of the samples. Printing was performed using a water-based ink and it is likely that water remained in the tablets. The drying process was not optimized in this study. Samples post-dried during storage, which is also supported by the increasing T_g of the samples (Table 3).

Drug release from tablets was fast and all dosage forms released 80% of KTZ within 15–30 min (Fig. 6). Drug release was similar even though DoP tablets had a higher porosity. Copovidone is a well soluble polymer and KTZ was amorphous. Fast dissolution and the small size of the tablets are possibly the reason that no differentiation was possible. Both types of tablets eroded in a similar manner upon contact with the dissolution medium. It is likely that in case of DoP tablets the dissolution medium led to swelling of the polymer on the tablet surface, making the dissolution independent from the tablet porosity. This effect was described for compressed amorphous melt extrudate by Flügel et al. (2021).

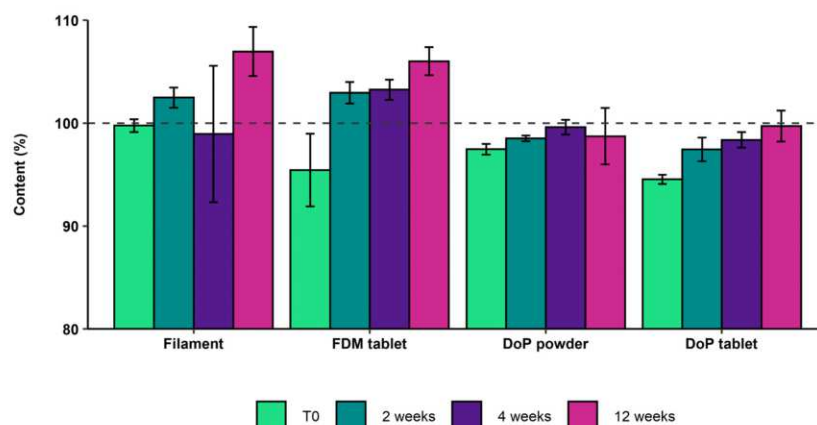


Fig. 5. KTZ content for filament, tablets and DoP powder (mean drug content \pm SD, $n = 3$).

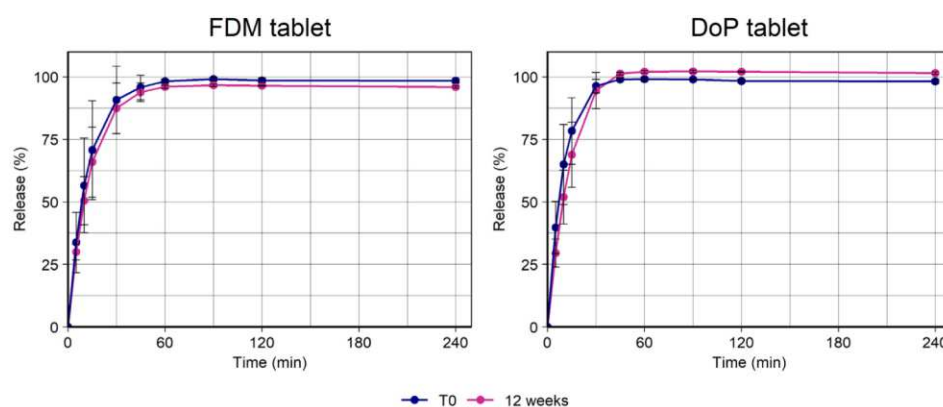


Fig. 6. Sink-dissolution of FDM and DoP tablets (mean release \pm SD, $n = 3$).

3.5. Comparison of techniques

The choice on which 3DP techniques to employ depends greatly on the material properties. In case of a brittle formulation, the filament production and printability will be more difficult and may require additional equipment to enable printing. Furthermore, the production of filaments is challenging, especially the production of amorphous filament at high drug loads, as the parameter settings for ASDs (high screw speeds) and filament (low screw speeds) can be contradicting and need extensive investigation of a sweet spot. Several techniques have been employed to bypass the step of filament production by, e.g., direct powder extrusion (Goyanes et al., 2019; Zheng et al., 2021) or modification of the feeding mechanism (Gottschalk et al., 2021). Nevertheless, the use of filament as an intermediate is especially beneficial for production of dosage forms as the solid state reduces the risk of operator exposure (Quodbach et al., 2021). However, even though the material in this study was in a solid state, it imposes the risk of small splinters during handling of the filament or detaching tablets from the build plate when material is too brittle.

In case of an ASD being too brittle for FDM, DoP printing presents a suitable alternative printing technique. However, an additional milling step is necessary to achieve printable powder bed material. To reduce the number of processing steps and further bypass thermal stress during HME, also the use of spray-dried ASDs would be conceivable. Still, a thorough assessment of possible inks and printing parameters is necessary (Gottschalk et al., 2022a). The high surface area combined with

high hygroscopicity of copovidone presented a challenge during the manufacturing process, which makes it necessary to perform manufacturing at controlled conditions. Furthermore, a powder-based process naturally requires additional safety precautions. On the other hand, milling of extrudate is easier than the production of homogenous filaments for FDM printing and formulation development is facilitated as the process is mainly independent from the mechanical properties of the formulation.

In DoP, the printability of customized inks was reported to present a major challenge and intensive formulation development is required to achieve optimal properties in terms of surface tension, viscosity and density (Prasad and Smyth, 2016). This study used a simple ink composition, which occasionally led to malfunction of individual nozzles, wherefore it was necessary to replace the print cartridge. This was sufficient for the number of tablets produced in this study. Three cartridges were used to print the whole number of tablets. At a larger scale, the ink needs to be optimized for the respective printhead in order to ensure the longevity of printheads. In addition, this study used organic solvents in the ink composition to ensure faster evaporation and prevent recrystallisation. The presence of residual amounts of solvent in the tablets is likely, wherefore, tablets would have to be additionally tested to meet the limits of the ICH Q3C (R8) on residual solvents in pharmaceuticals. In this study a mixture of ethanol and water was used. Ethanol, being a class 3 solvents, is a solvent with low toxic potential. However, the comparison in the prior study indicated that the higher volatile solvent methanol resulted in less recrystallization at higher drug loads.

The use of more volatile solvents may be necessary to increase the drug loading or for APIs with a higher recrystallization tendency. Furthermore, residual water was not fully removed during drying. Drying of tablets is a critical process and the impact of residual moisture in the DoP tablets should be further investigated.

Great differences between the two techniques are the appearance and dimensional properties of the tablets. FDM tablets showed poor resolution compared to DoP printed tablets. The resolution in DoP printing is mainly dependent on the particle size of the powder material (Infanger et al., 2019) whereas the resolution in FDM depends on the nozzle size (Kiński and Pietkiewicz, 2020) and the viscosity of molten material. A nozzle with a diameter of 0.4 mm was used in this study. Smaller nozzles are available but it has to be considered that this would also result in a higher printing duration. The poor resolution of FDM tablets has been widely described (Brambilla et al., 2021) and a study among children revealed that FDM tablets were favored least compared to tablets produced by selective laser sintering, semi-solid extrusion and digital light processing due to their rough and hard appearance (Januskaite et al., 2020). This eventually results in impaired patient compliance wherefore printing parameters and tablet geometries in FDM have to be chosen wisely and might require post-processing. Contributing to that, tablet mass variations of FDM tablets were higher compared to DoP in most batches, which was possibly a result of the filament quality. As filament extrusion is very challenging another approach could be to optimize FDM printers for the production of SODFs by equipping them with control mechanism that adapt to changes in filament diameter and deposited mass. DoP tablets were not as dense as FDM tablets due to the lower bulk density of the powder bed. Higher porosity can be beneficial regarding API release but also challenging when high doses of API have to be applied. Several approaches have been reported for powder-based printing processes to increase powder material density, such as the use of powder with bimodal particle size distribution (Sofia et al., 2018). From these observations we conclude that FDM tablets are rather suited when high doses have to be applied due to their higher mass-to-volume ratio, whereas DoP tablets are suited for the application of porous systems. For both printing techniques, the 3D design has to be adapted to the respective material density to achieve the required dose.

Both 3DP techniques were capable in producing amorphous and physically stable SODFs. It has to be pointed out, though, that even small traces of crystallinity, as in the case of DoP tablets, resulted in a slightly impaired supersaturation performance, which may reduce oral absorption. The DoP technique is prone to recrystallization when using an ASD as powder bed material wherefore very high drug loads might be difficult to achieve. Higher drug loads are likely feasible in FDM but the effects of the API on the processing conditions and mechanical properties of filaments have to be considered.

The storage stability of the feedstock materials is more important than the stability of 3D printed tablets, as tablets for on-demand production will not have long shelf-life. With FDM, the quality of filaments during storage must be ensured, to prevent changes in terms of dimensional and mechanical properties such as embrittlement, which was observed in this study.

In FDM, a homogenous drug distribution in the filament is crucial since inhomogeneities in filaments can result in over- or underdosing of tablets. This study indicated small variations of drug content uniformity in filaments produced on a small-scale extruder. However, at different extrusion setups or for different formulations, variations could be more pronounced and hence, more critical. In the event that blend segregation is likely to occur, it may be necessary to include a granulation step prior to extrusion to ensure content uniformity. For DoP printing, the usage of a hot melt extruded single-phase material is beneficial as content fluctuations can be balanced out by milling of the extrudate and subsequent homogenization. Another benefit is that segregation of DoP powder components during the manufacturing process is not possible since the API is embedded in the polymer. Even though it appears that

optimization of the extrusion process is not as necessary as in FDM, it is also important in DoP printing of ASDs that the API is equally distributed in the polymer as local supersaturations will recrystallize to a greater degree upon contact with the ink.

The choice of 3DP technique will also depend on the respective API. Due to FDM printing being a thermo-intensive process, degradation of temperature-sensitive APIs may be possible. If water-based inks are used in DoP, this will present a challenge to APIs sensitive to hydrolysis. These two scenarios were not covered in this study.

4. Conclusion

In this study, we demonstrated that printing of an ASD was successful using the printing techniques FDM and DoP printing. Tablets with a high drug loading were achieved in which the API was amorphous and physically stable. We elaborated on the advantages and drawbacks of each printing technique and the respective aspects that have to be considered in the manufacturing process. If mechanical properties allow the production of flexible filaments, FDM is preferable for the production of high dose ASDs due to the lower chances of recrystallization. It has to be considered, though, that production of filament is challenging and operators should pay particular attention to filament uniformity. DoP printing presents a good alternative for brittle ASDs. DoP tablets were further advantageous compared to FDM tablets in terms of mass uniformity. However, high drug loaded ASDs and formulations that are sensitive to moisture and recrystallization will be difficult to be printed with DoP printing as well as high doses due to the higher porosity of SODFs. The choice of manufacturing process with an ASD depends on the API, targeted dose and physical stability in the respective polymer matrix. Each 3DP technique has its potential that can be leveraged for different applications.

Funding

Parts of this work were supported by the German Ministry of Education and Research [grant number 13XP5064].

CRediT authorship contribution statement

Nadine Gottschalk: Conceptualization, Investigation, Methodology, Formal analysis, Writing – original draft, Visualization. **Malte Bogdahn:** Conceptualization, Supervision, Writing – review & editing. **Julian Quodbach:** Conceptualization, Supervision, Writing – review & editing.

Declaration of Competing Interest

The authors declare the following financial interests/personal relationships which may be considered as potential competing interests:

Malte Bogdahn has patent Process for the manufacture of a solid pharmaceutical administration form pending to Merck Patent GmbH. Julian Quodbach has patent Process for the manufacture of a solid pharmaceutical administration form pending to Merck Patent GmbH. Nadine Gottschalk has patent Process for the manufacture of a solid pharmaceutical administration form pending to Merck Patent GmbH.

Data availability

No data was used for the research described in the article.

Acknowledgements

The authors would like to thank Marcel Wedel for his technical support during the DoP experiments and Alessandro-Giuseppe Elia for his support during hot-melt extrusion. The authors would also like to thank the German Federal Ministry of Education and Research, as parts

of this work were funded through the initiative ProMatLeben (grant number 13XP5064).

Appendix A. Supplementary data

Supplementary data to this article can be found online at <https://doi.org/10.1016/j.ijph.2023.100179>.

References

- Alhijaj, M., Nasereddin, J., Belton, P., Qi, S., 2019. Impact of processing parameters on the quality of pharmaceutical solid dosage forms produced by Fused Deposition Modeling (FDM). *Pharmaceutics* 11, 633. <https://doi.org/10.3390/pharmaceutics11120633>.
- Antic, A., Zhang, J., Amini, N., Morton, D.A.V., Hapgood, K.P., Ft, F., 2021. Screening pharmaceutical excipient powders for use in commercial 3D binder jetting printers. *Adv. Powder Technol.* 32, 2469–2483. <https://doi.org/10.1016/j.apt.2021.05.014>.
- Anwar, J., Khan, S., Lindfors, L., 2015. Secondary crystal nucleation: Nuclei breeding factory uncovered. *Angew. Chem. Int. Ed.* 54, 14681–14684. <https://doi.org/10.1002/anie.201501216>.
- Araújo, M.R.P., Sa-barreto, L.L., Gratiéri, T., Gelfuso, G.M., Cunha-filho, M., 2019. The digital pharmacies era: How 3D Printing technology using fused deposition modeling can become a reality? *Pharmaceutics* 11, 128. <https://doi.org/10.3390/pharmaceutics11030128>.
- Brambilla, C.R.M., Okafor-muo, O.L., Hassanin, H., Elshaer, A., 2021. 3DP printing of oral solid formulations: a systematic review. *Pharmaceutics* 13. <https://doi.org/10.3390/pharmaceutics13030358>.
- Buyukgoz, G.G., Kossor, C.G., Davé, R.N., 2021. Enhanced supersaturation via fusion-assisted amorphization during 3D printing of crystalline poorly soluble drug loaded filaments. *Pharmaceutics* 13. <https://doi.org/10.3390/pharmaceutics13111857>.
- Chamberlain, R., Windolf, H., Geissler, S., Quodbach, J., Breitkreutz, J., 2022. Precise dosing of pramipexole for low-dosed filament production by hot melt extrusion applying various feeding methods. *Pharmaceutics* 14, 216. <https://doi.org/10.3390/pharmaceutics14010216>.
- Chang, S., Jin, J., Yan, J., Dong, X., Chaudhuri, B., 2021. Development of a pilot-scale HuskyJet binder jet 3D printer for additive manufacturing of pharmaceutical tablets. *Int. J. Pharm.* 605, 120791. <https://doi.org/10.1016/j.ijpharm.2021.120791>.
- Clark, E.A., Alexander, M.R., Irvine, D.J., Roberts, C.J., Wallace, M.J., Yoo, J., Wildman, R.D., 2020. Making tablets for delivery of poorly soluble drugs using photoinitiated 3D inkjet printing. *Int. J. Pharm.* 578, 118805. <https://doi.org/10.1016/j.ijpharm.2019.118805>.
- Flügel, K., Schmidt, K., Mareczek, L., Gäbe, M., Hennig, R., Thommes, M., 2021. Impact of incorporated drugs on material properties of amorphous solid dispersions. *Eur. J. Pharm. Biopharm.* 159, 88–98. <https://doi.org/10.1016/j.ejpb.2020.12.017>.
- Fuenmayor, E., Forde, M., Healy, A., Devine, D., Lyons, J., McConville, C., Major, I., 2018. Material considerations for fused-filament fabrication of solid dosage forms. *Pharmaceutics* 10, 44. <https://doi.org/10.3390/pharmaceutics10020044>.
- Gottschalk, N., Bogdahn, M., Harms, M., Quodbach, J., 2021. Brittle polymers in fused deposition modeling: an improved feeding approach to enable the printing of highly drug loaded filament. *Int. J. Pharm.* 597, 120216. <https://doi.org/10.1016/j.ijpharm.2021.120216>.
- Gottschalk, N., Burkard, A., Quodbach, J., Bogdahn, M., 2022a. Drop-on-powder 3D printing of amorphous high dose oral dosage forms: process development, opportunities and printing limitations. *Int. J. Pharm.* X 100151. <https://doi.org/10.1016/j.ijph.2022.100151>.
- Gottschalk, N., Quodbach, J., Elia, A.-G., Hess, F., Bogdahn, M., 2022b. Determination of feed forces to improve process understanding of Fused Deposition Modeling 3D printing and to ensure mass conformity of printed solid oral dosage forms. *Int. J. Pharm.* 614, 121416. <https://doi.org/10.1016/j.ijpharm.2021.121416>.
- Goyanes, A., Allahham, N., Trenfield, S.J., Stoyanov, E., Gaisford, S., Basit, A.W., 2019. Direct powder extrusion 3D printing: fabrication of drug products using a novel single-step process. *Int. J. Pharm.* 567, 118471. <https://doi.org/10.1016/j.ijpharm.2019.118471>.
- Ilyés, K., Kovács, N.K., Balogh, A., Borbás, E., Farkas, B., Casian, T., Marosi, G., Tomuță, I., Nagy, Z.K., 2019. The applicability of pharmaceutical polymeric blends for the fused deposition modelling (FDM) 3D technique: Material considerations—printability—process modulation, with consecutive effects on in vitro release, stability and degradation. *Eur. J. Pharm. Sci.* 129, 110–123. <https://doi.org/10.1016/j.ejps.2018.12.019>.
- Infanger, S., Haemmerli, A., Iliev, S., Baier, A., Stoyanov, E., Quodbach, J., 2019. Powder bed 3D-printing of highly loaded drug delivery devices with hydroxypropyl cellulose as solid binder. *Int. J. Pharm.* 555, 198–206. <https://doi.org/10.1016/j.ijpharm.2018.11.048>.
- Jamróz, W., Szafraniec, J., Kurek, M., Jachowicz, R., 2018. 3D printing in pharmaceutical and medical applications – recent achievements and challenges. *Pharm. Res.* <https://doi.org/10.1007/s11095-018-2454-x>.
- Januskaitė, P., Xu, X., Ranmal, S.R., Gaisford, S., Basit, A.W., Tuleu, C., Goyanes, A., 2020. I spy with my little eye: a paediatric visual preferences survey of 3D printed tablets. *Pharmaceutics* 12, 1–16. <https://doi.org/10.3390/pharmaceutics12111100>.
- Kanaujia, P., Lau, G., Ng, W.K., Widjaja, E., Hanefeld, A., Fischbach, M., Maio, M., Tan, R.B.H., 2011. Nanoparticle formation and growth during in vitro dissolution of ketoconazole solid dispersion. *J. Pharm. Sci.* 100, 2876–2885. <https://doi.org/10.1002/jps.22491>.
- Keen, J.M., Martin, C., MacHado, A., Sandhu, H., McGinity, J.W., Dinunzio, J.C., 2014. Investigation of process temperature and screw speed on properties of a pharmaceutical solid dispersion using corotating and counter-rotating twin-screw extruders. *J. Pharm. Pharmacol.* 66, 204–217. <https://doi.org/10.1111/jphp.12106>.
- Kiński, W., Pietkiewicz, P., 2020. Influence of the printing nozzle diameter on tensile strength of produced 3D models in FDM technology. *Agric. Eng. 24*, 31–38. <https://doi.org/10.1515/agriceng-2020-0024>.
- Kissi, E.O., Nilsson, R., Nogueira, L.P., Larsson, A., Tho, I., 2021. Influence of drug load on the printability and solid-state properties of 3D-printed Naproxen-based amorphous solid dispersion. *Molecules* 26, 4492. <https://doi.org/10.3390/molecules26154492>.
- Melocchi, A., Parietti, F., Maroni, A., Foppoli, A., Gazzaniga, A., Zema, L., 2016. Hot-melt extruded filaments based on pharmaceutical grade polymers for 3D printing by fused deposition modeling. *Int. J. Pharm.* 509, 255–263. <https://doi.org/10.1016/j.ijpharm.2016.05.036>.
- Nasereddin, J.M., Wellner, N., Alhijaj, M., Belton, P., Qi, S., 2018. Development of a simple mechanical screening method for predicting the feedability of a pharmaceutical FDM 3D printing filament. *Pharm. Res.* 35, 151. <https://doi.org/10.1007/s11095-018-2432-3>.
- Patel, N.G., Serajuddin, A.T.M., 2022. Moisture sorption by polymeric excipients commonly used in amorphous solid dispersion and its effect on glass transition temperature: I. Polyvinylpyrrolidone and related copolymers. *Int. J. Pharm.* 616, 121532. <https://doi.org/10.1016/j.ijpharm.2022.121532>.
- Ponsar, H., Wiedey, R., Quodbach, J., 2020. Hot-melt extrusion process fluctuations and their impact on critical quality attributes of filaments and 3D-printed dosage forms. *Pharmaceutics* 12, 511. <https://doi.org/10.3390/pharmaceutics12060511>.
- Prasad, L.K., Smyth, H., 2016. 3D Printing technologies for drug delivery: a review. *Drug Dev. Ind. Pharm.* <https://doi.org/10.3109/03639045.2015.1120743>.
- Prasad, E., Islam, M.T., Goodwin, D.J., Megarry, A.J., Halbert, G.W., Florence, A.J., Robertson, J., 2019. Development of a hot-melt extrusion (HME) process to produce drug loaded Affinisol™ 15LV filaments for fused filament fabrication (FFF) 3D printing. *Addit. Manuf.* 29, 100776. <https://doi.org/10.1016/j.addma.2019.06.027>.
- Quodbach, J., Bogdahn, M., Breitkreutz, J., Chamberlain, R., Eggenreich, K., Elia, A.G., Gottschalk, N., Gunkel-Grabole, G., Hoffmann, L., Kapote, D., Kipping, T., Klinken, S., Loose, F., Marquetant, T., Windolf, H., Geißler, S., Spitz, T., 2021. Quality of FDM 3D printed medicines for pediatrics: considerations for formulation development, filament extrusion, printing process and printer design. *Ther. Innov. Regul. Sci.* <https://doi.org/10.1007/s43441-021-00354-0>.
- Rajjada, D., Genina, N., Fors, D., Wisaeus, E., Peltonen, J., Rantanen, J., Sandler, N., 2013. A step toward development of printable dosage forms for poorly soluble drugs. *J. Pharm. Sci.* 102, 3694–3704. <https://doi.org/10.1002/jps.23678>.
- Shah, N., Sandhu, H., Choi, D.S., Chokshi, H., Malick, A.W. (Eds.), 2014. *Dissolution of Amorphous Solid Dispersions: Theory and Practice*. Springer. https://doi.org/10.1007/978-1-4939-1598-9_15.
- Sofia, D., Chirone, R., Lettieri, P., Barletta, D., Poletto, M., 2018. Selective laser sintering of ceramic powders with bimodal particle size distribution. *Chem. Eng. Res. Des.* 136, 536–547. <https://doi.org/10.1016/j.cherd.2018.06.008>.
- Ting, J.M., Porter, W.W., Mecca, J.M., Bates, F.S., Reineke, T.M., 2018. Advances in polymer design for enhancing oral drug solubility and delivery. *Bioconjug. Chem.* 29, 939–952. <https://doi.org/10.1021/acs.bioconjchem.7b00646>.
- Ullrich, A., Schiffer, H.A., 2018. The influence of polymer excipients on the dissolution and recrystallization behavior of ketoconazole: Application, variation and practical aspects of a pH shift method. *Eur. J. Pharm. Biopharm.* 133, 20–30. <https://doi.org/10.1016/j.ejpb.2018.09.018>.
- Vaz, V.M., Kumar, L., 2021. 3D printing as a promising tool in personalized medicine. *AAPS PharmSciTech* 22, 49. <https://doi.org/10.1208/s12249-020-01905-8>.
- Wang, X., Han, X., Chen, R., Li, J., Gao, J., Zhang, H., Liu, N., Gao, X., Zheng, A., 2021. Innovative color jet 3D printing of levettiracetam personalized paediatric preparations. *Asian J. Pharm. Sci.* 16, 374–386. <https://doi.org/10.1016/j.ajps.2021.02.003>.
- Wickström, H., Palo, M., Rijckaert, K., Kolakovic, R., Nyman, J.O., Määttä, A., Ihalainen, P., Peltonen, J., Genina, N., de Beer, T., Löbmann, K., Rades, T., Sandler, N., 2015. Improvement of dissolution rate of indomethacin by inkjet printing. *Eur. J. Pharm. Sci.* 75, 91–100. <https://doi.org/10.1016/j.ejps.2015.03.009>.
- Windolf, H., Chamberlain, R., Quodbach, J., 2021. Predicting drug release from 3D Printed oral medicines based on the surface area to volume ratio of tablet geometry. *Pharmaceutics* 13, 1453. <https://doi.org/10.3390/pharmaceutics13091453>.
- Yu, D., Branford-White, C., Yang, Y.-C., Zhu, L., Welbeck, E.W., Yang, X., 2009. A novel fast disintegrating tablet fabricated by three-dimensional printing. *Drug Dev. Ind. Pharm.* 35, 1530–1536. <https://doi.org/10.3109/03639040903059359>.
- Zhang, J., Feng, X., Patil, H., Tiwari, R.V., Repka, M.A., 2017. Coupling 3D printing with hot-melt extrusion to produce controlled-release tablets. *Int. J. Pharm.* 519, 186–197. <https://doi.org/10.1016/j.ijpharm.2016.12.049>.
- Zheng, Y., Deng, F., Wang, B., Wu, Y., Luo, Q., Zuo, X., Liu, X., Cao, L., Li, M., Lu, H., Cheng, S., Li, X., 2021. Melt extrusion deposition (MEDTM) 3D printing technology – a paradigm shift in design and development of modified release drug products. *Int. J. Pharm.* 602, 120639. <https://doi.org/10.1016/j.ijpharm.2021.120639>.

4. Summary and conclusion

This work discussed the processability of highly loaded ASDs through 3DP and properties of printed dosage forms. For this purpose, highly loaded filaments were manufactured through HME with the aim to use them in the FDM process. Filaments contained the drug substance ketoconazole at 40 % drug load and different polymers commonly used in HME, namely copovidone, polyvinyl caprolactam-polyvinyl acetate-polyethylene glycol graft copolymer and basic butylated methacrylate copolymer. Filaments with a suitable dimensional conformity were successfully produced, however printing using the common feeding mechanism of the printer was not possible, as the filaments broke between the feeding gears. The mechanical properties were further assessed using the three-point bending test and compared to respective formulations without API. Overall, the filaments showed a brittle behavior and further an increase in brittleness of drug loaded filaments. In order to overcome the feedability issue, the feeding mechanism was modified to piston feeding to enable printing of the brittle materials. Therefore, a rigid guide was designed and placed on top of the print head in which the brittle filaments were placed, preventing filament bending and breakage. The brittle filament was moved through a flexible filament, which was guided into the rigid guide using the bowden extruder at the back of the printer. Highly drug loaded tablets were successfully printed. The filaments from copovidone and polyvinyl caprolactam-polyvinyl acetate-polyethylene glycol graft copolymer were amorphous, but traces of crystallinity were found in filament from basic butylated methacrylate copolymer, which triggered in recrystallization during printing. Even though printing parameters had been optimized to reduce crystallinity in tablets, full amorphization was not achieved as the transition time of the filament in the hotend is short, demonstrating the necessity of fully amorphous filaments after extrusion. Tablets printed from copovidone and basic butylated methacrylate copolymer showed immediate release, which was not achieved for tablet from polyvinyl caprolactam-polyvinyl acetate-polyethylene glycol graft copolymer, demonstrating the influence of the polymer on the dissolution and the need of fast dissolving polymers to achieve immediate release dosage forms through FDM printing. Modification of the feeding mechanism from feeding gears to piston feeding enabled printing of materials. By employing such a feeding system in newly developed printers, the printable range of materials or material combinations can be extended and formulation development can be facilitated. It has to be pointed out that even though very brittle materials may be printable with this feeding system, they carry the risk of breaking during handling. Small particles of split API-containing material have to be considered in terms of operator safety and potential cross-contamination within the printing system. Further, the mechanical properties must also be considered in terms tablet removal from the build plate and potential post-processing

steps. A drawback of this feeding system was its discontinuity. Re-engineering would be required to develop printers that can automatically change filament sticks. Depending on the changing system, different mechanical specifications will have to be defined. On a larger scale, the automatized production of filaments will also determine the specifications for the mechanical properties. This will potentially also require formulation development or even the development of novel polymers that are dedicated for the use in pharmaceutical FDM printing.

A high drug load can further affect the rheological properties and consequently printing conditions. In order to predict suitable printing conditions, a new method, the feed force tester was developed. The feed force tester mimics the printing process and measures the force, which is required at a specified nozzle temperature and vertical movement of the filament through the hotend (correlating printing speed). Comparative printing experiments were conducted at equal printing conditions using commercially available filaments. Printed test specimen were characterized in terms of absolute mass and mass uniformity. At certain printing conditions, especially when printing speed is high or nozzle temperature low, the absolute tablet mass was smaller than the targeted mass and batch variability is high. This was explained by insufficient melting in the hotend and discontinuous forward propulsion of the filament leading to underextrusion, which became also visible through μ CT-measurements. Consequently, the melt viscosity has to reach a level where the feeding gears are capable to push the softened material through the nozzle. From these printing trials a force limit of the printer could be derived. Thus, the feed force tester can be used to identify printing conditions that fall below the feed force limit of the printer ensuring that the targeted absolute mass is printed as well as mass uniformity. Regarding pharmaceutical formulations, filaments containing polyvinyl alcohol and 20 % and 40 % of ketoconazole, respectively, were manufactured and compared to placebo filaments. Feed forces decreased with increasing drug load, which was attributed to decrease in melt viscosity and confirmed through melt rheology measurements. The feed force tester was capable of determining suitable printing conditions. Thereby, it is also possible to optimize the printing process in terms of printing speed and nozzle temperature. In addition, a better process understanding was gained by the acquisition of feed force data. Measurement of feed forces during the printing process could possibly be implemented as an in-process control in pharmaceutical printers to ensure uniform mass deposition and act as an indicator of feeding system wear. It could also be a useful method to assess the feed forces of filaments after storage. It is likely that, depending on the storage conditions, properties may change, e.g., through water absorption. As filaments are the storage material for FDM, it is important that they maintain their properties to ensure reproducibility of the process. Other approaches have been reported for the prediction of print parameters. One of these

is a machine learning approach, taking into consideration e.g., melt rheology and mechanical properties to predict the printability, extrusion and printing temperatures (Elbadawi et al., 2020b; Muñiz Castro et al., 2021). However, this approach did not include variations of print parameters other than nozzle temperature, which was only determined by visual assessment of the melt at the die. Another approach can be in silico simulation of the printing process. By now, different models have been proposed, which consider printing speeds and nozzle geometries. However, these models are mainly limited to filaments made from a single material (Kattinger et al., 2022). Pharmaceutical formulations can contain a multitude of materials, which makes modeling even more complex. In addition, they require a magnitude of data on the respective formulation, which may not be available at an early stage of development. In comparison, the feed force tester is advantageous as it provides information on suitable printing conditions without both, a significant invest in data mining and material.

The principles of the modified feeding approach and the feed force tester were further applied to print the Merck pipeline API peposertib. Peposertib is an API with poor solubility and potentially high dosages. However, the challenge in formulating an ASD with peposertib lies in its high melting point and degradation post melting. Therefore, suitable extrusion and printing parameters had to be identified that allow amorphization of the drug and limiting the percentage of degradation products in the formulation. A formulation containing 30 % of peposertib and the polymer copovidone was used. In order to achieve amorphous filaments high screw speeds up to 600 rpm were utilized. However, this also resulted in diameter fluctuations in the range of $\pm 0.10 - 0.15$ mm instead of the targeted ± 0.05 mm. Diameter fluctuations can have an impact on the tablet mass uniformity and should be kept at a low level. This may conflict with high melting and thermo-sensitive APIs such as peposertib. However, filament should be fully amorphous prior to printing, as the transition time in the hotend may not be sufficient to amorphize the drug as also described in the prior section. Therefore, a good selection of extrusion parameters is crucial to manufacture amorphous filament as well as filament with suitable dimensional uniformity. The feed force tester was used to select the nozzle temperature, indicating that temperatures > 170 °C were required. Further, due to the brittleness of the filaments the modified printer setup was used. However, it became apparent that build plate adhesion and inter-layer bonding are also important factors, which could not be determined with the feed force tester and were adapted using a trial-and-error approach. Finally, printing parameters were identified, where it was possible to print a whole batch without complications. Another limit of the feed force tester is the prediction of potential degradation products. Filament, which had been processed in the feed force tester showed lower content of degradation products compared to the material, which had been printed as a tablet,

which is possibly due to the fact that the nozzle is in contact with the material for a longer duration in time during printing. Further tests would be necessary to show the influence of printing parameters such as printing speed on API degradation. A tablet batch was successfully printed, passing the pharmacopeia test “Uniformity of mass” (Ph. Eur. 2.9.5.). The tablets were fully amorphous but did not exhibit immediate release such as tablets printed from ketoconazole and copovidone as peposertib recrystallized upon contact with the dissolution medium. Changes to the tablet design and the formulation would be necessary to improve dissolution. The model API peposertib posed a challenge for its use in FDM, thereby emphasizing the constraints of this method, which could potentially be addressed by employing alternative 3DP techniques.

Therefore, the feasibility of using amorphous melt extrudate as raw material in DoP printing was evaluated. As this technique uses liquids to bind the powder particles to create the 3D object, the effects of print parameters on the extend of API recrystallization were assessed. Formulations containing plain copovidone as well as formulations containing copovidone and 20 % or 40 % of ketoconazole were assessed. The formulations were extruded and finely milled to serve as powder feed material for the printer. Different ink compositions and drug loads were assessed, and the printed tablets were analyzed with regards to solid state and mechanical stability. The aim was to identify printing parameters that will result in tablets with suitable tensile strength and no recrystallization. Here, a water-based ink containing 30 % water and 70 % ethanol (v/v%) showed a higher tendency for recrystallization of the powder material compared a water-free ink containing 100 % methanol. This became visible when printing with a drug load of 40 %, which resulted in strong recrystallization using the water-based and almost no recrystallization for the water-free ink. Material with 20% drug load, however, was printable with both inks without recrystallization. Regarding mechanical properties of the printed tablets, printing with the water-based inks resulted in higher tensile strengths. In addition, the physical stability of the printed tablets was assessed over a period of twelve weeks at 40 °C. At drug loads of 20 %, tablets were stable over the tested storage duration whereas tablets with 40 % of ketoconazole partially recrystallized after twelve weeks indicating limitations of this method for very high drug loads. It has to be pointed out that even though the amorphous material was sensitive to recrystallization during the printing process, it was observed that small traces of crystallinity remained localized during storage. The porosity and small number of connection points between the powder particles possibly contributed to the containment of crystals. However, loose connections between the particles are also a factor for poor mechanical stability, wherefore a sweet spot has to be identified to achieve proper tablet integrity as well as physical stability of the ASD. The process developed in this work demonstrated

a feasibility approach and was assessed for a single compound with low recrystallization tendency belonging to the GFA class III. The applicability to other APIs has to be evaluated.

The printing techniques FDM and DoP printing were further compared and discussed with regards to processability, physical stability and tablet properties. Therefore, filaments from copovidone were extruded with 20 % of ketoconazole. One part of the filaments was used for FDM printing and the other part was milled and used for DoP printing. Optimized printing parameters were chosen as discussed in the previous sections and printed tablets were characterized in terms of solid state, dissolution, content and physical stability after storage. Regarding processability and the production of the intermediates, filament production for FDM was more challenging than the production of the intermediate for DoP printing. As also confirmed by the study on peposertib, identifying extrusion parameters that result in amorphous but also dimensional uniform filament can be difficult. Brittle formulations are, as discussed earlier, an additional challenge for this process. However, to produce intermediates for DoP printing, brittle materials are more easily to handle. Nevertheless, the step of milling increased the surface area of the hygroscopic material to a great extent, leading to water absorption, which affected powder recoating. Filaments on the other hand exhibited cracks during storage, further increasing the brittleness of the material, which would impair the feedability. This highlights the importance of defined process conditions as well as storage conditions for the intermediates. In terms of physical stability, both techniques were capable in producing amorphous and physically stable dosage forms. It was discussed that the porous structure of DoP printed tablets, which also applies to the intermediate, contributed to the physical stability. In comparison, FDM printed tablets and filaments are inherently dense, wherefore it has to be considered that traces of crystallinity may carry the risk to spread all over as the whole melt is connected. Regarding tablet properties, the high density of FDM tablets is beneficial for the production of dosage forms with high dosages as FDM tablets showed an approximately 1.7fold higher mass. Nevertheless, it is important to also consider drug release in addition to having a high dose. In the comparative study with ketoconazole, a fast release was achieved. However, this can be very dependent on the respective formulation as shown by the poor release from peposertib tablets. Further, FDM and DoP printed tablets differed strongly in terms of appearance. DoP printed tablets were more similar to commonly available tablets due to their opacity. Januskaite et al. (2020) had shown that tablets prepared by SLS, another powder-based 3DP technique, resulted in the highest visual preferences in children. Likewise, it is to expect that DoP printed tablets are also more likely to be accepted by patients. FDM tablets on the other hand were transparent and had rough edges, hence two factors, which were described to impair patient preference in the aforementioned paper. Even though FDM printed tablets

showed poor resolution, the surface of these tablets was smoother compared to the DoP printed tablets. DoP tablets were rough, which could possibly result in poorer swallowability. Bogdahn et al. (2021) proposed that FDM printed tablets compared to their compressed porous counterparts could exhibit a smoother surface upon contact with water, resulting in an improved swallowability. However, FDM printed tablets exhibit sharp edges, which could possibly lead to micro-injuries during deglutition. The design should therefore be optimized with respect to the utilized printing technique to achieve good acceptability and swallowability, which is an important step in the establishment of 3D printed products in the pharmaceutical sector.

In summary, this work demonstrated that poorly soluble APIs are successfully printable as an amorphous SODF form using either the 3DP technique FDM or DoP printing. The use of high drug loads requires the use of a minimum of excipients in the formulation to ensure a high dose and a small tablet volume. In the field of FDM, this contrasts with previous publications that focus on intensive formulation development by adding excipients to adjust the mechanical properties of the formulation. This work presented a reverse approach by re-engineering the printer setup for the formulation and by highlighting the necessity of printing systems that are capable to process materials in a broad range of mechanical properties. Improvement of printing systems for pharmaceutical applications should not only include adaption of the feeding mechanism, but also inclusion of sensory in-process controls. The assessment of feed forces during printing was linkable to important quality parameters such as mass conformity and could hence, be part of the sensory tools in FDM printers for pharmaceutical applications. As a melt-based 3DP technique, FDM was well suitable for printing of highly dosed tablets from ASDs. Nevertheless, prolonged process times and challenges in terms of scalability limit its use mainly for production of small batches, which can be beneficial in a point-of-care environment. In contrast, DoP printing presents a 3DP technique that can easily be scaled up, enabling manufacturing of large batches, holding a high potential for the pharmaceutical industry. Compared to conventional manufacturing processes, DoP printing offers a simplified manufacturing process as the resulting SODFs can be directly printed from powder blends. This work demonstrated that next to highly dosed powders containing a highly soluble API also highly dosed powders containing a poorly soluble API in its amorphous form are possible. Extending the range of APIs from highly to poorly soluble compounds is beneficial in the pharmaceutical industry as many pipeline compounds belong to BCS class II. It was shown that each printing technique has its advantages and disadvantages, which define the application of each technique. The different 3DP techniques are versatile, which should be considered as an opportunity to enhance and accelerate future drug product development.

5. Materials and methods

The following sections describe materials and methods, which were applied for the manufacturing and characterization of filament and tablets containing peposertib in section 3.1.3.

5.1. Materials

Substance	Abbreviation/ synonym	Supplier	Batch	Use
Peposertib	-	Merck KGaA, Darmstadt, Germany	PR-00951	API
Copovidone (Kollidon® VA64)	-	BASF, Ludwigshafen, Germany	00183656P0	Polymer matrix
Acetonitrile (gradient grade)	ACN	Merck KGaA, Darmstadt, Germany	Various	Eluent, solvent
Sodium chloride	NaCl	Merck KGaA, Darmstadt, Germany	K51096300919	Preparation of SGF _{sp} medium
Hydrochloric acid 1 mol/L	HCl 1 M	Merck KGaA, Darmstadt, Germany	Various	Dissolution medium
Glacial acetic acid	CH ₃ COOH	Merck KGaA, Darmstadt, Germany	Various	pH adjustment
Ammonium acetate	NH ₄ CH ₃ CO ₂	Merck KGaA, Darmstadt, Germany	Various	Eluent preparation

5.2. Methods

5.2.1. Manufacturing methods

5.2.1.1. Hot-melt extrusion

Blending was performed in a 50 L container blender by Servolift (Offenburg, Germany). The powder blend contained 30 % of peposertib and 70 % of copovidone and was roller compacted to enhance flowability. Therefore, the Mini-Factor® by Gerteis (Jona, Switzerland) was utilized. Knurled rolls with a roll size of 25 mm were used. Compaction force was set to 5 kN/cm, roll gap

to 3 mm and roll speed to 5 rpm. The resulting compactate was used for extrusion. Extrusion was carried out on a co-rotating twin-screw extruder (Pharma 11, Thermo Fisher Scientific, Waltham, USA). An elongated die (length: 3 cm) with a diameter of 1.75 mm was used. The screw configuration is displayed in Table 2.

Table 2: Screw configuration (CE: conveying element; ME: mixing element; EE: extrusion element)

No. of elements	Element type	Length	Helix
4	CE	2 L/D	3/2 L/D
1	CE	1 L/D	1 L/D
2	CE	1 L/D	2/3 L/D
6	ME	0.25 L/D	-
3	CE	2 L/D	3/2 L/D
2	CE	1 L/D	2/3 L/D
6	ME	0.25 L/D	-
2	CE	2 L/D	3/2 L/D
2	CE	1 L/D	2/3 L/D
6	ME	0.25 L/D	-
4	CE	2 L/D	3/2 L/D
1	CE	1 L/D	2/3 L/D
1	EE	1.5 L/D	-

The compactate was gravimetrically fed using a Congrav[®] OP 1T (Brabender Technologie GmbH & Co. KG, Duisburg, Germany). The extrusion of uniform and amorphous filament required different extrusion settings, which are displayed in Table 3. Filament diameter was measured using a three-axis laser measurement system (Odac Trio33, Zumbach Electronic AG, Orpund, Switzerland) and the filament diameter was adjusted manually by altering the conveyor belt speed (Brabender Technologie GmbH & Co. KG, Duisburg, Germany).

Table 3: Extrusion parameters

Run	Screw speed (rpm)	Feed rate (kg/h)	Zone 1	Zone 2	Zone 3	Zone 4	Zone 5	Zone 6	Zone 7	Die
1.1	300	0.2	80	160	160	160	160	160	160	170
1.2	400	0.2	80	160	160	160	160	160	160	170
1.3	500	0.2	80	160	160	160	160	160	160	170
1.4	500	0.2	80	165	165	165	165	165	165	170
2.1	600	0.3	100	165	165	165	165	165	165	165
2.2	600	0.3	100	160	160	160	160	160	160	175
2.3	600	0.3	100	165	165	165	165	165	165	175
2.4	600	0.3	100	165	165	165	165	165	165	170
2.5	600	0.3	100	170	170	170	170	170	170	170
2.6	600	0.3	100	170	170	170	170	170	170	175
2.7	600	0.3	80	130	170	170	170	170	170	180

5.2.1.2. Printing

Printing was carried out on an Ultimaker 3 (Ultimaker, Utrecht, Netherlands) equipped with an Ultimaker printcore (0.4 mm, type BB). The modified printing setup according to Gottschalk et al. (2021) was applied to enable printing of brittle filaments. A cylindrical tablet (height 2.4 mm, diameter 10 mm) was designed in Fusion 360 (Autodesk, San Rafael, USA) and saved as stereolithography (.stl) file format. The G-code was generated in Simplify3D (version 4.0.1., Simplify3D, Cincinnati, USA). Several trials were performed to identify suitable print parameters, which are displayed in Table 4. All tablets were printed with 0.2 mm layer height, 0.4 mm line width, two shell layers, 100 % infill density, and a rectilinear infill pattern. The initial layer printing speed was reduced to 30 % of the set printing speed.

Table 4: Print parameters

Run	Speed (mm/s)	Build plate temperature (°C)	Nozzle temperature (°C)	Printing surface
1	30	60	175	Original glass build plate
2		70	175	
3		80	175	
4		60	180	
5		70	180	
6		80	185	
7		70	185	
8		80	180	
9		85	190	
10	10	70	165	Adhesion tape: 3M Scotch 2090
11		80	165	
12		70	170	
13		70	175	
14		70	180	
15		80	180	
16		80	185	
17*	30	70	165	

*Ten brim layers with direct contact to the tablet were printed

5.2.2. Analytical methods

5.2.2.1. Differential scanning calorimetry

Thermal analysis was performed on a DSC 1 (Mettler Toledo, Gießen, Germany). Approximately 7 – 9 mg of pure peposertib, compacted powder blend, ground filament and FDM printed tablets were exactly weighed (MCA6.6S-2S00-M Cubis®, Sartorius, Goettingen, Germany) and analyzed in triplicate. Samples were weighed into 100 µL aluminum pans and hermetically sealed. Prior to analysis, lids were pierced by the automatic piercing unit. Analysis was performed under a nitrogen environment at 50 mL/min. Two heating and cooling cycles from 0 °C – 230 °C and 230 °C – 0 °C were applied at 10 K/min.

5.2.2.2. Polarized light microscopy

Raw materials, intact filament and ground tablets were assessed using a IX73P1F microscope (Olympus, Tokyo, Japan) in white and polarized light at 5x and 10x magnification. Images were recorded using Olympus cellSens Standard software (version 1.18).

5.2.2.3. X-ray powder diffraction

XRPD was performed on a Bruker D2 Phaser (Bruker, Billerica, USA) in Bragg-Brentano arrangement. X-rays were generated by a copper radiation source at 30 kV and 10 mA. Nickel foil was used to reduce $K\beta$ radiation. Ground samples were prepared on zero-background holders with well and scanned from 6° to 35° with a step size of 0.02° and measurement time of 6 s per step. Rotation speed of the samples was 5 rpm. A SSD160 detector was used in 1D mode.

5.2.2.4. Three-point bending test

Ten filament sticks of approximately 70 mm length were tested regarding their mechanical properties on a Texture Analyser TA-XT (Stable Micro Systems, Godalming, UK) equipped with a three-point bending rig. The gap between the bearings was set to 30 mm. Filament diameter was assessed prior to the measurement using a three-axis laser measurement system (Odac Trio33, Zumbach Electronic AG, Orpund, Switzerland). The average diameter of the filament was used to determine stress and strain at break according to Prasad et al. (2019). The test punch speed was set to 5 mm/s and upon contact with the test specimen reduced to 0.1 mm/s. Data were acquired using Exponent software (version 6.1.16.0).

5.2.2.5. Feed force testing

The feed force tester was used according to Gottschalk et al. (2022) on a Texture Analyser (TA-XT, Stable Micro Systems, Godalming, UK). Tests were performed in triplicate at 1.00 mm/s (corresponding 30 mm/s printing speed) at 170 °C, 180 °C and 190 °C.

5.2.2.6. Content and purity analysis

Chromatographic analysis was carried out by high-performance liquid chromatography (HPLC) on an Agilent LC (Agilent, Santa Clara, USA) using a Poroshell 120 EC-C8 column by Agilent (100 mm x 4.6 mm, particle size: 2.7 μm , pore size 120 Å) constantly heated up to 35 °C. Detection was performed at a wavelength of 273 nm. Eluents consisted of acetate buffer at pH 4.5 and acetonitrile (ACN) at ratios of 95:5 and 5:95, which were pumped through the system at a flow rate of 1.55 mL/min for 27 min. Injection volume was 10 μL . Acetate buffer was prepared by dissolving 19.27 g ammonium acetate in purified water and adjusting the pH with acetic acid to 4.5 using a pH-meter (780/810, Metrohm, Herisau, Switzerland). Calibration was performed with solutions of peposertib in ACN and purified water (50:50) at a concentration of 25 $\mu\text{g/mL}$ and concentrations ranging from 50 to 400 $\mu\text{g/mL}$ in steps of 50 $\mu\text{g/mL}$.

Sample preparation:

Purity profile: Approximately 6 mg of filament, tablets and samples after analysis with the feed force tester were dissolved in 10 mL of a mixture of ACN and purified water (60:40). Approximately 20 mg of pure peposertib was weighed as standard and reference and 65 mg of compactate. Material was dissolved in 100 mL of the aforementioned solvent.

Tablet content: Three tablets were assessed by dissolving each tablet in a volumetric flask with a mixture of ACN and purified water (60:40) in an ultrasonic bath (5510, Branson, Brookfield, USA) for 20 min. After dissolution the volumetric flask was filled up to a volume of 500 mL.

5.2.2.7. Dissolution

Dissolution of printed tablets ($n = 6$) was performed in a USP 2 dissolution apparatus (Smart AT7, Sotax, Aesch, Switzerland) in simulated gastric fluid without pepsin (SGF_{sp}). SGF_{sp} was prepared by dissolving 10 g in 2.5 L of purified water, adding 400 mL of 1 N HCl and filling up to 5 L with purified water. Tablets were weighed prior to the analysis using an analytical balance (XS205DU/M, Mettler Toledo, Gießen, Germany). Dissolution was performed in 900 mL of medium at 37 °c and at a paddle speed 75 rpm. A sampling volume of 5 mL was withdrawn from the vessels at 5, 10, 15, 20, 30, 45, 60, 90, 120, 180 and 240 min. For HPLC analysis 500 µL of sample were diluted with 500 µL of ACN. Tablet content (5.2.2.6.) was used to determine the percentage of release. As the dissolution resulted in very low concentrations, calibration was performed with solutions of peposertib in ACN and purified water (60:40) at concentration of 1, 2.5, 5, 10, 15, 20, 25 µg/mL. To assess the release kinetics of peposertib tablets, the Korsmeyer-Peppas-Equation was utilized (Ritger and Peppas, 1987):

$$\frac{M_t}{M_\infty} = k * t^n \quad (4)$$

Here, the quotient of M_t and M_∞ represents the proportion of drug released after time (t) and k the release rate constant. The release exponent n is dependent on the geometry of the dosage form and a value of 0.45 was used for the calculations due to the cylindrical design of the tablets.

5.2.2.8. Tablet characterization

Tablet mass was determined using an analytical balance (XS205DU/M, Mettler Toledo, Gießen, Germany). "Uniformity of mass" was determined according to Ph. Eur. 2.9.5.

6. List of publications and conference contributions

6.1. Research papers

- I. N. Gottschalk, M. Bogdahn, M. Harms, J. Quodbach; Brittle polymers in Fused Deposition Modeling: An improved feeding approach to enable the printing of highly drug loaded filament; International Journal of Pharmaceutics, Volume 597, 2021, 120216, <https://doi.org/10.1016/j.ijpharm.2021.120216>.
- II. N. Gottschalk, J. Quodbach, A. Elia, F. Hess, M. Bogdahn; Determination of feed forces to improve process understanding of Fused Deposition Modeling 3D printing and to ensure mass conformity of printed solid oral dosage forms; International Journal of Pharmaceutics, Volume 614, 2022, 121416, <https://doi.org/10.1016/j.ijpharm.2021.121416>.
- III. N. Gottschalk, A. Burkard, J. Quodbach, M. Bogdahn; Drop-on-powder 3D printing of amorphous high dose oral dosage forms: Process development, opportunities and printing limitations; International Journal of Pharmaceutics: X, Volume 5, 2023, 100151, <https://doi.org/10.1016/j.ijpx.2022.100151>.
- IV. N. Gottschalk, J. Quodbach, M. Bogdahn; 3D Printing of amorphous solid dispersions: A comparison of fused deposition modeling and drop-on-powder printing; International Journal of Pharmaceutics: X, Volume 5, 2023, 100179, <https://doi.org/10.1016/j.ijpx.2023.100179>

6.2. Patent application

- I. Patent application: N. Gottschalk, M. Bogdahn, J. Quodbach, S. Geißler; Process for the manufacture of a solid pharmaceutical administration form, European Patent Office, no. EP22190883.3, application date: 18.08.2022

6.3. Poster presentations

- I. N. Gottschalk; M. Bogdahn; J. Quodbach; S. Geißler; „3D-Druck fester oraler Darreichungsformen – Einfluss der Prozessparameter auf Masse und Dimension“; 1. Doktoranden- und PostDoc-Konferenz im Rahmen der BMBF-Fördermaßnahme ProMatLeben; Berlin 2019
- II. N. Gottschalk; T. Marquetant; K. Bauer; J. Quodbach; A. Elia; T. Kipping; M. Bogdahn; „3D-Druck neuartiger Polymere zur Herstellung wirkstoffhaltiger Arzneiformen“; 2.

- Doktoranden- und PostDoc-Konferenz im Rahmen der BMBF-Fördermaßnahme ProMatLeben; 2021 (virtual)
- III. N. Gottschalk; M. Bogdahn; J. Quodbach; “Optimization of processing times and temperature for 3D-printing of tablets”; 12th World Meeting on Pharmaceutics, Biopharmaceutics and Pharmaceutical Technology; 2021 (virtual)
- IV. N. Gottschalk; T. Marquetant; K. Bauer; A. Elia; T. Kipping; J. Quodbach; M. Bogdahn; „3D-Druck von Tabletten: Entwicklung eines Vorschubkrafttesters um Drucktemperaturen für neue Materialien und verschiedene Formulierungen vorherzusagen“; 3. Doktoranden- und PostDoc-Konferenz im Rahmen der BMBF-Fördermaßnahme ProMatLeben; 2021 (virtual)
- V. N. Gottschalk; M. Bogdahn; J. Quodbach; “Influence of High Drug Load on Printability of Filaments via Fused Deposition Modeling”, PharmSci 360, 2021 (virtual)
- VI. N. Gottschalk; F. Hess; A. Elia; T. Kipping; M. Bogdahn; J. Quodbach; “Dimensional conformity of filaments in hot-melt extrusion: Design of experiment and process optimization”; PharmSci 360; Boston 2022
- VII. N. Gottschalk; A. Burkard; M. Bogdahn; J. Quodbach; “Enabling Manufacturing of Amorphous Highly Dosed Tablets by Drop-on-Powder 3D printing”; European Conference on Pharmaceutics; Marseille 2023

7. References

Aho, J., Bøtker, J.P., Genina, N., Edinger, M., Arnfast, L., Rantanen, J., 2019. Roadmap to 3D-printed oral pharmaceutical dosage forms: feedstock filament properties and characterization for fused deposition modeling. *J. Pharm. Sci.* 108, 26–35.

Alhijaj, M., Belton, P., Qi, S., 2016. An investigation into the use of polymer blends to improve the printability of and regulate drug release from pharmaceutical solid dispersions prepared via fused deposition modeling (FDM) 3D printing. *Eur. J. Pharm. Biopharm.* 108, 111–125.

Alhijaj, M., Nasereddin, J., Belton, P., Qi, S., 2019. Impact of processing parameters on the quality of pharmaceutical solid dosage forms produced by Fused Deposition Modeling (FDM). *Pharmaceuticals* 11, 633.

Alhnan, M.A., Okwuosa, T.C., Sadia, M., Wan, K.W., Ahmed, W., Arafat, B., 2016. Emergence of 3D printed dosage forms: Opportunities and challenges. *Pharm. Res.* 33, 1817–1832.

Alqahtani, M.S., Kazi, M., Alsenaidy, M.A., Ahmad, M.Z., 2021. Advances in oral drug delivery. *Front. Pharmacol.* 12, 1–21.

Amidon, G.L., Lennernäs, H., Shah, V.P., Crison, J.R., 1995. A theoretical basis for a biopharmaceutic drug classification: The correlation of in vitro drug product dissolution and in vivo bioavailability. *Pharm. Res.* 12, 413–420.

Antic, A., Zhang, J., Amini, N., Morton, D.A. V, Hapgood, K.P., Ft, F., 2021. Screening pharmaceutical excipient powders for use in commercial 3D binder jetting printers. *Adv. Powder Technol.* 32, 2469–2483.

Arafat, B., Wojsz, M., Isreb, A., Forbes, R.T., Isreb, M., Ahmed, W., Arafat, T., Alhnan, M.A., 2018. Tablet fragmentation without a disintegrant: A novel design approach for accelerating disintegration and drug release from 3D printed cellulosic tablets. *Eur. J. Pharm. Sci.* 118, 191–199.

Auch, C., Harms, M., Mäder, K., 2018. Melt-based screening method with improved predictability regarding polymer selection for amorphous solid dispersions. *Eur. J. Pharm. Sci.* 124, 339–348.

Baird, J.A., Eerdenbrugh, B.V.A.N., Taylor, L.S., 2010. A classification system to assess the crystallization tendency of organic molecules from undercooled melts. *J. Pharm. Sci.* 99, 3787–3806.

Blaabjerg, L.I., Lindenberg, E., Löbmann, K., Grohgan, H., Rades, T., 2016. Glass forming ability of amorphous drugs investigated by continuous cooling and isothermal transformation. *Mol. Pharm.* 13, 3318–3325.

Bogdahn, M., Torner, J., Krause, J., Grimm, M., Weitschies, W., 2021. Influence of the geometry of 3D printed solid oral dosage forms on their swallowability. *Eur. J. Pharm. Biopharm.* 167, 65–72.

Boniatti, J., Januskaite, P., da Fonseca, L.B., Viçosa, A.L., Amendoeira, F.C., Tuleu, C., Basit, A.W., Goyanes, A., Ré, M.I., 2021. Direct powder extrusion 3D printing of praziquantel to overcome neglected disease formulation challenges in paediatric populations. *Pharmaceutics* 13, 1114.

- Borgers, M., Van den Bossche, H., De Brabander, M., 1983. The mechanism of action of the new antimycotic ketoconazole. *Am. J. Med.* 74, 2–8.
- Brostow, W., Hagg Lobland, H.E., Khoja, S., 2015. Brittleness and toughness of polymers and other materials. *Mater. Lett.* 159, 478–480.
- Buanz, A.B.M., Belaunde, C.C., Soutari, N., Tuleu, C., Gul, M.O., Gaisford, S., 2015. Ink-jet printing versus solvent casting to prepare oral films: Effect on mechanical properties and physical stability. *Int. J. Pharm.* 494, 611–618.
- Buanz, A.B.M., Saunders, M.H., Basit, A.W., Gaisford, S., 2011. Preparation of personalized-dose salbutamol sulphate oral films with thermal ink-jet printing. *Pharm. Res.* 28, 2386–2392.
- Buckley, S.T., Frank, K.J., Fricker, G., Brandl, M., 2013. Biopharmaceutical classification of poorly soluble drugs with respect to “enabling formulations.” *Eur. J. Pharm. Sci.* 50, 8–16.
- Bühler, V., 2005. Polyvinylpyrrolidone excipients for pharmaceuticals. Springer, Berlin, Heidelberg, Germany, pp. 189–190
- Butler, J.M., Dressman, J.B., 2010. The developability classification system: Application of biopharmaceutics concepts to formulation development. *J. Pharm. Sci.* 99, 4940–4954.
- Butreddy, A., Sarabu, S., Bandari, S., Batra, A., Lawal, K., Chen, N.N., Bi, V., Durig, T., Repka, M.A., 2021. Influence of Plasdone™ S630 Ultra - an improved copovidone on the processability and oxidative degradation of quetiapine fumarate amorphous solid dispersions prepared via hot-melt extrusion technique. *AAPS PharmSciTech* 22, 1–13.
- Cader, H.K., Rance, G.A., Alexander, M.R., Gonçalves, A.D., Roberts, C.J., Tuck, C.J., Wildman, R.D., 2019. Water-based 3D inkjet printing of an oral pharmaceutical dosage form. *Int. J. Pharm.* 564, 359–368.
- Chamberlain, R., Windolf, H., Geissler, S., Quodbach, J., Breitzkreutz, J., 2022. Precise dosing of pramipexole for low-dosed filament production by hot melt extrusion applying various feeding methods. *Pharmaceutics* 14, 216.
- Chang, S., Jin, J., Yan, J., Dong, X., Chaudhuri, B., 2021. Development of a pilot-scale HuskyJet binder jet 3D printer for additive manufacturing of pharmaceutical tablets. *Int. J. Pharm.* 605, 120791.
- Chang, S., Wan, S., Kowsari, K., Shetty, A., Sorrells, L., Sen, K., Nagapudi, K., Chaudhuri, B., Ma, A.W.K., 2020. Binder-jet 3D printing of indomethacin-laden pharmaceutical dosage forms. *J. Pharm. Sci.* 109, 3054–3063.
- Chasse, T., Conway, S.L., Danzer, G.D., Feng, L., Leone, A.M., McNevin, M., Smoliga, J., Stroud, P.A., van Lishaut, H., 2022. Industry white paper: Contemporary opportunities and challenges in characterizing crystallinity in amorphous solid dispersions. *J. Pharm. Sci.* 111, 1543–1555.
- Chen, L., Lin, Y., Irdam, E., Madden, N., Osei-Yeboah, F., 2022. Improving the manufacturability of cohesive and poorly compactable API for direct compression of mini-tablets at high drug loading via particle engineering. *Pharm. Res.* 3185–3195.
- Chiou, W.L., Riegelman, S., 1971. Pharmaceutical applications of solid dispersion systems. *J. Pharm. Sci.* 60, 1281–1302.

- Clark, E.A., Alexander, M.R., Irvine, D.J., Roberts, C.J., Wallace, M.J., Yoo, J., Wildman, R.D., 2020. Making tablets for delivery of poorly soluble drugs using photoinitiated 3D inkjet printing. *Int. J. Pharm.* 578, 118805.
- Coogan, T., Kazmer, D., 2019. In-line rheological monitoring of Fused Deposition Modeling. *J. Rheol.* 63, 141–155.
- Crump, S., 1992. Apparatus and method for creating three-dimensional objects. Patent US005121329A.
- Cui, M., Pan, H., Su, Y., Fang, D., Qiao, S., Ding, P., Pan, W., 2021. Opportunities and challenges of three-dimensional printing technology in pharmaceutical formulation development. *Acta Pharm. Sin. B* 11, 2488–2504.
- Curatolo, W., Nightingale, J.A., Herbig, S.M., 2009. Utility of hydroxypropylmethylcellulose acetate succinate (HPMCAS) for initiation and maintenance of drug supersaturation in the GI milieu. *Pharm. Res.* 26, 1419–1431.
- Daly, R., Harrington, T.S., Martin, G.D., Hutchings, I.M., 2015. Inkjet printing for pharmaceuticals – A review of research and manufacturing. *Int. J. Pharm.* 494, 554–567.
- Dedroog, S., Huygens, C., Van den Mooter, G., 2019. Chemically identical but physically different: A comparison of spray drying, hot melt extrusion and cryo-milling for the formulation of high drug loaded amorphous solid dispersions of naproxen. *Eur. J. Pharm. Biopharm.* 135, 1–12.
- Dedroog, S., Pas, T., Vergauwen, B., Huygens, C., Van den Mooter, G., 2020. Solid-state analysis of amorphous solid dispersions: Why DSC and XRPD may not be regarded as stand-alone techniques. *J. Pharm. Biomed. Anal.* 178, 112937.
- Dengale, S.J., Grohgan, H., Rades, T., Löbmann, K., 2016. Recent advances in co-amorphous drug formulations. *Adv. Drug Deliv. Rev.* 100, 116–125.
- Elbadawi, M., Gustaffson, T., Gaisford, S., Basit, A.W., 2020a. 3D printing tablets: Predicting printability and drug dissolution from rheological data. *Int. J. Pharm.* 590, 119868.
- Elbadawi, M., Muñiz Castro, B., Gavins, F.K.H., Ong, J.J., Gaisford, S., Pérez, G., Basit, A.W., Cabalar, P., Goyanes, A., 2020b. M3DISEEN: A novel machine learning approach for predicting the 3D printability of medicines. *Int. J. Pharm.* 590, 119837.
- EMA, 2013. European Medicines Agency recommends suspension of marketing authorisations for oral ketoconazole. EMA/458028/2013.
- Evans, R.C., Kyeremateng, S.O., Asmus, L., Degenhardt, M., Rosenberg, J., Wagner, K.G., 2018. Development and performance of a highly sensitive model formulation based on torasemide to enhance hot-melt extrusion process understanding and process development. *AAPS PharmSciTech* 19, 1592–1605.
- Fanous, M., Gold, S., Hirsch, S., Ogorka, J., Imanidis, G., 2020. Development of immediate release (IR) 3D-printed oral dosage forms with focus on industrial relevance. *Eur. J. Pharm. Sci.* 155, 105558.
- Feuerbach, T., Callau-Mendoza, S., Thommes, M., 2019. Development of filaments for fused deposition modeling 3D printing with medical grade poly(lactic-co-glycolic acid) copolymers. *Pharm. Dev. Technol.* 24, 487–493.

- Feuerbach, T., Kock, S., Thommes, M., 2018. Characterisation of fused deposition modeling 3D printers for pharmaceutical and medical applications. *Pharm. Dev. Technol.* 23, 1136–1145.
- Field, J.E., 1971. Brittle fracture: Its study and application. *Contemp. Phys.* 12, 1–31.
- Flügel, K., Schmidt, K., Mareczek, L., Gäbe, M., Hennig, R., Thommes, M., 2021. Impact of incorporated drugs on material properties of amorphous solid dispersions. *Eur. J. Pharm. Biopharm.* 159, 88–98.
- Fridgeirsdottir, G.A., Harris, R., Fischer, P.M., Roberts, C.J., 2016. Support tools in formulation development for poorly soluble drugs. *J. Pharm. Sci.* 105, 2260–2269.
- Fuenmayor, E., Forde, M., Healy, A., Devine, D., Lyons, J., McConville, C., Major, I., 2018. Material considerations for fused-filament fabrication of solid dosage forms. *Pharmaceutics* 10, 44.
- Gao, J., Walsh, G.C., Bigio, D., Briber, R.M., Wetzel, M.D., 2000. Mean residence time analysis for twin screw extruders. *Polym. Eng. Sci.* 40, 227–237.
- Gentis, N.D., Betz, G., 2012. Compressibility of binary powder formulations: Investigation and evaluation with compaction equations. *J. Pharm. Sci.* 101, 777–793.
- Gottschalk, N., Bogdahn, M., Harms, M., Quodbach, J., 2021. Brittle polymers in Fused Deposition Modeling: An improved feeding approach to enable the printing of highly drug loaded filament. *Int. J. Pharm.* 597, 120216.
- Gottschalk, N., Quodbach, J., Elia, A.-G., Hess, F., Bogdahn, M., 2022. Determination of feed forces to improve process understanding of Fused Deposition Modeling 3D printing and to ensure mass conformity of printed solid oral dosage forms. *Int. J. Pharm.* 614, 121416.
- Goyanes, A., Allahham, N., Trenfield, S.J., Stoyanov, E., Gaisford, S., Basit, A.W., 2019. Direct powder extrusion 3D printing: Fabrication of drug products using a novel single-step process. *Int. J. Pharm.* 567, 118471.
- Goyanes, A., Buanz, A.B.M., Basit, A.W., Gaisford, S., 2014. Fused-filament 3D printing (3DP) for fabrication of tablets. *Int. J. Pharm.* 476, 88–92.
- Goyanes, A., Chang, H., Sedough, D., Hatton, G.B., Wang, J., Buanz, A., Gaisford, S., Basit, A.W., 2015a. Fabrication of controlled-release budesonide tablets via desktop (FDM) 3D printing. *Int. J. Pharm.* 496, 414–420.
- Goyanes, A., Robles Martinez, P., Buanz, A., Basit, A.W., Gaisford, S., 2015b. Effect of geometry on drug release from 3D printed tablets. *Int. J. Pharm.* 494, 657–663.
- Gross, B.C., Erkal, J.L., Lockwood, S.Y., Chen, C., Spence, D.M., 2014. Evaluation of 3D printing and its potential impact on biotechnology and the chemical sciences. *Anal. Chem.* 86, 3240–3253.
- Gueche, Y.A., Sanchez-Ballester, N.M., Bataille, B., Aubert, A., Leclercq, L., Rossi, J.-C., Soulairol, I., 2021. Selective laser sintering of solid oral dosage forms with copovidone and paracetamol using a CO₂ laser. *Pharmaceutics* 13, 160.
- Guo, C., Zhang, M., Bhandari, B., 2019. Model building and slicing in food 3D printing processes: A review. *Compr. Rev. Food Sci. Food Saf.* 18, 1052–1069.

- Guo, Z., Lu, M., Li, Y., Pang, H., Lin, L., Liu, X., Wu, C., 2014. The utilization of drug-polymer interactions for improving the chemical stability of hot-melt extruded solid dispersions. *J. Pharm. Pharmacol.* 66, 285–296.
- Gupta, A.K., Lyons, D.C.A., 2015. The rise and fall of oral ketoconazole. *J. Cutan. Med. Surg.* 19, 352–357.
- Hancock, B.C., Zografi, G., 1997. Characteristics and significance of the amorphous state in pharmaceutical systems. *J. Pharm. Sci.* 86, 1–12.
- Hirshfield, L., Giridhar, A., Taylor, L.S., Harris, M.T., Reklaitis, G. V., 2014. Dropwise additive manufacturing of pharmaceutical products for solvent-based dosage forms. *J. Pharm. Sci.* 103, 496–506.
- Hoffmann, L., Breitreutz, J., Quodbach, J., 2022. Fused Deposition Modeling (FDM) 3D printing of the thermo-sensitive peptidomimetic drug enalapril maleate. *Pharmaceutics* 14, 2411.
- Hsiao, W.-K., Lorber, B., Reitsamer, H., Khinast, J., 2018. 3D printing of oral drugs: a new reality or hype? *Expert Opin. Drug Deliv.* 15, 1–4.
- Huang, S., O'Donnell, K.P., Delpon de Vaux, S.M., O'Brien, J., Stutzman, J., Williams, R.O., 2017. Processing thermally labile drugs by hot-melt extrusion: The lesson with gliclazide. *Eur. J. Pharm. Biopharm.* 119, 56–67.
- Hue P. Le, 1998. Progress and trends in ink-jet printing technology. *J. Imaging Sci. Technol.* 42, 49–62.
- Hughey, J.R., DiNunzio, J.C., Bennett, R.C., Brough, C., Miller, D.A., Ma, H., Williams, R.O., McGinity, J.W., 2010. Dissolution enhancement of a drug exhibiting thermal and acidic decomposition characteristics by fusion processing: A comparative study of hot melt extrusion and KinetiSol® dispersing. *AAPS PharmSciTech* 11, 760–774.
- Hutchings, I.M., Martin, G.D., Hoath, S.D., 2016. Introductory Remarks, in: Hoath, S.D. (Ed.), *Fundamentals of Inkjet Printing*. Wiley-VCH Verlag, Weinheim, Germany, p. 5.
- Ilyés, K., Kovács, N.K., Balogh, A., Borbás, E., Farkas, B., Casian, T., Marosi, G., Tomuță, I., Nagy, Z.K., 2019. The applicability of pharmaceutical polymeric blends for the fused deposition modelling (FDM) 3D technique: Material considerations–printability–process modulation, with consecutive effects on in vitro release, stability and degradation. *Eur. J. Pharm. Sci.* 129, 110–123.
- Infanger, S., Haemmerli, A., Iliev, S., Baier, A., Stoyanov, E., Quodbach, J., 2019. Powder bed 3D-printing of highly loaded drug delivery devices with hydroxypropyl cellulose as solid binder. *Int. J. Pharm.* 555, 198–206.
- Iwasaki, T., Takahara, M., Sonoda, R., Watano, S., 2007. Dry grinding of mefenamic acid particles for enhancement of its water dissolution rate. *Part. Part. Syst. Charact.* 24, 236–241.
- Jammalamadaka, U., Tappa, K., 2018. Recent advances in biomaterials for 3D printing and tissue engineering. *J. Funct. Biomater.* 9, 22.
- Jamróz, W., Kurek, M., Czech, A., Szafraniec, J., Gawlak, K., Jachowicz, R., 2018. 3D printing of tablets containing amorphous aripiprazole by filaments co-extrusion. *Eur. J. Pharm. Biopharm.* 131, 44–47.

- Januskaite, P., Xu, X., Ranmal, S.R., Gaisford, S., Basit, A.W., Tuleu, C., Goyanes, A., 2020. I spy with my little eye: A paediatric visual preferences survey of 3D printed tablets. *Pharmaceutics* 12, 1–16.
- Jermain, S. V., Brough, C., Williams, R.O., 2018. Amorphous solid dispersions and nanocrystal technologies for poorly water-soluble drug delivery – An update. *Int. J. Pharm.* 535, 379–392.
- Kanaujia, P., Lau, G., Ng, W.K., Widjaja, E., Hanefeld, A., Fischbach, M., Maio, M., Tan, R.B.H., 2011a. Nanoparticle formation and growth during in vitro dissolution of ketoconazole solid dispersion. *J. Pharm. Sci.* 100, 2876–2885.
- Kanaujia, P., Lau, G., Ng, W.K., Widjaja, E., Schreyer, M., Hanefeld, A., Fischbach, M., Saal, C., Maio, M., Tan, R.B.H., 2011b. Investigating the effect of moisture protection on solid-state stability and dissolution of fenofibrate and ketoconazole solid dispersions using PXRD, HSDSC and Raman microscopy. *Drug Dev. Ind. Pharm.* 37, 1026–1035.
- Kattinger, J., Ebinger, T., Kurz, R., Bonten, C., 2022. Numerical simulation of the complex flow during material extrusion in fused filament fabrication. *Addit. Manuf.* 49, 102476.
- Kempin, W., Domsta, V., Grathoff, G., Brecht, I., Semmling, B., Tillmann, S., Weitschies, W., Seidlitz, A., 2018. Immediate release 3D-printed tablets produced via Fused Deposition Modeling of a thermo-sensitive drug. *Pharm. Res.* 35, 124.
- Khaled, S.A., Alexander, M.R., Wildman, R.D., Wallace, M.J., Sharpe, S., Yoo, J., Roberts, C.J., 2018. 3D extrusion printing of high drug loading immediate release paracetamol tablets. *Int. J. Pharm.* 538, 223–230.
- Khaled, S.A., Burley, J.C., Alexander, M.R., Yang, J., Roberts, C.J., 2015. 3D printing of tablets containing multiple drugs with defined release profiles. *Int. J. Pharm.* 494, 643–650.
- Kiefer, O., Fischer, B., Breitzkreutz, J., 2021. Fundamental investigations into metoprolol tartrate deposition on orodispersible films by inkjet printing for individualised drug dosing. *Pharmaceutics* 13, 247.
- Kokott, M., Klinken, S., Breitzkreutz, J., Wiedey, R., 2023. Downstream processing of amorphous solid dispersions into orodispersible tablets. *Int. J. Pharm.* 631, 122493.
- Korte, C., Quodbach, J., 2018. Formulation development and process analysis of drug-loaded filaments manufactured via hot-melt extrusion for 3D-printing of medicines. *Pharm. Dev. Technol.* 23, 1117–1127.
- Kozakiewicz-Latała, M., Nartowski, K.P., Dominik, A., Malec, K., Gołkowska, A.M., Złocińska, A., Rusińska, M., Szymczyk-Ziółkowska, P., Ziółkowski, G., Górnjak, A., Karolewicz, B., 2022. Binder jetting 3D printing of challenging medicines: From low dose tablets to hydrophobic molecules. *Eur. J. Pharm. Biopharm.* 170, 144–159.
- Lang, B., McGinity, J.W., Williams, R.O., 2014. Hot-melt extrusion – basic principles and pharmaceutical applications. *Drug Dev. Ind. Pharm.* 40, 1133–1155.
- Lawal, A., Kalyon, D.M., 1995. Mechanisms of mixing in single and co-rotating twin screw extruders. *Polym. Eng. Sci.* 35, 1325–1338.

- Lee, K.J., Kang, A., Delfino, J.J., West, T.G., Chetty, D., Monkhouse, D.C., Yoo, J., 2003. Evaluation of critical formulation factors in the development of a rapidly dispersing captopril oral dosage form. *Drug Dev. Ind. Pharm.* 29, 967–979.
- Lehmkemper, K., Kyeremateng, S.O., Heinzerling, O., Degenhardt, M., Sadowski, G., 2017. Long-term physical stability of PVP- and PVPVA-amorphous solid dispersions. *Mol. Pharm.* 14, 157–171.
- Leister, D., Geilen, T., Geissler, T., 2012. Twin-screw extruders for pharmaceutical hot-melt extrusion: Technology, techniques and practices, in: Douroumis, D. (Ed.), *Hot-melt extrusion: Pharmaceutical applications*. John Wiley & Sons, Greenwich, United Kingdom, p. 24
- Li, J., Rossignol, F., Macdonald, J., 2015. Inkjet printing for biosensor fabrication: Combining chemistry and technology for advanced manufacturing. *Lab Chip* 15, 2538–2558.
- Li, M., Gogos, C.G., Ioannidis, N., 2015. Improving the API dissolution rate during pharmaceutical hot-melt extrusion I: Effect of the API particle size, and the co-rotating, twin-screw extruder screw configuration on the API dissolution rate. *Int. J. Pharm.* 478, 103–112.
- Li, S., Tian, Y., Jones, D.S., Andrews, G.P., 2016. Optimising drug solubilisation in amorphous polymer dispersions: Rational selection of hot-melt extrusion processing parameters. *AAPS PharmSciTech* 17, 200–213. h
- Ligon, S.C., Liska, R., Stampfl, J., Gurr, M., Mülhaupt, R., 2017. Polymers for 3D printing and customized additive manufacturing. *Chem. Rev.* 117, 10212–10290.
- Lima, A.L., Pires, F.Q., Hilgert, L.A., Sa-Barreto, L.L., Gratieri, T., Gelfuso, G.M., Cunha-Filho, M., 2022. Oscillatory shear rheology as an in-process control tool for 3D printing medicines production by fused deposition modeling. *J. Manuf. Process.* 76, 850–862.
- Liu, X., Feng, X., Williams, R.O., Zhang, F., 2018. Characterization of amorphous solid dispersions. *J. Pharm. Investig.* 48, 19–41.
- Löbmann, K., Grohgan, H., Laitinen, R., Strachan, C., Rades, T., 2013. Amino acids as co-amorphous stabilizers for poorly water soluble drugs - Part 1: Preparation, stability and dissolution enhancement. *Eur. J. Pharm. Biopharm.* 85, 873–881.
- Luebbert, C., Klanke, C., Sadowski, G., 2018. Investigating phase separation in amorphous solid dispersions via Raman mapping. *Int. J. Pharm.* 535, 245–252.
- Manero, A., Smith, P., Sparkman, J., Dombrowski, M., Courbin, D., Kester, A., Womack, I., Chi, A., 2019. Implementation of 3D printing technology in the field of prosthetics: Past, present and future. *Int. J. Environ. Res. Public Health* 16, 1641.
- Marsac, P.J., Shamblin, S.L., Taylor, L.S., 2006. Theoretical and practical approaches for prediction of drug-polymer miscibility and solubility. *Pharm. Res.* 23, 2417–2426.
- Matić, J., Alva, C., Witschnigg, A., Eder, S., Reusch, K., Paudel, A., Khinast, J., 2020. Towards predicting the product quality in hot-melt extrusion: Small scale extrusion. *Int. J. Pharm.* X 2,
- Meléndez, P.A., Kane, K.M., Ashvar, C.S., Albrecht, M., Smith, P.A., 2008. Thermal inkjet application in the preparation of oral dosage forms: Dispensing of prednisolone solutions and polymorphic characterization by solid-state spectroscopic techniques. *J. Pharm. Sci.* 97, 2619–2636.

- Melocchi, A., Briatico-Vangosa, F., Uboldi, M., Parietti, F., Turchi, M., von Zeppelin, D., Maroni, A., Zema, L., Gazzaniga, A., Zidan, A., 2021. Quality considerations on the pharmaceutical applications of fused deposition modeling 3D printing. *Int. J. Pharm.* 592, 119901.
- Melocchi, A., Parietti, F., Maroni, A., Foppoli, A., Gazzaniga, A., Zema, L., 2016. Hot-melt extruded filaments based on pharmaceutical grade polymers for 3D printing by fused deposition modeling. *Int. J. Pharm.* 509, 255–263.
- Miyajima, H., Rahman, K.M., Da, M., Williams, C.B., 2020. Effect of fine powder particles on quality of binder jetting parts. *Addit. Manuf.* 36, 101587.
- Monschke, M., Kayser, K., Wagner, K.G., 2021. Influence of particle size and drug load on amorphous solid dispersions containing pH-dependent soluble polymers and the weak base ketoconazole. *AAPS PharmSciTech* 22, 1–11.
- Moseson, D.E., Parker, A.S., Beaudoin, S.P., Taylor, L.S., 2020. Amorphous solid dispersions containing residual crystallinity: Influence of seed properties and polymer adsorption on dissolution performance. *Eur. J. Pharm. Sci.* 146, 105276.
- Muñiz Castro, B., Elbadawi, M., Ong, J.J., Pollard, T., Song, Z., Gaisford, S., Pérez, G., Basit, A.W., Cabalar, P., Goyanes, A., 2021. Machine learning predicts 3D printing performance of over 900 drug delivery systems. *J. Control. Rel.* 337, 530–545.
- Nasereddin, J.M., Wellner, N., Alhijaj, M., Belton, P., Qi, S., 2018. Development of a simple mechanical screening method for predicting the feedability of a pharmaceutical FDM 3D printing filament. *Pharm. Res.* 35, 151.
- Nichols, G., 2006. Light Microscopy, in: Hilfiker, R. (Ed.): *Polymorphism in the pharmaceutical industry*. Wiley-VCH Verlag, Weinheim, Germany, pp. 167–209.
- Nikzad, M., Masood, S.H., Sbarski, I., 2011. Thermo-mechanical properties of a highly filled polymeric composites for Fused Deposition Modeling. *Mater. Des.* 32, 3448–3456.
- Nollenberger, K., Albers, J., 2012. Applications of poly(meth)acrylate polymers in melt extrusion, in: Douroumis, D. (Ed.), *Hot-melt extrusion: Pharmaceutical applications*. John Wiley & Sons, Greenwich, United Kingdom, p. 120.
- Norman, J., Madurawe, R.D., Moore, C.M.V., Khan, M.A., Khairuzzaman, A., 2017. A new chapter in pharmaceutical manufacturing: 3D-printed drug products. *Adv. Drug Deliv. Rev.* 108, 39–50.
- Okafor-Muo, O.L., Hassanin, H., Kayyali, R., Elshaer, A., 2020a. 3D printing of solid oral dosage forms: Numerous challenges with unique opportunities. *J. Pharm. Sci.* 109, 3535–3550.
- Okwuosa, T.C., Pereira, B.C., Arafat, B., Cieszynska, M., Isreb, A., Alhnan, M.A., 2017. Fabricating a shell-core delayed release tablet using dual FDM 3D printing for patient-centred therapy. *Pharm. Res.* 34, 427–437.
- Parhi, R., 2021. A review of three-dimensional printing for pharmaceutical applications: Quality control, risk assessment and future perspectives. *J. Drug Deliv. Sci. Technol.* 64, 102571.
- Perkins, W., 1999. Polymer toughness and impact resistance. *Polym. Eng. Sci.* 39, 2445–2460.

- Pflieger, T., Venkatesh, R., Dachtler, M., Eggenreich, K., Laufer, S., Lunter, D., 2022. Novel approach to pharmaceutical 3D-printing omitting the need for filament - Investigation of materials, process and product characteristics. *Pharmaceutics* 14, 2488.
- Ponsar, H., Wiedey, R., Quodbach, J., 2020. Hot-melt extrusion process fluctuations and their impact on critical quality attributes of filaments and 3D-printed dosage forms. *Pharmaceutics* 12, 511.
- Prasad, E., Islam, M.T., Goodwin, D.J., Megarry, A.J., Halbert, G.W., Florence, A.J., Robertson, J., 2019. Development of a hot-melt extrusion (HME) process to produce drug loaded Affinisol™ 15LV filaments for fused filament fabrication (FFF) 3D printing. *Addit. Manuf.* 29, 100776.
- Prasad, L.K., Smyth, H., 2016. 3D Printing technologies for drug delivery: a review. *Drug Dev. Ind. Pharm.*
- Prestidge, C.A., Barnes, T.J., Lau, C.H., Barnett, C., Loni, A., Canham, L., 2007. Mesoporous silicon: A platform for the delivery of therapeutics. *Expert Opin. Drug Deliv.* 4, 101–110.
- Prudic, A., Ji, Y., Luebbert, C., Sadowski, G., 2015. Influence of humidity on the phase behavior of API/polymer formulations. *Eur. J. Pharm. Biopharm.* 94, 352–362.
- Raijada, D., Genina, N., Fors, D., Wisaeus, E., Peltonen, J., Rantanen, J., Sandler, N., 2013. A step toward development of printable dosage forms for poorly soluble drugs. *J. Pharm. Sci.* 102, 3694–3704.
- Repka, M.A., Bandari, S., Kallakunta, V.R., Vo, A.Q., McFall, H., Pimparade, M.B., Bhagurkar, A.M., 2018. Melt extrusion with poorly soluble drugs – An integrated review. *Int. J. Pharm.* 535, 68–85.
- Ritger, P.L., Peppas, N.A., 1987. A simple equation for description of solute release I. Fickian and non-fickian release from non-swellable devices in the form of slabs, spheres, cylinders or discs. *J. Control. Rel.* 5, 23–36.
- Rowe, C.W., Katstra, W.E., Palazzolo, R.D., Giritlioglu, B., Teung, P., Cima, M.J., 2000. Multimechanism oral dosage forms fabricated by three dimensional printing. *J. Control. Rel.* 66, 11–17.
- Rudolf, R., 2008. General overview of the compounding process: Tasks, selected applications and process zones, in: Kohlgrüber, K. (Ed.), *Co-Rotating Twin-Screw Extruder - Fundamentals, Technology and Applications*. Carl Hanser Verlag, München, Germany, pp. 66–67.
- Sachs, E.M., Haggerty, J., Cima, M.J., Williams, P.A., 1993. Three-dimensional printing techniques. Patent US005204055A.
- Sadia, M., Arafat, B., Ahmed, W., Forbes, R.T., Alhnan, M.A., 2018. Channelled tablets: An innovative approach to accelerating drug release from 3D printed tablets. *J. Control. Rel.* 269, 355–363.
- Samaro, A., Janssens, P., Vanhoorne, V., Renterghem, J. Van, Eeckhout, M., Cardon, L., 2020. Screening of pharmaceutical polymers for extrusion-based additive manufacturing of patient-tailored tablets. *Int. J. Pharm.* 586, 119591.

- Santos, J. dos, Deon, M., da Silva, G.S., Beck, R.C.R., 2021. Multiple variable effects in the customisation of fused deposition modelling 3D-printed medicines: A design of experiments (DoE) approach. *Int. J. Pharm.* 597, 120331.
- Sarabu, S., Butreddy, A., Bandari, S., Batra, A., Lawal, K., Chen, N.N., Kogan, M., Bi, V., Durig, T., Repka, M.A., 2022. Preliminary investigation of peroxide levels of Plasdone™ copovidones on the purity of atorvastatin calcium amorphous solid dispersions: Impact of plasticizers on hot melt extrusion processability. *J. Drug Deliv. Sci. Technol.* 70, 103190.
- Schenck, L., Lowinger, M., Troup, G.M., Li, L., McKelvey, C., 2019. Achieving a hot melt extrusion design space for the production of solid solutions, in: *Chemical Engineering in the Pharmaceutical Industry*. John Wiley & Sons, Hoboken, NJ, USA, pp. 469–487.
- Schulz, M.N., 2020. Systematic development of a binder containing ink suitable for binder jetting. Master thesis. Heinrich Heine University, Düsseldorf.
- Scoutaris, N., Alexander, M.R., Gellert, P.R., Roberts, C.J., 2011. Inkjet printing as a novel medicine formulation technique. *J. Control. Rel.* 156, 179–185.
- Sen, K., Manchanda, A., Mehta, T., Ma, A.W.K., Chaudhuri, B., 2020. Formulation design for inkjet-based 3D printed tablets. *Int. J. Pharm.* 584, 119430.
- Sen, K., Mehta, T., Sansare, S., Sharifi, L., Ma, A.W.K., Chaudhuri, B., 2021. Pharmaceutical applications of powder-based binder jet 3D printing process – A review. *Adv. Drug Deliv. Rev.* 177, 113943.
- Shah, N., Sandhu, Ha., Choi, D.S., Chokshi, H., Malick, A.W. (Eds.), 2014. *Dissolution of amorphous solid dispersions: Theory and practice*. Springer, New York, USA. pp. 81–83
- Skowrya, J., Pietrzak, K., Alhnan, M.A., 2015. Fabrication of extended-release patient-tailored prednisolone tablets via fused deposition modelling (FDM) 3D printing. *Eur. J. Pharm. Sci.* 68, 11–17.
- Sofia, D., Chirone, R., Lettieri, P., Barletta, D., Poletto, M., 2018. Selective laser sintering of ceramic powders with bimodal particle size distribution. *Chem. Eng. Res. Des.* 136, 536–547.
- Souto, E.B., Campos, J.C., Filho, S.C., Teixeira, M.C., Martins-Gomes, C., Zielinska, A., Carbone, C., Silva, A.M., 2019. 3D printing in the design of pharmaceutical dosage forms. *Pharm. Dev. Technol.* 24, 1044–1053.
- Tabriz, A.G., Scoutaris, N., Gong, Y., Hui, H.W., Kumar, S., Douroumis, D., 2021. Investigation on hot melt extrusion and prediction on 3D printability of pharmaceutical grade polymers. *Int. J. Pharm.* 604, 120755.
- Takagi, T., Ramachandran, C., Bermejo, M., Yamashita, S., Yu, L.X., Amidon, G.L., 2006. A provisional biopharmaceutical classification of the top 200 oral drug products in the United States, Great Britain, Spain, and Japan. *Mol. Pharm.* 3, 631–643.
- Tambe, S., Jain, D., Meruva, S.K., Rongala, G., Juluri, A., Nihalani, G., Mamidi, H.K., Nukala, P.K., Bolla, P.K., 2022. Recent advances in amorphous solid dispersions: Preformulation, formulation strategies, technological advancements and characterization. *Pharmaceutics* 14., 2203.

- Thabet, Y., Lunter, D., Breitzkreutz, J., 2018a. Continuous inkjet printing of enalapril maleate onto orodispersible film formulations. *Int. J. Pharm.* 546, 180–187.
- Thabet, Y., Sibanc, R., Breitzkreutz, J., 2018b. Printing pharmaceuticals by inkjet technology: Proof of concept for stand-alone and continuous in-line printing on orodispersible films. *J. Manuf. Process.* 35, 205–215.
- Thakral, N.K., Zanon, R.L., Kelly, R.C., Thakral, S., 2018. Applications of powder X-ray diffraction in small molecule pharmaceuticals: Achievements and aspirations. *J. Pharm. Sci.* 107, 2969–2982.
- Thompson, S.A., Williams, R.O., 2021. Specific mechanical energy – An essential parameter in the processing of amorphous solid dispersions. *Adv. Drug Deliv. Rev.* 173, 374–393.
- Tian, P., Yang, F., Yu, L., Lin, M.-M., Lin, W., Lin, Q., Lv, Z., Huang, S., Chen, Y., 2019. Applications of excipients in the field of 3D printed pharmaceuticals. *Drug Dev. Ind. Pharm.* 45, 905–913.
- Ting, J.M., Porter, W.W., Mecca, J.M., Bates, F.S., Reineke, T.M., 2018. Advances in polymer design for enhancing oral drug solubility and delivery. *Bioconjug. Chem.* 29, 939–952.
- Trasi, N.S., Taylor, L.S., 2012. Effect of polymers on nucleation and crystal growth of amorphous acetaminophen. *CrystEndComm* 14, 5188–5197.
- Trenfield, S.J., Madla, C.M., Basit, A.W., Gaisford, S., 2018. Binder jet printing in pharmaceutical manufacturing, in: Basit, A.W., Gaisford, S. (Eds.), *3D printing of pharmaceuticals*, AAPS Advances in the Pharmaceutical Sciences Series. Springer, Cham, Switzerland, pp. 44, 46, 51, 52.
- U.S. Food and Drug Administration, 2013. FDA Drug Safety Communication: FDA limits usage of Nizoral (ketoconazole) oral tablets due to potentially fatal liver injury and risk of drug interactions and adrenal gland problems.
- van den Heuvel, K.A., Berardi, A., Buijvoets, L.B., Dickhoff, B.H.J., 2022. 3D-Powder-bed-printed pharmaceutical drug product tablets for use in clinical studies. *Pharmaceutics* 14, 2320.
- van den Heuvel, K.A., de Wit, M.T.W., Dickhoff, B.H.J., 2021. Evaluation of lactose based 3D powder bed printed pharmaceutical drug product tablets. *Powder Technol.* 390, 97–102.
- van Tyle, J., 2013. Ketoconazole; Mechanism of action, spectrum of activity, pharmacokinetics, drug interactions, adverse reactions and therapeutic use. *Pharmacotherapy* 4, 343–373.
- Vasconcelos, T., Marques, S., das Neves, J., Sarmiento, B., 2016. Amorphous solid dispersions: Rational selection of a manufacturing process. *Adv. Drug Deliv. Rev.* 100, 85–101.
- Vaz, V.M., Kumar, L., 2021. 3D printing as a promising tool in personalized medicine. *AAPS PharmSciTech* 22, 49.
- Venkataraman, N., Rangarajan, S., Matthewson, M.J., Harper, B., Safari, A., Danforth, S.C., Wu, G., Langrana, N., Gucer, S., Yardimci, A., 2000. Feedstock material property - Process relationships in fused deposition of ceramics (FDC). *Rapid Prototyp. J.* 6, 244–252.

- Verstraete, G., Samaro, A., Grymonpré, W., Vanhoorne, V., Snick, B. Van, Boone, M.N., 2018. 3D printing of high drug loaded dosage forms using thermoplastic polyurethanes. *Int. J. Pharm.* 536, 318–325.
- Wang, C.-C., Tejwani (Motwani), M.R., Roach, W.J., Kay, J.L., Yoo, J., Surprenant, H.L., Monkhouse, D.C., Pryor, T.J., 2006. Development of near zero-order release dosage forms using three-dimensional printing (3-DP™) technology. *Drug Dev. Ind. Pharm.* 32, 367–376.
- Wang, Z., Han, X., Chen, R., Li, J., Gao, J., Zhang, H., Liu, N., Gao, X., Zheng, A., 2021. Innovative color jet 3D printing of levetiracetam personalized paediatric preparations. *Asian J. Pharm. Sci.* 16, 374–386.
- Wickström, H., Palo, M., Rijckaert, K., Kolakovic, R., Nyman, J.O., Määttänen, A., Ihalainen, P., Peltonen, J., Genina, N., de Beer, T., Löbmann, K., Rades, T., Sandler, N., 2015. Improvement of dissolution rate of indomethacin by inkjet printing. *Eur. J. Pharm. Sci.* 75, 91–100.
- Windolf, H., Chamberlain, R., Quodbach, J., 2021. Predicting drug release from 3D printed oral medicines based on the surface area to volume ratio of tablet geometry. *Pharmaceutics* 13, 1453.
- Wu, B.M., Borland, S.W., Giordano, R.A., Cima, L.G., Sachs, E.M., Cima, M.J., 1996. Solid free-form fabrication of drug delivery devices. *J. Control. Rel.* 40, 77–87.
- Xu, P., Li, J., Meda, A., Osei-Yeboah, F., Peterson, M.L., Repka, M., Zhan, X., 2020. Development of a quantitative method to evaluate the printability of filaments for fused deposition modeling 3D printing. *Int. J. Pharm.* 588, 119760.
- Yasuhiro, T., Mudie, D.M., Langguth, P., Amidon, G.E., Amidon, G.L., 2014. The Biopharmaceutics classification system: Subclasses for in vivo predictive dissolution (IPD) methodology and IVIVC. *Eur. J. Pharm. Sci.* 57, 152–163.
- Yoo, J., Bradbury, T.J., Bebb, T.J., Iskra, J., Surprenant, H.L., West, T.G., 2014. Three-dimensional printing system and equipment assembly. Patent US008888480B2.
- Yu, D., Branford-White, C., Yang, Y.-C., Zhu, L., Welbeck, E.W., Yang, X., 2009. A novel fast disintegrating tablet fabricated by three-dimensional printing. *Drug Dev. Ind. Pharm.* 35, 1530–1536.
- Yu, D., Yang, X., Huang, W.D., Liu, J., Wang, Y.G., Xu, H., 2007. Tablets with material gradients fabricated by three-dimensional printing. *J. Pharm. Sci.* 96, 2446–2456.
- Zhang, J., Allardyce, B.J., Rajkhowa, R., Wang, X., Liu, X., 2021. 3D printing of silk powder by binder jetting technique. *Addit. Manuf.* 38, 101820.
- Zhang, J., Feng, X., Patil, H., Tiwari, R. V., Repka, M.A., 2017. Coupling 3D printing with hot-melt extrusion to produce controlled-release tablets. *Int. J. Pharm.* 519, 186–197.
- Zhang, J., Xu, P., Vo, A.Q., Bandari, S., Yang, F., Durig, T., Repka, M.A., 2019. Development and evaluation of pharmaceutical 3D printability for hot melt extruded cellulose-based filaments. *J. Drug Deliv. Sci. Technol.* 52, 292–302.
- Zheng, Y., Deng, F., Wang, B., Wu, Y., Luo, Q., Zuo, X., Liu, X., Cao, L., Li, M., Lu, H., Cheng, S., Li, X., 2021. Melt extrusion deposition (MED™) 3D printing technology – A paradigm shift in design and development of modified release drug products. *Int. J. Pharm.* 602, 120639.

Zhou, Z., Buchanan, F., Mitchell, C., Dunne, N., 2014. Printability of calcium phosphate: Calcium sulfate powders for the application of tissue engineered bone scaffolds using the 3D printing technique. *Mater. Sci. Eng. C* 38, 1–10.

Ziaee, M., Crane, N.B., 2019. Binder jetting: A review of process, materials, and methods. *Addit. Manuf.* 28, 781–801.

8. Danksagung

Diese Arbeit entstand unter der Leitung von Prof. Dr. Jörg Breitzkreutz und der Betreuung durch Dr. Malte Bogdahn und Dr. Julian Quodbach im Rahmen der Fördermaßnahme „Materialinnovationen für gesundes Leben: ProMatLeben – Polymere“ und meiner Tätigkeit als Doktorandin bei Merck Healthcare KGaA in der Abteilung „Pharmaceutical Technologies“.

Ein besonderer Dank geht an Dr. Malte Bogdahn und Dr. Julian Quodbach für die intensive Betreuung meiner Arbeit. Ihre Expertise und Ihr Engagement haben meine Arbeit bereichert. Ich bin außerordentlich dankbar für die zahlreichen Ratschläge sowie die regelmäßigen Diskussionen, die mich gelehrt haben meine Ergebnisse kritisch zu hinterfragen sowie diese in einem größeren Kontext zu stellen.

Ich möchte auch Prof. Dr. Jörg Breitzkreutz meinen Dank aussprechen für die Möglichkeit an diesem Forschungsthema als Teil seines Arbeitskreises zu arbeiten.

Mein Dank geht ebenfalls an Prof. Dr. Anne Seidlitz für die Übernahme der Rolle der zweiten Gutachterin.

Ein sehr großer Dank geht an Alicia Burkard für ihre Unterstützung im Labor während ihres Pharmaziepraktikums. Ihr Engagement und sorgfältige Arbeitsweise haben Publikation Nr. 3 überhaupt erst ermöglicht.

Vielen Dank dem gesamten PolyPrint Konsortium für die Zusammenarbeit. Meine Arbeit im Rahmen dieses interdisziplinären Konsortiums durchführen zu dürfen, habe ich sehr geschätzt. Ein großer Dank geht hier insbesondere an Alessandro-Giuseppe Elia für die vielen Stunden, die wir gemeinsam versucht haben gleichförmige Filamente zu extrudieren und von dessen Extrusionserfahrung ich sehr viel gelernt habe.

Ein großer Dank geht an das Team von DDI. Ich möchte Dr. Simon Geißler dafür danken, dass er mir die Möglichkeit gegeben hat, diese Arbeit in seiner Gruppe durchzuführen zu können. Ein großer Dank geht an Marcel Wedel für seine technische Unterstützung, insbesondere dann, wenn ein 3D-Drucker mal wieder nicht tat, was er sollte und der stets eine passende Lösung parat hatte. Ich möchte mich auch ganz herzlich bei Martina Jeschke und Catharina Stietzel für die unermüdliche und wertvolle Unterstützung bedanken, die sie mir im Labor bei verschiedenen Fragen, insbesondere im Bereich UPLC, zukommen haben lassen. Dank ihrer Erfahrung und ihres Know-hows konnte ich sehr viel lernen. Vielen Dank auch an Patrizia Boniforte und Dr. Robert

Hennig bei allen Fragen zu Peposertib. Und zu guter Letzt bedanke ich mich bei Reiner Vonderschmitt, der immer mit Rat und Tat bei Fragen jeglicher Art zur Stelle war.

Ich möchte mich auch herzlich bei den vielen Doktoranden/Leidensgenossen in PharmTech für den regen Austausch zu fachlichen Themen, aber auch jeglichen Tipps und Tricks für das Doktorandensein bedanken. Ganz nach dem Motto „Geteiltes Leid ist halbes Leid“. Auch wenn unsere gemeinsame Zeit durch Covid erschwert wurde, bin ich sehr froh, dass wir gemeinsame Freizeitaktivitäten im Anschluss an unsere Doktorandenzeit noch nachgeholt haben/bzw. nachholen.

Ein ganz großer Dank geht an meine Bürokolleginnen Dominique Schädel, Franziska Kuhn, Lena Mareczek und Nicole Hofmann und ihre unermüdliche emotionale Unterstützung während der wenigen Hochs und besonders vielen Tiefs der Doktorandenzeit. In diesem thematischen Rahmen möchte ich zudem Dr. Melinda Kern hervorheben, die war nicht in unserem Büro saß, aber bestimmt genauso oft dort war. Ich möchte mich bei ihr ganz herzlich bedanken für die wertvolle Unterstützung zu Beginn meiner Doktorandenzeit, die schönen gemeinsamen Unternehmungen, die vielen leckeren Gebäckspezialitäten und ganz besonders für ihr offenes Ohr und ihre Freundschaft während der besonders schwierigen Phasen.

Ein großer Dank geht an meine langjährigen Freunde außerhalb der Wissenschaftswelt, die mir stets ein wichtiger Ausgleich zum Doktorandenalltag gewesen sind und mich immer wieder erinnern haben, dass es im Leben noch mehr gibt als die Doktorarbeit. Für all das und noch so vieles mehr danke ich euch von ganzem Herzen!

Vielen Dank auch an meine Familie, insbesondere an meine Mutter, für all das, was sie gegeben hat, um mir ein gutes Leben zu ermöglichen und für ihr Vertrauen in meine Entscheidungen und den Weg, den ich eingeschlagen habe. Ebenso danke ich meinen Großeltern, meiner Oma für ihre Fürsorge und Vorbildfunktion in Sachen Durchhaltevermögen und meinem Opa dafür, dass er immer bereit war, mit mir Neues auszuprobieren und meine Neugierde zu fördern.

Ein abschließender Dank geht an meinen Partner Alex. Danke für deine Geduld und Bereitschaft dir meine Gedankengänge anzuhören und deine humorvolle Art, die mich stets wieder aufgemuntert hat. Dank dir drehen nicht nur die Förderräder dieser Dissertation in die richtige Richtung. Vielen Dank für deine bedingungslose Unterstützung!

9. Eidesstattliche Erklärung

Ich versichere an Eides Statt, dass die Dissertation von mir selbständig und ohne unzulässige fremde Hilfe unter Beachtung der „Grundsätze zur Sicherung guter wissenschaftlicher Praxis an der Heinrich-Heine-Universität Düsseldorf“ erstellt worden ist.

Nadine Gottschalk